

NASA Contractor Report 178216

Flight Survey of the 757 Wing Noise Field And Its Effects on Laminar Boundary Layer Transition

Volume I — Program Description and Data Analysis

Boeing Commercial Airplane Company
P.O. Box 3707, Seattle, WA 98124

Contract NAS1-15325
March 1987

MAR 24 1989

Publicly Released 3/89

(NASA-CR-178216) FLIGHT SURVEY OF THE 757
WING NOISE FIELD AND ITS EFFECTS ON LAMINAR
BOUNDARY LAYER TRANSITION. VOLUME 1: PROGRAM
DESCRIPTION AND DATA ANALYSIS Report, NOV.
1984 - Jul. 1985 (Boeing Commercial

N89-18665

Unclas
G3/34 0192940

The limitations
contained in this legend will be considered void after March 1989. ~~_____~~



National Aeronautics and
Space Administration

Langley Research Center
Hampton, Virginia 23665
AC 804 865-2000

NASA Contractor Report 178216

**Flight Survey of the 757 Wing Noise Field
And Its Effects on Laminar Boundary
Layer Transition**

**Volume I — Program Description and
Data Analysis**

**Boeing Commercial Airplane Company
P.O. Box 3707, Seattle, WA 98124**

**Contract NAS1-15325
March 1987**

**NATIONAL AERONAUTICS AND SPACE ADMINISTRATION
LANGLEY RESEARCH CENTER**

FOREWORD

This report presents the results of the 757 Wing Noise Survey and Glove Flight Test conducted under NASA Contract NAS1-15325 from November 1984 through July 1985. This work was managed by the Laminar Flow Control Project Office (LFCPO) at the NASA Langley Research Center. Mr. R. D. Wagner is Head of the LFCPO and Mr. D. B. Middleton, and Mr. D. W. Bartlett were the technical monitors for the contract.

The work was performed under the direction of the New Product Development staff of the Boeing Commercial Airplane Company. A number of organizations including the Engineering, Manufacturing, and Flight Test departments contributed to the successful completion of the total project as planned. Key contractor personnel responsible for this effort were—

C. F. Watson
L. B. Gratzner
J. H. Armstrong
G. W. Bielak
T. J. Kelly
R. A. Mangiarotty
J. F. McGuire
A. L. Nagel
M. J. Omoth
E. I. Plunkett
L. J. Runyan
A. C. Chen
J. T. Skomorowski
R. Q. Taylor
H. M. Tomlinson
W. H. Walter

Manager-NASA Programs
Laminar Flow Program Manager
757 Project Test Pilot
Acoustics Technology
Developmental Manufacturing/Engineering
Acoustics Technology
Structures Technology Supervision
Aerodynamics Supervision
Systems Technology
Acoustics Laboratory
Aerodynamics Technology
Aerodynamics Technology
Structural Design
Materials Technology
Structures Design Supervision
Flight Test Engineering

CONTENTS

	Page
1.0 SUMMARY.....	1
2.0 INTRODUCTION.....	3
3.0 SYMBOLS AND ABBREVIATIONS	5
3.1 Acronyms.....	5
3.2 Mathematical Symbols.....	5
3.3 Subscripts	6
4.0 PROGRAM PLAN	7
4.1 Objectives	7
4.2 Technical Approach.....	7
5.0 NATURAL LAMINAR FLOW GLOVE DESIGN	15
5.1 Aerodynamic Design.....	15
5.2 Attachment Line Stability.....	17
5.3 Final Glove Geometry	17
5.4 Transonic Analysis Results	18
5.5 Leading Edge Protective Cover.....	48
6.0 INSTRUMENTATION	53
6.1 Airplane Instrumentation Systems.....	53
6.2 Glove Aerodynamic Instrumentation	53
6.2.1 Static Pressure Belts	53
6.2.2 Hot-Film Sensors	54
6.3 Acoustic Instrumentation.....	54
6.3.1 Surface-Mounted Microphones.....	54
6.3.2 Probe-Mounted Microphones	54
6.3.3 Microphone Installation.....	55
6.4 Data Acquisition Systems	55
6.4.1 Online Data Reduction Instrumentation	55
6.4.2 Calibrations.....	55
6.4.3 Data Acquisition Procedure.....	55
6.5 Acoustic Data Reduction	55
6.5.1 Online Data Reduction.....	55
6.5.2 Offline Data Reduction	55
6.5.3 Disposition of Data.....	57
7.0 GLOVE FABRICATION AND INSTALLATION	83
7.1 Fabrication	83
7.2 Installation	83
7.3 Surface Checking and Finishing.....	85

PRECEDING PAGE BLANK NOT FILMED

CONTENTS (Concluded)

	Page
8.0 TEST DATA ANALYSIS	103
8.1 Flight Test Conditions	103
8.2 Acoustic Environment	104
8.2.1 Sound Level Distributions	104
8.2.2 One-Third-Octave Data Spectra	105
8.2.3 Compressor Bleed Flow Noise	106
8.2.4 Altitude Normalization	107
8.2.5 Noise Correlation With Engine Parameters	108
8.2.6 Narrowband Analysis	108
8.3 Aerodynamic Characteristics	158
8.3.1 Static Pressure Data	158
8.3.2 Transition Location Data	159
8.3.3 Sideslip Effects	160
8.4 Effect of Engine Power on Transition	160
9.0 CONCLUSIONS AND RECOMMENDATIONS	177
10.0 REFERENCES	179
APPENDIX A PROBE DEVELOPMENT	181
A.1 Sting-Mounted Probes	181
A.2 Transducer Vent Tube Modifications	181
ABSTRACT	201

Figure	FIGURES Title	Page
4-1	757 Airplane With NLF Glove	9
4-2	Typical 757 Wing Section Pressures	10
4-3	Natural Laminar Flow Glove Installation Concept	11
4-4	Wing Instrumentation Concept.	12
4-5	Range of Conditions for Glove Flight Test.	13
5-1	757 Natural Laminar Flow Glove Concept	19
5-2	757 Natural Laminar Flow Glove Arrangement.	20
5-3	Disturbance Growth Analysis for Laminar Boundary Layers	21
5-4	Transition Criteria for Laminar Boundary Layers	22
5-5	Boundary Layer Transition Analysis for Glove Upper Surface, $M = 0.80$, $C_L = 0.548$	23
5-6	Boundary Layer Transition Analysis for Glove Lower Surface, $M = 0.80$, $C_L = 0.548$	24
5-7	Boundary Layer Transition Analysis for Glove Upper Surface, $M = 0.84$, $C_L = 0.420$	25
5-8	Boundary Layer Transition Analysis for Glove Lower Surface, $M = 0.70$, $C_L = 0.522$	26
5-9	Attachment Line Momentum Thickness Reynolds Number vs Span	27
5-10	757 Glove Planform Definition	28
5-11	Airfoil Sections for 757 Glove	30
5-12	757 Glove Notch Geometry	31
5-13	Theoretical Glove Pressure Distribution — Case SS, $M = 0.84$, $C_L = 0.420$	33
5-14	Theoretical Glove Pressure Distribution — Case VV, $M = 0.84$, $C_L = 0.345$	34
5-15	Theoretical Glove Pressure Distribution — Case YY, $M = 0.82$, $C_L = 0.452$	35
5-16	Theoretical Glove Pressure Distribution — Case TT, $M = 0.82$, $C_L = 0.388$	36
5-17	Theoretical Glove Pressure Distribution — Case OO, $M = 0.80$, $C_L = 0.548$	37
5-18	Theoretical Glove Pressure Distribution — Case PP, $M = 0.80$, $C_L = 0.436$	38
5-19	Theoretical Glove Pressure Distribution — Case QQ, $M = 0.80$, $C_L = 0.380$	39
5-20	Theoretical Glove Pressure Distribution — Case AB, $M = 0.80$, $C_L = 0.243$	40
5-21	Theoretical Glove Pressure Distribution — Case ZZ, $M = 0.78$, $C_L = 0.473$	41
5-22	Theoretical Glove Pressure Distribution — Case XX, $M = 0.75$, $C_L = 0.503$	42
5-23	Theoretical Glove Pressure Distribution — Case RR, $M = 0.75$, $C_L = 0.399$	43
5-24	Theoretical Glove Pressure Distribution — Case WW, $M = 0.70$, $C_L = 0.522$	44
5-25	Theoretical Glove Pressure Distribution — Case UU, $M = 0.70$, $C_L = 0.433$	45
5-26	Glove Pressure Distribution Characteristics Summary — WBL 325	46
5-27	Theoretical Glove Streamlines on Upper and Lower Surfaces, $M = 0.80$, $C_L = 0.548$, $R_\rho/ft = 1.471 \times 10^6$	47
5-28	Evaluation of Glove Cover Parameters, T-33 Flight Test.	50
5-29	Glove Cover and Removal Apparatus — Flights 1, 2, and 3	51
5-30	Insect Impingement on Glove for Flight 4.	52

FIGURES (Continued)

Figure	Title	Page
6-1	Video Monitor for Flight Parameters.....	58
6-2	757 NLF Glove Instrumentation	59
6-3	Pressure Belt Installation	60
6-4	Transition Sensing System Using Hot Films	64
6-5	Microphone Arrays on Wing Upper and Lower Surfaces.....	65
6-6	Acoustic Sensor Types and Specifications	66
6-7	Probe-Mounted Microphone Arrangements	68
6-8	Instrumentation Array on Wing Upper Surface	69
6-9	Instrumentation Array on Wing Lower Surface	70
6-10	Instrumentation Array on Glove Upper Surface.....	71
6-11	Instrumentation Array on Glove Lower Surface.....	72
6-12	Typical Upper Surface Probe Installations	73
6-13	Typical Lower Surface Probe Installations	74
6-14	Typical Surface-Mounted Microphone Installations	75
6-15	Typical Surface-Mounted Microphone Installations	76
6-16	Data Acquisition System Schematic.....	77
6-17	Acoustic Signal Conditioning Electronics	78
6-18	Acoustic Data Recording System	79
6-19	Online Data Reduction System.....	80
6-20	Typical Frequency Response Calibration Data — Normalized to 250 Hz.....	81
6-21	Typical Ambient Noise Floor Microphone 11	82
7-1	Machining Sequence for Glove Leading Edge Segments	87
7-2	Machined Leading Edge Foam Piece	88
7-3	Machined Upper Surface Foam Panel	89
7-4	Glove Parts Arrangement	90
7-5	Glove Installation Technique	91
7-6	Wing Cocoon for Glove Installation	92
7-7	Assembly Mismatches for Glove Upper Surface	93
7-8	Assembly Mismatches for Glove Lower Surface	94
7-9	Glove Surfaces Prior to Fiberglass Installation	95
7-10	Steps in Glove Contouring and Finishing Process	96
7-11	Deviation of Glove Contour from Design Loft.....	97
7-12	Smoothness Criteria for Laminar Flow Surfaces	98
7-13	Waviness Survey for Glove Upper Surface	99
7-14	Waviness Survey for Glove Lower Surface	100
7-15	Finished Glove Upper Surface Instrumentation Installed	101
7-16	Finished Glove Lower Surface Instrumentation Installed	102

FIGURES (Continued)

Figure	Title	Page
8-1	OASPL Distribution on 757 Wing, Category 5, Condition 219	114
8-2	OASPL Distribution on 757 Wing, Category 6, Condition 223	115
8-3	OASPL Distribution on 757 Wing, Category 7, Condition 231	116
8-4	OASPL Distribution on 757 Wing, Category 8, Condition 243	117
8-5	Normalized OASPL on Wing Lower Surface, Probe Microphones	118
8-6	Normalized OASPL on Wing Lower Surface, Leading Edge Surface Microphones	119
8-7	Normalized OASPL on Wing Upper Surface, Probe Microphones	120
8-8	Normalized OASPL on Wing Upper Surface, Leading Edge Surface Microphones	121
8-9	Engine Power Effects on Wing Lower Surface Spectra, Probe Microphones	122
8-10	Engine Power Effects on Wing Lower Surface Spectra, Probe Microphones	123
8-11	Engine Power Effects on Wing Lower Surface Spectra, Probe Microphones	124
8-12	Engine Power Effects on Wing Lower Surface Spectra, Probe Microphones	125
8-13	Engine Power Effects on Wing Lower Surface Spectra, Leading Edge Surface Microphones	126
8-14	Engine Power Effects on Wing Lower Surface Spectra, Leading Edge Surface Microphones	127
8-15	Engine Power Effects on Wing Lower Surface Spectra, Leading Edge Surface Microphones	128
8-16	Engine Power Effects on Wing Lower Surface Spectra, Leading Edge Surface Microphones	129
8-17	Engine Power Effects on Wing Upper Surface Spectra, Probe Microphones	130
8-18	Engine Power Effects on Wing Upper Surface Spectra, Probe Microphones	131
8-19	Engine Power Effects on Wing Upper Surface Spectra, Probe Microphones	132
8-20	Engine Power Effects on Wing Upper Surface Spectra, Probe Microphones	133
8-21	Engine Power Effects on Wing Upper Surface Spectra, Leading Edge Surface Microphones	134
8-22	Engine Power Effects on Wing Upper Surface Spectra, Leading Edge Surface Microphones	135
8-23	Engine Power Effects on Wing Upper Surface Spectra, Leading Edge Surface Microphones	136
8-24	Engine Power Effects on Wing Upper Surface Spectra, Probe Microphones	137
8-25	Engine Bleed Effects on Wing Lower Surface Spectra, Probe Microphones	138
8-26	Engine Bleed Effects on Wing Lower Surface Spectra, Leading Edge Surface Microphones	139
8-27	Engine Bleed Effects on Wing Upper Surface Spectra, Probe Microphones	140
8-28	Engine Bleed Effects on Wing Upper Surface Spectra, Leading Edge Surface Microphones	141
8-29	OASPL Correlation With Ambient Pressure	142
8-30	Altitude Normalization of Noise Spectra, Upper Surface Microphone 1	143

FIGURES (Continued)

Figure	Title	Page
8-31	Effect of Altitude Normalization, Upper Surface Microphone 1	144
8-32	Effect of Altitude Normalization, Lower Surface Microphone 10	145
8-33	Engine Parameters Correlation, Lower Surface Microphone 10	146
8-34	Effect of Airplane Electrical Power System Interference on Narrowband (37.5 Hz) Spectra	148
8-35	Effect of Various Noise Sources on Narrowband (37.5 Hz) Spectra	149
8-36	Effect of Various Noise Sources on Narrowband (37.5 Hz) Spectra	150
8-37	Effect of Various Noise Sources on Narrowband (37.5 Hz) Spectra	151
8-38	Effect of Various Noise Sources on Narrowband (37.5 Hz) Spectra	152
8-39	Effect of Various Noise Sources on Narrowband (37.5 Hz) Spectra	153
8-40	Effect of Various Noise Sources on Narrowband (37.5 Hz) Spectra	154
8-41	Effect of Various Noise Sources on Narrowband (37.5 Hz) Spectra	155
8-42	Effect of Various Noise Sources on Narrowband (37.5 Hz) Spectra	156
8-43	Effect of Various Noise Sources on Narrowband (37.5 Hz) Spectra	157
8-44	Laminar Areas on Glove in Flight — Design Condition.	166
8-45	Spanwise Effects on Glove Pressure Distributions	167
8-46	Comparison of Inboard Glove Pressure Distributions — Effect of C_L	168
8-47	Comparison of Outboard Glove Pressure Distributions — Effect of C_L	169
8-48	Comparison of Outboard Glove Pressure Distributions — Effect of Mach Number	170
8-49	Comparison of Inboard Glove Pressure Distributions — Effect of Mach Number	171
8-50	Transition Distribution on 757 Glove — Effect of C_L	172
8-51	Transition Distribution on 757 Glove — Effect of Mach Number	173
8-52	Transition Variation With Sideslip (Sweep) — Effect of C_L	174
8-53	Effect of Sideslip on Glove Pressure Distributions	175
8-54	Effect of Engine Power Setting on Extent of Laminar Flow	176
A1	Close-Up View of Transducer Installation on NA001 for Probe Evaluation Flight Tests ..	183
A2	Test Setup in LTC for Probe Directivity Comparison	184
A3	B&K 4134 Reference Spectrum.	185
A4	Side-Mounted Transducer Probe Configuration Tested With Unvented Kulite	186
A5	B&K Bullet Nose Probe Configuration — No Modification to Vent Tube	187
A6	Test Setup in Quiet Air Facility for Probe Self-Noise Test	188
A7	B&K Bullet Nose Probe Configuration Self-Noise Test	189
A8	Side-Mounted Transducer Probe Configuration Self-Noise Test	190
A9	Kulite Transducer Installation on NA001 for Probe Evaluation Flight Tests	191
A10	Flight Test Data From February 22, 1985 Probe Evaluation Test	192
A11	Flight Evaluation of Surface-Mounted Microphone	193
A12	Flight Evaluation of Probe Microphone (B&K Nose Cone)	194

FIGURES (Concluded)

Figure	Title	Page
A13	Flight Evaluation of Probe Microphone (Side Mount)	195
A14	XCW-093-5 Transducer — No Modifications to Vent Tube	196
A15	LQ-101-125-5 Transducer — No Modification Made to Vent Tube	197
A16	B&K Bullet Nose Probe Configuration — 3 ft Length of Tygon Tubing Spliced to Transducer Vent Tube	198
A17	XCE-093-5 Transducer With 0.008-in Wire Inserted in Vent Tube	199
A18	LQ-101-125-5 Transducer With 0.008-in Wire Inserted in Vent Tube	200

TABLES		
Table	Title	Page
5-1	757 Glove Airfoil Coordinates	29
5-2	Aerodynamic Analysis Results Summary — Glove Upper Surface	32
5-3	Aerodynamic Analysis Results Summary — Glove Lower Surface	32
6-1	Static Pressure Orifice Locations	61
6-2	Hot-Film Locations for Flights 1 and 2	62
6-3	Hot-Film Locations for Flights 3 and 4	63
6-4	Microphone Installation Geometry Specification	67
8-1	Noise Related Airplane and Engine Data — Flight 1	109
8-2	Noise Related Airplane and Engine Data — Flight 2	110
8-3	One-Third-Octave Band Plot Categories — Flight 1	111
8-4	One-Third-Octave Band Plot Categories — Flight 2	112
8-4	One-Third-Octave Band Plot Categories — Flight 2 (Continued)	113
8-5	Prominent Turbomachinery Tones for P&W 2037 Engine	147
8-6	Flight Test Data Summary — Flight 1	162
8-7	Flight Test Data Summary — Flight 2	163
8-8	Flight Test Data Summary — Flight 3	164
8-9	Flight Test Data Summary — Flight 4	165

PRECEDING PAGE BLANK NOT FILMED

1.0 SUMMARY

It has been previously observed that an incident acoustic field on a wing with laminar flow can cause transition to turbulent flow if the fluctuating acoustic velocities are of sufficient amplitude and in the critical frequency range for an unstable laminar boundary layer (ref. 1). Although some data on the Northrop X-21A LFC airplane have been previously taken, very little acoustic environment data measured on the wing of a modern transport aircraft are available. Accordingly, NASA awarded a contract to The Boeing Company to perform a flight test program using the Boeing 757 flight research aircraft with wing-mounted high-bypass ratio engines (PW 2037 engines) to obtain acoustic spectral data on the wing surfaces. As part of this effort, a section of the wing was modified with a natural laminar flow (NLF) glove to allow direct measurement of the effect of varying engine noise on the extent of laminar flow.

The NLF glove was installed on the right wing panel just outboard of the engine. The glove had a leading edge sweep of 21 deg, a span of approximately 10 ft, and extended chordwise about 6 ft. The glove was instrumented with hot films for measuring the extent of laminar flow, and pressure belts were used to obtain the chordwise pressure distributions at two spanwise stations. A combination of surface and probe microphones were distributed over the upper and lower wing surfaces to measure sound spectra. A range of flight conditions was selected to provide coverage of the normal cruise condition and to assess the effects of off-design operation.

The flight test program was completed in June, 1985. A maximum of about 29% chord laminar flow was obtained on the upper surface and about 28% on the lower surface. This exceeded the design objectives for the NLF glove.

At each flight condition, the engine power was varied from about 2600 r/min (idle) to about 4500 r/min (maximum continuous power). This produced changes in sound pressure level over 20 dB on the wing lower surface, depending on the proximity to the engine. On the wing upper surface, the sound pressure levels were relatively independent of engine power but did exhibit significant variations with airplane Mach number. The spectral data provides considerable insight into the influences of the various sound sources that contribute to the overall noise levels. Additional analysis will be required to assess the impact of these sources on boundary layer transition.

The location of transition was affected by a number of operational parameters including Reynolds number, Mach number, C_L , and sideslip (sweep). The trends exhibited were generally in accord with those expected from analysis and other experiments. For the conditions prevailing in these tests, the effect of engine power on transition was negligible on the upper surface and small (1% - 2% chord) on the lower surface. For situations involving longer laminar runs (e.g., with HLFC) and for higher engine noise levels, significant effects of engine noise on the extent of laminar flow cannot be ruled out.

These results demonstrate that substantial laminar flow on the wing of a transport configuration with wing-mounted engines can be obtained.

2.0 INTRODUCTION

Application of a laminar flow wing design to commercial transports offers the potential of significant airplane drag reductions. However, a major concern has been whether laminar flow can be sustained in the presence of the noise environment on the wing of a commercial transport with conventional wing-mounted turbofan engines. To resolve this issue, and thereby avoid possible design limitations, it was planned to obtain flight test wing noise environment data on a current production commercial aircraft. To assess the effect of engine noise on laminar flow, it was also planned to establish an area of laminar flow on the wing and thus allow direct measurement of the effect of varying engine noise level on the extent of laminar flow.

Reference 1 provides a limited amount of one-third octave sound pressure level data measured on a chordwise array of eight microphones installed close to the outboard engine nacelle on the wing under-surface of a 747-200 airplane. In addition, single microphone measurements on the wing surfaces of smaller aircraft (ref. 2) are available. Some sound surveys have been made on the wing of the Northrop X-21A LFC airplane (ref. 3), but these measurements were of overall sound pressures only and were obtained 12 to 18 inches above and below the wing surfaces. Although evaluation of this limited data indicates that noise may not be a major constraint to successful application of laminar flow on wing-mounted engine configuration arrangements, acoustical spectra data extending over most of the upper and lower wing surfaces are needed to substantiate these conclusions and to guide future configuration designs using laminar flow concepts.

The 757-200 airplane is a suitable testbed for investigating the effects of noise from wing-mounted engines on the extent of laminar flow because it is typical of the size and configuration of airplanes currently being considered for laminar flow applications. A number of possibilities were considered for obtaining laminar flow over a limited area of the 757 wing. An approach involving suction through holes or slots in the surface to stabilize the boundary layer would make it possible to achieve extensive laminar flow at the existing leading edge sweep angle of 28 deg. However, such an approach would be more expensive than one that relies on natural laminar flow (NLF). Based on existing evidence, it became apparent that in order to obtain a significant chordwise extent of NLF, the leading edge sweep angle would have to be reduced.

The above considerations suggested an approach with an NLF glove installed on the 757-200 wing in the vicinity of the engines with the leading edge sweep angle of the glove significantly less than that of the wing. Implementation of the NLF glove and measurement of aerodynamic and acoustic data in flight on the 757 are the subject of this report.

Volume I of this report contains the program description and data analysis. Volume II is a compilation of all of the flight test data.

PRECEDING PAGE BLANK NOT FILMED

3.0 SYMBOLS AND ABBREVIATIONS

3.1 ACRONYMS

C-F	Crossflow
CIR	Circle
HLFC	Hybrid laminar flow
LE	Leading edge
LFC	Laminar flow control
NLF	Natural laminar flow
OASPL	Overall sound pressure level
SPL	Sound pressure level = $20 \log \frac{P_{rms}}{0.002 \text{ dynes/cm}^2}$
STR	Straight
T-S	Tollmien-Schlichting
WBL	Wing buttock line

3.2 MATHEMATICAL SYMBOLS

A	disturbance amplitude
A_o	Disturbance amplitude at neutral stability point
c	Chord
C_L	Airplane lift coefficient
C_p	Pressure coefficient
h	Indicated double wave amplitude measured with waviness gauge
$\ell_n A/A_o$	Disturbance amplification factor
M	Mach number
M_{AP}	Airplane Mach number
M_{FAN}	Fan jet exhaust Mach number
N	Disturbance amplification factor
N_1	Engine fan revolutions per minute r/min)
N_{1C}	N_1 corrected to standard day temperature (59°F)
N_{CF}	Crossflow amplification factor
N_{TS}	Tollmien-Schlichting amplification factor
P	Pressure
P_{40}	Reference pressure ambient pressure at 40,000 ft altitude on standard day
Re_C	Reynolds number based on chord
$Re_{\theta_{AL}}$	Reynolds number based on momentum thickness and velocity at attachment line
s	Arc length along surface from leading edge
s/c	Normalized arc length along surface from leading edge
x	Distance from leading edge along airfoil chord

x/c	Normalized distance from leading edge along airfoil chord
y/δ	Distance above glove surface normalized by boundary layer thickness
z	Airfoil ordinate
α	Airplane angle of attack
β	Airplane sideslip angle (positive nose left)
δ	Boundary layer thickness
γ	Ratio of specific heats
Λ	Sweep angle
ψ	Angle of disturbance wavenumber vector with respect to local potential flow velocity direction
ρ	Density
ω^*	Dimensional disturbance frequency

3.3 SUBSCRIPTS

amb	Ambient
E2	Engine no. 2 (on glove side)
max	Maximum
tr	Transition
∞	Undisturbed reference condition

4.0 PROGRAM PLAN

4.1 OBJECTIVES

Objectives of the 757 flight program were as follows:

- To survey upper and lower surfaces of the 757 wing to provide the noise distribution over a major portion of the wing as a function of flight condition and engine power setting.
- To measure directly the effect of engine noise on the extent of natural laminar flow in a representative critical area.

It was recognized that providing the means to accomplish the above would also contribute significantly to important secondary goals as follows:

- To assess the feasibility of maintaining extensive natural laminar flow in a noise and interference environment generated by wing-mounted engines.
- To validate and improve current wing surface noise field prediction methods that are supported by low-speed wind tunnel data and limited flight test data.
- To further the development of aero-acoustic transfer functions for predicting the effects on the stability of a laminar flow boundary layer resulting from an impinging external acoustic field.

4.2 TECHNICAL APPROACH

The 757 airplane shown in Figure 4-1 was selected to be the testbed for the subject series of flight tests. This airplane is representative of a modern transport type for which the application of laminar flow technology could be expected in the future. The airplane is shown with the NLF glove installed. The no. 4 slat was locked in the retracted position to be compatible with the absence of the no. 7 slat, which was removed to allow installation of the glove. A modest load factor restriction was imposed for operation at the TOGW limit. Although the remaining slats were fully operable, a nominal increase in landing speed was imposed to eliminate possible low-speed operational concerns. The flight envelope for test operations and conditions was unrestricted.

Preliminary analysis had shown that the pressure distribution on that portion of the wing just outboard of the engine was likely to be quite conducive to the maintenance of natural laminar flow (NLF). The pressure distributions shown in Figure 4-2 are for two different flight conditions that were selected as being most nearly ideal for NLF on both the upper and lower surfaces. Differences in Mach number and lift coefficient were judged to be not significant in this context. Thus, the basic wing characteristics were found to be compatible with the glove concept. The remaining concerns involved the 757 leading edge sweep (28 deg) which appeared too large, and the need to provide a smooth wave-free surface.

The diagram of Figure 4-3a shows a plan view of the wing with the glove outline in the appropriate location to meet the above requirements. Although a leading edge sweep of 23 deg was initially chosen, it was decided to reduce the sweep further if structural requirements could be met and the configuration asymmetry did not impose significant flight restrictions on the airplane. The need was recognized for special leading edge treatment near the strut-wing intersection to avoid turbulent flow transfer onto the leading edge with resulting adverse effects on the laminar flow. This ultimately took the form of a leading edge notch, the design of which is discussed later.

The structural arrangement selected was simple in concept and provided an ideal basis for meeting performance and operational requirements at low cost. Figure 4-3b illustrates the design approach, which involves the minimum use of structural supporting members, i.e., ribs and a spanwise beam, which were attached to the slat support points and the end ribs respectively. Foam blocks machined to contour provided the structural base. After removal of the no. 7 slat and installation of the new supporting members, the foam blocks were to be bonded to existing fixed structure. The arrangement was completed with an overlay of fiberglass-epoxy. Final contouring and finish were expected to be accomplished through accepted techniques for a one-of-a-kind installation of this type.

The instrumentation layout is shown in Figure 4-4. The top part of the figure indicates the location of the two different types of microphone installations used on the wing. Probe-mounted types were considered necessary behind the front spar in order to avoid undue influence from thick turbulent boundary layers. Near the leading edge this consideration was judged to be less significant and the use of surface-mounted sensors was planned.

In the lower part of the figure showing the glove detail, the locations of static pressure belts for basic aerodynamic characteristics and sensors to indicate transition are illustrated. The arrangement was tailored to avoid any interference with the critical laminar areas while allowing full assessment of the aerodynamic characteristics with maximum extent of laminar flow. The placement of the microphones was also selected to be compatible with the above objectives. While the instrumentation arrangement is shown here for the upper surface, both surfaces were provided with the same instrumentation array.

The flight test plan was based on the need to acquire data over a representative range of cruise conditions for a commercial transport while allowing sufficient latitude to meet expected off-design conditions for typical operations. A further requirement involved defining the flight envelope to permit acquisition of data sufficient to define trends in terms of engine and flight parameters.

Figure 4-5 illustrates the range of flight conditions selected to meet the above objectives. It will be noted that the focus is on cruise conditions, but that a substantial range of speed and altitude is also provided to cover an appropriate range of Mach number and unit Reynolds numbers. For each flight condition, the right-hand engine power was to be varied from flight idle to maximum continuous power (MCT). For most conditions, level flight could be maintained by suitable adjustment of engine power on the opposite side. In cases where this was not possible a slow descent rate compatible with data acquisition requirements was allowed.

- Remaining slats are operable
- TOGW limit - 220,000 lb (1.7g)
- Normal flight envelope

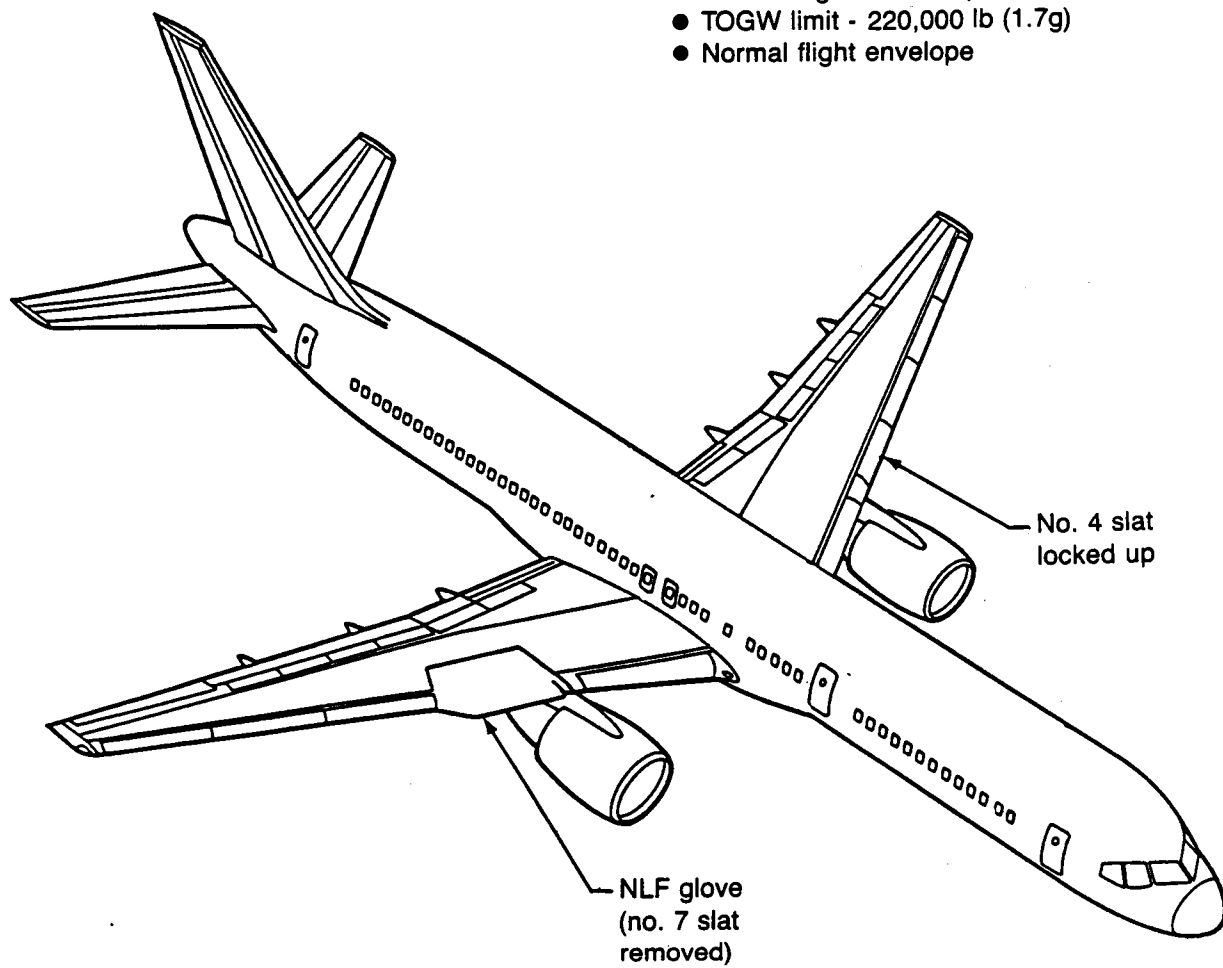


Figure 4-1. 757 Airplane With NLF Glove

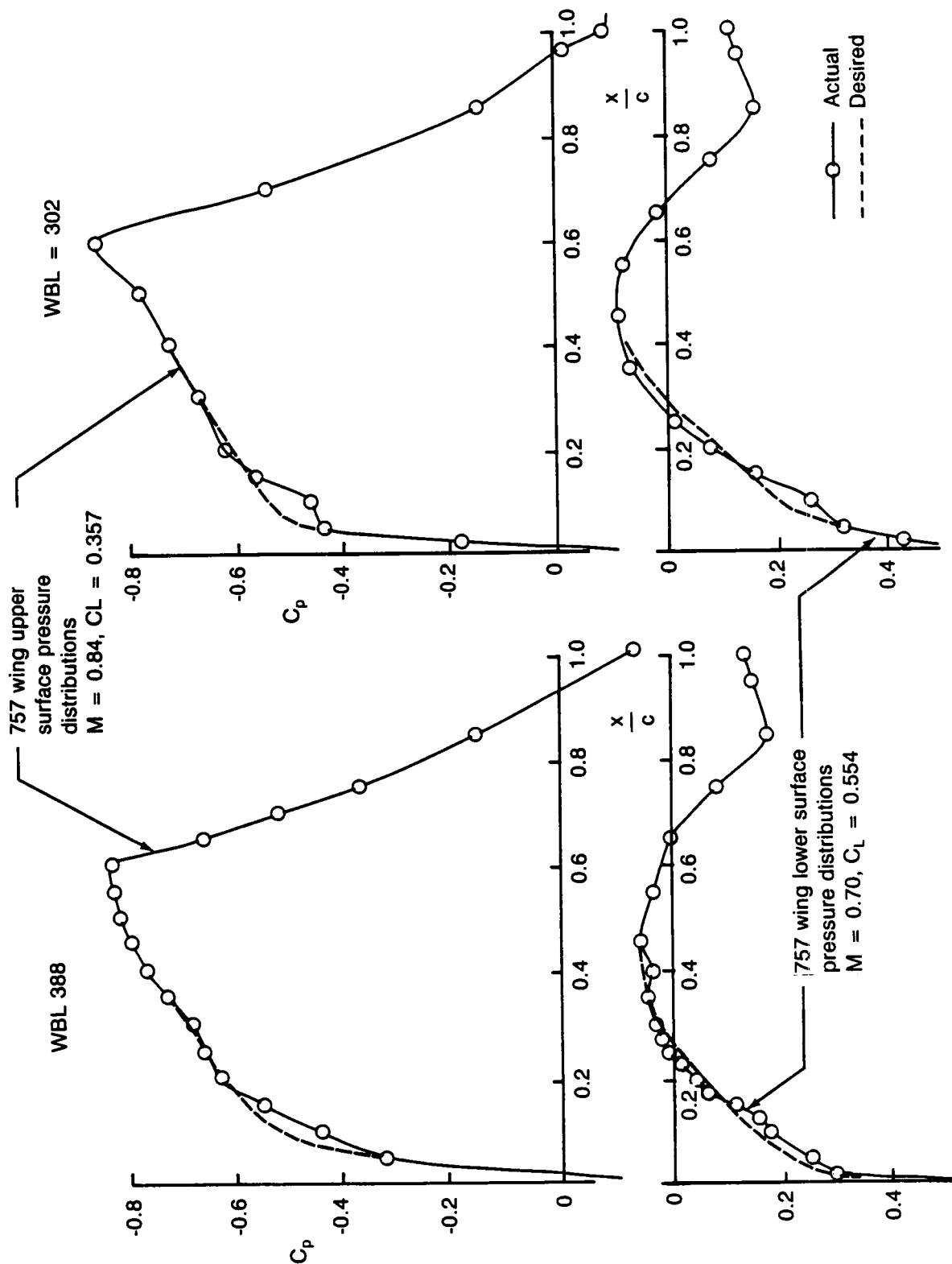


Figure 4-2. Typical 757 Wing Section Pressures

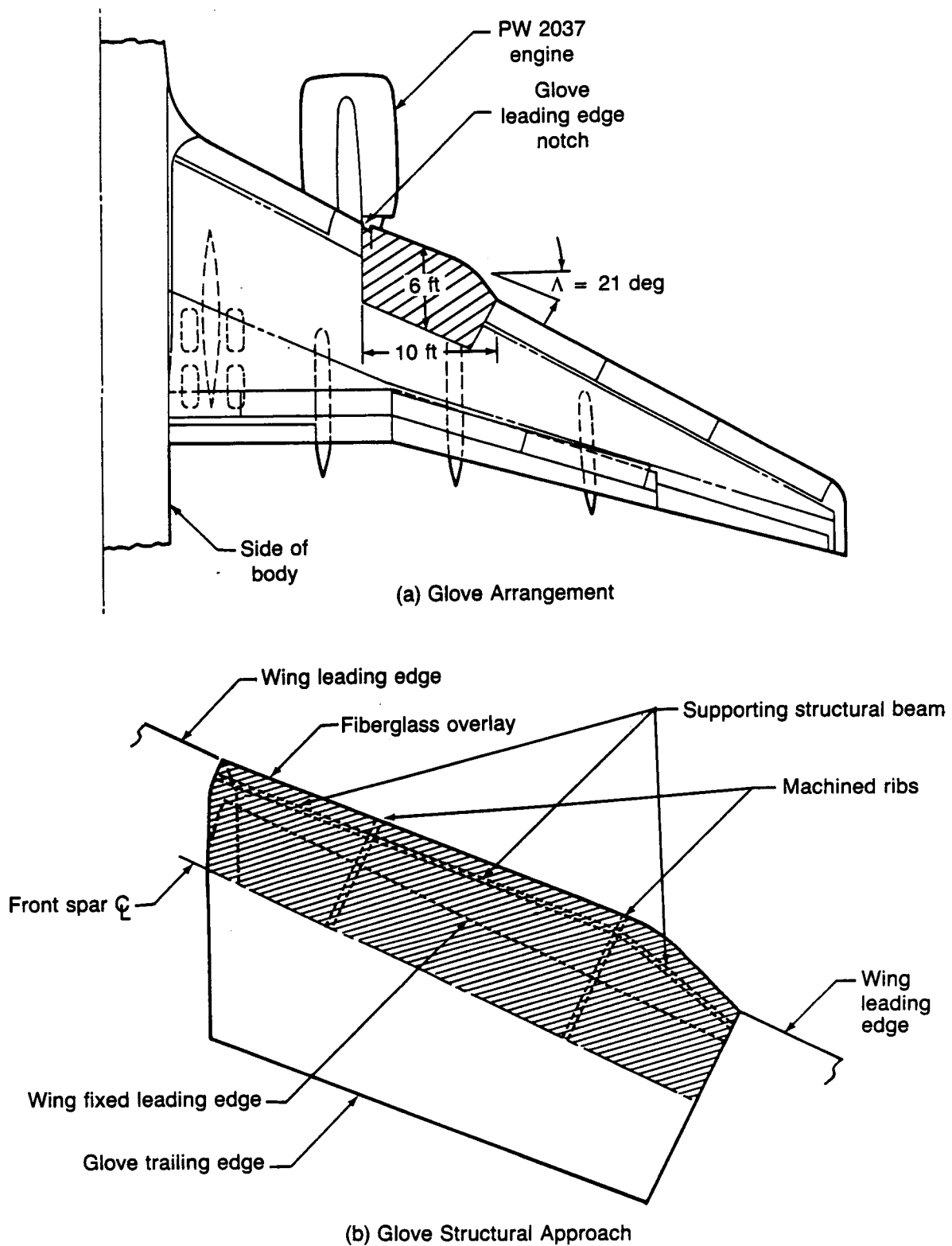


Figure 4-3. Natural Laminar Flow Glove Installation Concept

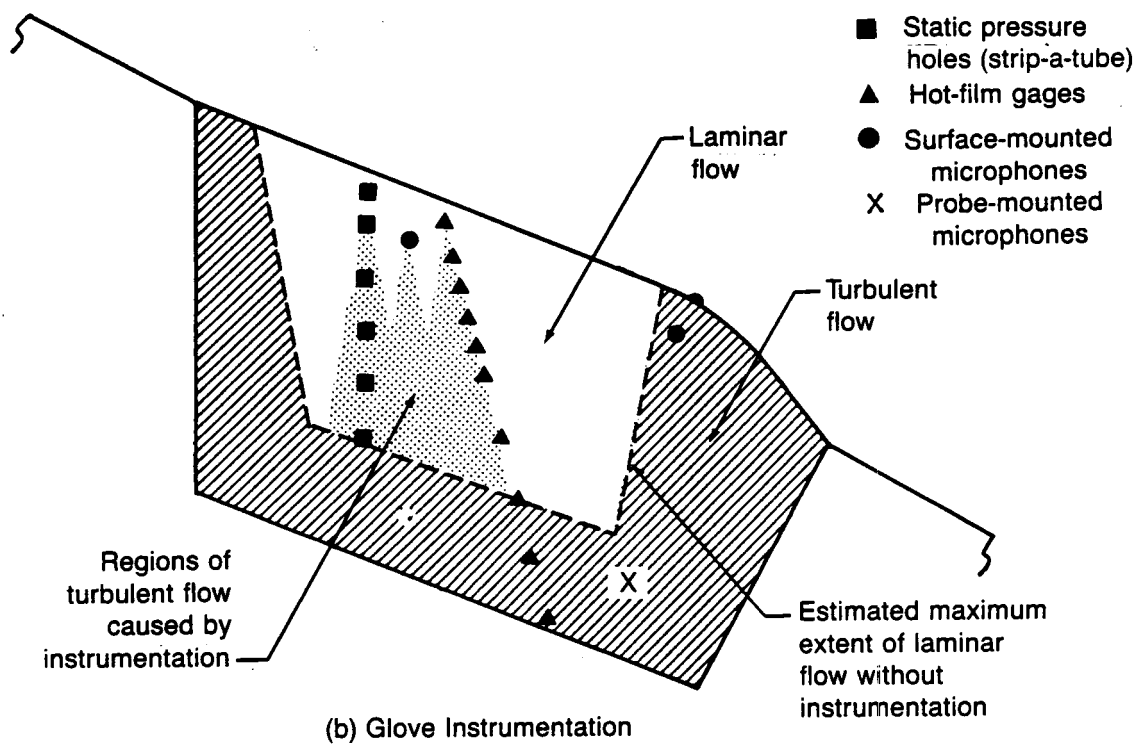
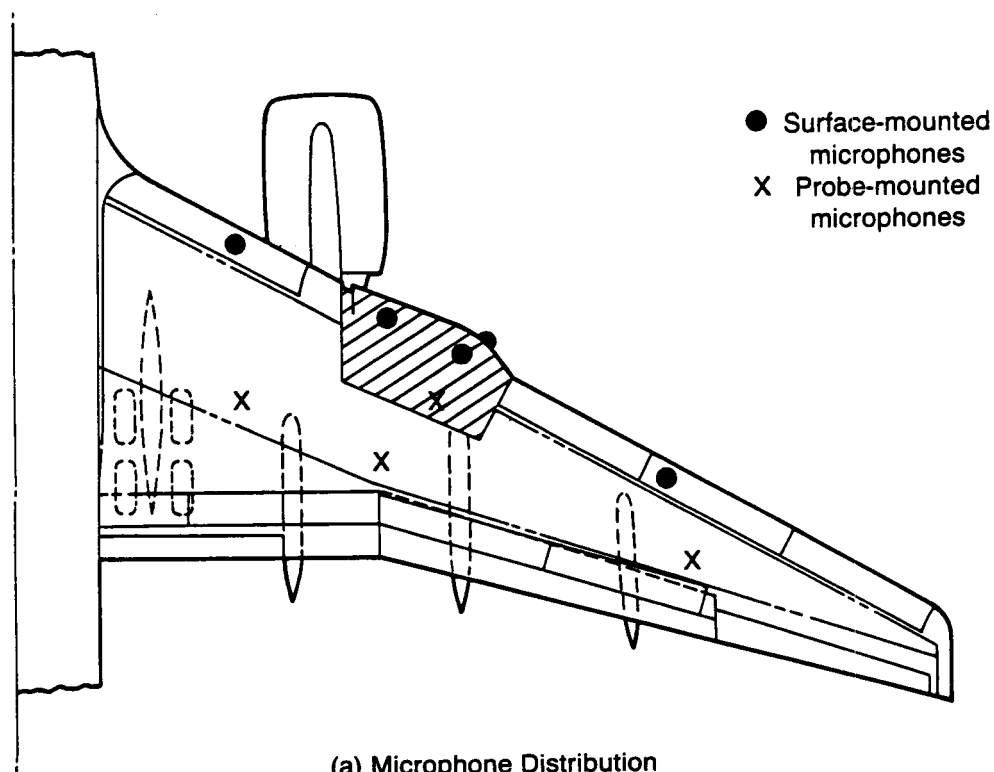


Figure 4-4. Wing Instrumentation Concept

W = 170,000 lb
S = 1951 ft²

● Basic flight conditions

Engine power varied from idle to MCT

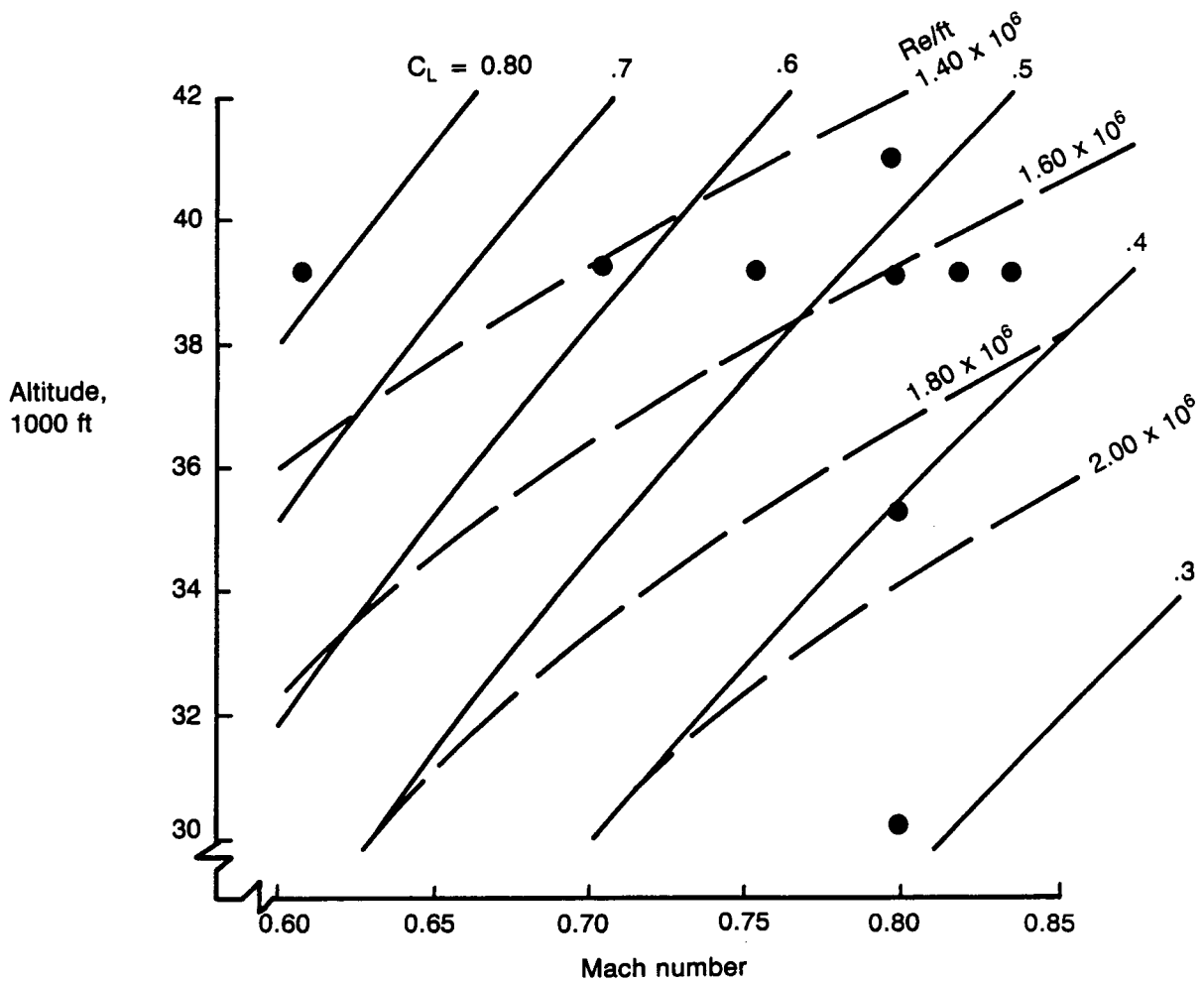


Figure 4-5. Range of Conditions for Glove Flight Test

5.0 NATURAL LAMINAR FLOW GLOVE DESIGN

5.1 AERODYNAMIC DESIGN

The objective of the 757 NLF glove design was to obtain enough natural laminar flow to allow the effect of engine noise on the extent of laminar flow to be observed. On the basis of previous experience, an appropriate objective was judged to be 3 to 4 ft. chordwise extent of laminar flow. The glove location was chosen to be immediately outboard of the no. 2 engine at slat location no. 7, as shown in Figure 5-1. This location was chosen in order to obtain maximum engine noise exposure on the glove. The glove was designed with the constraint that it have straight spanlines within the prime test region in order to facilitate its manufacture. It also was designed with the constraint that it match the existing wing at $x/c = .35$ in order to minimize the size of the glove (this constraint was relaxed slightly on the upper surface late in the design process).

Because the glove was considered to be a relatively small departure from the existing 757 wing for which both wind tunnel and flight data are available, no wind tunnel testing was considered necessary to substantiate the glove design. The availability of accurate transonic aerodynamic codes was also a factor in the decision to dispense with testing.

The extent of natural laminar flow that is obtained with a given pressure distribution is a strong function of leading edge sweep. Therefore, the leading edge sweep of the glove was made as low as possible. However several limitations were considered in arriving at the final sweep selection. As the leading edge sweep angle is reduced, the load on the outboard rib tends to become excessive due to the glove projection beyond the basic planform (see structural arrangement in fig. 5-2). Also, the airplane asymmetry increases, thereby placing possible limits on the flight envelope. At some point, the benefits of decreasing sweep become marginal so that the final selection becomes a compromise. In this case the lower limit was determined by a structural analysis of the glove, which indicated that the minimum allowable sweep was 23 deg for a 2.5-g load limit and 21 deg for a 2.0-g load limit. The 2.0-g load limit was used, allowing 21 deg to be used for the glove leading edge sweep angle.

The glove aerodynamic design was evolved using an iterative procedure with suitable computational analysis codes. The design condition was chosen to be $M = .80$, $C_L = .548$, and altitude = 41,000 ft. The high altitude was chosen in order to minimize the Reynolds number, thus favoring the maintenance of laminar flow. The Mach number and lift coefficient were chosen so that a significant extent of laminar flow could be obtained on both the upper and lower surface simultaneously. The Boeing transonic analysis code, A488G, was used to analyze each glove geometric iteration to obtain pressures and isobars. For selected design iterations, the pressure distribution at the glove midspan (WBL 325) was used in the boundary layer stability analysis procedure illustrated in Figure 5-3 to estimate the chordwise extent of laminar flow. This stability analysis procedure uses a Boeing laminar boundary layer code (A552) that computes compressible boundary layer parameters on infinite swept wings. The output from this program is used as input to the Boeing boundary layer stability code A566, which is a modified version of a program developed by Mack (ref. 8). This program solves the boundary layer stability equations for three-dimensional, linearized, parallel flow for a perfect gas and can calculate either spatial (used in this application) or temporal stability. The output from the program consists of boundary layer disturbance growth curves, such as those indicated in Figure 5-3, where A is the disturbance amplitude at a given point and A_0 is the disturbance amplitude at the neutral stability point. The quantity $\ln A/A_0$ is called the amplification factor (also N-factor).

On a high-speed swept wing there are four types of laminar boundary layer instability to be considered. These are: (1) Tollmien-Schlichting (T-S), (2) crossflow (C-F), (3) Taylor-Goertler, and (4) leading edge attachment line stability.

The T-S instability has a direction of propagation (direction of wave number vector) that is typically within 20 to 50 degrees of the local freestream direction. Amplification of T-S disturbances is small in regions of favorable pressure gradient and large in regions of adverse pressure gradient.

The typical C-F instability has wave fronts that are nearly parallel to the local freestream direction at the edge of the boundary layer. C-F in the boundary layer results from the combination of wing sweep and pressure gradient and is most severe in the wing leading edge and trailing edge regions, where pressure gradients are largest.

Taylor-Goertler instability occurs primarily in the flow over concave surfaces. Because the 757 natural laminar flow glove does not have concave surfaces in the region designed to have laminar flow, this type of instability was not considered in the glove stability analysis.

Attachment line instability is related to the behavior of the boundary layer along the forward stagnation or attachment line; i.e., the locus of points for which the chordwise velocity is zero. The boundary layer flow along the attachment line can be either laminar or turbulent depending on Reynolds number and environment, as described in Reference 9. If the attachment line flow does become turbulent, the flow over the surface downstream will be turbulent also.

Leading edge attachment line contamination differs fundamentally from T-S and C-F instabilities. The latter begin as very small disturbances that are either damped or amplified until they cause transition. However, leading edge attachment line contamination refers to the spanwise propagation along the attachment line of turbulence originating from such sources as large leading edge roughness elements or upstream turbulent sources. Such turbulence can spread both spanwise and chordwise. It has been observed experimentally that the attachment line boundary layer is usually laminar when the Reynolds number based on momentum thickness at the attachment line, $Re_{\theta_{AL}}$, is less than about 100 (ref. 9), even in the presence of a turbulent attachment line inboard, such as that which might be caused by the body boundary layer at the wing-body junction. This is because the predominately viscous effects in the attachment line boundary layer at these low Reynolds numbers suppress the formation of turbulent eddies in the boundary layer. Detailed stability calculations are not useful to assess attachment line contamination because of the strong disturbances which cause it. The boundary layer state depends primarily on $Re_{\theta_{AL}}$. In the absence of large initial disturbances, the attachment line boundary layer will remain laminar for $Re_{\theta_{AL}}$ values of 150 to 200 (ref. 9).

For each glove iteration the T-S and C-F stabilities were analyzed. T-S disturbances were followed downstream keeping wave angle and frequency fixed, with the wave angle corresponding closely to that for maximum disturbance amplification. A range of frequencies was analyzed to define a T-S disturbance envelope. C-F disturbances were followed downstream keeping the frequency fixed at zero and letting the wave angle vary in accordance with the irrotationality condition, as proposed by Mack (ref. 10). Only zero frequency (stationary) crossflow disturbances were analyzed because they are usually close to being the most highly amplified (refs. 10, 11, and 12). It is this approach for analyzing C-F disturbances that was calibrated against flight test data in a previous study (ref. 13). The data was obtained on an NLF wing glove installed on an F-111 airplane. Figure 5-4 illustrates the results of that calibration. The data points in the figure show calculated T-S and C-F amplification factors (N-factors) at the measured transition location for a number of different flight conditions and sweep angles on the upper surface of the F-111 glove. Taken together these data can be used as transition criteria for situations similar to those experienced on the F-111 aircraft.

In the design of the 757 glove, N-factors were calculated as a function of chordwise position and the results superimposed on Figure 5-4. The transition location for a given design iteration was then judged to be within the range where the N-factor trajectory penetrated the F-111 data band. The boundary layer stability results for the final glove design at the design condition on the upper surface are shown in Figure 5-5. The pressure distribution at WBL 325, which is near the glove midspan, and the upper surface isobars are shown in the upper part of the figure. It can be seen that the isobar sweep is about 21 deg near the glove leading edge and increases significantly further back, where the basic wing tends to dominate the pressures. Since the laminar boundary layer code produces precise results only for infinite yawed wings, which corresponds to constant isobar sweep, the stability analysis was carried out for two separate regions and the solutions were then patched together. A sweep angle of 21 deg was used from $s/c = 0$ to $s/c = .06$, and a sweep angle of 29 deg was used from $s/c = .06$ to $s/c = .40$. The C-F and T-S

disturbance amplification curves are shown in the lower left of the figure. It can be seen that from the leading edge to $s/c = .05$, the C-F disturbances grow very rapidly because of the large pressure gradients, and T-S disturbances do not grow at all, because the large favorable pressure gradients are stabilizing for T-S disturbances. The decrease in pressure gradient between $s/c = .05$ and $s/c = .20$ results in a decrease of C-F disturbance growth rate and an increase in T-S disturbance growth rate. Aft of $s/c = .20$, the higher pressure gradient again increases the C-F growth rate while it tends to damp out the T-S disturbances. The trajectory curve of the combined T-S and C-F disturbances in the N_{TS} vs. N_{CF} plane is shown in the lower right of the figure. It is apparent that the transition criteria band is nearly penetrated at $s/c = .20$ before the curve moves away from the band. The transition criteria band is actually penetrated at $s/c = .36$ on the lower side and $s/c = .39$ on the upper side, indicating that transition would be expected to occur somewhere between these values. However, it should be recognized that the criteria are not precise and that variations from assumed conditions such as might occur in the actual glove pressure distributions could result in the criteria band being penetrated near $s/c = .20$. However, this would still meet the design objective of 3 to 4 ft of laminar flow, so the upper surface design was judged to be satisfactory.

The boundary layer stability analysis results for the lower surface at the design condition are shown in Figure 5-6 on the basis stated above. They indicate that transition should be expected somewhere between $s/c = .23$ and $s/c = .29$.

Stability analyses were also carried out for selected off-design conditions. Figure 5-7 shows results for the upper surface at the off-design condition of $M = .84$, $C_L = .420$. Transition is predicted to occur somewhere between $s/c = .23$ and $s/c = .28$. A comparison of the results at this condition with those at the design condition, shown in Figure 5-5, shows that the effect of the higher Mach number is to eliminate the "flattening" of the pressure distribution between $s/c = .05$ and $s/c = .20$, resulting in increased C-F disturbance growth and decreased T-S disturbance growth. Although the expected transition point is not significantly different from that predicted for the design case, the C-F mode rather than the T-S mode appears to be more critical and thus more likely to cause transition.

For the lower surface, the results of a stability analysis for the off-design condition, $M = .70$ and $C_L = .522$ are shown in Figure 5-8. Transition is predicted somewhere between $s/c = .23$ and $s/c = .26$. A comparison with the stability results for the design condition in Figure 5-6 shows that the C-F disturbances are more highly amplified and the T-S disturbances are less highly amplified at this condition. The results in this comparison are quite similar to those for the upper surface, which were discussed previously.

5.2 ATTACHMENT LINE STABILITY

The attachment line stability parameter on the final glove iteration and on the wing at the design condition is shown in Figure 5-9. As previously pointed out, when the Reynolds number based on momentum thickness at the attachment line $Re_{\theta_{AL}}$ is less than 100, the attachment line boundary layer will usually be laminar, even if the boundary layer is initially turbulent on the wing just inboard of the glove. The figure shows that $Re_{\theta_{AL}}$ varies from about 65 at the inboard edge of the glove to 130 at the outboard edge. Thus, the attachment line boundary layer was expected to be laminar over the entire span of the glove, since as the laminar boundary layer inboard propagates into the region where $Re_{\theta_{AL}}$ is greater than 100 it will tend to remain laminar. If the high $Re_{\theta_{AL}}$ values had occurred inboard, it would have been unacceptable, since an initially turbulent boundary layer coming from the basic wing leading edge would remain turbulent until $Re_{\theta_{AL}}$ dropped below 100.

5.3 FINAL GLOVE GEOMETRY

To facilitate installation and finishing of the glove, the new surface was designed to have straight span lines between WBL 296.3 and WBL 355.7. A further constraint required that the glove fair smoothly into the basic wing at about $s/c = .35$ on both upper and lower surfaces. Since the glove was

considered to be a modest departure from the basic wing for which detailed aerodynamic information was already available, it was decided to proceed with glove definition without wind tunnel testing to validate the design. The availability of sophisticated transonic aerodynamic analysis codes with which considerable experience has been accumulated, provided further confidence that a satisfactory design could be developed within the above constraints. With the planform defined (see fig. 5-10) and the objective pressure distributions established, the iterative technique previously mentioned was used to create candidate designs. The final glove geometry was selected for compatibility with design objectives and the ability to accommodate a substantial range of off-design conditions. Chordwise cuts of the selected glove are shown for five locations in relation to the existing 757 wing in Figure 5-11. The forward chordwise extension is the most obvious feature and is brought about by the reduced sweep of the glove. Coordinates of the glove sections at the two control stations are given in Table 5-1.

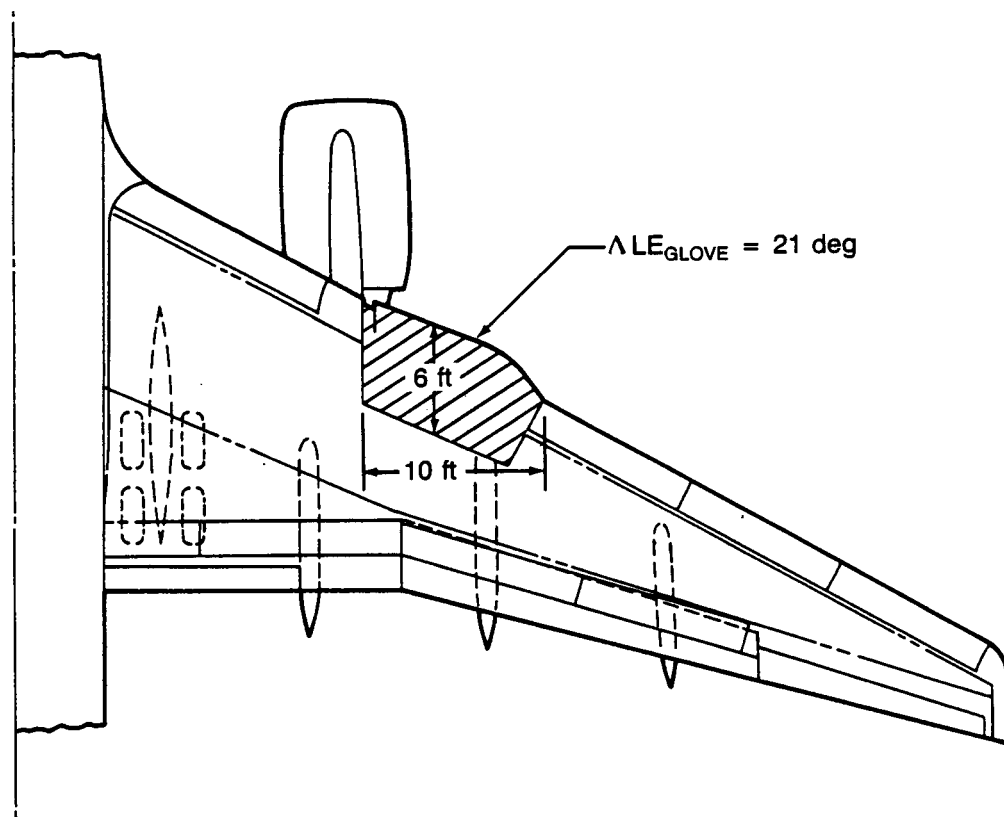
Even though the attachment line stability parameter variation on the glove was well within the acceptable range, a leading edge notch was incorporated in the glove design at the inboard end. This was provided as an additional safety factor since the severity of disturbances at the strut-wing intersection were unknown. The primary purpose of the notch was to prevent turbulence from the leading edge of the basic wing on the engine strut from propagating onto the glove leading edge. The geometry was chosen with the objective of starting a new attachment line boundary layer at the outboard edge of the notch and diverting the flow rearward from the strut wing intersection area. Figure 5-12 shows the notch details in plan view. It is about 3 in deep (in the chordwise direction) and 7 in wide at the leading edge. Particular attention is given to avoiding sharp corners on the outboard portions of the notch in order to smooth transition to the new stagnation area near points 4 and 5. Streamwise surface extensions from the circular arc traces are gently and smoothly faired to blend with the airfoil contour on both upper and lower glove surfaces about 18 in behind the leading edge.

5.4 TRANSONIC ANALYSIS RESULTS

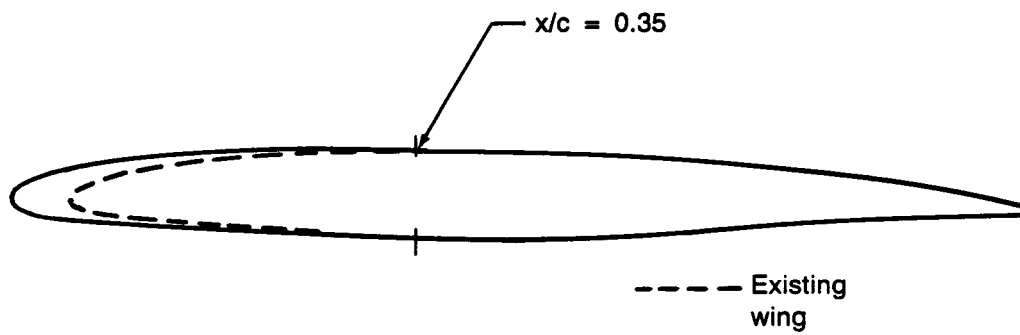
The final glove design was analyzed at 13 different conditions corresponding to Mach number and lift combinations covering the expected flight envelope. Table 5-2 lists these conditions and summarizes some of the important characteristics of the upper surface pressure distributions and isobars. Table 5-3 shows a similar summary for the lower surface. Figures 5-13 through 5-25 show pressure distributions and isobars determined from the transonic code analysis for each of the 13 conditions. Taken as a whole, the pressure distributions generally meet the design objectives set forth originally. The gradients are appropriate for the maintenance of laminar flow, particularly in the midspan region that comprises the critical test area. The spanwise variations do not appear large but do produce a generally increasing isobar sweep behind the leading edge, which reflects the influence of the basic wing geometry. Since the most critical area is in the immediate vicinity of the leading edge, the isobar pattern was judged to be acceptable. This was confirmed by the results of the boundary layer stability analysis for the appropriate range of cruise conditions.

Figure 5-26 summarizes the pressure distribution data for the glove midspan portion (WBL 325) for 12 of the 13 cases. The results show the expected trends for both Mach number and C_L variations. Examination indicates that they will be compatible with significant areas of NLF for a range of off-design conditions.

Figure 5-27 shows upper surface and lower surface streamlines at the design condition. The upper part of the figure exhibits the streamline pattern on the glove surface whereas the lower part of the figure shows conditions at the edge of the boundary layer. The differences are significant and must be considered in determining the instrumentation array used to define the extent of laminar flow. In general the streamline pattern is used to establish the approximate locations of the disturbance wedges emanating from each sensor. In each case the most critical streamline pattern was used depending on the specific sensor pair involved and a margin was provided to compensate for deficiencies in the calculation procedures as well as for off-design operation.



757 Wing Planform



Typical Glove Section

Figure 5-1. 757 Natural Laminar Flow Glove Concept

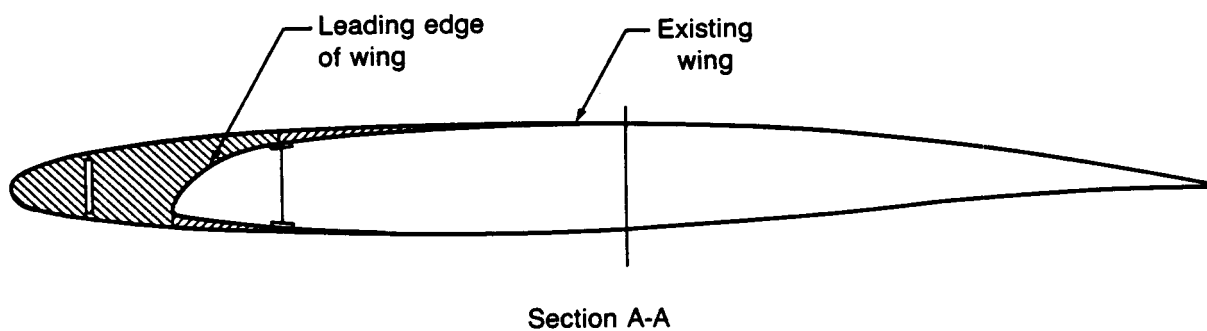
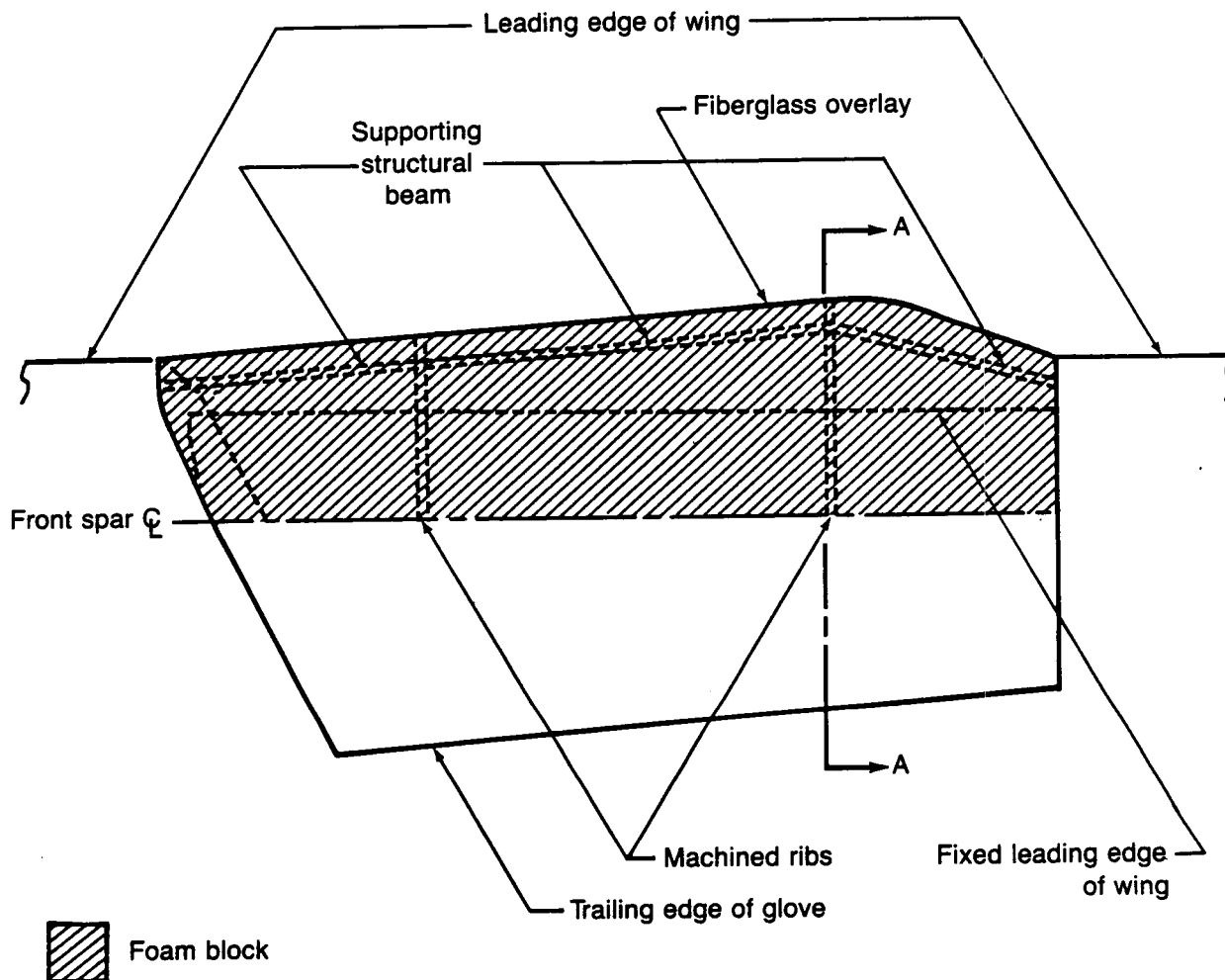
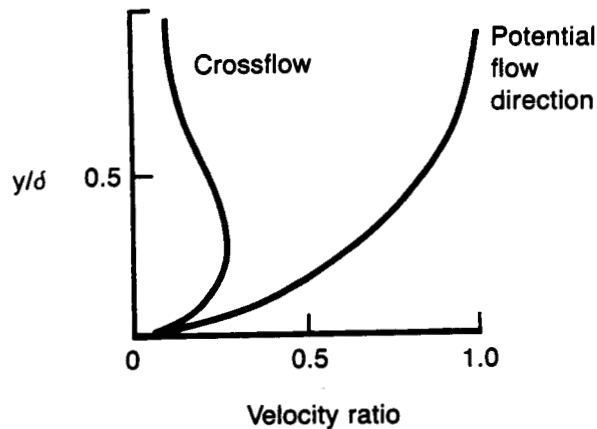


Figure 5-2. 757 Natural Laminar Flow Glove Arrangement

- Boeing laminar boundary layer code
 - Infinite swept wing
 - Compressible



Boundary layer
velocity profiles



- Modified MACK stability code (Boeing)
 - Spatial or temporal stability
 - Compressible or incompressible



Boundary layer
stability analysis

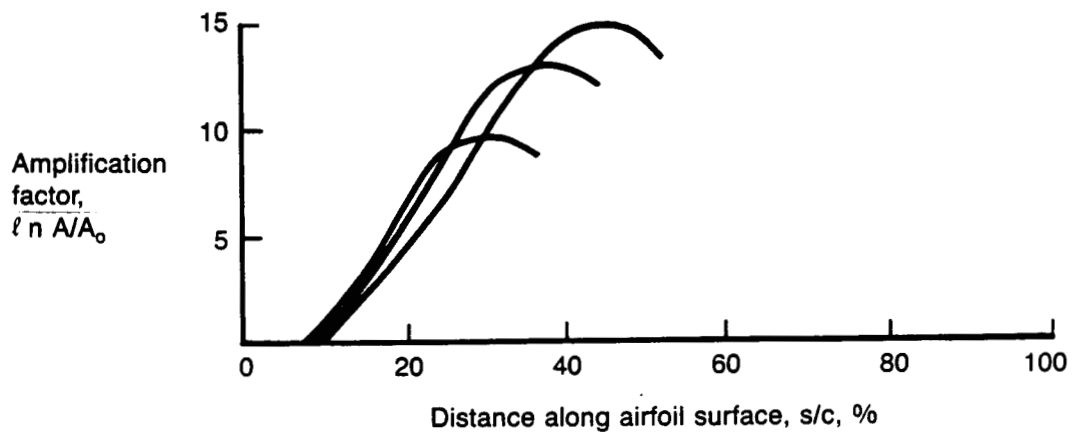


Figure 5-3 Disturbance Growth Analysis for Laminar Boundary Layers

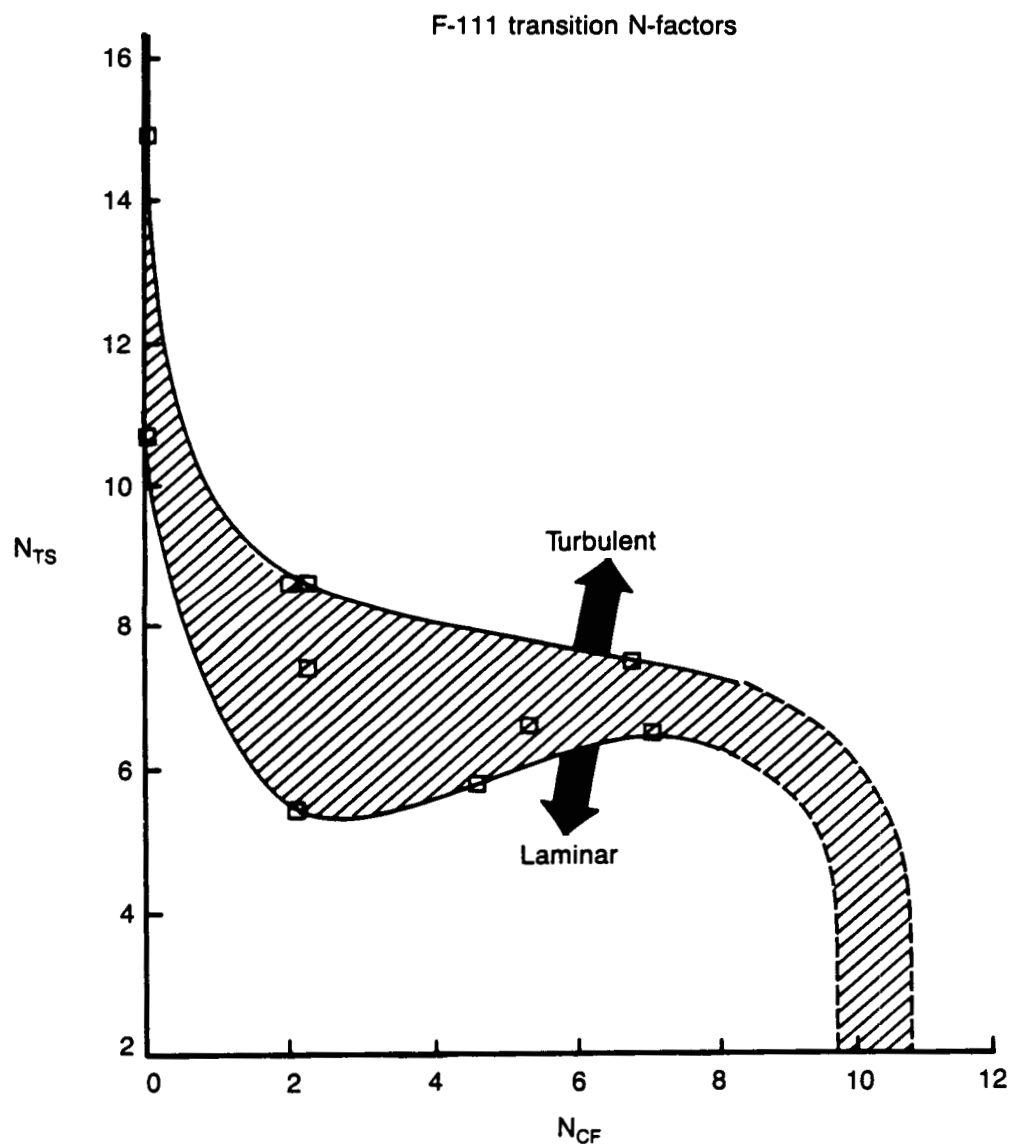


Figure 5-4. Transition Criteria for Laminar Boundary Layers

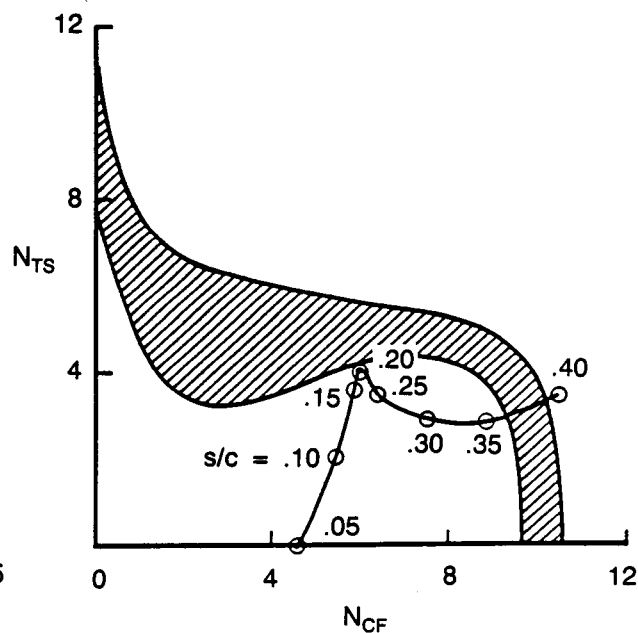
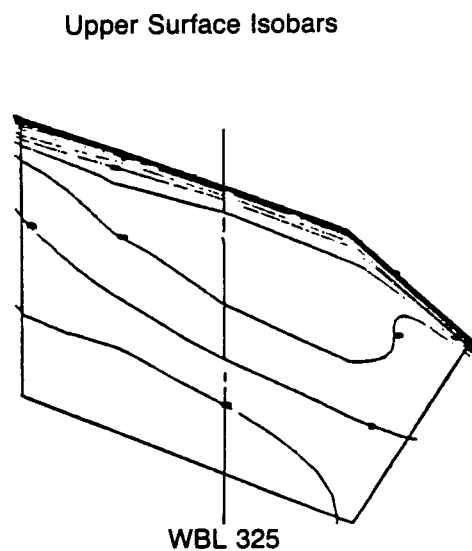
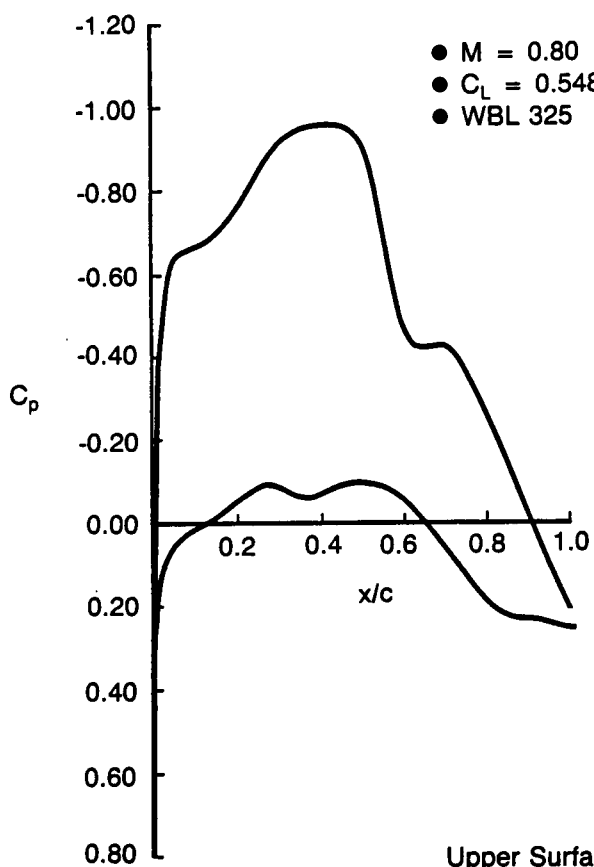
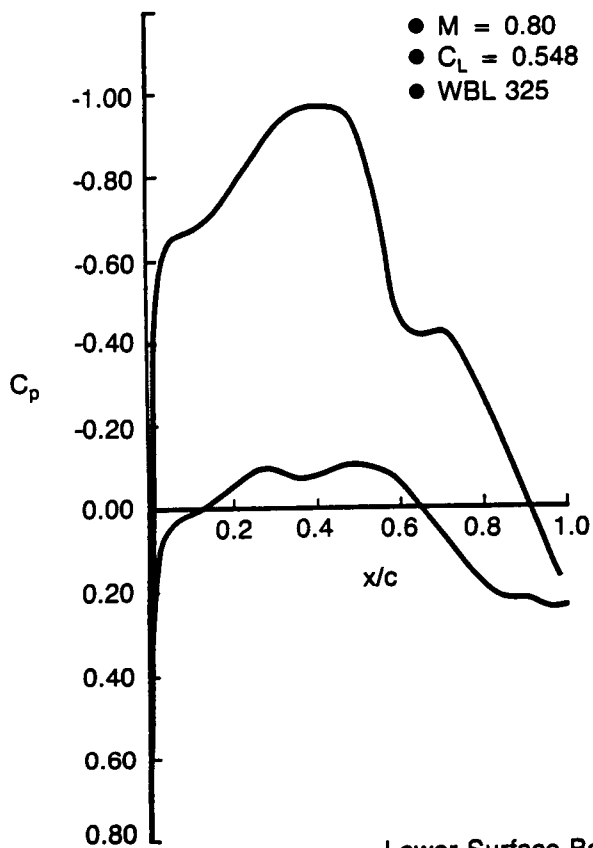
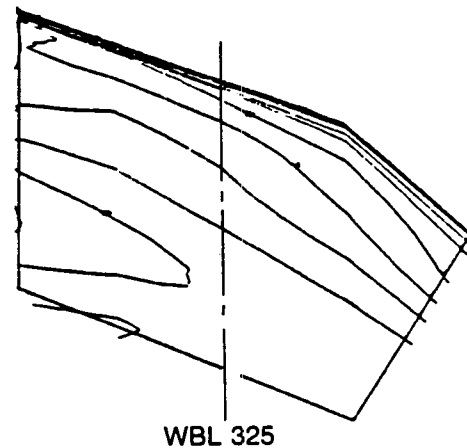


Figure 5-5. Boundary Layer Transition Analysis for Glove Upper Surface, $M = 0.80$, $C_L = 0.548$



Lower Surface Isobars



Lower Surface Boundary Layer Stability

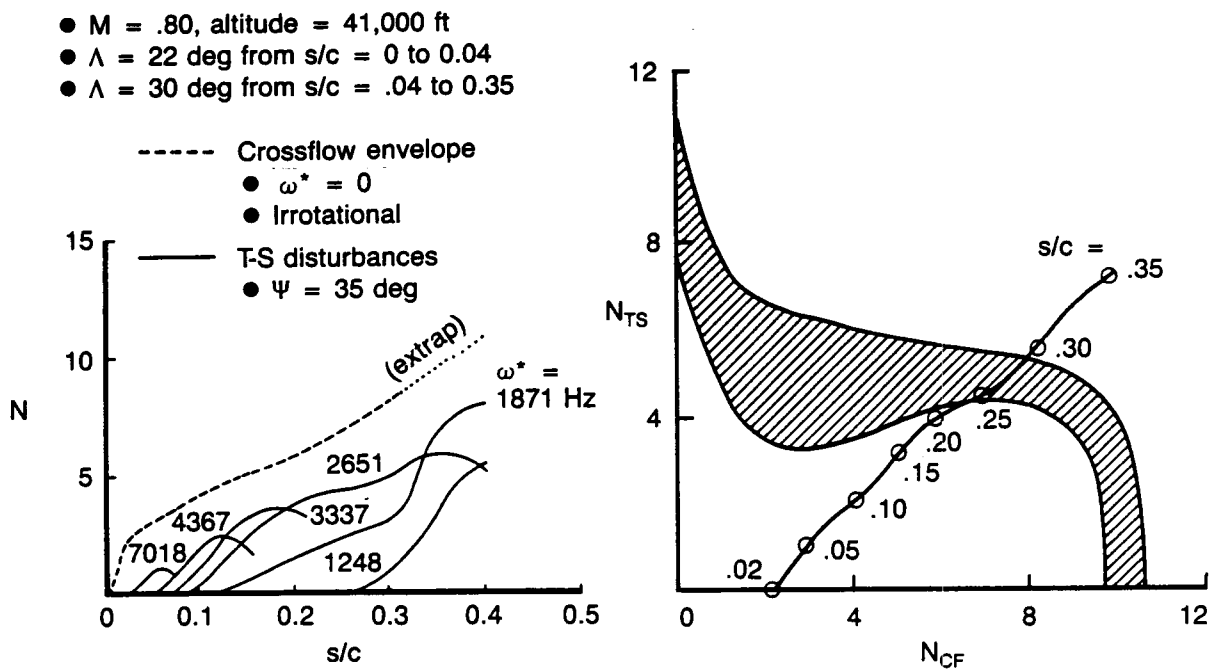


Figure 5-6. Boundary Layer Transition Analysis for Glove Lower Surface, $M = 0.80$, $C_L = 0.548$

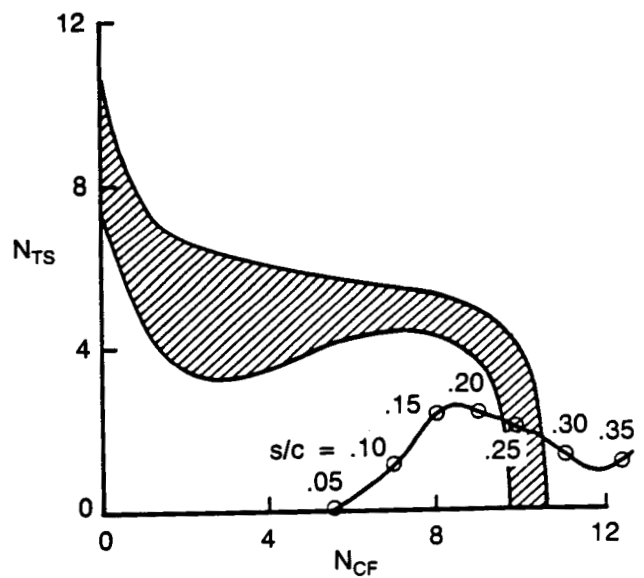
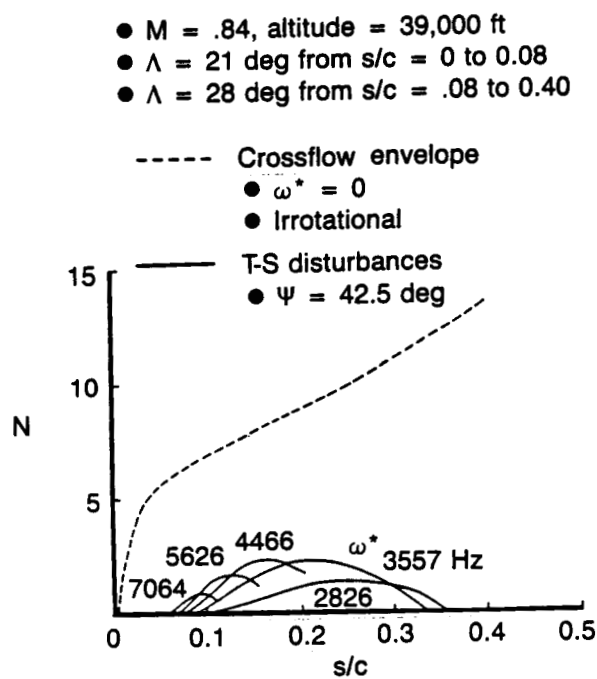
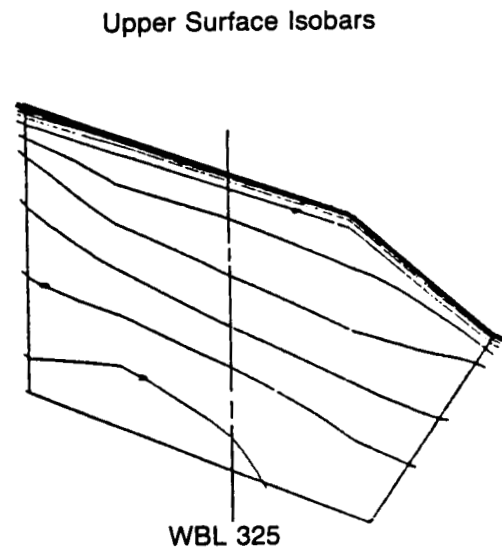
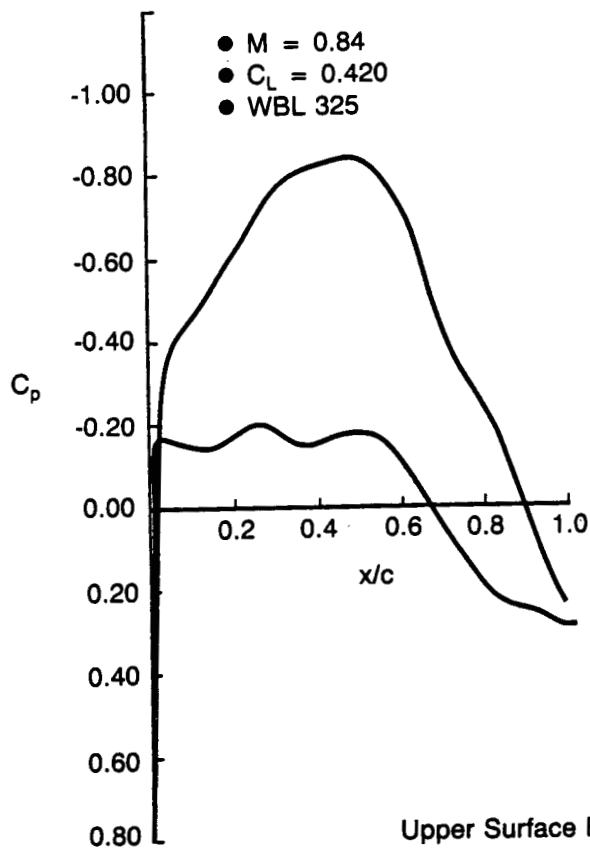


Figure 5-7. Boundary Layer Transition Analysis for Glove Upper Surface, $M = 0.84$, $C_L = 0.420$

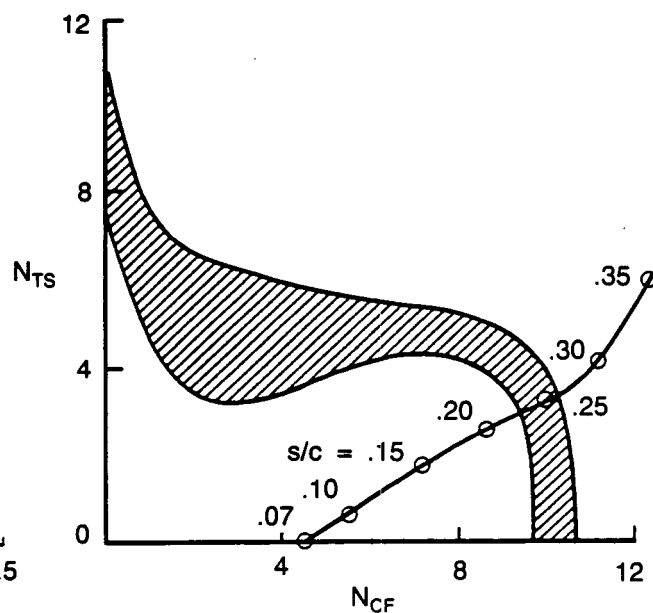
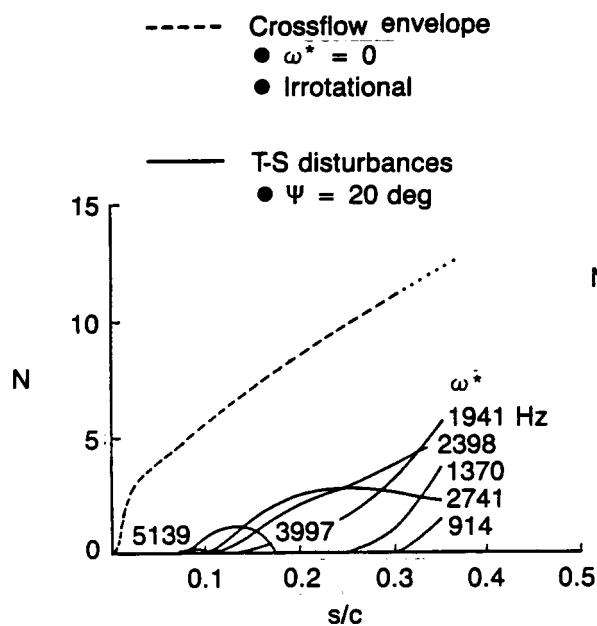
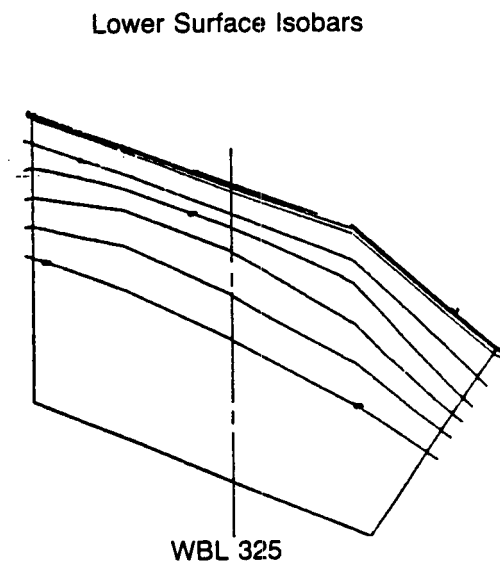
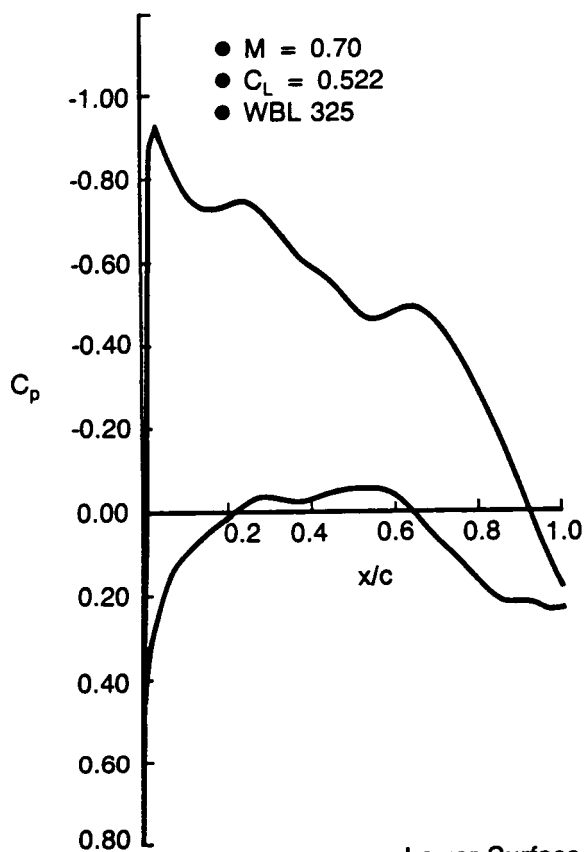


Figure 5-8. Boundary Layer Transition Analysis for Glove Lower Surface, $M = 0.70$, $C_L = 0.522$

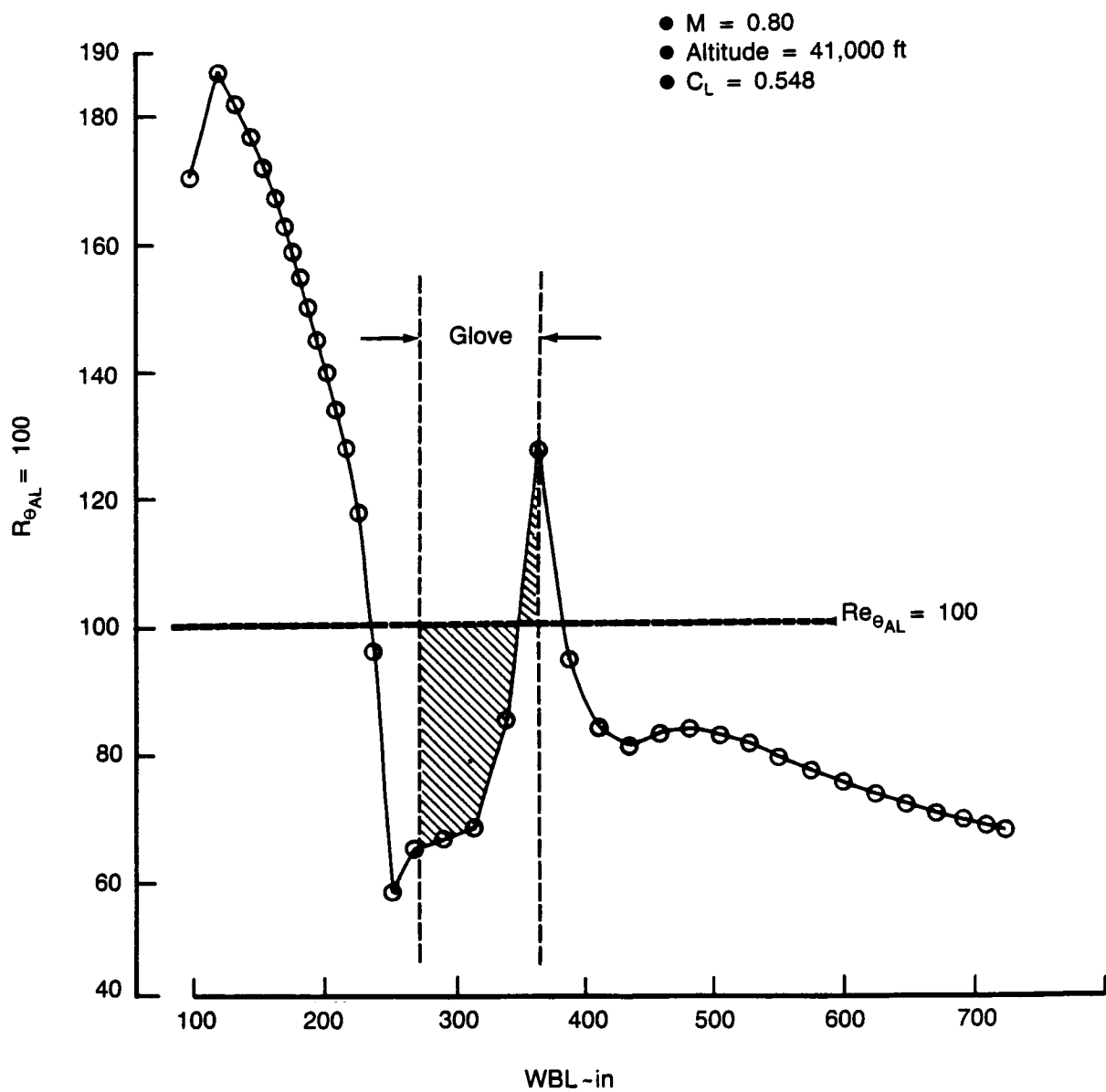


Figure 5-9. Attachment Line Momentum Thickness Reynolds Number vs. Span

Key coordinates and dimensions

Station	WBL (in)	X _{LE} (in) Glove	X _{TE} (in) Wing	C (in)
1	268.9	148.00	360.85	215.87
2	276.0	147.71	360.85	213.14
3	300.0	156.92	360.85	203.93
4	355.7	178.30	374.65	197.35
5	369.83	188.52	378.15	189.63
6	385.7	207.95	382.08	174.13

Note: Wing apex is at X = 0, WBL = 0

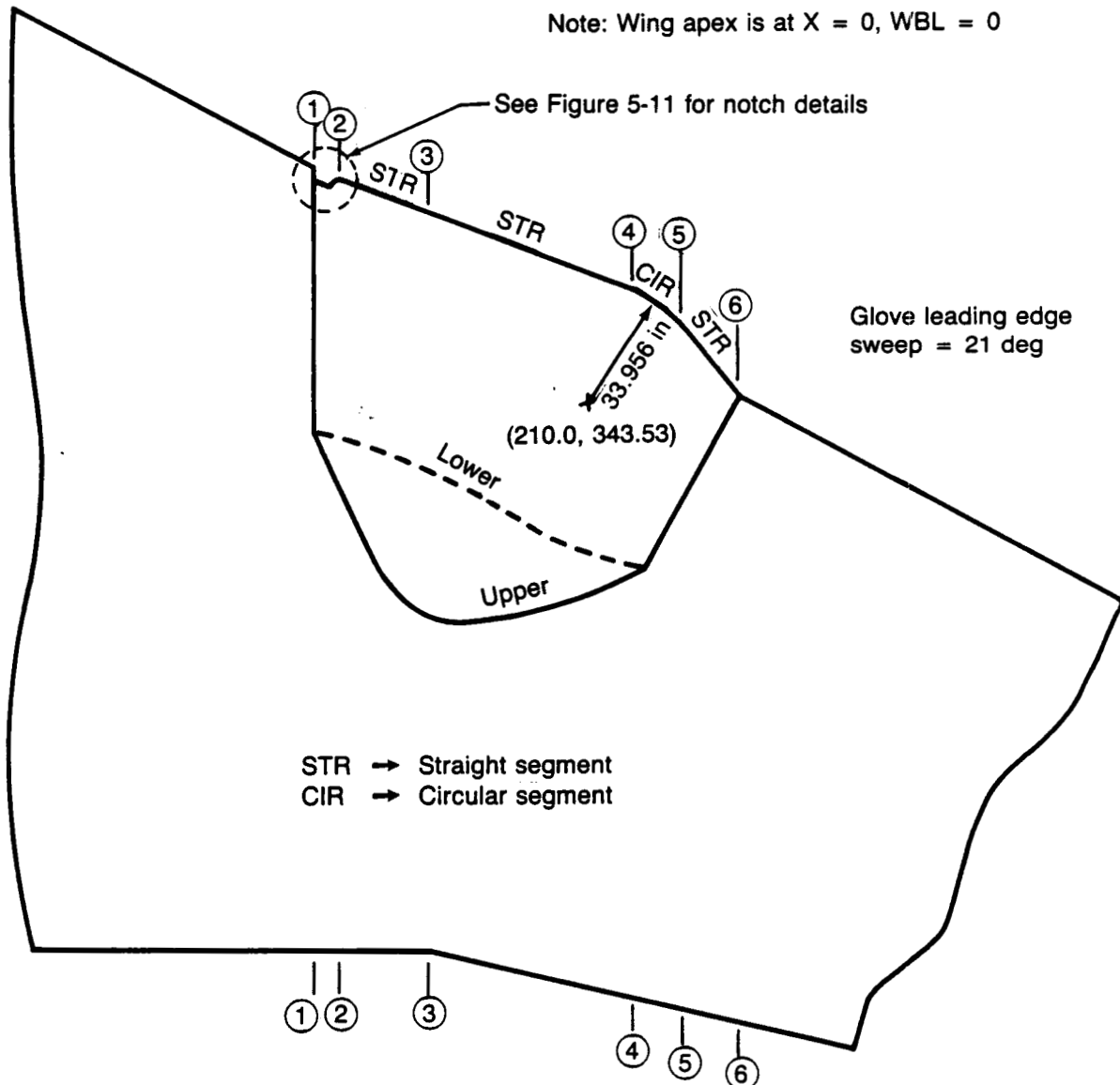


Figure 5-10. 757 Glove Planform Definition

Table 5-1. 757 Glove Airfoil Coordinates

WBL 296.3				WBL 355.7			
Upper		Lower		Upper		Lower	
$x-x_{LE}(in)$	$z(in)$	$x-x_{LE}(in)$	$z(in)$	$x-x_{LE}(in)$	$z(in)$	$x-x_{LE}(in)$	$z(in)$
0.0	2.259	0.0	2.259	0.0	1.843	0.0	1.843
0.066	2.714	0.066	1.800	0.064	2.434	0.064	1.297
0.131	2.901	0.131	1.609	0.127	2.686	0.127	1.085
0.262	3.163	0.262	1.342	0.254	3.039	0.254	0.800
0.524	3.527	0.524	0.975	0.509	3.521	0.508	0.423
0.916	3.920	0.916	0.596	0.890	4.020	0.890	0.046
1.309	4.224	1.309	0.319	1.271	4.393	1.271	-0.229
1.963	4.628	1.963	-0.017	1.906	4.874	1.906	-0.569
2.618	4.955	2.618	-0.268	2.541	5.254	2.541	-0.827
3.926	5.484	3.926	-0.657	3.812	5.849	3.811	-1.218
6.543	6.316	6.543	-1.290	6.352	6.706	6.352	-1.786
9.160	7.017	9.160	-1.849	8.893	7.344	8.892	-2.237
13.086	7.921	13.086	-2.580	12.703	8.086	12.703	-2.796
17.012	8.708	17.011	-3.213	16.514	8.658	16.513	-3.235
20.937	9.429	20.937	-3.770	20.324	9.120	20.323	-3.608
26.171	10.310	26.171	-4.416	25.405	9.629	25.404	-4.041
32.714	11.276	32.713	-5.118	31.756	10.140	31.755	-4.509
39.256	12.112	39.255	-5.723	38.106	10.535	38.106	-4.909
52.341	13.348	52.340	-6.635	50.808	11.008	50.807	-5.486
65.426	13.853	65.424	-6.922	63.509	11.137	63.508	-5.759
78.510	13.806	78.509	-6.937	76.210	11.086	76.209	-5.771
91.594	13.222	91.593	-6.816	88.911	11.043	88.910	-5.675
94.211	13.041	94.210	-6.745	91.452	11.034	91.451	-5.644
96.828	12.843	96.827	-6.660	93.992	11.023	93.991	-5.612
99.445	12.635	99.444	-6.561	96.532	11.006	96.531	-5.573
102.062	12.423	102.061	-6.451	99.072	10.979	99.071	-5.521

Note: Airfoils are defined only to approximate end of glove

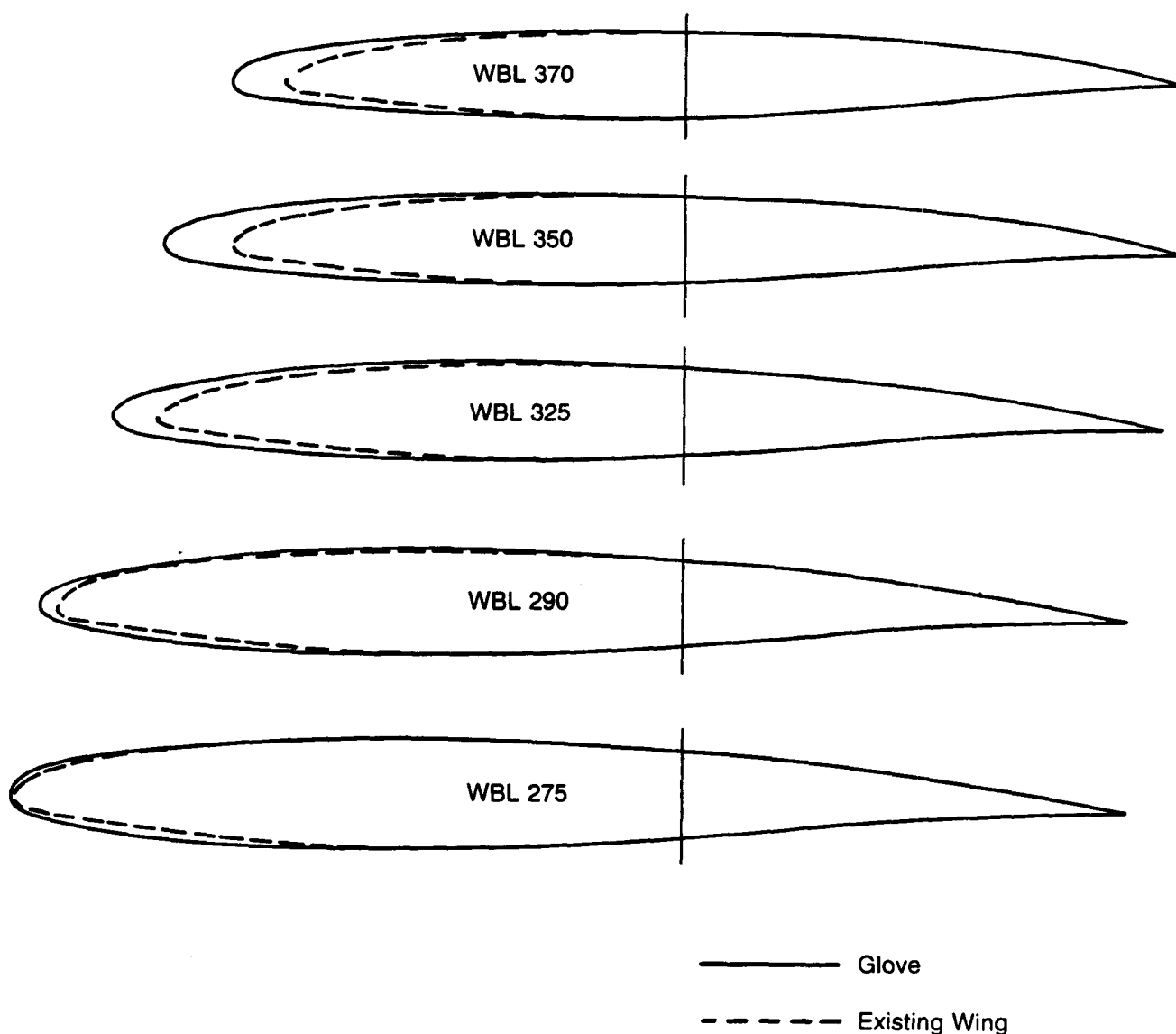


Figure 5-11. Airfoil Sections for 757 Glove

Point	WBL (in)	x (in)
A	272.57	148.10
B	275.50	149.00
1	268.90	148.00
2	272.11	149.26
3	273.40	149.03
4	274.58	147.97
5	276.00	147.71
6	300.00	156.92

Note: Wing apex is at X = 0, WBL = 0

STR → Straight Segment

CIR → Circular Segment

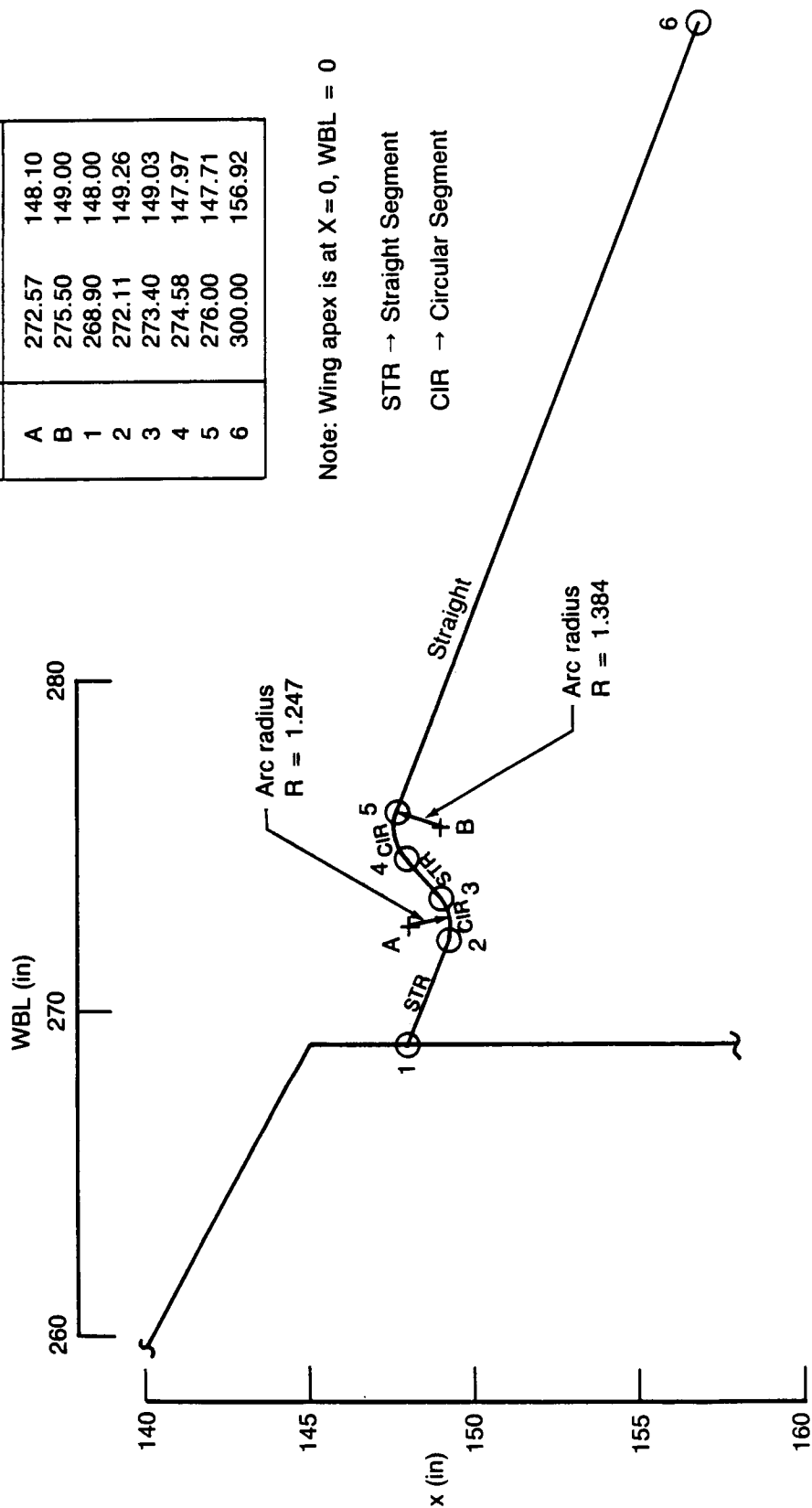


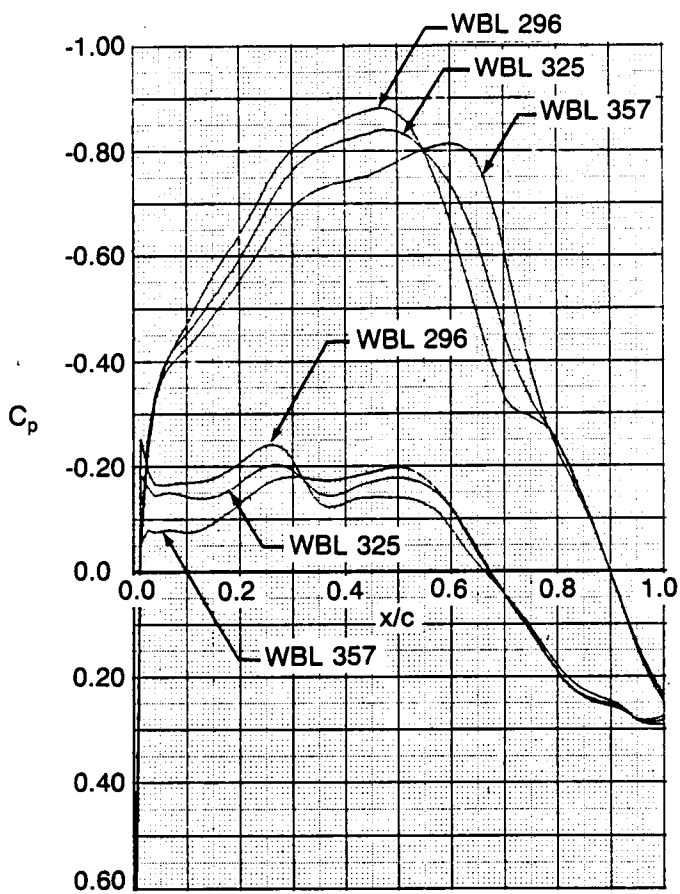
Figure 5-12. 757 Glove Notch Geometry

Table 5-2. Aerodynamic Analysis Results Summary — Glove Upper Surface

Case	M	α	C_L	WBL 325 d C_p/d x/c	$C_{P_{MIN}}$	Peakiness (1-10) (10 = Very Peaky)	Isobar Sweep (Deg)	Rating (1-10) (1 = Best)
SS	.84	1.30	.420	- 1.55	-.84	2	21 - 28	3
VV	.84	0.80	.345	- 1.60	-.78	1	21 - 28	3
YY	.82	1.90	.452	- 1.35	-.89	3	21 - 29	4
TT	.82	1.40	.388	- 1.43	-.82	2	21 - 29	4
OO	.80	2.96	.548	- 1.11	-.96	4	21 - 29	4
PP	.80	2.00	.436	- 1.22	-.87	3	21 - 30	5
QQ	.80	1.52	.381	- 1.30	-.80	2	21 - 29	4
AB	.80	0.27	.243	- 1.46	-.60	1	21 - 28	3
ZZ	.78	2.50	.473	- .95	-.89	7	21 - 31	6
XX	.75	3.00	.503	- .31	-.83	9	21 - 35	7
RR	.75	2.00	.399	- .58	-.69	8	21 - 35	7
WW	.70	3.50	.522	+ 1.15	-.95	10	—	—
UU	.70	2.60	.433	+ .25	-.69	10	—	—

Table 5-3. Aerodynamic Analysis Results Summary — Glove Lower Surface

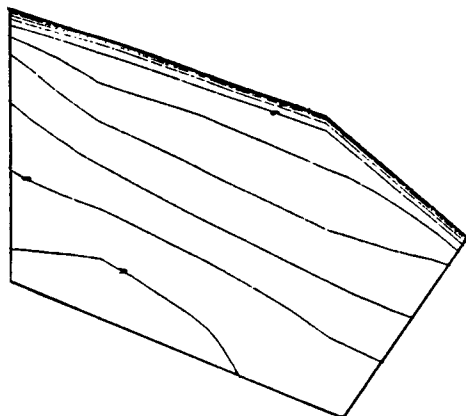
Case	M	α	C_L	WBL 325 d C_p/d x/c	$C_{P_{MIN}}$	Peakiness (1-10) (10 = Very Peaky)	Isobar Sweep (Deg)	Rating (1-10) (1 = Best)
SS	.84	1.30	.420	- .09	-.21	8	—	—
VV	.84	0.80	.345	+ .31	-.31	10	—	—
YY	.82	1.90	.452	- .51	-.16	4	23 - 37	9
TT	.82	1.40	.388	- .21	-.19	6	23 - 37	9
OO	.80	2.96	.548	- .63	-.09	1	22 - 32	6
PP	.80	2.00	.436	- .49	-.14	3	23 - 35	8
QQ	.80	1.52	.381	- .34	-.17	6	23 - 39	9
ZZ	.78	2.50	.473	- .63	-.11	1	22 - 33	7
XX	.75	3.00	.503	- .73	-.08	1	22 - 30	4
RR	.75	2.00	.399	- .52	-.13	1	23 - 35	8
WW	.70	3.50	.522	- .82	-.04	1	21 - 28	3
UU	.70	2.60	.433	- .64	-.09	1	22 - 31	5



- $M = 0.84$
- $C_L = 0.420$
- $\alpha = 1.30$
- Inviscid

Isobars

Upper



Lower

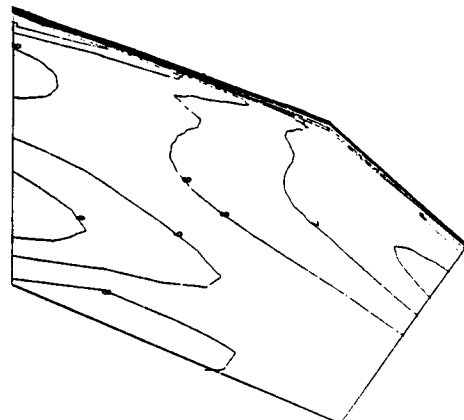
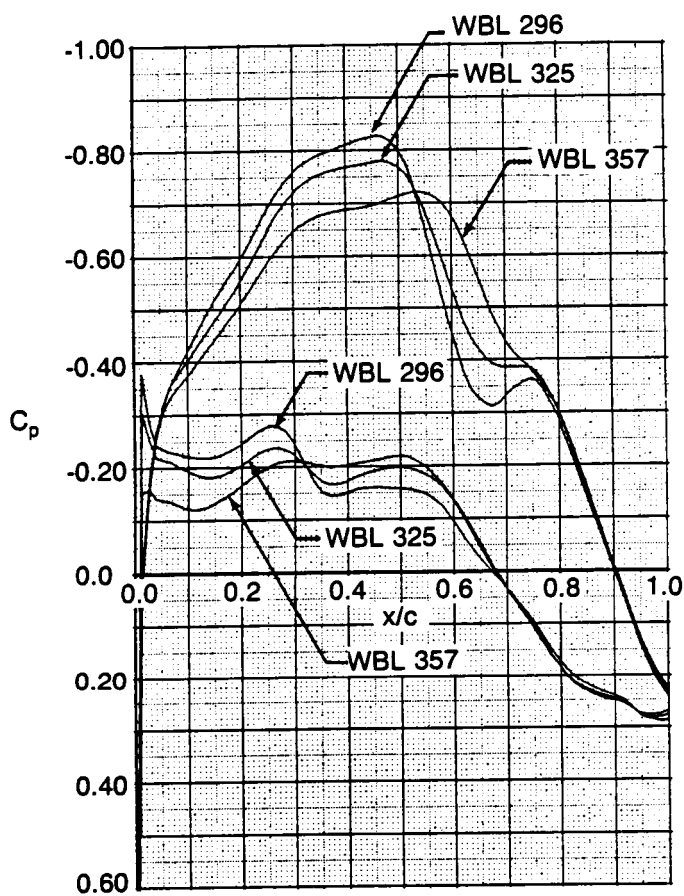


Figure 5-13. Theoretical Glove Pressure Distribution—Case SS, $M = 0.84$, $C_L 0.420$



- $M = 0.84$
- $C_L = 0.345$
- $\alpha = .80 \text{ deg}$
- Inviscid

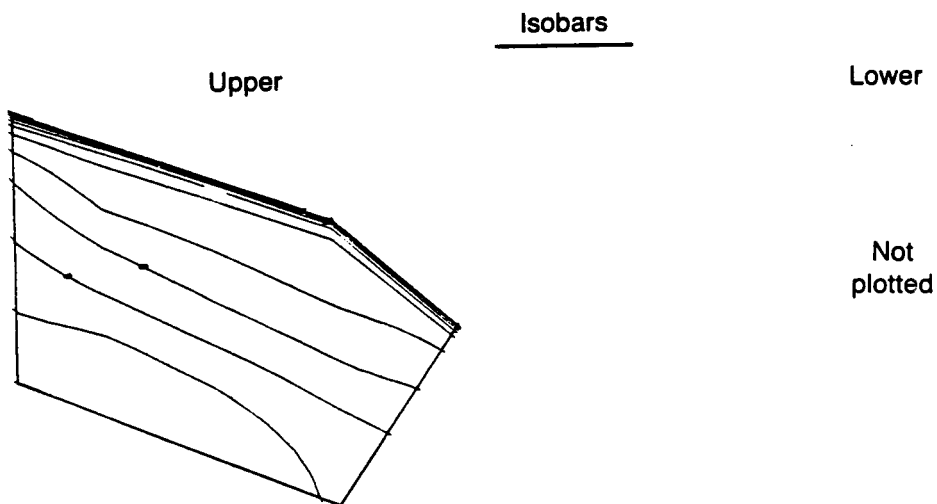
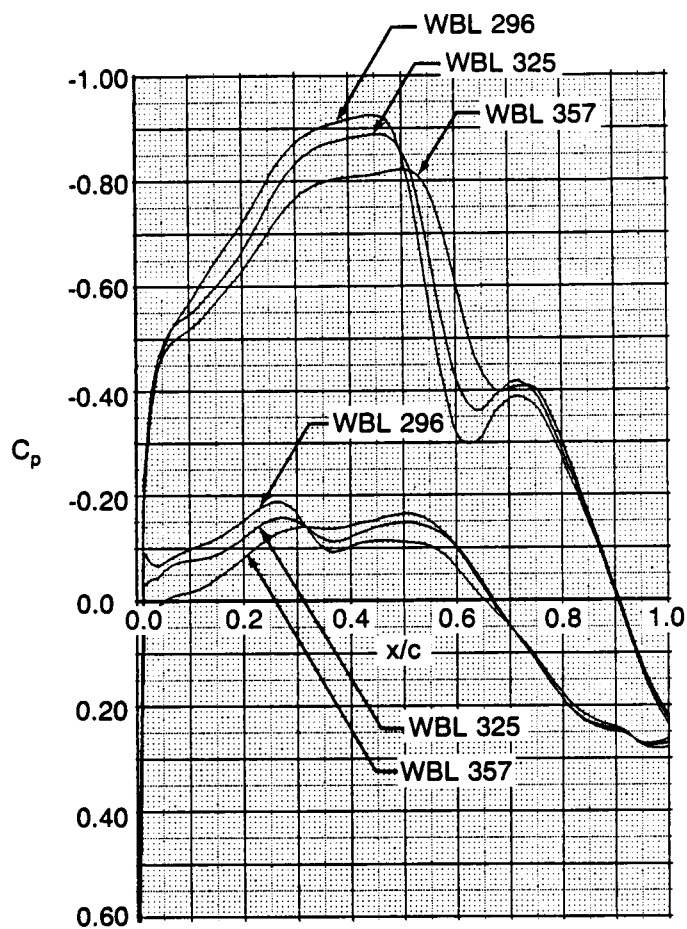


Figure 5-14. Theoretical Glove Pressure Distribution—Case VV, $M = 0.84$, $C_L = 0.345$



- $M = 0.82$
- $C_L = 0.452$
- $\alpha = 1.90$ deg
- Inviscid

Isobars

Upper

Lower

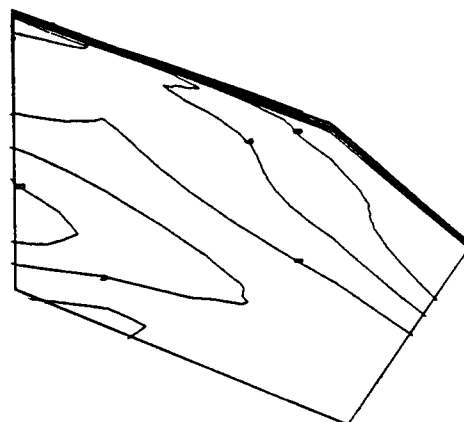
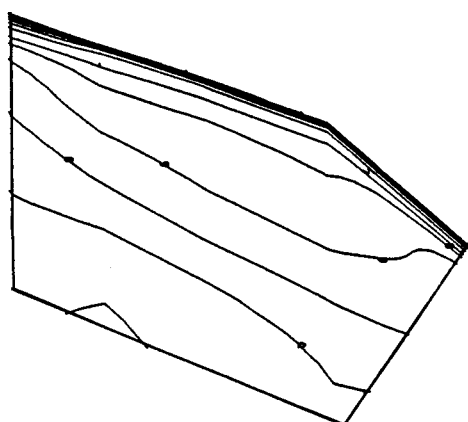
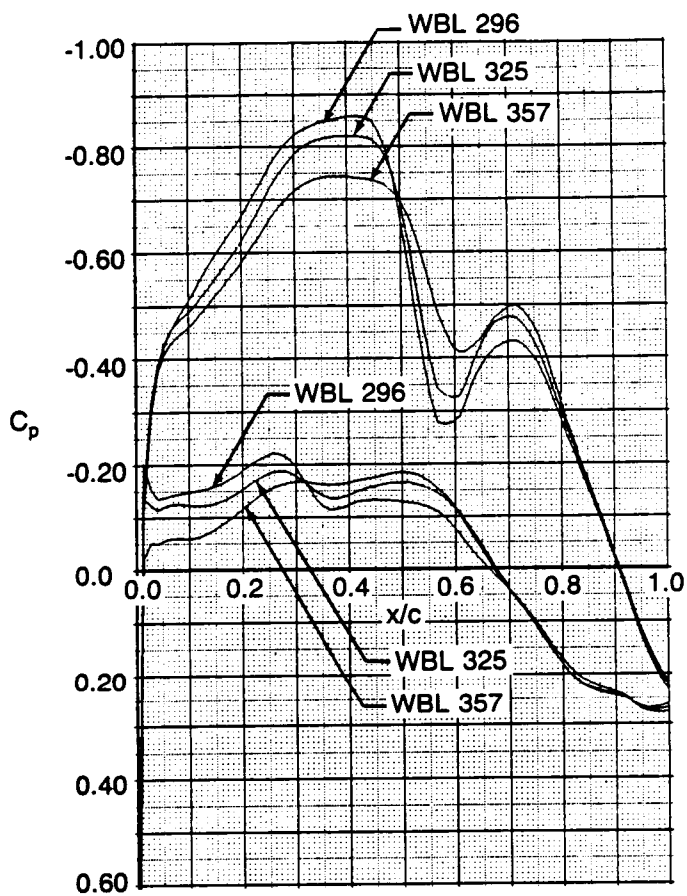


Figure 5-15. Theoretical Glove Pressure Distribution—Case YY, $M = 0.82$, $C_L = 0.452$



- $M = 0.82$
- $C_L = 0.388$
- $\alpha = 1.40$ deg
- Inviscid

Isobars

Upper

Lower

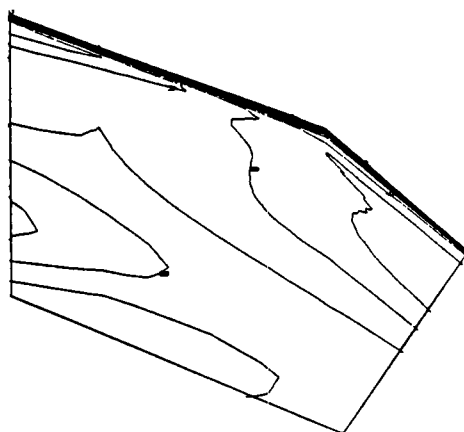
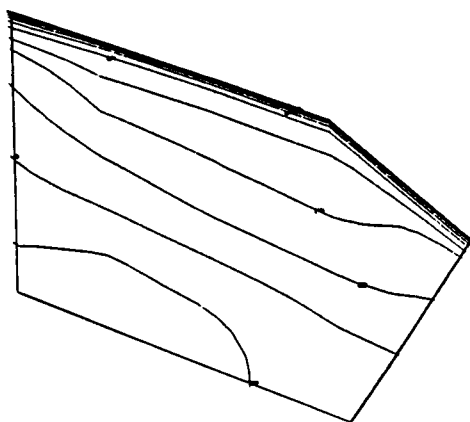
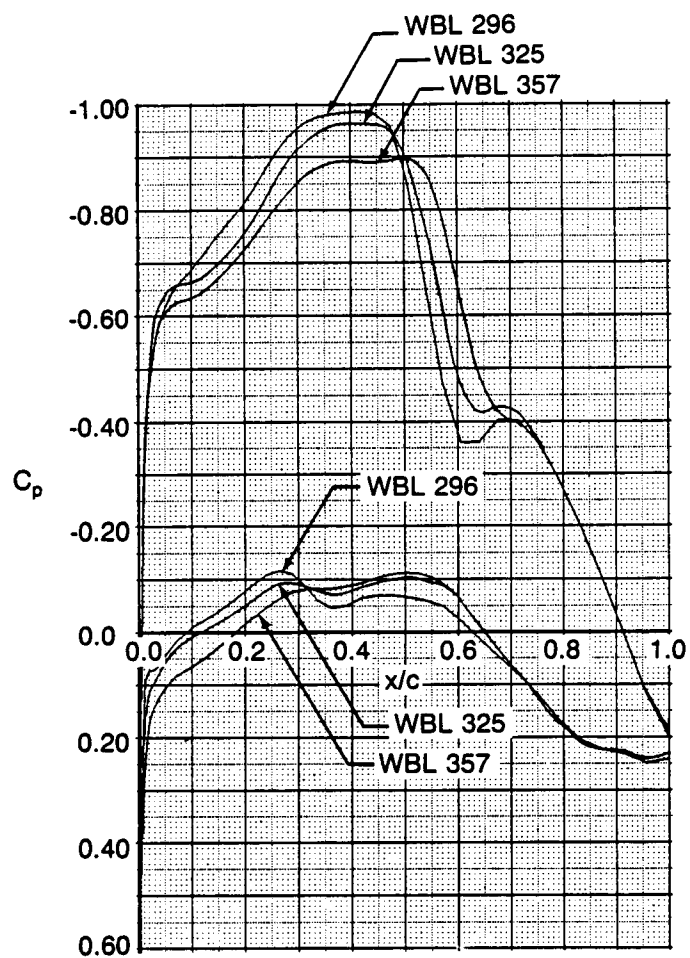


Figure 5-16. Theoretical Glove Pressure Distribution—Case TT, $M = 0.82$, $C_L = 0.388$



- $M = 0.80$
- $C_L = 0.548$
- $\alpha = 2.96 \text{ deg}$
- Viscous

Isobars

Upper

Lower

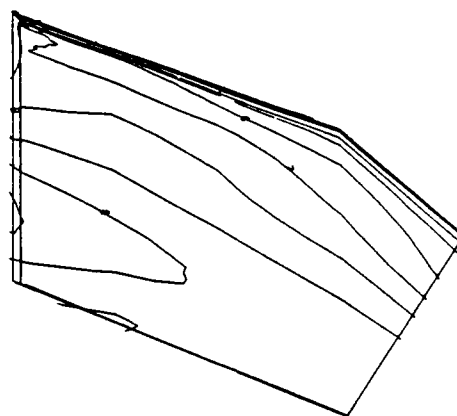
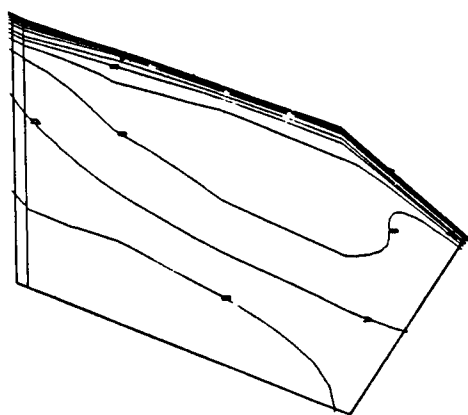
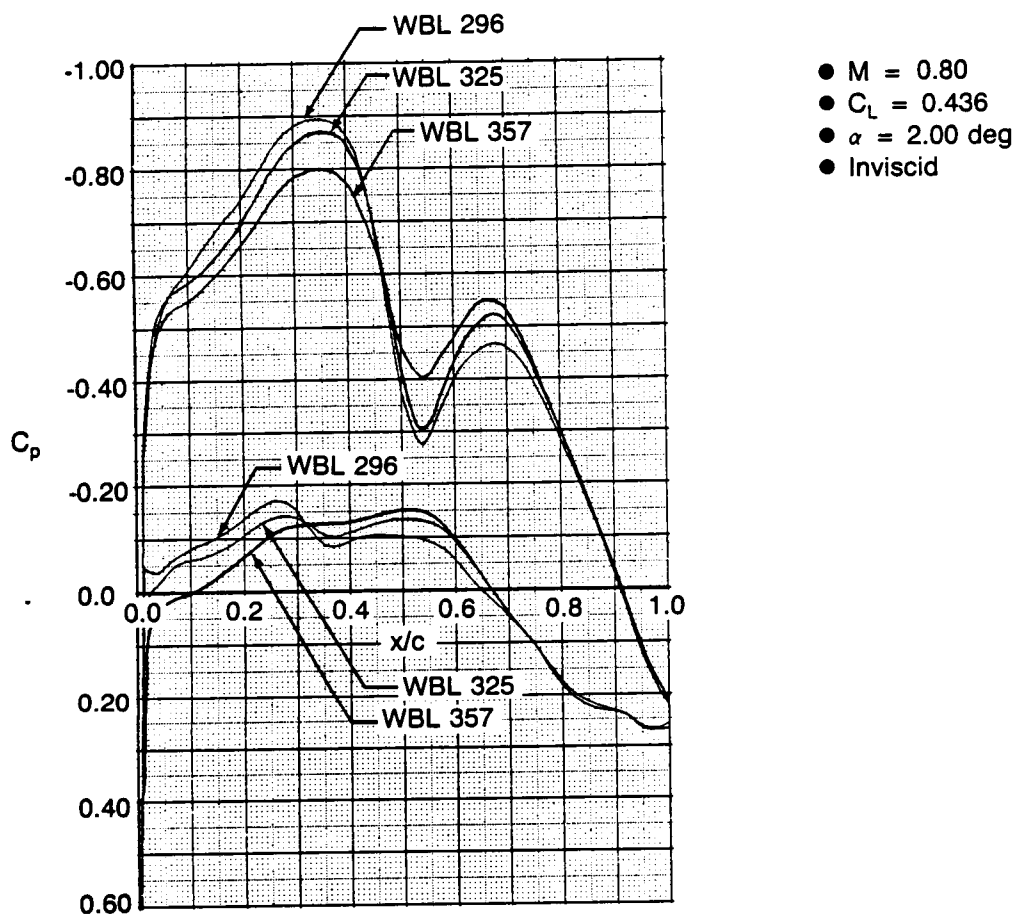


Figure 5-17. Glove Pressure Distribution—Case OO, $M = 0.80$, $C_L = 0.548$



- $M = 0.80$
- $C_L = 0.436$
- $\alpha = 2.00$ deg
- Inviscid

Isobars

Upper

Lower

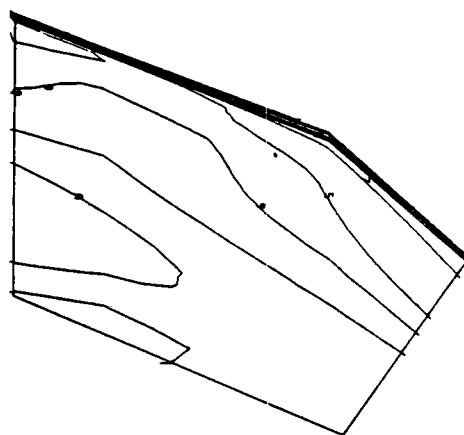
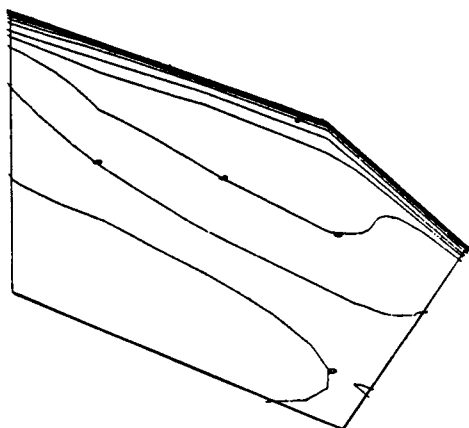
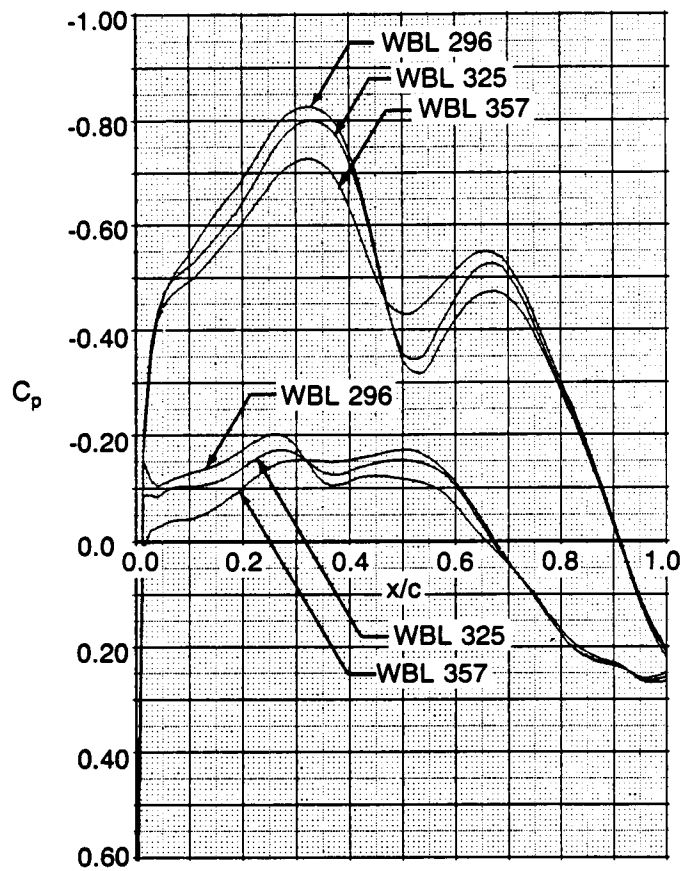


Figure 5-18. Theoretical Glove Pressure Distribution—Case PP, $M = 0.80$, $C_L = 0.436$



- $M = 0.80$
- $C_L = 0.380$
- $\alpha = 1.52^\circ$
- Inviscid

Isobars

Upper

Lower

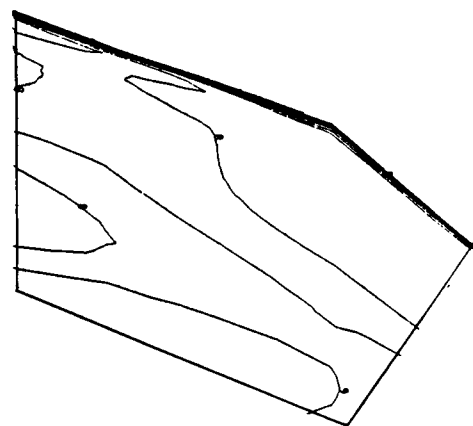
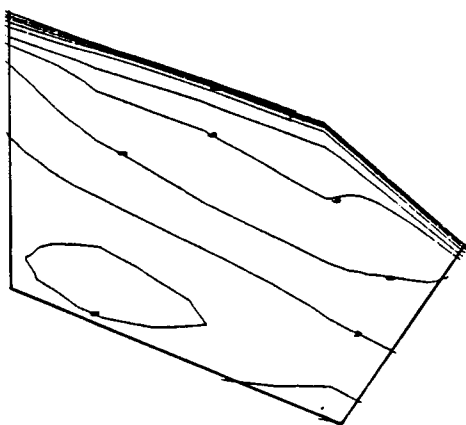
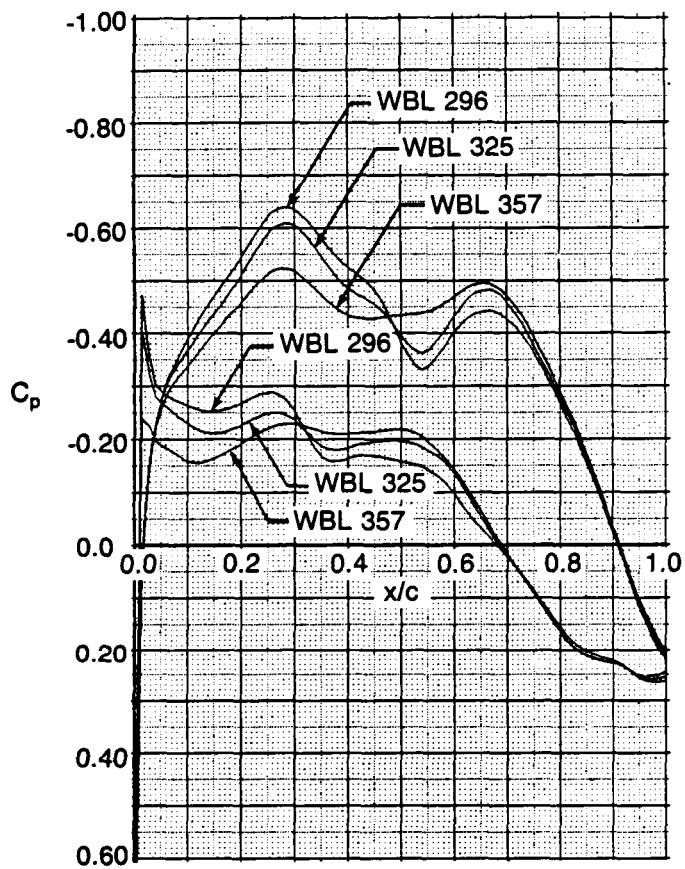


Figure 5-19. Theoretical Glove Pressure Distribution—Case QQ, $M = 0.80$, $C_L = 0.380$



- $M = 0.80$
- $C_L = 0.243$
- $\alpha = 0.27$ deg
- Inviscid

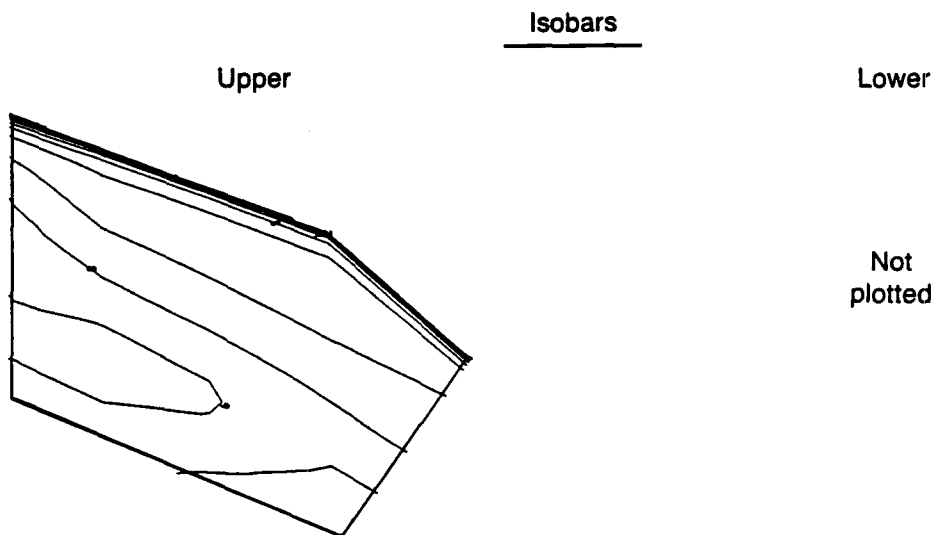
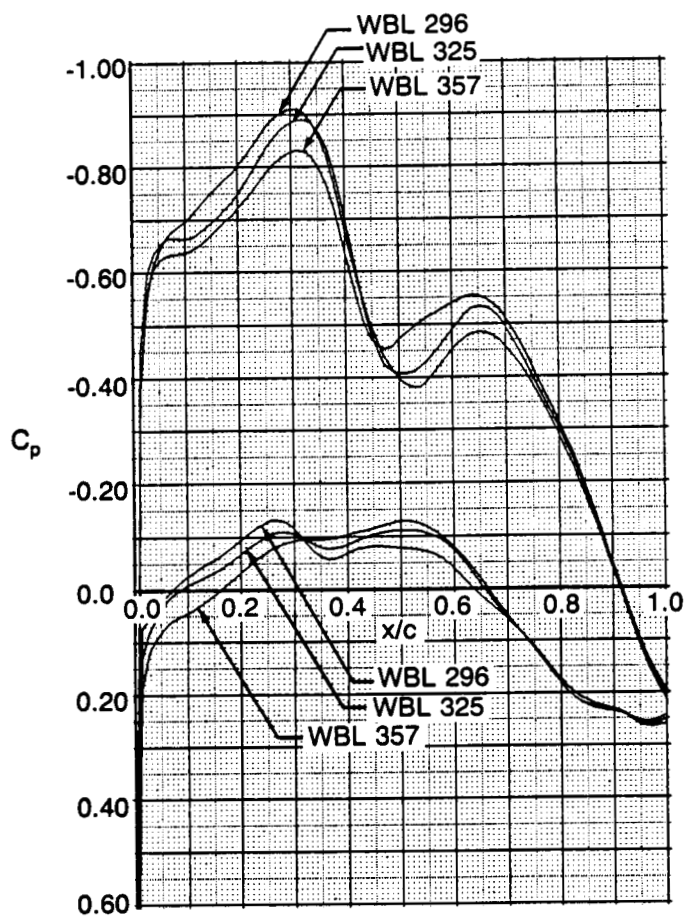


Figure 5-20. Theoretical Glove Pressure Distribution—Case AB, $M = 0.80$, $C_L = 0.243$



- $M = 0.78$
- $C_L = 0.473$
- $\alpha = 2.50$ deg
- Inviscid

ORIGINAL PAGE IS
OF POOR QUALITY

Isobars

Upper

Lower

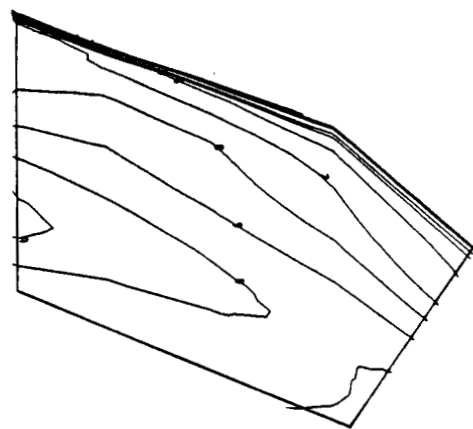
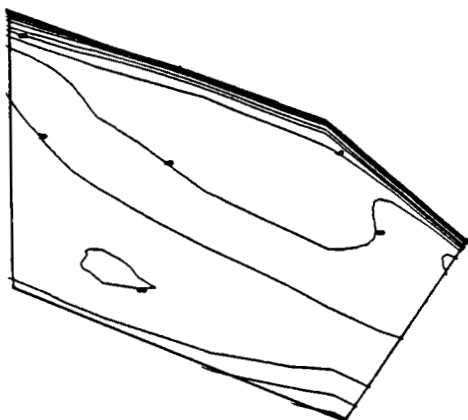
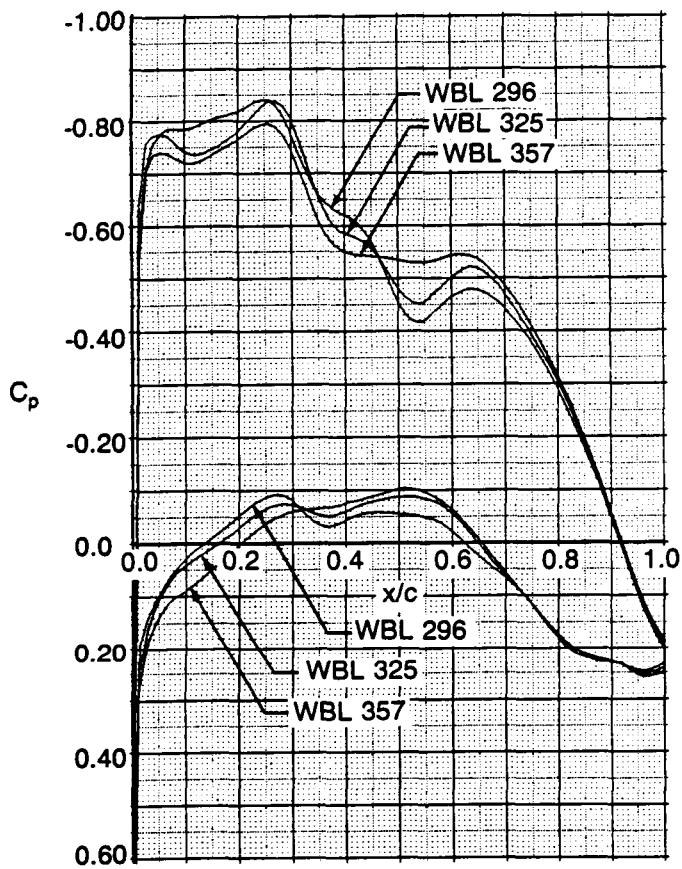


Figure 5-21. Theoretical Glove Pressure Distribution—Case ZZ, $M = 0.78$, $C_L = 0.473$



- $M = 0.75$
- $C_L = 0.503$
- $\alpha = 3.0$ deg
- Inviscid

Isobars

Upper

Lower

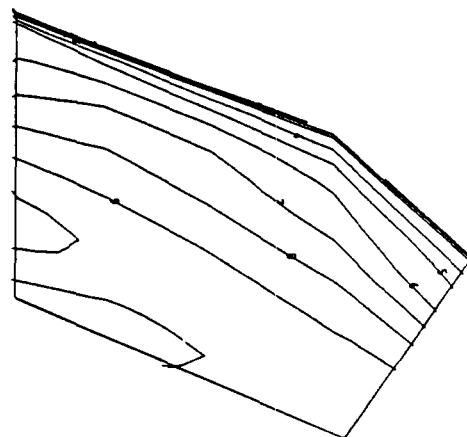
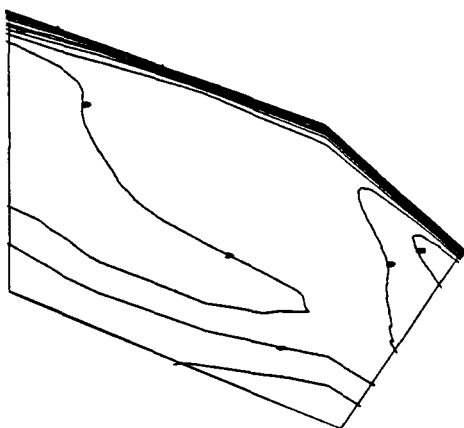
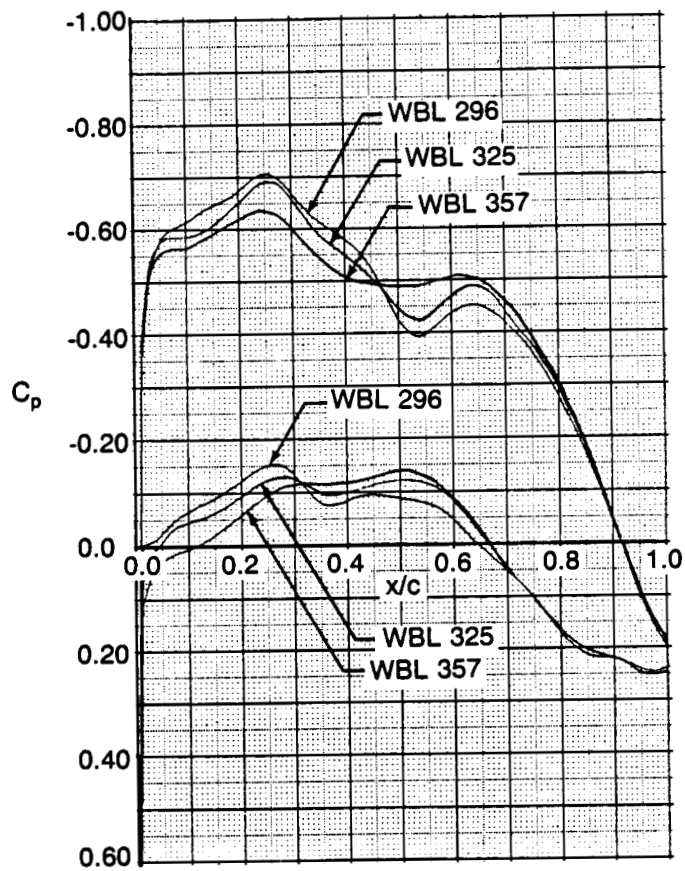


Figure 5-22. Theoretical Glove Pressure Distribution—Case XX, $M = 0.75$, $C_L = 0.503$

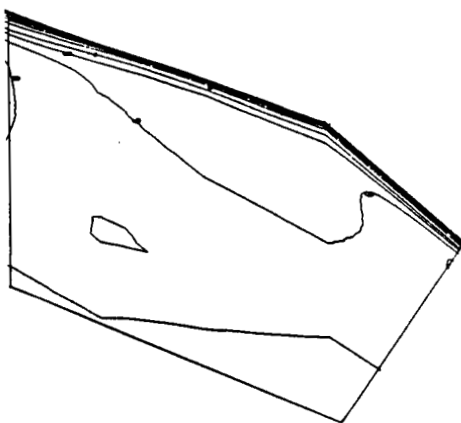
ORIGINAL PAGE IS
OF POOR QUALITY



- $M = 0.75$
- $C_L = 0.399$
- $\alpha = 2.00$ deg
- Inviscid

Isobars

Upper



Lower

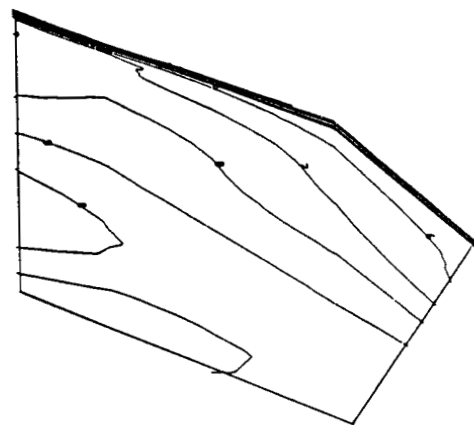
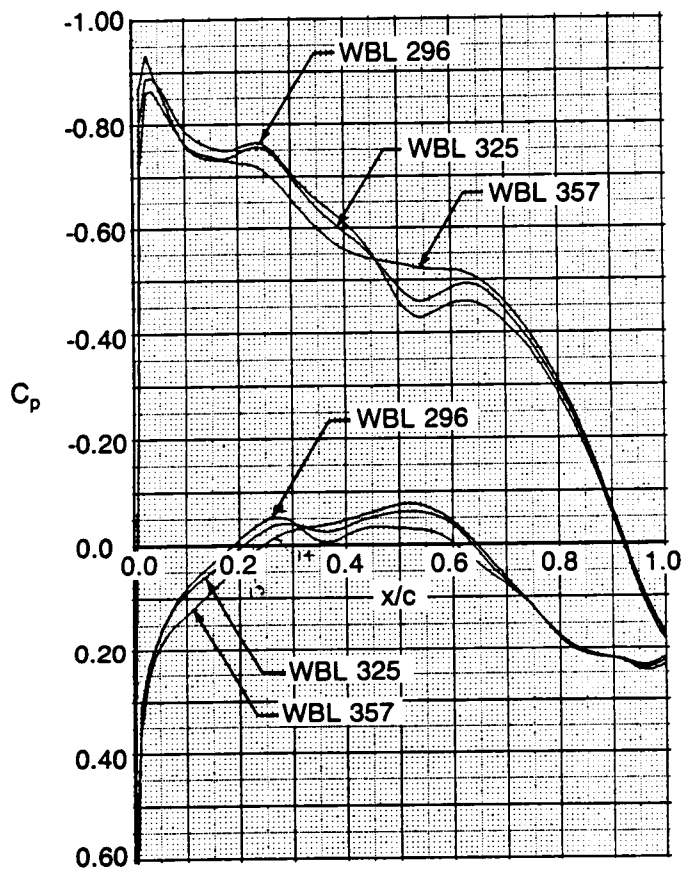


Figure 5-23. Theoretical Glove Pressure Distribution—Case RR, $M = 0.75$, $C_L = 0.399$



- $M = 0.70$
- $C_L = 0.522$
- $\alpha = 3.50$ deg
- Inviscid

Isobars

Upper

Lower

Not
plotted

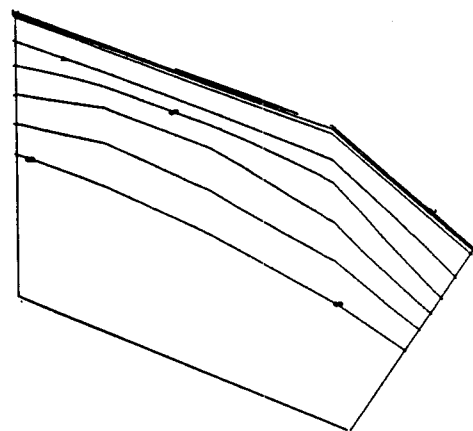
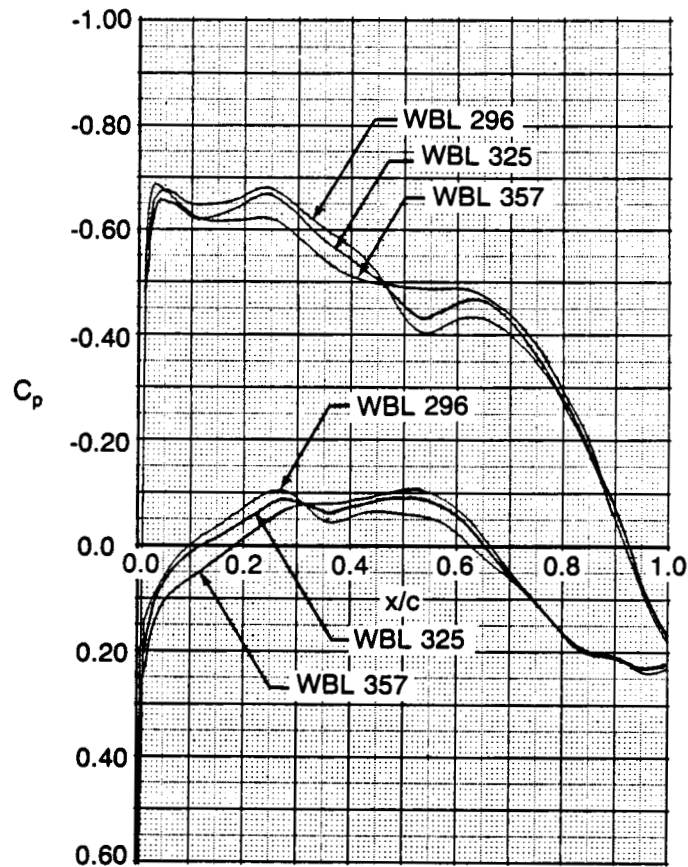


Figure 5-24. Theoretical Glove Pressure Distribution—Case WW, $M = 0.70$, $C_L = 0.522$

ORIGINAL PAGE IS
OF POOR QUALITY



- $M = 0.70$
- $C_L = 0.433$
- $\alpha = 2.60$ deg
- Inviscid

Upper

Isobars

Not plotted

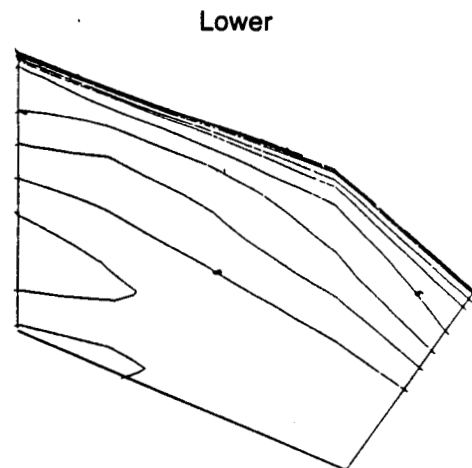


Figure 5-25. Theoretical Glove Pressure Distribution—Case UU, $M = 0.70$, $C_L = 0.433$

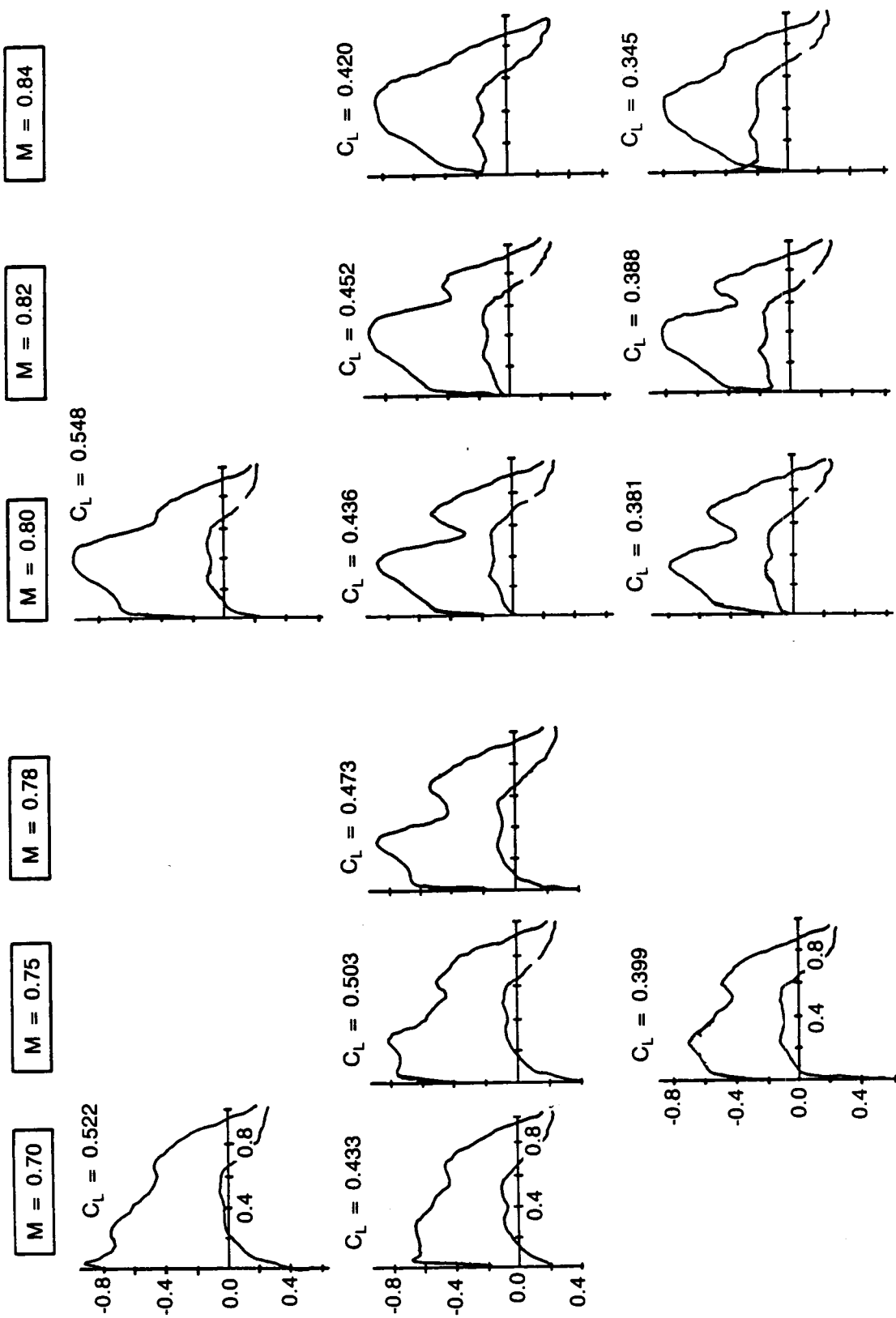
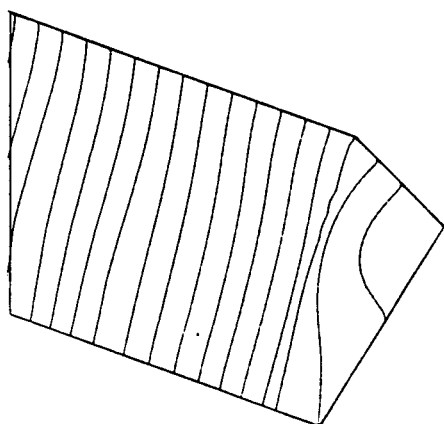


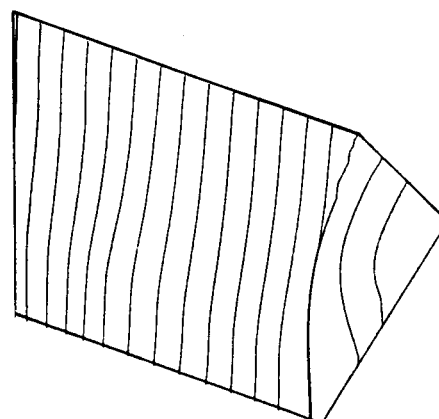
Figure 5-26. Glove Pressure Distribution Characteristics Summary—WBL 325

Streamlines at Glove Surface

Upper

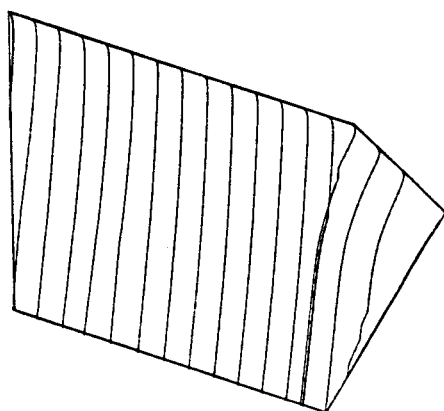


Lower



Streamlines at Outer Edge
of Boundary Layer

Upper



Lower

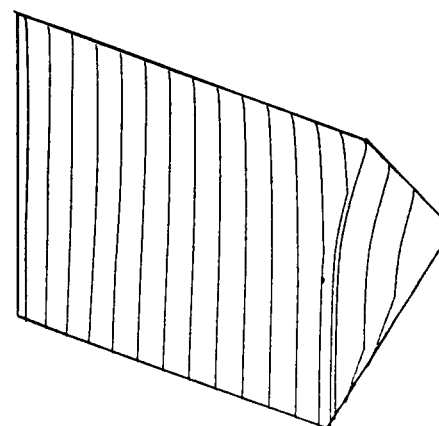


Figure 5-27. Theoretical Glove Streamlines on Upper and Lower Surfaces, $M = 0.80$, $C_L = 0.548$, $R_\theta/\text{ft} = 1.471 \times 10^6$

5.5 LEADING EDGE PROTECTIVE COVER

Because the 757 NLF glove flight testing took place during the month of June, it was necessary to protect the glove from insect impingement that would result in contamination of the laminar flow. After considering a number of alternatives, the most cost effective approach appeared to be one involving the use of a paper cover over the glove test areas (including the leading edge) during takeoff and climb. Existing data tends to show that the insect concentration is small above 5000 ft so the cover could then be removed above this level. The technique of ripping along the leading edge allowing the cover halves to be carried away in the airstream was successfully used on the King Cobra flight test program (ref. 14), so this approach was ultimately chosen for the 757 test.

There was some question, however, whether such a cover would tend to come off prematurely as a result of the aerodynamic forces acting on it, particularly on the upper surface at high angles of attack. In order to provide some guidance on this point, four tests were conducted in conjunction with other flight testing using a Boeing-owned T-33 airplane. No provisions were made for removal of the paper in flight during this testing, since the primary objective was to determine whether the paper would stay on up to at least 5000 feet. Figure 5-28 shows the size and configuration of the covers tested on each flight. In all cases the inboard edge of the paper was swept at a 30-deg angle to the streamwise direction, and the outboard edge was swept at a 10-deg angle. These angles were the largest that could be used on the actual 757 glove without the risk of getting tape residue on the glove surface in the laminar region. It was felt that large angles would provide a better chance of the paper ripping off cleanly along the edge of the tape (which remains on the surface) because the velocity component normal to the tape edge is made as large as possible.

In Flight 1 the cover was 3 ft wide by 2 ft long. This was less than half the width of that to be used on the actual 757 glove, but because of safety considerations it was decided to approach the full size incrementally in later flights. The first flight results showed a partial loss of paper on both surfaces at an altitude of 5000 ft. In Flight 2 the paper width was increased to 4 ft and the length to 3 ft, and the aft edge of the paper on the lower surface was taped. There was again a partial loss of paper on both surfaces, similar to the first flight. In Flight 3 the width of the paper was 6 ft and the length 2 ft. This was the largest width that could be tested. In Flight 4 the paper dimensions were the same, but the paper was taped intermittently along the aft edge on both surfaces. More paper was lost on Flight 4 than on Flight 3, apparently because of the tape on the aft edge. The configuration used in Flight 3 was chosen for use on the 757 glove.

The details of the insect protection covers used on the 757 NLF glove are shown in Figure 5-29. The covers extended from the outboard edge of the notch (about WBL 276) to just beyond the edge of the straight leading edge portion of the glove (about WBL 357), making them about 7 ft wide. For Flight 1, the chordwise extent was 3 ft long on the lower surface and 2 ft long the upper surface, but for Flight 2 the chordwise length was reduced to 1 ft on the upper surface. For Flight 3, the upper surface length was again increased to 2 ft. The paper used was similar to butcher paper in strength and thickness, with a thin film of wax on one side which was put next to the glove surface. The system for removing the paper in flight consisted of a heavy nylon rip cord (60-lb test for Flights 1 and 2 and 100-lb test for Flight 3) led from inside the body through a .25-inch-dia copper tube and secured to body and wing surfaces. It was further led under the leading edge of the cover to its outboard end and then back through a small paper envelope attached to the outside leading edge of the cover. The line was attached to the cover at its inboard end and was protected from the airflow by the envelope. The glove cover was positioned to place the rip cord near the stagnation line so that when the cord was pulled, thereby ripping the cover along the leading edge, the cover would fly away in two pieces, over upper and lower surfaces of the glove.

On Flight 1 most of the upper surface paper eroded away shortly after takeoff but the lower surface paper remained more nearly intact. However, on the upper side about 6 in remained along the entire span so that the portion of the glove most likely to be struck by insects, the region near the stagnation line, was still protected when the rip cord was pulled at about 5000-ft altitude to remove the cover. After

repeated attempts, the line broke without complete ripping of the cover due to excessive friction in the system. However, the cover was gradually eroded away during high-speed flight to the point where the execution of several "roller-coaster" maneuvers resulted in complete cover removal. Data from Flight 1 showed no evidence of insect contamination, so the cover was successful in spite of upper side erosion early in the flight.

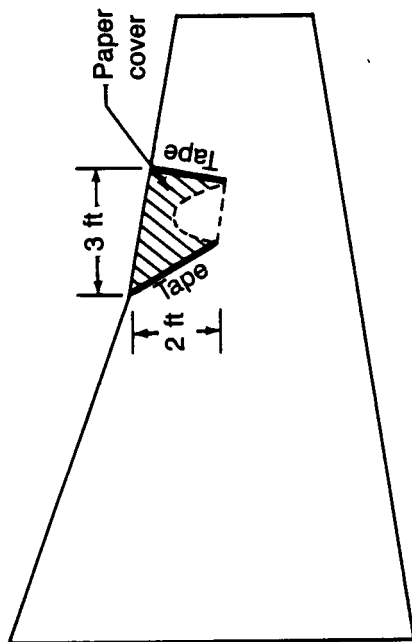
Preparation for Flight 2 included careful cleaning and avoidance of any contaminating influence that would cause line friction. Lubrication of the nylon line was used upon reinstallation. Since an inadequate flare on the end of the copper tube inside the body was suspected as a contributing cause of the premature line break in Flight 1, the tube end was carefully flared for Flight 2. Also for Flight 2 the upper surface cover length was shortened to 1 ft to reduce the fluttering of the free edge. Furthermore, the portion behind had been lost very early on Flight 1, so was deemed unnecessary for upper surface protection in this case also.

On Flight 2, however, the cover upper surface eroded even more quickly than previously so that along most of the glove span only 3 to 4 in of chordwise length remained by the time an altitude of 5000 ft was attained. The nylon line again broke during an attempt to rip the cover so a considerable period was used to effect cover removal. Again there was no evidence of insect contamination in the Flight 2 data, so the cover did provide sufficient protection in this case also.

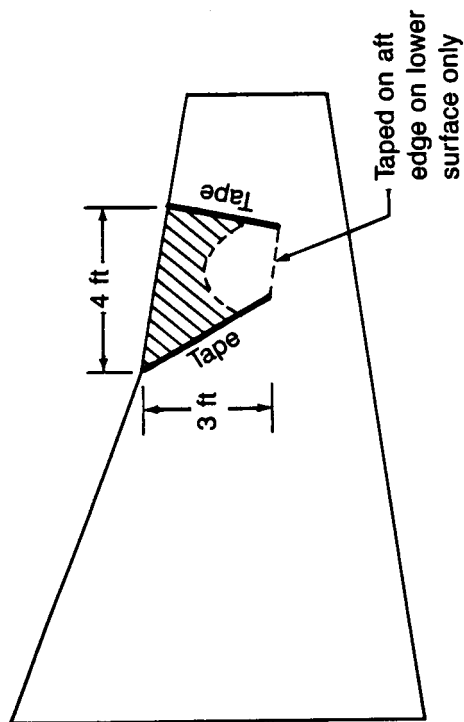
Preparation for Flight 3 included a more direct routing of the copper tube to reduce the friction force during the rip cord pull. The copper tubing had originally been routed behind the inboard microphone at 60% chord on the upper surface to minimize the risk of introducing an unwanted noise source. Since noise data was not taken on Flight 3, this was no longer a concern. The length of the cover on the upper surface was increased again to about 2 ft, since the Flight 1 configuration appeared better than for Flight 2. Finally, a new braided nylon line was used with 100-lb test capability. This time the cover was ripped successfully. The partly eroded upper side came off immediately and the lower side came off a short time later during a maneuver to move the stagnation line above the leading edge of the remaining paper. There again was no evidence of insect contamination in the data from Flight 3.

Since the purpose of Flight 4 was to obtain pressure data, no glove protection cover was used. Laminar flow sensor data was taken on the flight, however, which did indicate a loss of laminar flow in some areas of the glove relative to the Flight 3 results. It was suspected that this was due to insect contamination although this could not be visually confirmed in flight. After landing, an inspection of the glove leading edge showed that seven insects had hit the glove in the vicinity of the stagnation line, as shown in Figure 5-30. It is not known how many of these were picked up during takeoff and climbout. However, this evidence together with the reduced extent of laminar flow in corresponding areas of the glove, indicates that the cover served its essential purpose on the three flights for which it was used.

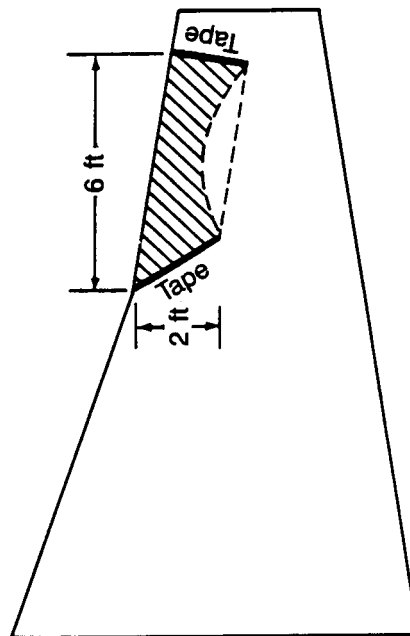
Flight 1



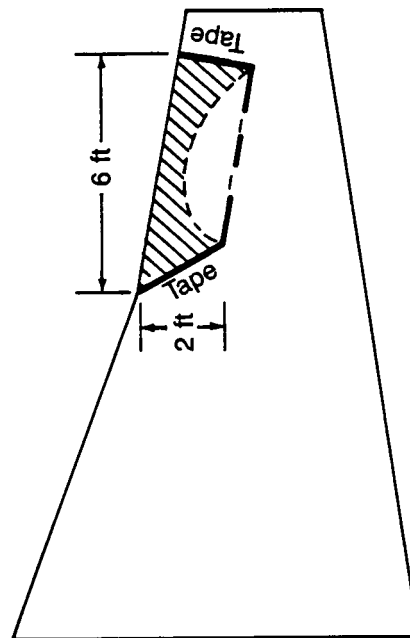
Flight 2



Flight 3



Flight 4



Notes: 1. The dashed line indicates the extent of paper loss on both surfaces at 5000-ft altitude

2. In all cases the inboard edge of the paper makes a 30-deg angle with the streamwise direction and the outboard a 10-deg angle

Figure 5-28. Evaluation of Glove Cover Parameters, T-33 Flight Tests

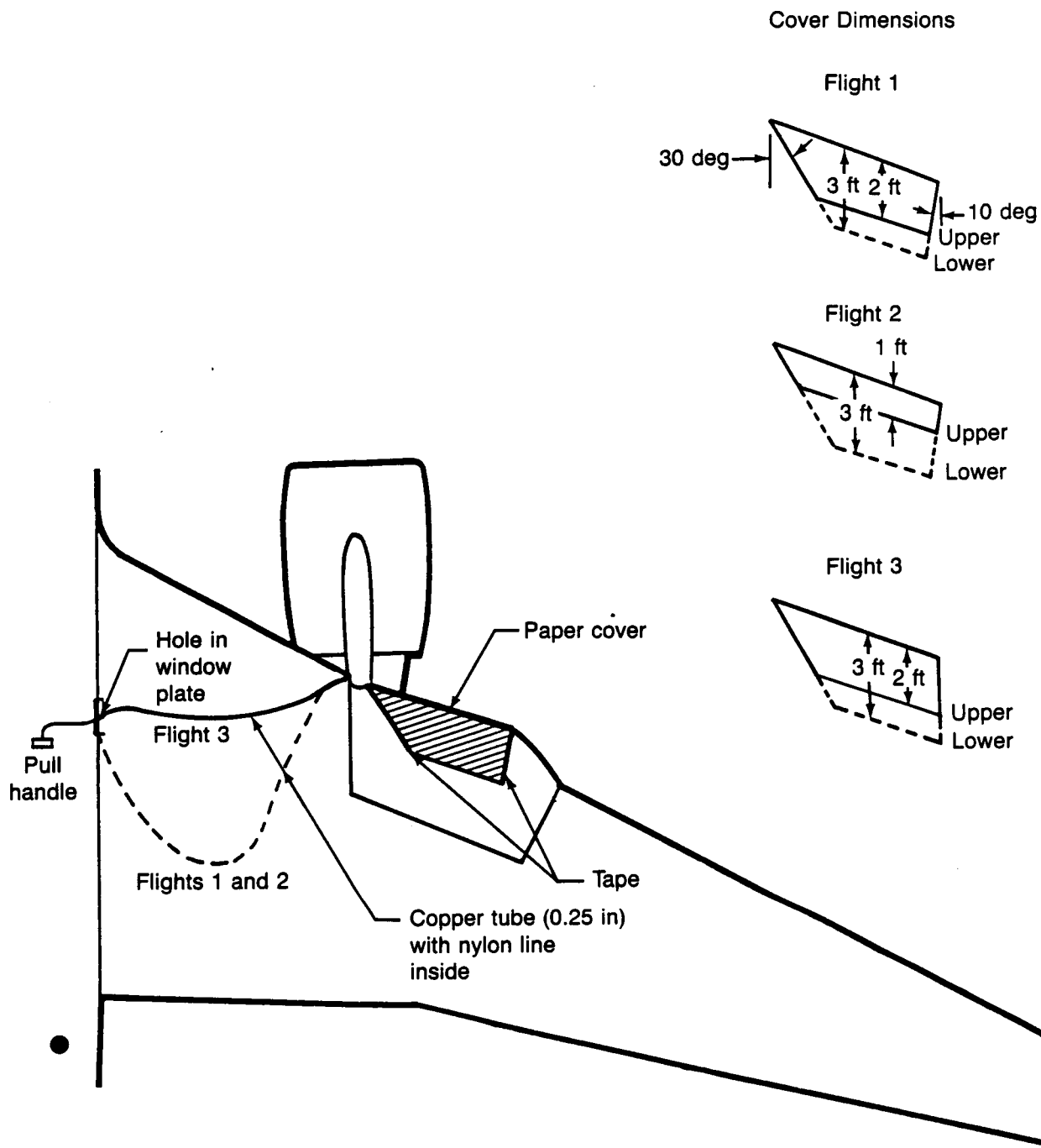


Figure 5-29. Glove Cover and Removal Apparatus — Flights 1, 2, and 3

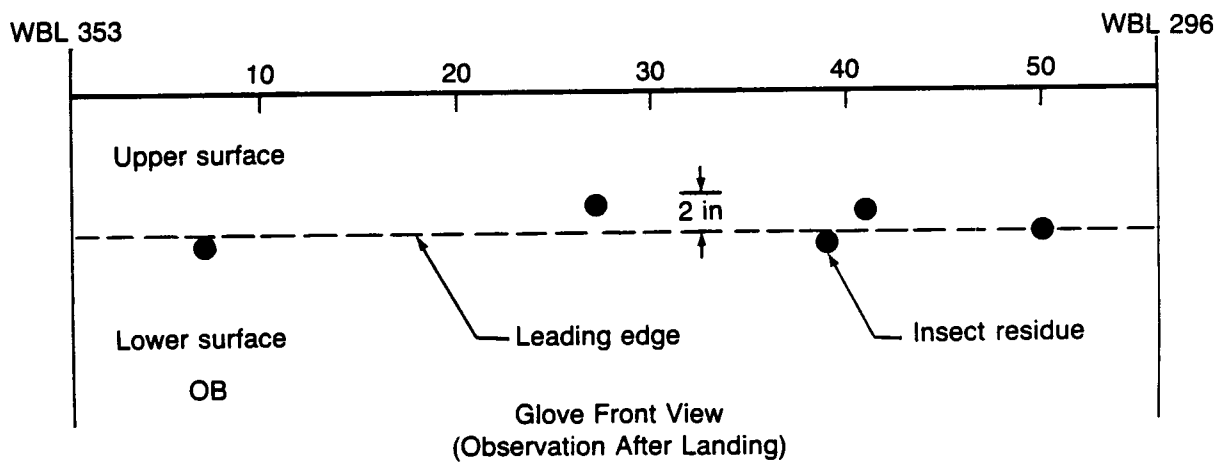
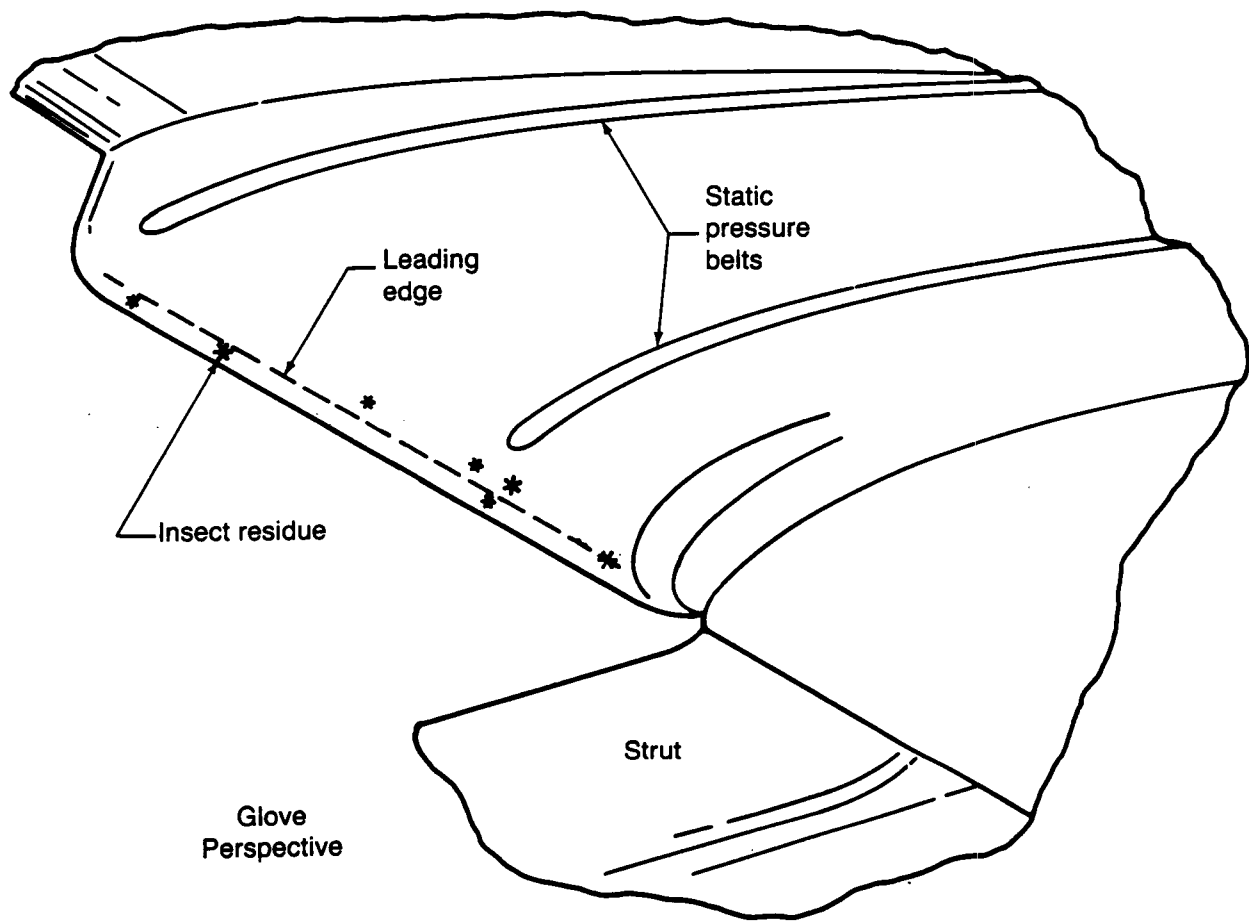


Figure 5-30. Insect Impingement on Glove for Flight 4

6.0 INSTRUMENTATION

6.1 AIRPLANE INSTRUMENTATION SYSTEMS

The 757 airplane (NA001) used in the flight survey is a Boeing-owned test airplane that is used for a variety of flight test and development activities. As such it carries an instrumentation complement that allows a complete description of the parameters that are likely to be important in assessing the performance and flight characteristics in a given test program. Provisions for online data acquisition allow inflight monitoring and assessment of results. Complete recording of about 50 data channels are also provided for offline data reduction and analysis. The normal flight management and control instrumentation is augmented to allow the flight crew to set up and maintain flight condition as required for efficient testing operations.

The total range of flight parameters recorded for the subject test series is discussed and enumerated elsewhere in this report. However, Figure 6-1 illustrates the online video display available to the test personnel to monitor the test progress and control the selection of flight conditions.

6.2 GLOVE AERODYNAMIC INSTRUMENTATION

The 757 NLF glove was instrumented to determine surface pressures, the state of the boundary layer, and noise levels as a function of flight condition. Surface pressures were measured using the pressure belt technique. The state of the boundary layer was indicated by means of hot films applied to the surface. Noise levels were determined using surface microphones and probe-mounted microphones. The noise instrumentation and measuring techniques are both discussed elsewhere.

The layout of the glove instrumentation for all four flights is shown in Figure 6-2. The noise instrumentation is included here to show its relationship to the aerodynamic instrumentation.

6.2.1 Static Pressure Belts

Glove surface pressures were measured using pressure belts ("strip-a-tube") installed on the glove surfaces. Figure 6-3 (upper) shows the strip-a-tube details, which differ from conventional strip-a-tube in that the surfaces are flat, rather than a series of circular arcs. This minimized pressure measurement errors that might be caused by crossflow over a cylindrical-type surface. Two 5-hole belts were located side-by-side. Plastic (PVC) wedge fairing was used to fair the edges of the belt. In the leading edge region, one belt was cut down to a 3-tube width and extended to the most forward position. This was done to minimize the flow disturbance due to the tube-end and the fairing which was used alongside and ahead of this part of the strip-a-tube. The lower part of Figure 6-3 shows the details of this arrangement.

For Flights 1 and 2, the strip-a-tube was installed at station WBL 296 and pressures measured at six chordwise locations on each surface, as shown in Figure 6-2. For Flights 3 and 4, another strip-a-tube belt was installed at station WBL 353 and pressures measured at seven chordwise locations on each surface. Table 6-1 provides the coordinates for all of these locations.

With the strip-a-tube technique there is inevitably some concern about the residual flow disturbance caused by the tube-end and its fairing. If the strip-a-tube had been wrapped continuously around the leading edge from upper to lower surface, the pressure disturbance would probably have been negligible. However, this could not be done without affecting the attachment line flow, so the installation was made as shown, with the expectation that only the most forward pressure indication would be affected. For Flight 4, the forward 3 in of the strip-a-tube was recessed into the glove surface so that the tube-end was flush with the surface. This allowed an evaluation of the pressure disturbance near the first hole position due to the local bump formed at the tube-end and fairing.

6.2.2 Hot-Film Sensors

The state of the boundary layer (ie., laminar vs. turbulent) on the glove was determined using the hot-film technique. As shown in Figure 6-2, there were ten hot films on each surface. For Flights 1 and 2, the hot films were placed along a line which made a 15-deg angle with the remote streamwise direction. This angle was felt to be the minimum that would prevent the turbulent wedge emanating from each hot film from affecting those further downstream. This line was swept outboard as shown in order to take advantage of the local streamline directions, which were swept inboard. The angle could not have been made this small if the streamlines had been swept outboard since insufficient margin would remain to accommodate differences between upper and lower surface flow and the various flight conditions. The row of hot films was located in the midspan region of the glove in such a way that turbulence caused by the surface-mounted microphones and the strip-a-tube would not affect them.

Based on the results from Flights 1 and 2, the hot-film locations were changed for Flights 3 and 4, as shown in Figure 6-2, to provide some definition of the spanwise variation of laminar flow transition on both surfaces. The hot-film locations for Flights 1 and 2 are defined in Table 6-2, and those for Flights 3 and 4 in Table 6-3.

The components of the transition sensing system are shown in Figure 6-4, which includes an expanded view of a typical hot-film sensor. The output from the hot film electronics box consisted of two types: (1) the fluctuating voltage traces that were recorded on tape and also displayed on a bank of 20 oscilloscopes; and (2) the RMS voltages, which were recorded on the airplane data system. The oscilloscope displays allowed immediate determination of the boundary layer state at each hot-film location throughout the course of the flight. The RMS output was recorded for later use in final data analysis.

6.3 ACOUSTIC INSTRUMENTATION

An array of microphones was provided on both upper and lower wing surfaces to establish the noise environment on the wing. Several types of installations were used to meet requirements peculiar to local conditions and provide definition of the noise spectra at each location. Certain limitations were recognized for the installation and sensor types being considered, so a period of analysis, development, and laboratory testing was necessary to define candidate installations for evaluation. Prior to final selection several flight tests were conducted with sensors mounted on the 757 wing to determine the characteristics of the most promising candidates. The appendix discusses the candidate evaluation and selection activity. The characteristics of the instrumentation package used for the flight survey of the wing noise environment follow. Figure 6-5 and Table 6-4 illustrate the configuration of the final microphone array and provide the geometry specification for each installation.

6.3.1 Surface-Mounted Microphones

Nine Kulite LQ-101-125-5 transducers were mounted directly on the upper and lower surfaces on the right wing of the airplane. Specifications are shown on Figure 6-6, which also presents an enlarged photograph of the LQ-101-125-5 transducer. Each surface-mounted transducer was modified by inserting a .016-in wire in the unit's vent tube to provide desired response characteristics.

6.3.2 Probe-Mounted Microphones

The eight probe-mounted microphones installed on the airplane wing incorporated Kulite XCW-093-5 transducers. Specifications for the transducer are given in Figure 6-6, which also shows a XCW-093-5 photograph along side a scale (50 divisions per inch) to indicate the size. The vent tube of each transducer was modified by inserting a .008-in wire to provide satisfactory response characteristics.

In a typical installation the transducer was placed inside a cylindrical probe, which was fitted with a Bruel and Kjaer (B&K) UA 0385 nosecone. This installation is similar to that used for B&K .25-in microphones. The probe assembly includes a base support for which the length is selected to provide the

appropriate height above the wing surface. This allowed placement of the microphone close to the edge of the boundary layer at the probe location. Figure 6-7 shows the typical probe general arrangement and dimensions. The lower part of the figure shows probes of several support lengths (i.e., 1.5, 2, 4, and 5 in).

6.3.3 Microphone Installation

The microphone locations were chosen to survey the entire wing with a limited number of transducers. It was also desired to use a denser distribution of microphones in the NLF glove region for monitoring sound effects on NLF. The microphone placement on the glove recognized that the microphones would trip the laminar boundary layer. Their locations were restricted so that the turbulent wedge flowing from them would not interfere with the hot film or pressure transducers. The upper glove surface probe located at WBL 350, $x/c = .3$ was originally planned to be located at WBL 308 but was moved to avoid the possibility of interference with the glove cover pull string upon separation of the cover from the wing in flight.

The probe distance from the wing surface was chosen so that the microphone would be slightly above the boundary layer as calculated for flight Mach number of .8. The probes were oriented in alignment with the local flow streamline at $M = .8$. To complement the information in Figure 6-2, a table of the noise transducer locations is included as Table 6-4.

Prior to the installation of the probe-mounted microphones, the wing surface finish was removed at the location where a probe was to be mounted. In cases where a probe was to be installed on the laminar flow glove, the glove surface was abraded before installation. After surface preparation, the sting-mounted probes were bonded to the wing surface per BAC Standard 5010 Type 70 (BMS J-92 Type 1). Aluminum contact tape was applied over the base of the probes after bonding in order to minimize the discontinuity at each base.

Surface-mounted microphones were bonded to the leading edge flaps per BAC Standard 5010 Type 44 (BMS J-26 Class B). Transducer edges were faired into the surface with Magic Bond (manufactured by U.S. Chemicals and Plastics) to provide a smooth transition to the wing surface. The vent tube end (with wire inserted) of each transducer was carefully left uncovered by adhesive or sealing materials in order to ensure proper venting.

Photographs showing the overall arrangement of the instrumentation arrays are given in Figure 6-8 (upper surface) and Figure 6-9 (lower surface). A closeup of the glove instrumentation is given in Figure 6-10 (upper surface) and Figure 6-11 (lower surface).

Photographs of typical surface-mounted and probe-mounted microphone installations are provided in Figures 6-12 to 6-15. The routing of the rip cord guide tube to avoid influences on the output of microphone 3 is shown in Figure 6-12.

6.4 DATA ACQUISITION SYSTEMS

A block diagram illustrating the noise data acquisition system is included in Figure 6-16. All Kulite transducers were connected to Boeing-built bridge and balance units that included the necessary power supply and also supplied 40 dB of preamplifier gain. The preamplified data channels were then routed through individual Ithaco amplifier units that were manually adjusted as conditions changed in order to maintain a nearly constant signal level for data recording. The data was then recorded on a 28-track Honeywell 5600E tape recorder at 15 in/s in wideband FM format. All data channels were monitored on separate oscilloscopes that were checked throughout the flight testing for signs of transducer failure or signal overload. In addition to transducer data, IRIG time code and voice annotation were also recorded. Photographs of the components discussed above and their installation in the airplane are given in Figures 6-17 and 6-18.

6.4.1 Online Data Reduction Instrumentation

The online data reduction system is also included in Figure 6-16. It consisted of a Boeing-built data multiplexer, a General Radio GR-1995 1/3-octave band spectrum analyzer, and a Hewlett-Packard HP-85 microcomputer (photograph in fig. 6-19). Six glove-mounted microphone data channels were selected for online analysis by connecting cables from the corresponding bridge and balance units to the inputs of the online system's data multiplexer. Under computer control, the system sequentially acquired 8 sec of data for each of the six input lines. After all data was acquired, the HP-85 printed a tabulation of 1/3-octave band sound pressure levels (SPL) for the six channels.

6.4.2 Calibrations

The noise transducers were individually calibrated for frequency response at 1/3-octave center frequencies between 50 Hz and 10 kHz, using an "infinite tube" apparatus. Example calibration curves for the LQ-101-125-5 and XCW-093-5 transducers are included as Figure 6-20. Calibration records were stored on a computer file and used in data reduction to correct the noise data for transducer frequency response.

A transducer sensitivity calibration was performed before and after each flight test. To accomplish this a 250 Hz, 150 dB test signal (from a Boeing-built Kulite calibrator) was applied to each transducer while the signal level displayed on the data acquisition system's voltmeter was read and logged. The voltage readings were used to calculate 1V equivalent values of SPL for the transducers which were then entered on the tape recorder log sheets. The 1V equivalent data was used in data reduction to correct noise data for transducer sensitivity.

Ambient noise floors were recorded with the airplane on the ground in a quiet environment. A typical set of 1/3-octave noise floors is shown in Figure 6-21. Measurements were made at gain settings of 18 dB, 30 dB, and 48 dB. The tone at 400 Hz is due to interference from the ground system electrical power supply. In flight, the electrical power came from generators driven by the airplane engines and the electrical interference was found to be much more severe.

6.4.3 Data Acquisition Procedure

Seventeen data channels were recorded at one switch position using the Honeywell 5600E 28-track recorder indicated in Figure 6-16 and shown by the photo of Figure 6-18. 60 sec of data were recorded after the airplane was stabilized on a given condition and a "condition set" announcement was made by the test director. Concurrent with analog data recording, data were acquired, sequentially, for six selected channels by the online data reduction system. The online system produced printed tabulations of 1/3-octave band sound pressure levels.

6.5 ACOUSTIC DATA REDUCTION

6.5.1 Online Data Reduction

The online system produced a paper tape listing of 1/3-octave band, octave band, and overall SPLs for each of six glove-mounted microphone data channels at the end of each condition. The printed listing was the only permanent record kept of the online data. In order to decrease data reduction time, no data was stored on the microcomputer's magnetic tape.

6.5.2 Offline Data Reduction

Analog magnetic tapes were reduced using the Boeing data reduction system consisting primarily of four B&K 2131 1/3-octave analyzers, controlled by a Prime 500 microcomputer. The Boeing system is more fully described in Reference 15. The 1/3-octave spectra for each condition and each data channel were written onto digital magnetic tapes for analysis.

6.5.3 Disposition of Data

Printouts of online data were provided in flight, as they were produced. Digital magnetic tapes were provided at the conclusion of data reduction. Analog magnetic tapes were retained by the Boeing laboratory and are stored in the tape vault with file number 85-10-086-(1-2). Tape recorder log sheets are stored with the tapes.

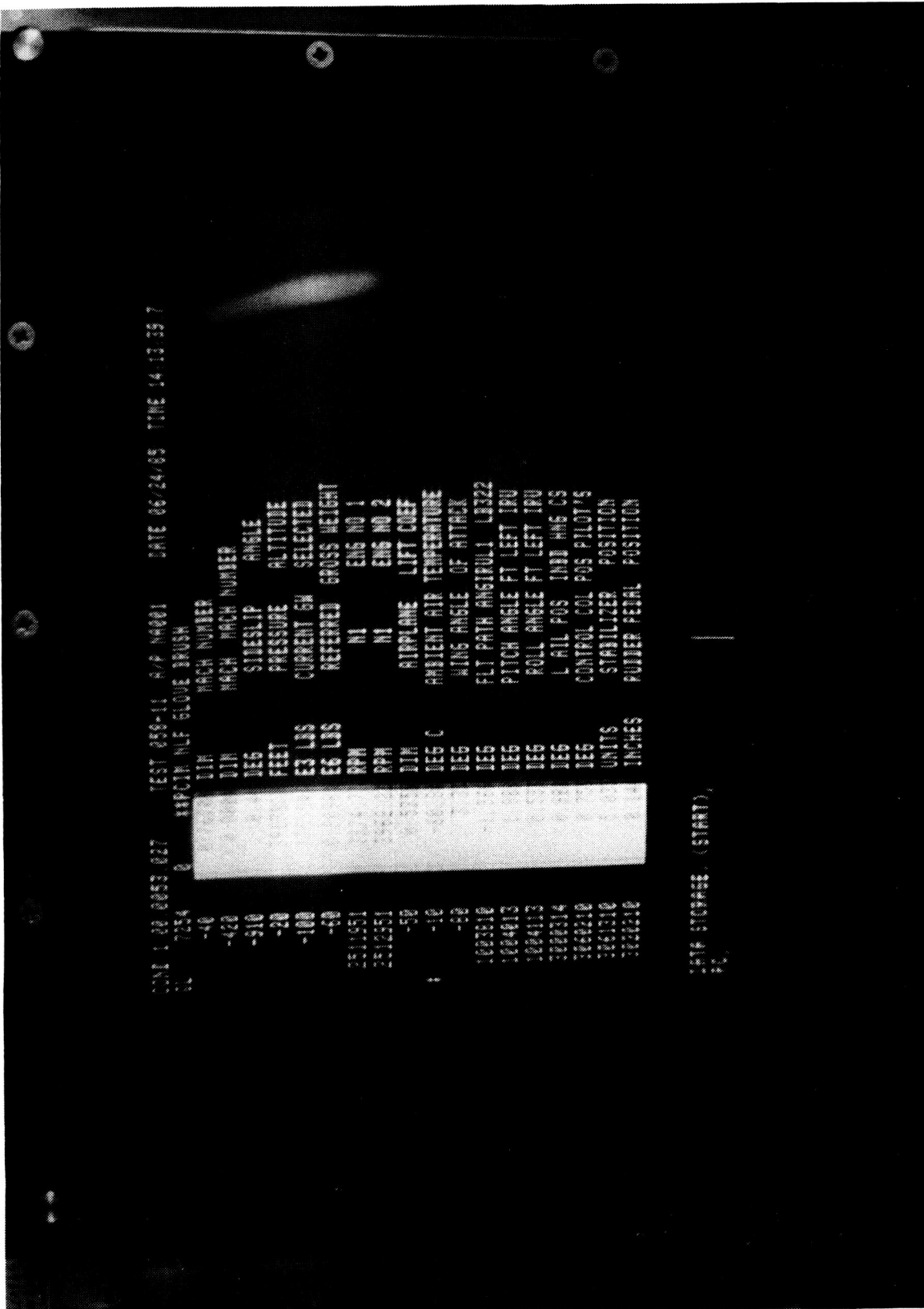


Figure 6-1. Video Monitor for Flight Parameters

- X Hot-film sensor
- Strip-a-tube static pressure
- + Probe-mounted microphone
- Surface-mounted microphone

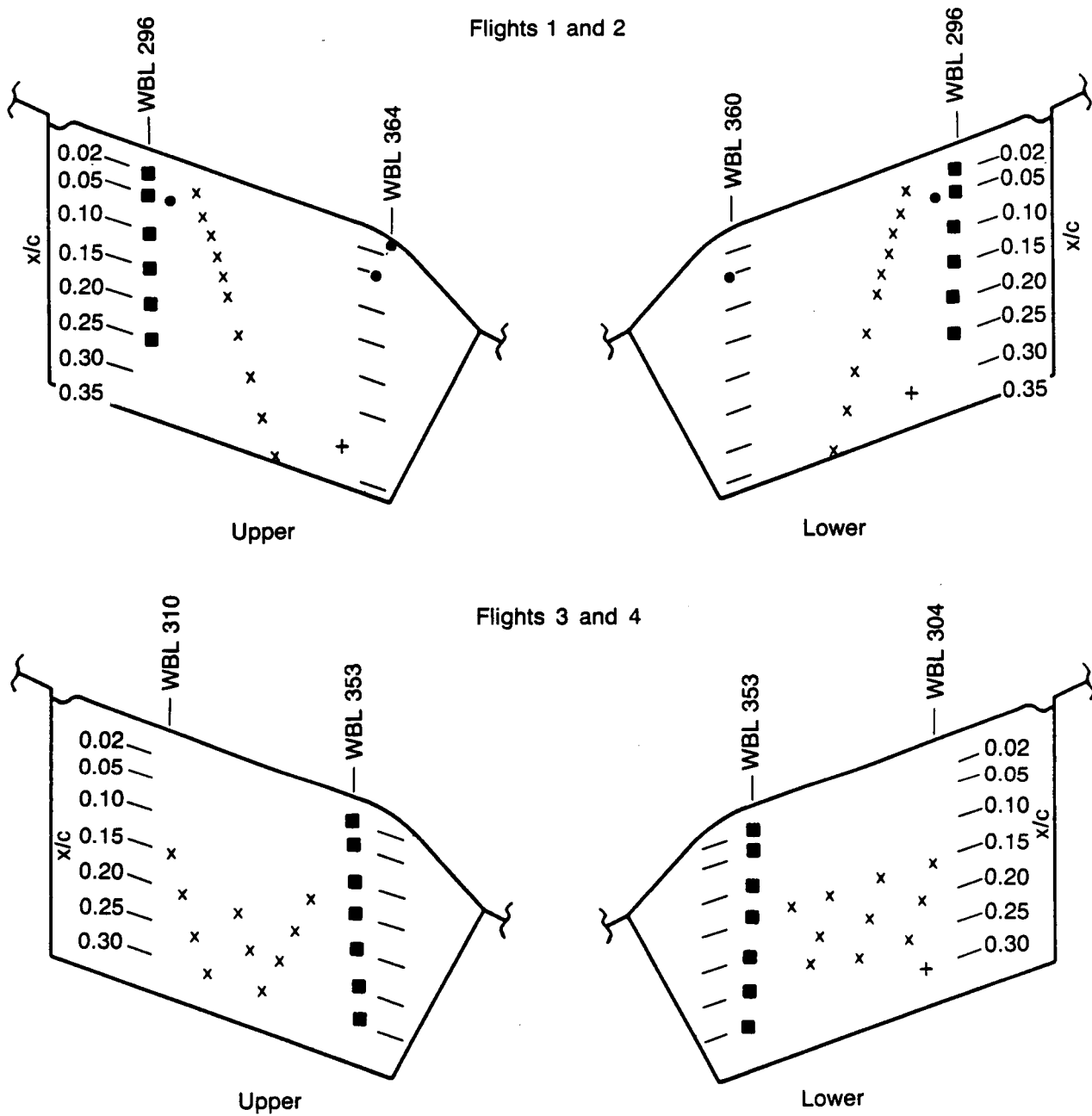
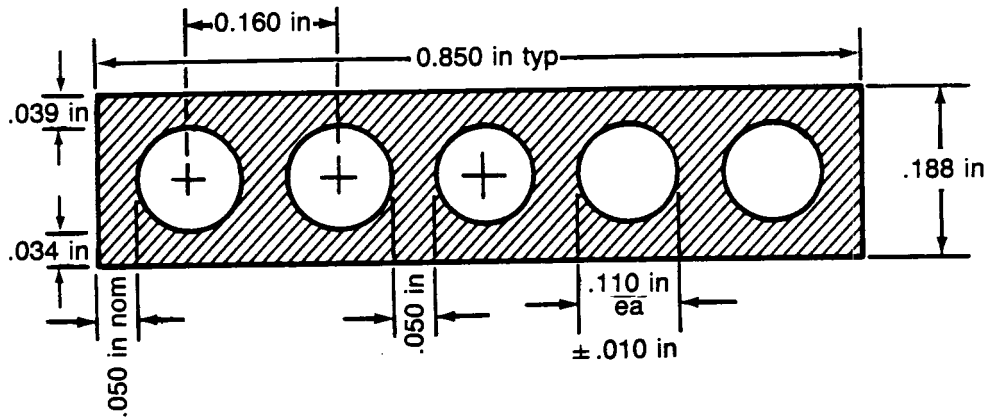


Figure 6-2. 757 NLF Glove Instrumentation

Strip-a-Tube Details
Single Belt Cross Section



PVC Wedge Fairing

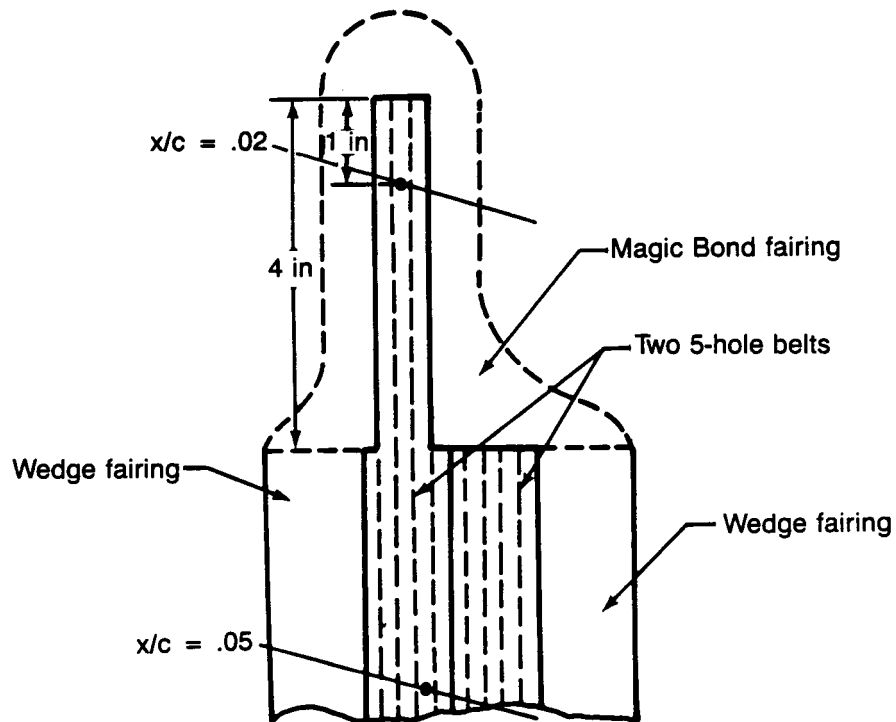
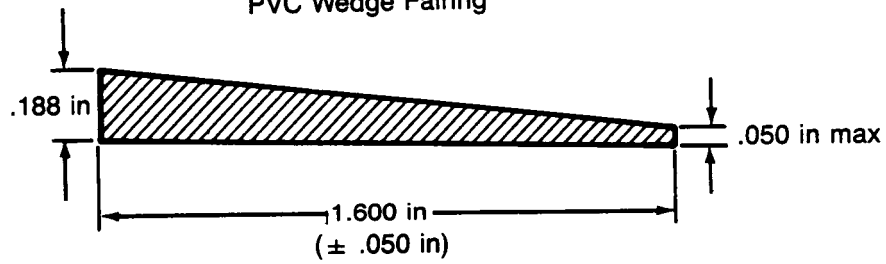
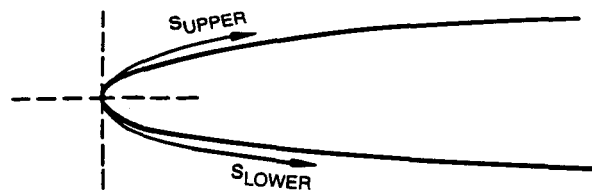


Figure 6-3. Pressure Belt Installation

Table 6-1. Static Pressure Orifice Locations

Inboard belt (center at WBL 296)			
Hole no.	x/c	s _{UPPER} (in)	s _{LOWER} (in)
1	0.02	5.6	5.4
2	0.05	12.0	11.7
3	0.10	22.5	22.1
4	0.15	32.9	32.4
5	0.20	43.3	42.8
6	0.25	53.6	53.0

Outboard belt (center at WBL 353)			
● c = 196.71 in			
Hole no.	x/c	s _{UPPER} (in)	s _{LOWER} (in)
1	0.02	6.0	5.4
2	0.05	12.1	11.4
3	0.10	22.1	21.3
4	0.15	32.0	31.2
5	0.20	41.8	41.1
6	0.25	51.7	50.9
7	0.30	61.5	60.7



Note: s is the distance along the wing surface from the most forward point of the wing

Table 6-2. Hot-Film Locations for Flights 1 and 2

- The WBL locations given below are for the most outboard point of a given sensor
- The x locations given below are for the most forward point of a given sensor

Upper surface					
Hot-film no.	WBL ~ in	c (in)	x/c	s/c	s (in)
1	310.0	202.57	0.02	0.0279	5.7
2	311.8	202.33	0.05	0.0584	11.8
3	313.3	202.12	0.075	0.0849	17.2
4	314.8	201.92	0.10	0.1103	22.3
5	316.3	201.71	0.125	0.1358	27.4
6	317.8	201.51	0.15	0.1610	32.4
7	320.8	201.10	0.20	0.2115	42.5
8	323.8	200.69	0.25	0.2618	52.5
9	326.8	200.29	0.30	0.3119	62.5
10	329.8	199.88	0.35	0.3619	72.3

Lower surface					
Hot-film no.	WBL ~ in	c (in)	x/c	s/c	s (in)
1	310.0	202.57	0.02	0.0266	5.4
2	311.8	202.33	0.05	0.0573	11.6
3	313.3	202.12	0.075	0.0826	16.7
4	314.8	201.92	0.10	0.1079	21.8
5	316.3	201.71	0.125	0.1330	26.8
6	317.8	201.51	0.15	0.1582	31.9
7	320.8	201.10	0.20	0.2083	41.9
8	323.8	200.69	0.25	0.2584	51.9
9	326.8	200.29	0.30	0.3084	61.8
10	329.8	199.88	0.35	0.3584	71.6

- Notes: 1. s is the distance along the wing surface from the most forward point of the wing at the y location of the sensor.
2. c is the local chord length including the glove and is given for reference.

Table 6-3. Hot-Film Locations for Flights 3 and 4

Upper surface			
Hot-film no.	y (WBL ~ in)	d (in)	x/c
1	302.5	6.9	0.15
2	305.5	10.1	0.20
3	308.5	13.3	0.25
4	311.5	16.5	0.30
5	320.8	26.4	0.20
6	323.8	29.6	0.25
7	326.8	32.8	0.30
8	331.5	37.8	0.25
9	336.5	43.1	0.20
10	341.0	47.9	0.15

Lower surface			
Hot-film no.	y (WBL ~ in)	d (in)	x/c
1	304.0	8.5	0.15
2	307.0	11.7	0.20
3	310.0	14.9	0.25
4	317.8	23.2	0.15
5	320.8	26.4	0.20
6	323.8	29.6	0.25
7	332.0	38.3	0.15
8	335.0	41.5	0.20
9	337.0	43.6	0.235
10	342.5	49.5	0.15

- The y locations are for the most outboard point of a given sensor
- The d values are the distances along the given x/c line from WBL 296

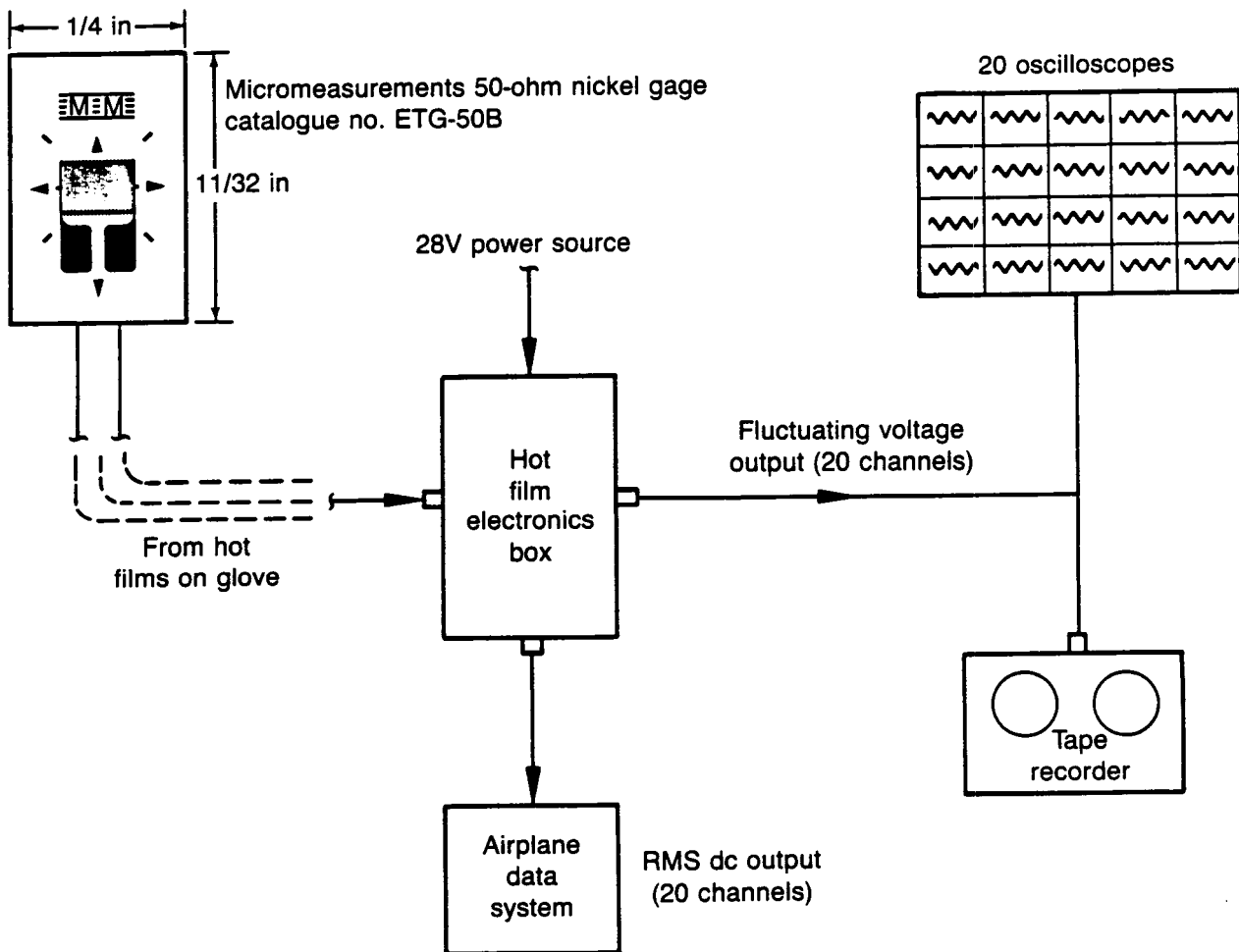


Figure 6-4. Transition Sensing System Using Hot Films

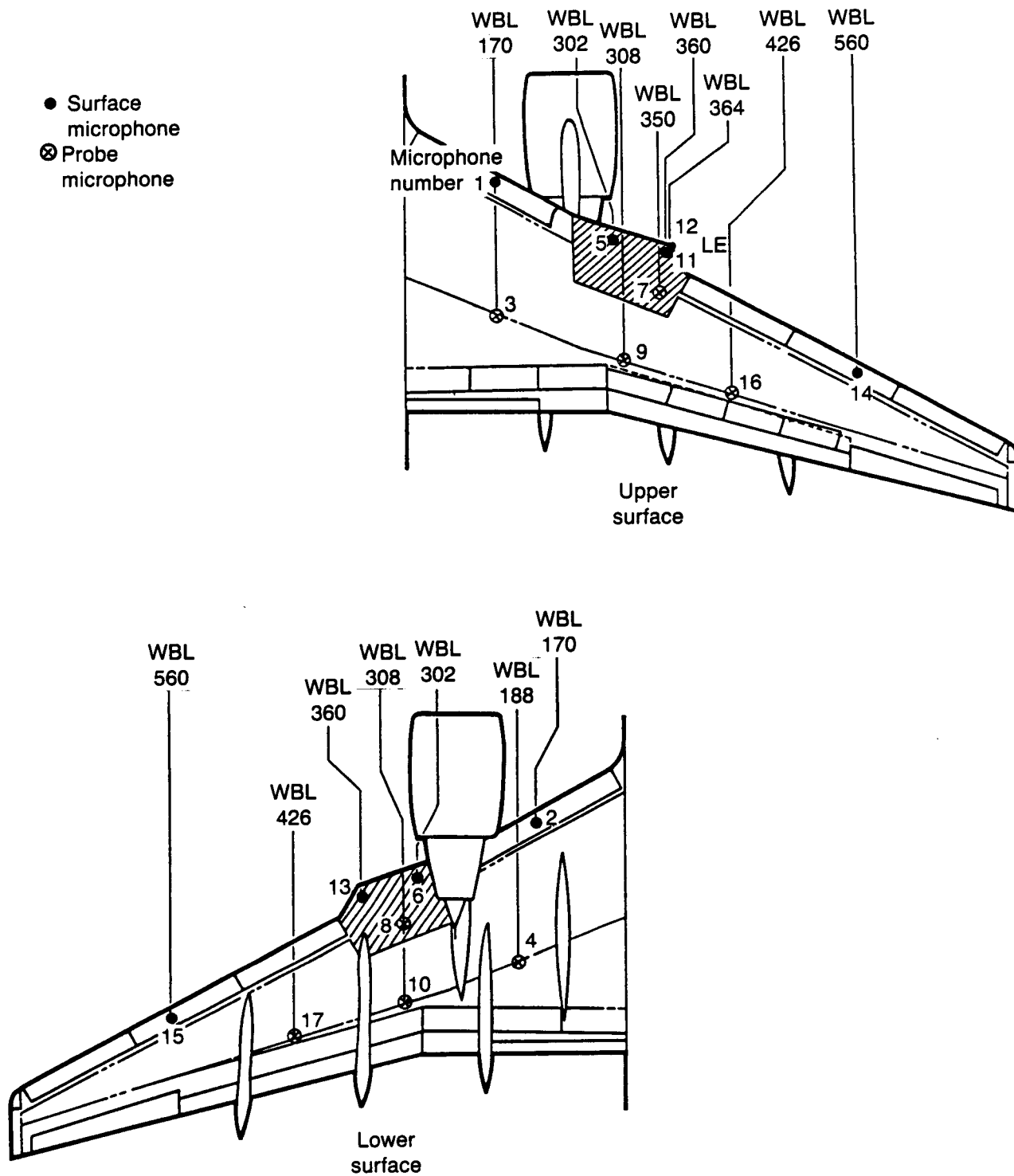
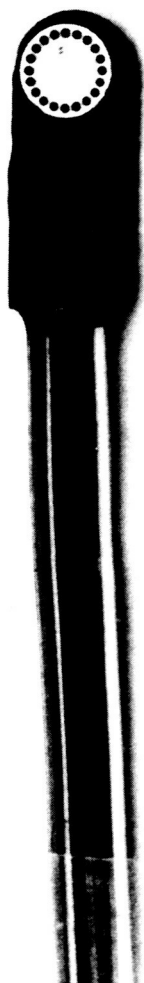
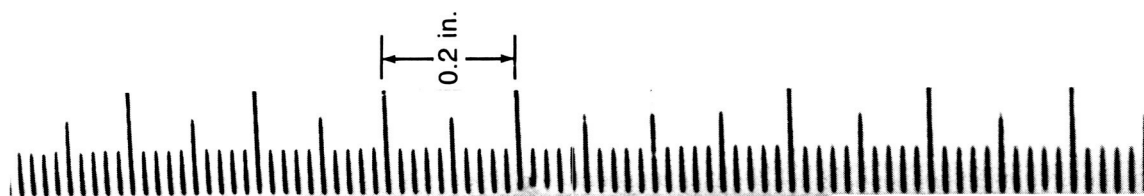
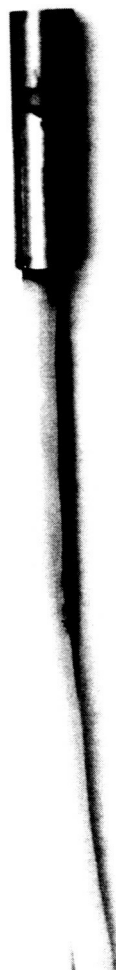


Figure 6-5. Microphone Arrays on Wing Upper and Lower Surfaces



LQ-101-125-5D (surface mounted)

Pressure range 0-5 lb/in²
 1V equiv sens 198.7 dB
 Noise floor 70 dB
 (1/3 OB, measured at 1 kHz)
 Excitation voltage 10V dc



XCW-093-5G (probe mounted)

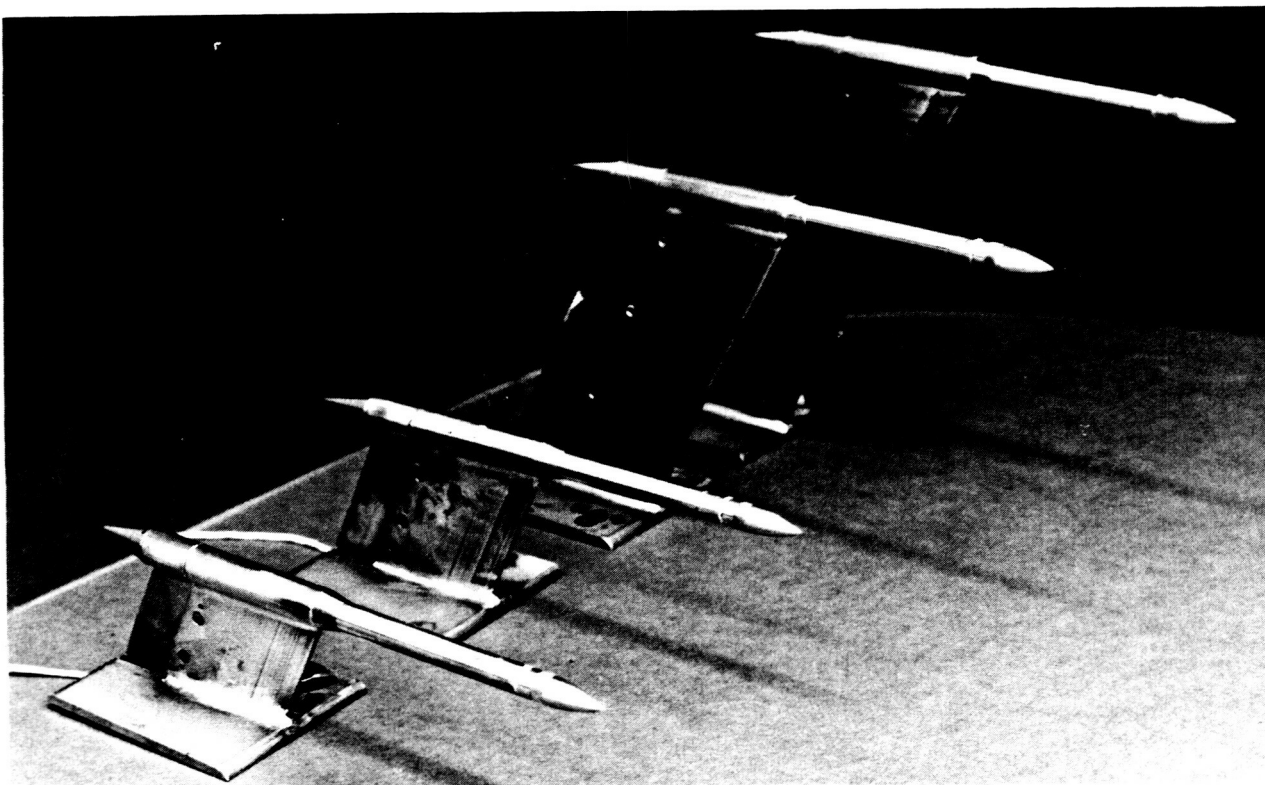
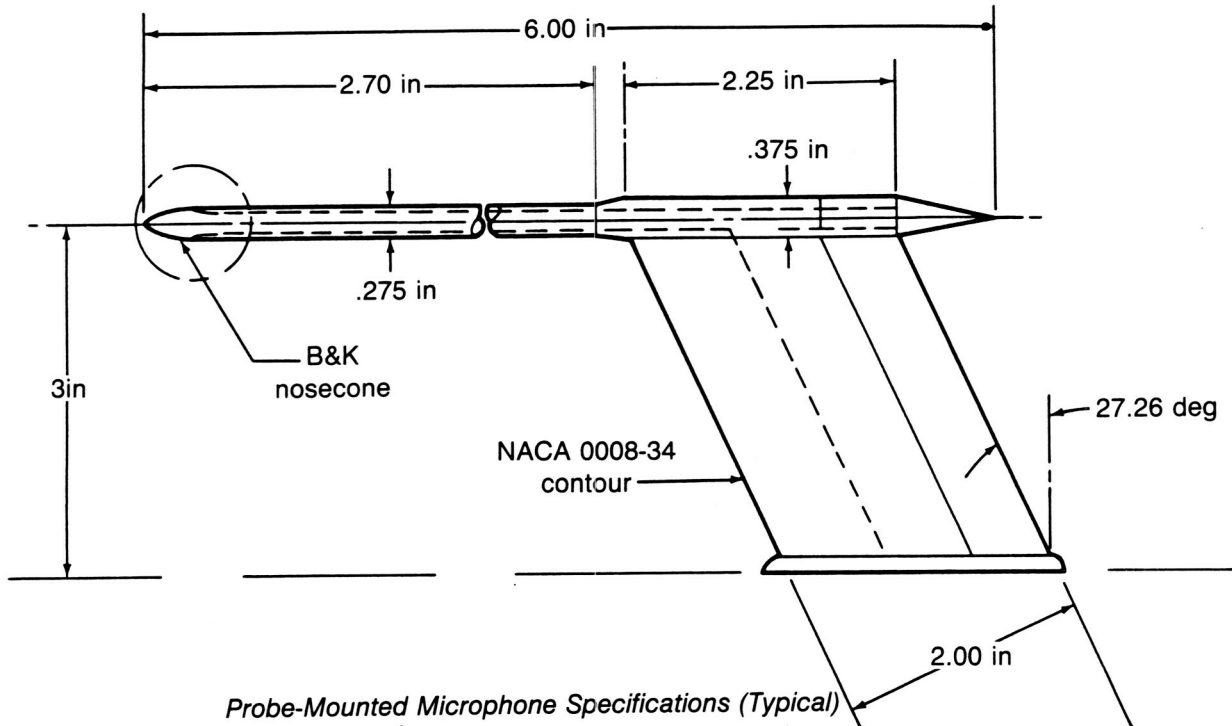
Pressure range 0-5 lb/in²
 1V equiv sens 202.8 dB
 Noise floor 70 dB
 (1/3 OB, measured at 1 kHz)
 Excitation voltage 15V dc

Figure 6-6. Acoustic Sensor Types and Specifications

Table 6-4. Microphone Installation Geometry Specification

Microphone no.	WBL	Wing surface	Nominal chord, x/c	Approximate distance from leading edge, in	Type	Probe height, in	Probe angle, deg
1	170	Upper	0.05	8	Surface		
2	170	Lower	0.05	8	Surface		
3	170	Upper	0.6	156	Probe	5	6
4	188	Lower	0.6	156	Probe	4	0
5	302	Upper glove	0.05	11.9	Surface		
6	302	Lower glove	0.05	11.7	Surface		
7	350	Upper glove	0.3	63.4	Probe	1.5	7
8	308	Lower glove	0.3	62.7	Probe	1.5	3
9	308	Upper	0.6	141	Probe	4	5
10	308	Lower	0.6	141	Probe	3	1
11	360	Upper glove	0.05	11.4	Surface		
12	364	Leading edge	0	0	Surface		
13	360	Lower glove	0.05	11.2	Surface		
14	560	Upper	0.05	8	Surface		
15	560	Lower	0.05	8	Surface		
16	426	Upper	0.6	109	Probe	3	6
17	426	Lower	0.6	109	Probe	2	1.5

ORIGINAL PAGE IS
OF POOR QUALITY



Probe-Mounted Microphone Configurations ($h = 1.5, 2, 4, 5$)

Figure 6-7. Probe-Mounted Microphone Arrangements

ORIGINAL PAGE IS
OF POOR QUALITY

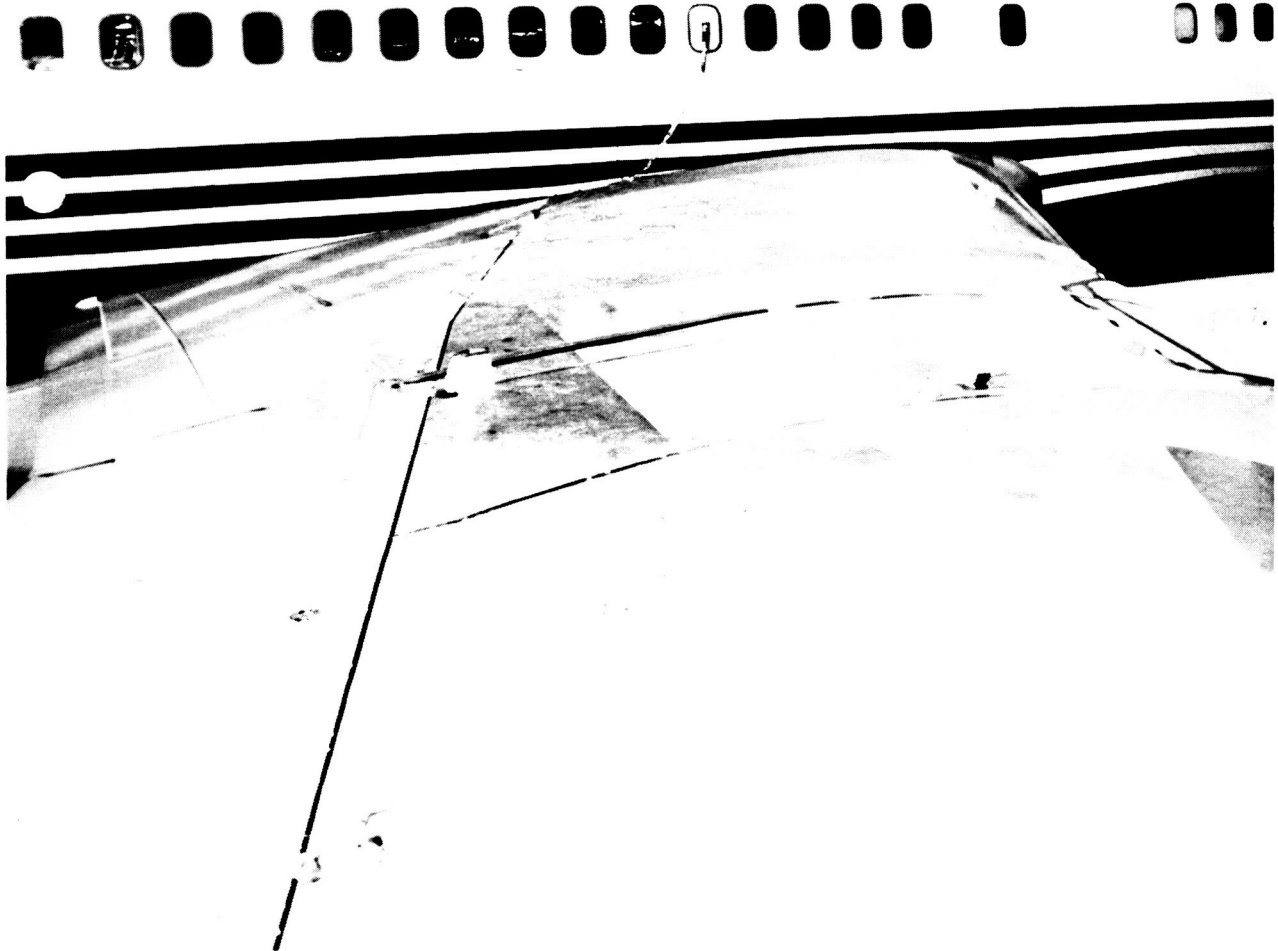
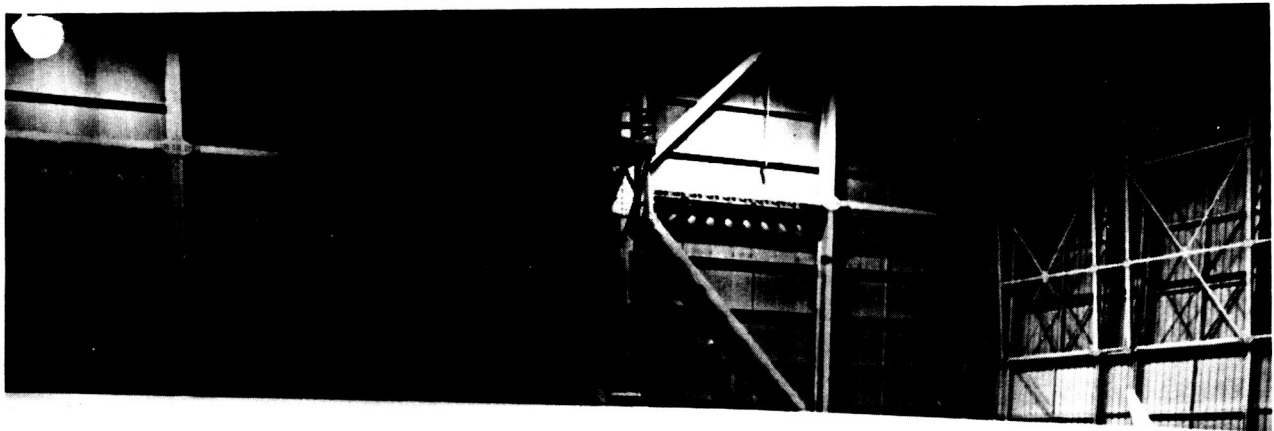


Figure 6-8. Instrumentation Array on Wing Upper Surface



Figure 6-9. Instrumentation Array on Wing Lower Surface

ORIGINAL PAGE IS
OF POOR QUALITY

ORIGINAL PAGE IS
OF POOR QUALITY

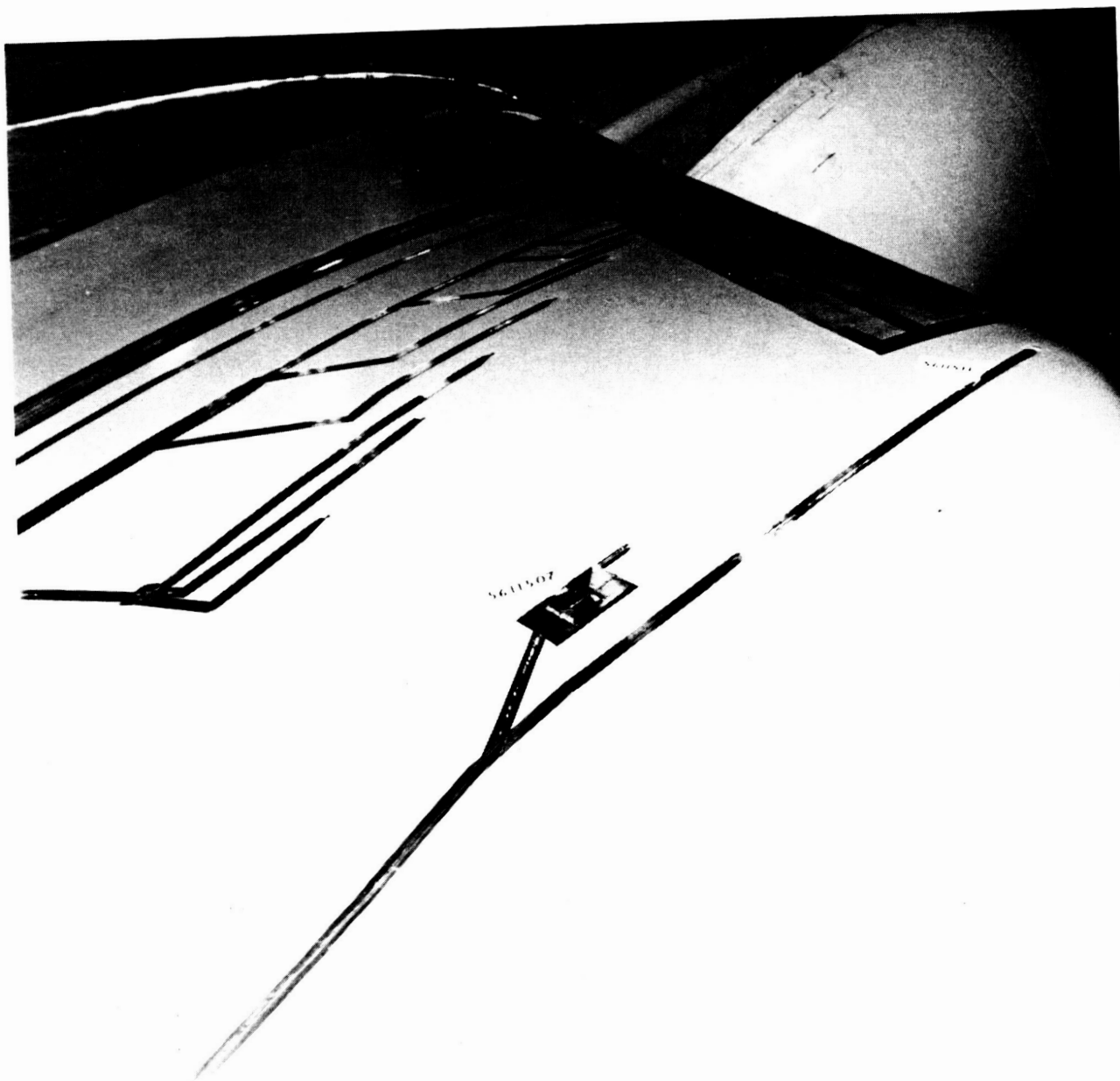


Figure 6-10. Instrumentation Array on Glove Upper Surface

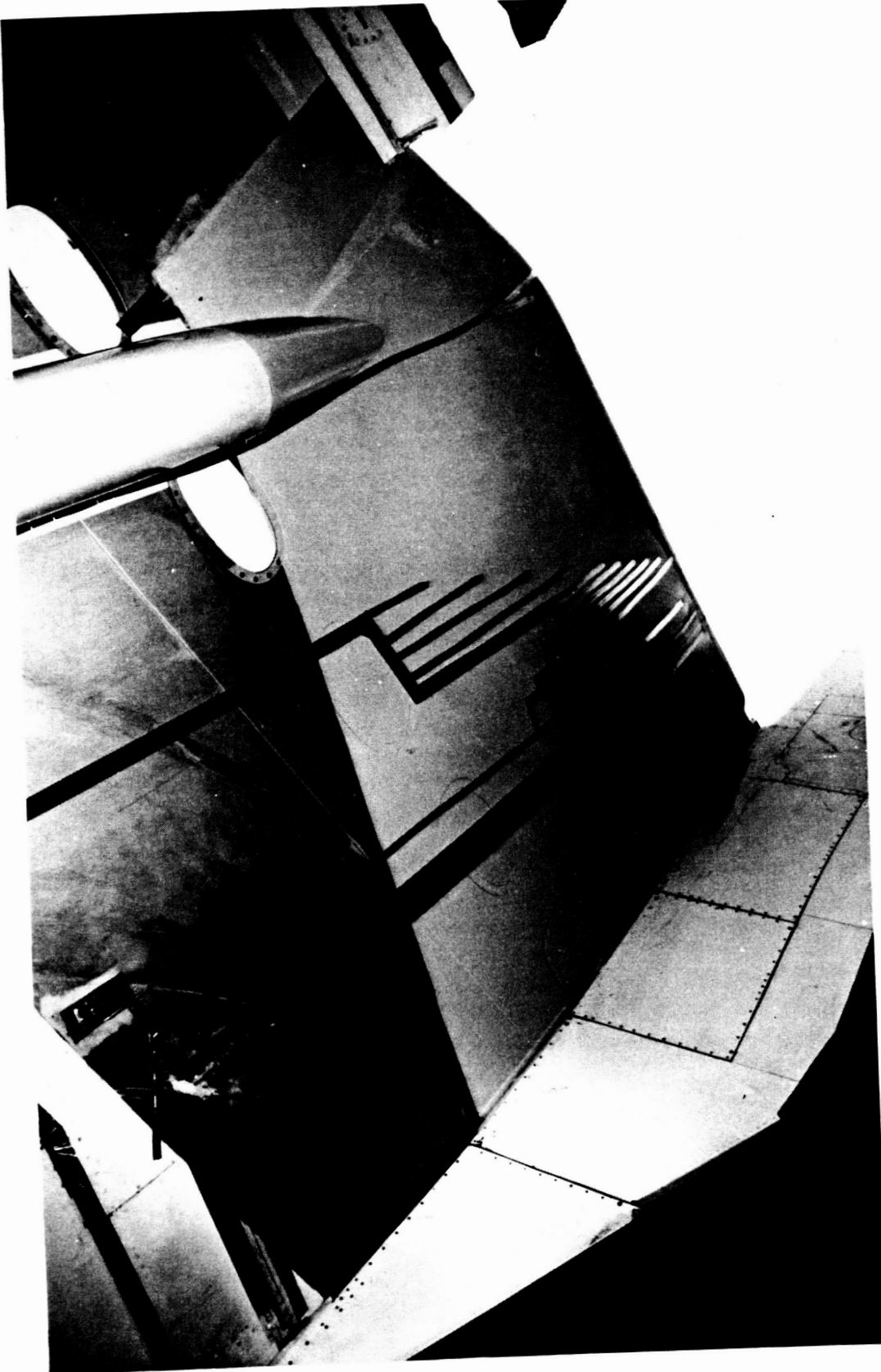
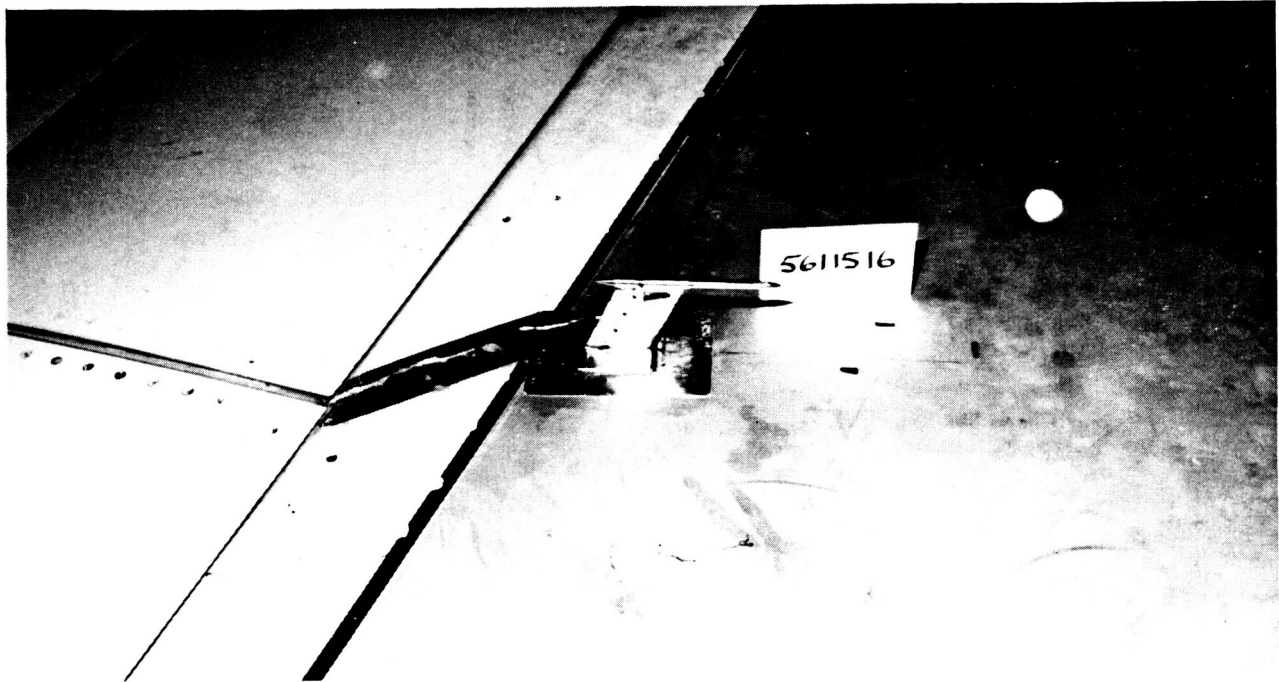


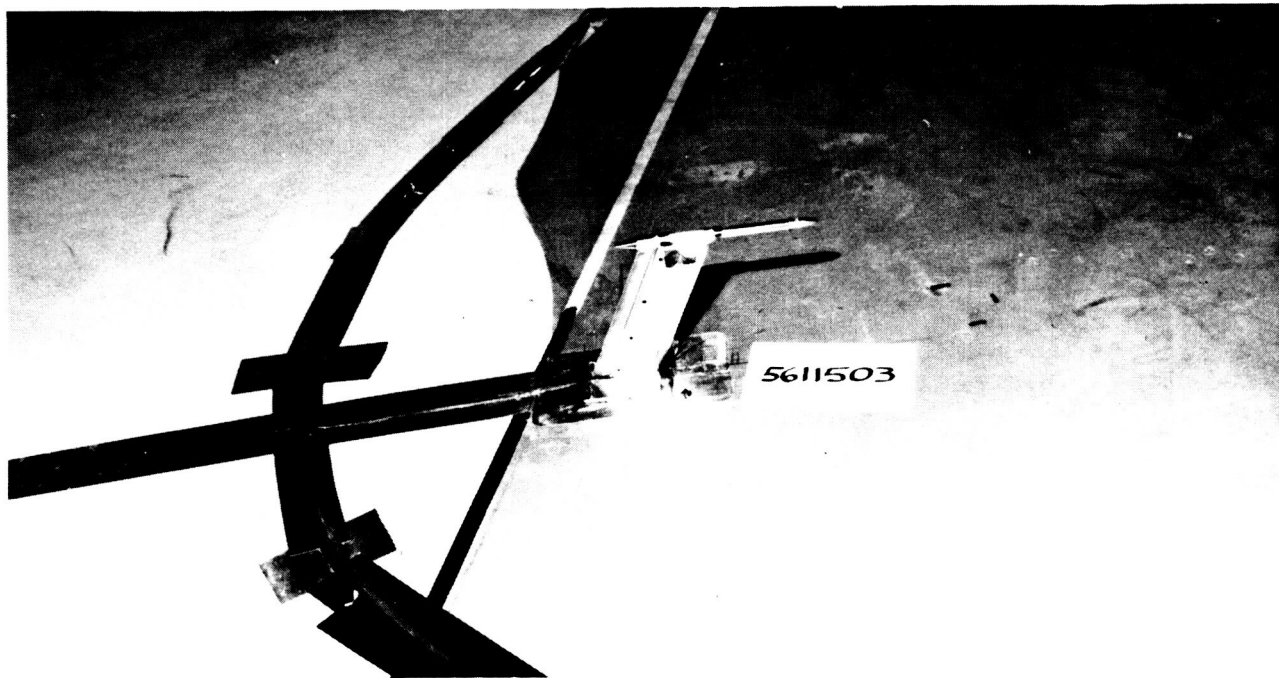
Figure 6-11. Instrumentation Array on Glove Lower Surface

ORIGINAL PAGE IS
OF POOR QUALITY

ORIGINAL PAGE IS
OF POOR QUALITY

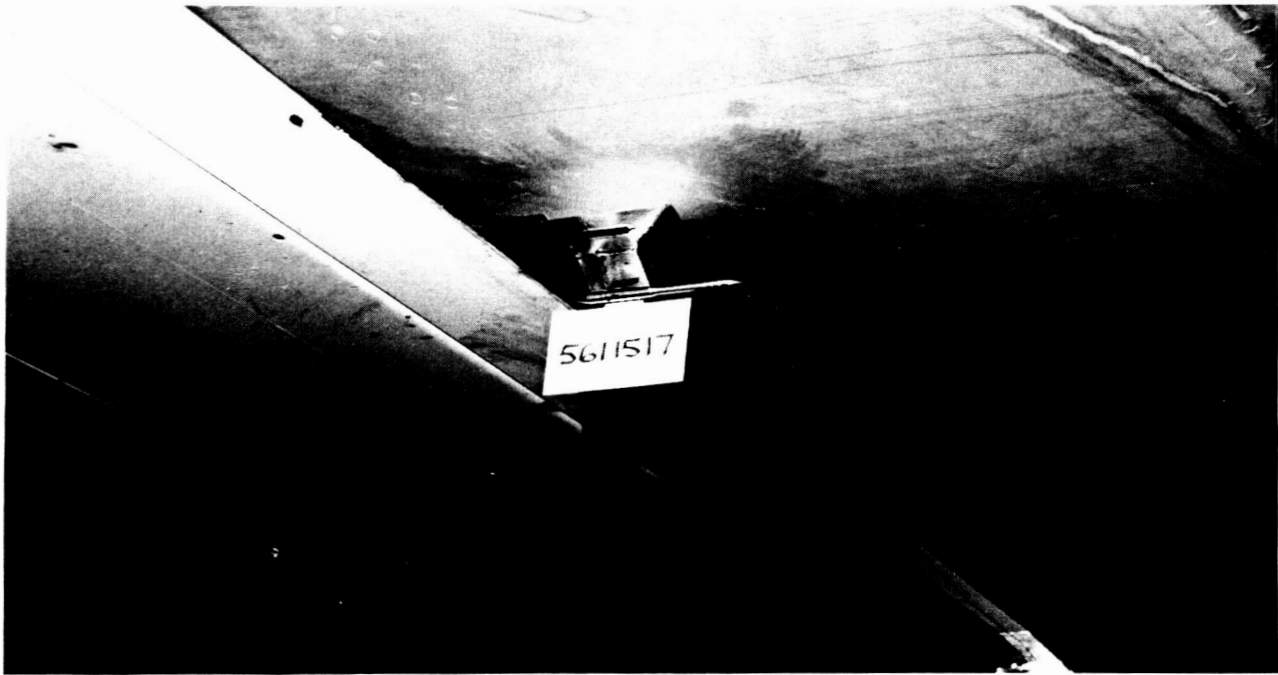


Outboard Probe Installation Microphone 16

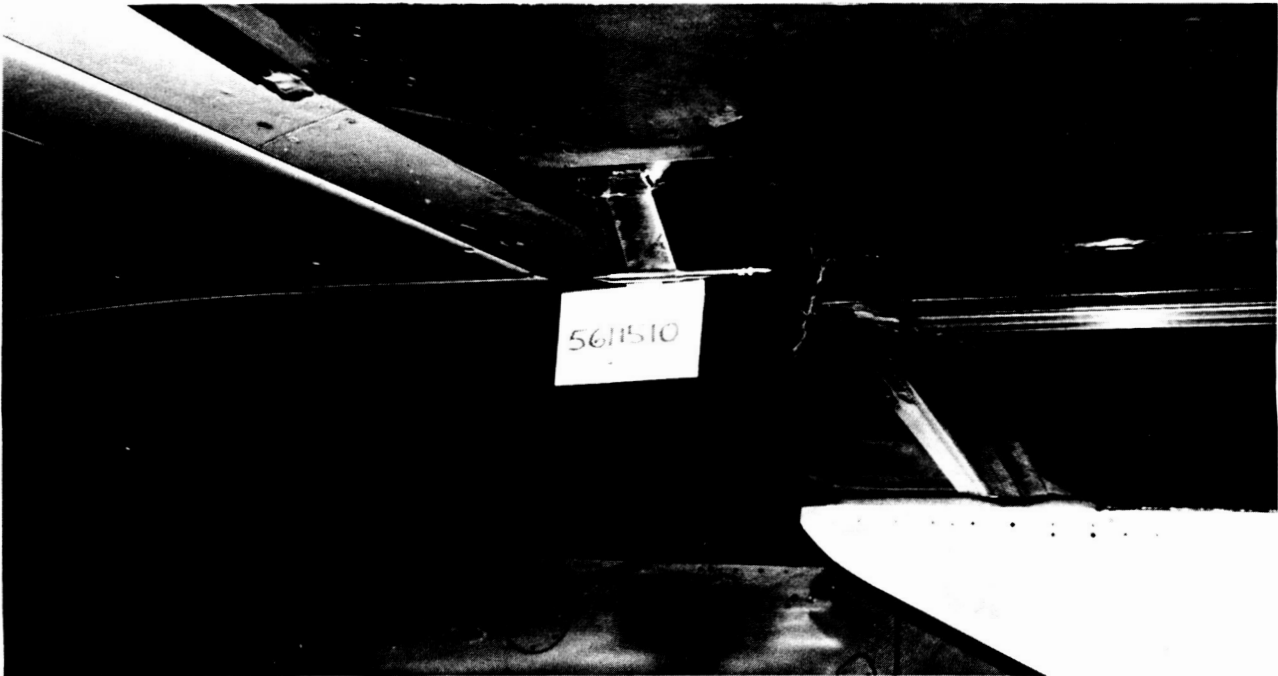


Inboard Probe Installation Microphone 3

Figure 6-12. Typical Upper Surface Probe Installations



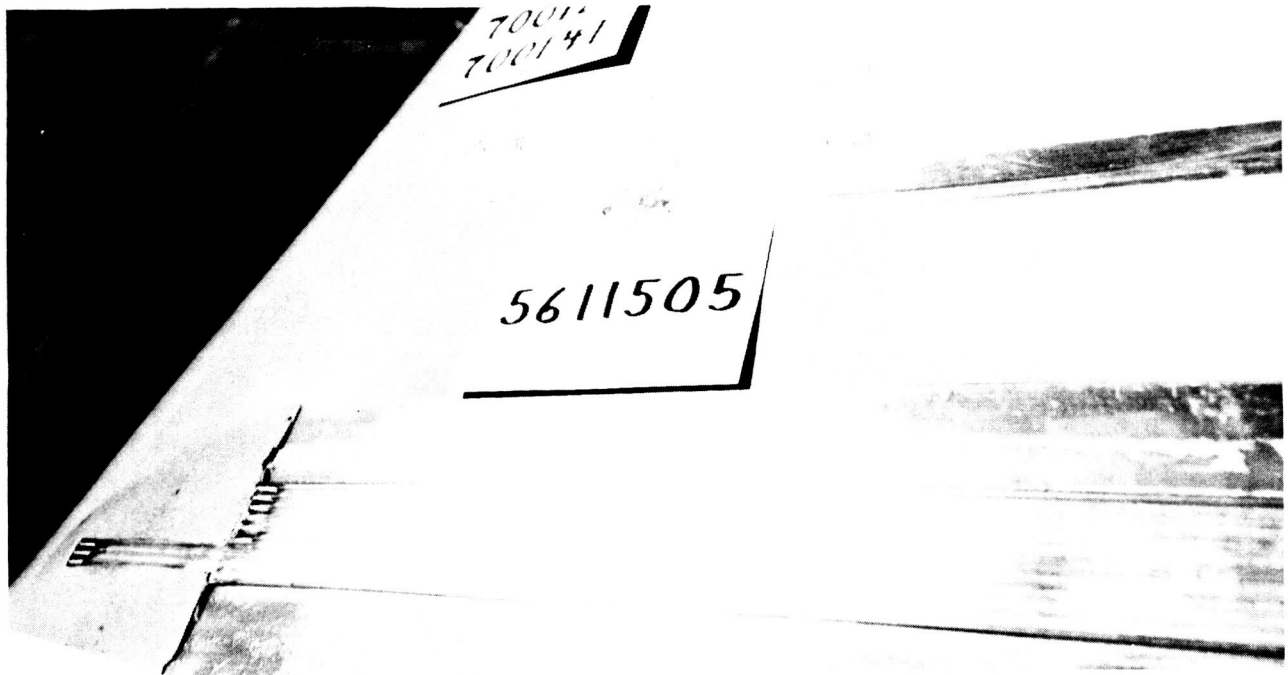
Outboard Probe Installation Microphone 17



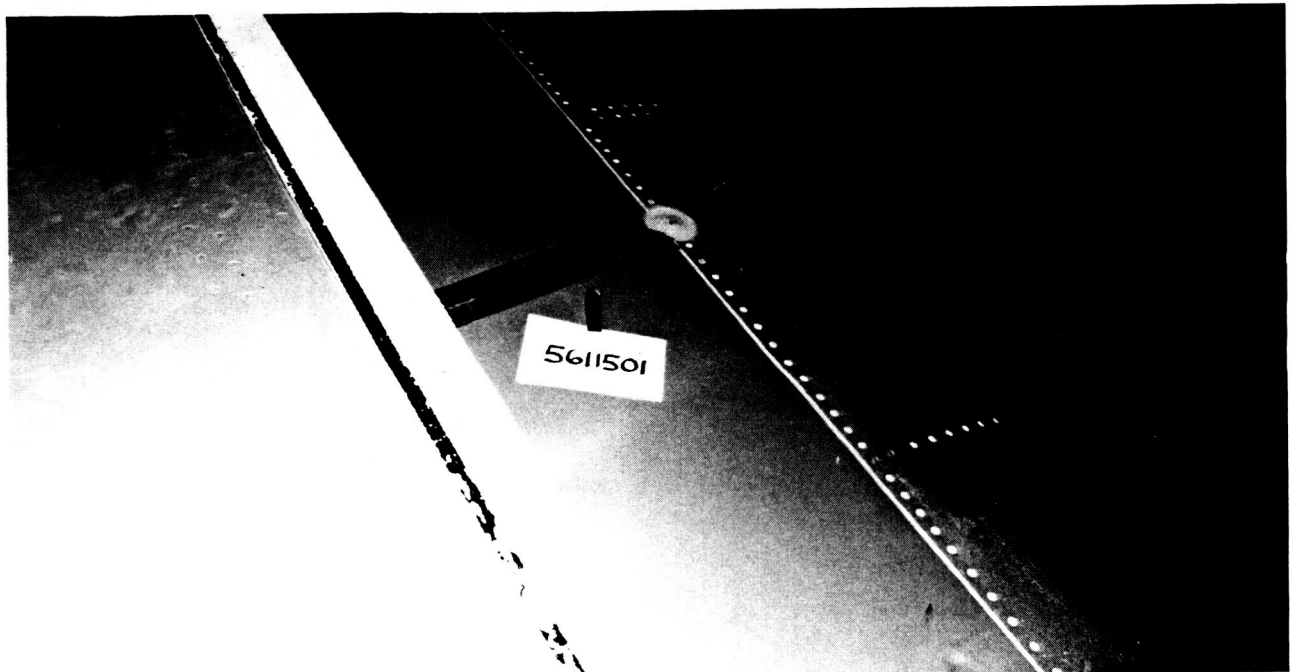
Midspan Probe Installation Microphone 10

Figure 6-13. Typical Lower Surface Probe Installations

ORIGINAL PAGE IS
OF POOR QUALITY

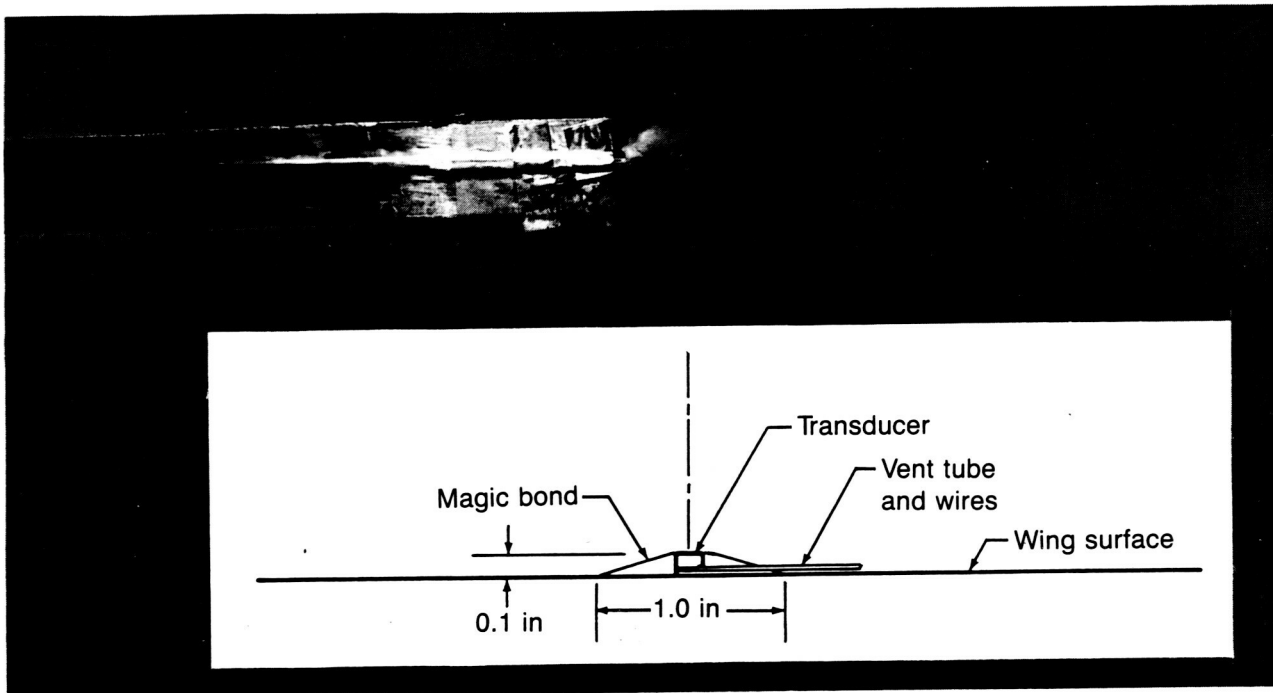


Glove Surface Microphone Installation (Mic 5)

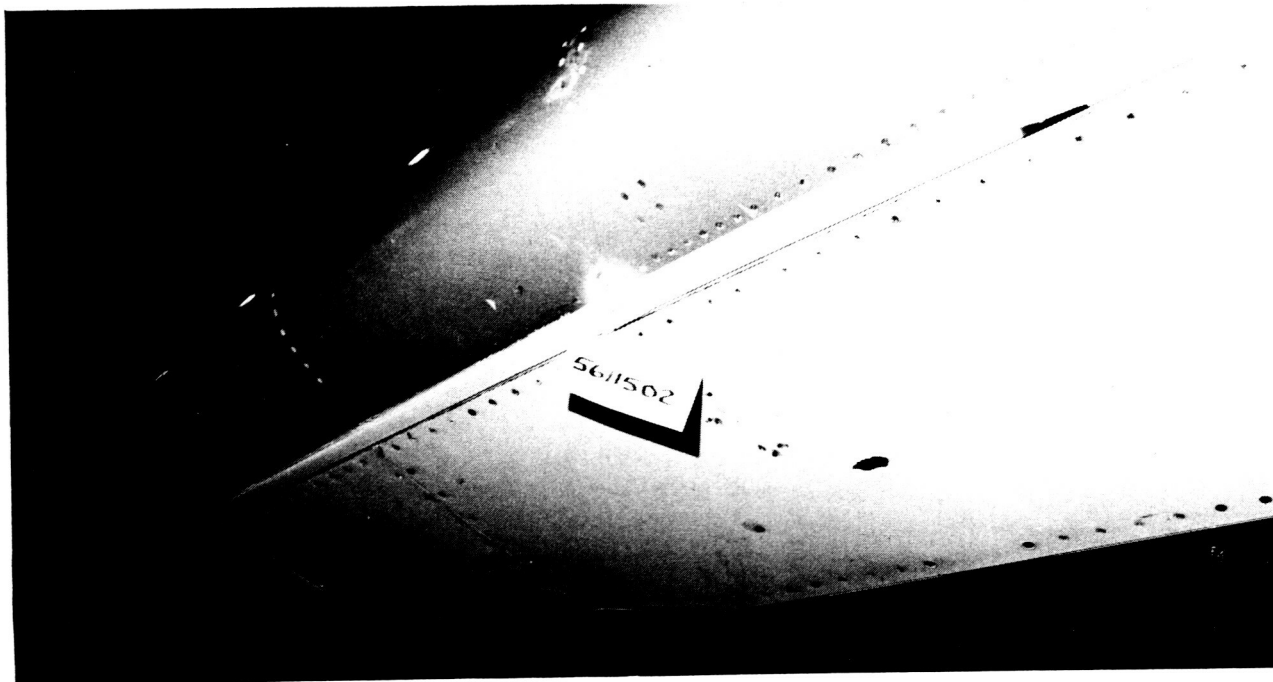


Leading Edge Slat Surface Microphone (Mic 1)

Figure 6-14. Typical Surface-Mounted Microphone Installations



Surface Microphone Fairing Detail



Lower Surface Microphone Installation

Figure 6-15. Typical Surface-Mounted Microphone Installations

ORIGINAL PAGE IS
OF POOR QUALITY

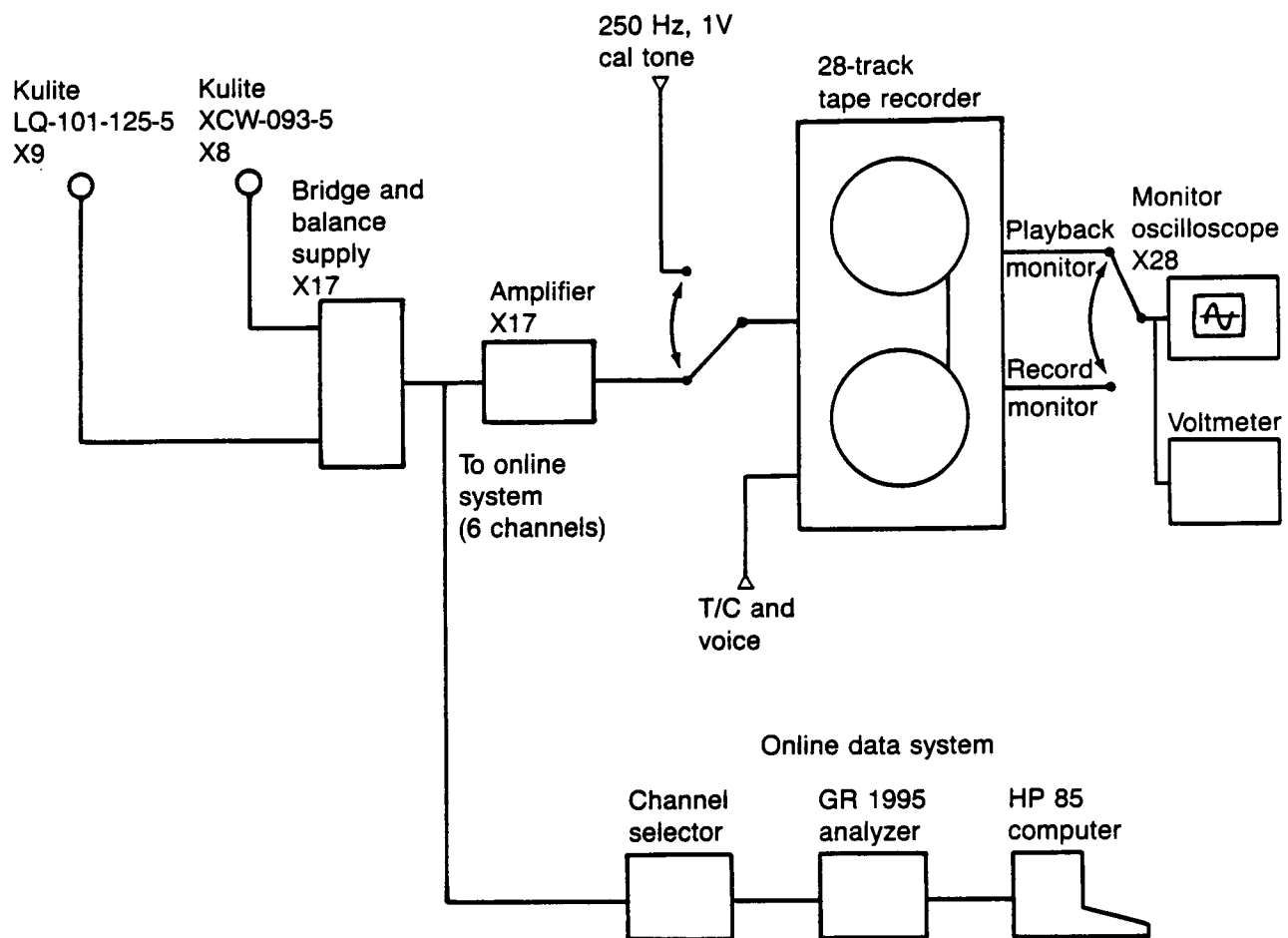


Figure 6-16. Data Acquisition System Schematic

ORIGINAL PAGE IS
OF POOR QUALITY

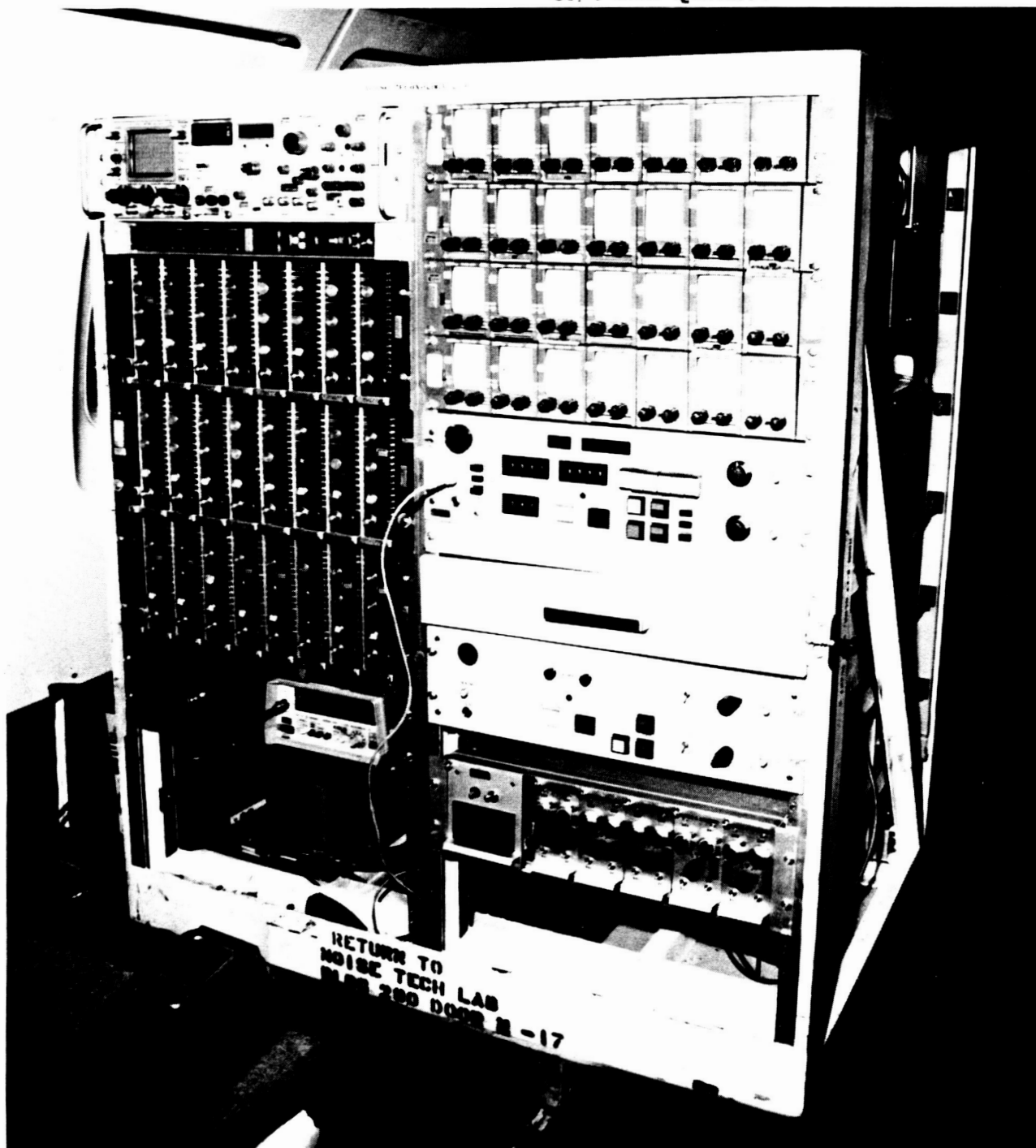


Figure 6-17. Acoustic Signal Conditioning Electronics

ORIGINAL PAGE IS
OF POOR QUALITY



Figure 6-18. Acoustic Data Recording System

ORIGINAL PAGE IS
OF POOR QUALITY



Figure 6-19. Online Data Reduction System

System no. 2
ID---LQ 2032-2-50
E and response, dB

14	0.29
15	0.16
16	0.19
17	0.13
18	0.11
19	0.08
20	0.06
21	0.05
22	0.04
23	0.02
24	0.00
25	-0.01
26	-0.02
27	-0.02
28	-0.02
29	-0.02
30	-0.02
31	0.03
32	0.05
33	-0.05
34	-0.14
35	-0.11
36	0.04
37	0.32
38	0.40
39	0.56
40	1.21
41	1.04
42	0.67
43	4.71

System no. 4
ID---LQ 404-6-83
E and response, dB

14	0.36
15	0.17
16	0.12
17	0.08
18	0.08
19	0.05
20	0.04
21	0.03
22	0.01
23	0.00
24	0.00
25	-0.01
26	-0.01
27	-0.01
28	-0.01
29	0.00
30	0.01
31	0.02
32	0.03
33	-0.01
34	-0.05
35	-0.10
36	0.02
37	0.18
38	0.45
39	0.41
40	0.63
41	0.49
42	0.94
43	2.50

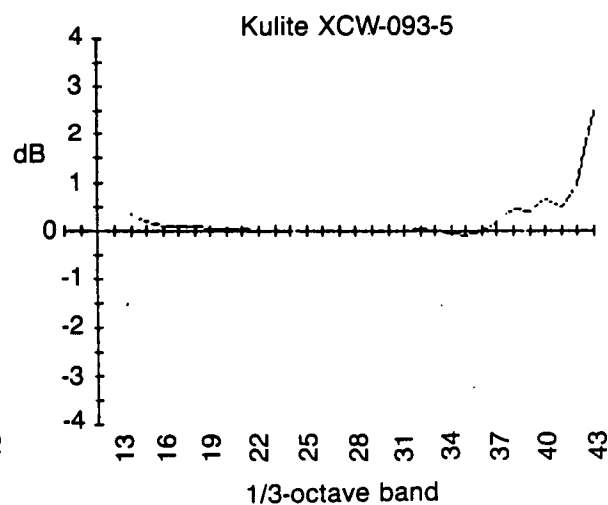
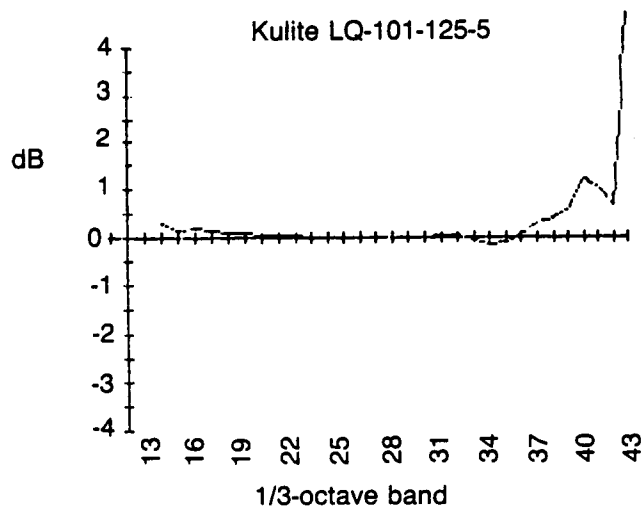


Figure 6-20. Typical Frequency Response Calibration Data — Normalized to 250 Hz

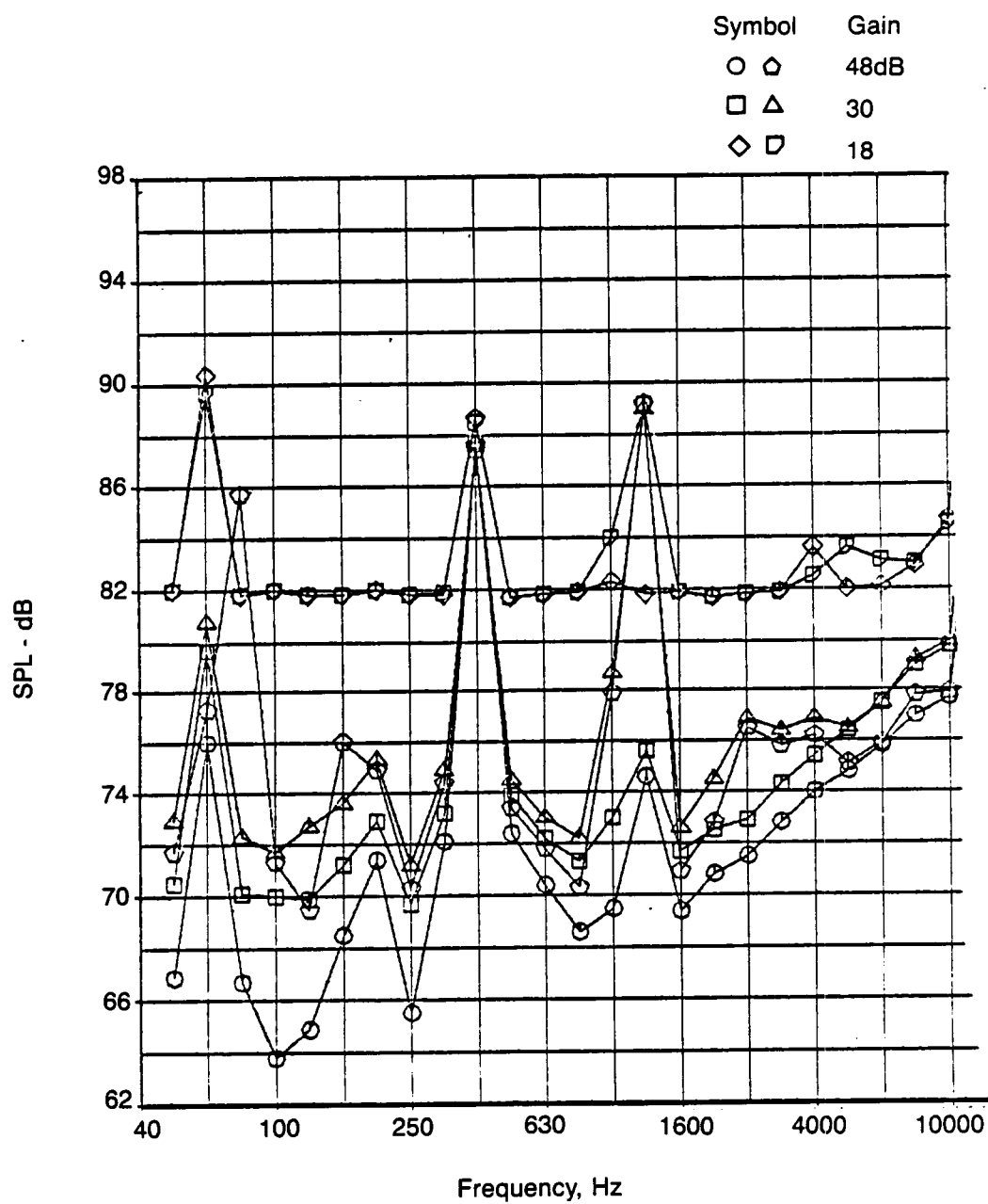


Figure 6-21. Typical Ambient Noise Floor Microphone 11

7.0 GLOVE FABRICATION AND INSTALLATION

The glove fabrication and installation were carried out according to a plan established in conjunction with the glove design and development phase. Particular attention was devoted to definition of an approach to minimize cost and to provide a method for glove contouring and final finishing to meet exacting requirements for laminar flow surfaces. The cost was controlled by selecting a concept requiring few parts and a method of assembly for which positive indexing could be used to assure adequate contour and shape control. For ease and control of final finish, the definition of two spanwise control stations from which straight-line spanwise elements could be projected was the central feature. Otherwise, generally accepted techniques for the assembly and installation of foam base structures with fiberglass-epoxy overlay were chosen on the basis of Boeing experience in this area. The final finish was essentially a manual process involving the use of personnel skilled in model making or tool and die techniques.

7.1 FABRICATION

Fabrication of all glove components took place in the Boeing Developmental Manufacturing shops located at North Boeing Field, Seattle. Installation of components, layup of the fiberglass cover, and application of the finish was accomplished by the Boeing Flight Test organization using people on loan from the appropriate Developmental Manufacturing shops.

With the exception of the urethane foam filler blocks, all component details were relatively conventional. The blocks made up the body of the glove with the inside contour matching that of the airplane wing and the outside contour forming the new airfoil surface. The blocks were machined in three pieces, which was the fewest number of pieces possible for the arrangement chosen. The three blocks comprised a large leading edge block, an upper wing panel, and a lower wing panel which were machined on a G&L NC mill with a horizontal spindle. Figure 7-1 illustrates the steps in the machining process for the large nose piece which was later cut into six pieces. Figure 7-2 is a photograph of the machined leading edge foam block taken before removal of indexing and supporting members. The upper and lower wing panels were machined using a backup panel to maintain stiffness during this process. Figure 7-3 is a photograph of the upper surface machined foam block taken with the supporting panel still in place.

Several of the steps involved in installation and finishing of the glove presented unusual problems, so it was advisable to conduct tests to prove out certain processes or materials selection. For example, the Materials and Technology unit made reduced-scale models of the segments of the wing leading edge and of the leading edge and join area between the glove and wing. These were used to test proposed treatments to protect the wing surface and to establish the adhesion characteristics and the flow of the material used to bond the foam blocks to the wing. Manufacturing Research and Development, using materials specified on the assembly drawing, laid up and cured a large fiberglass test panel on an overhead surface in order to verify the technique. Also, a series of fiberglass-epoxy test panels were made on which different fillers and finishes were applied to help in the selection of the final finishing processes.

7.2 INSTALLATION

All glove parts and supporting structure elements were completed prior to the airplane layup for installation. Figure 7-4 shows the main parts in their appropriate relationships for assembly on the wing. Before assembly could begin, removal of the slat and preparation of the mating surfaces was necessary. Modest revision to systems in the leading edge areas was also required in order to maintain normal operation of the remaining leading edge slats and other airplane systems. The various steps in the installation process including the final glove finishing and preparation for instrumentation are illustrated in Figure 7-5.

The large center leading edge foam block was used as a tool to locate other components of the glove. It was temporarily installed on the airplane wing .060 away from the wing surface and clamped in position. Metal support arms, beams, and attach angles were located to the center block and marked or

drilled in preparation for final assembly. They were then removed along with the foam block and the wing surfaces were sanded, reprimed, and the peel ply layers were installed in certain areas. The latter was necessary to protect the basic wing surfaces from damage that could involve extensive repair during refurbishment.

To prepare for the glove assembly bonding and finishing process, a plastic tent (fig. 7-6) was erected over the work area on the wing in order to maintain a temperature higher than 70°F, which was required to cure the adhesive being used. The actual installation proceeded in several steps starting with reinstallation of the metal support arms, beams, and angles. The three main leading edge foam blocks were then placed in position on the wing and the leading edge foam blocks secured in place on the support beams which were installed during the same operation. Liquid adhesive was then injected into the gaps between the foam blocks and wing, and the whole assembly was vacuum bagged. The temperature level in the tent was maintained for a period of 18 hr while the adhesive cured. When the bag was removed, it was discovered that one of the end foam blocks had moved during the bagging process. This area and the expected gaps along the support beams were filled and sanded to approximate the design contour. The upper and lower foam wing panels were then bonded to the wing, the assembly vacuum bagged and cured.

Some mismatches between the foam wing panels and the foam leading edge blocks were expected due to tolerance buildup and forces induced during the bagging and curing cycle. These did in fact occur on both upper and lower surfaces as illustrated in Figures 7-7 and 7-8. Filling was used in areas which were found too low or hollow on the basis of template checks. High areas that were clearly due to excessive adhesive or base layer thickness were sanded as required to bring the entire glove to within contour tolerances appropriate to this stage of the installation. Preparation for installation of the outer fiberglass layers included contour inspection and checking for adhesion in critical areas. Figure 7-9 shows the upper and lower surfaces of the glove in the final state prior to installation of the fiberglass outer shell.

It had been expected that two layup steps would be required for installation of the fiberglass-epoxy overlay—one for the first three plies and one for the final two plies. However, as the layup progressed, it was determined that all five layers could be installed at once. With the fiberglass in place the installation was vacuum bagged and cured for a period of 24 hr.

After application of the fiberglass surface and bag removal, rough sanding was used to remove adhesive accumulations, overlaps, and discontinuities. Templates were used to check the surface contours at WBL 296.3 and WBL 355.7, which are the inboard and outboard control stations, respectively, for that portion of the glove designed to have straight spanlines. Based upon those measurements, the surface was sanded and filled using accepted model finishing techniques. The control surfaces were worked to within $\pm .05$ in of the design contour over a strip about 3 in wide at both control stations. The waviness at these stations was then checked using a three-point waviness (or curvature) gage having a 2-in wheel-base and incorporating a dial indicator. The indication from the gage was interpreted in terms of the wave amplitude (i.e., crest to trough) for the range of wavelengths that are known to be critical for laminar flow.

After preparing the surfaces at stations WBL 296.3 and WBL 355.7, a rigid steel straightedge was used as a combination tool (fig. 7-10a) to sweep in filler or to define areas that required sanding between these two stations. The straightedge was kept parallel to the local spanlines and the surface was worked progressively (i.e., sanding and filling) until the gap between the straightedge and the surface was nominally within .001 in. Waviness checks in both chordwise and spanwise directions were also used (fig. 7-10b) during this process to highlight local areas where corrections were needed. The overall procedure described above was used in a step-by-step fashion to the point where the surface was judged to be within tolerances for both contour and waviness.

7.3 SURFACE CHECKING AND FINISHING

The measured contour deviations of the final glove surface (prior to painting) at stations WBL 296.3 and WBL 355.7 are shown in Figure 7-11. These are given relative to the design contour and were determined by measuring increments from a template applied to the glove surface at the appropriate locations. A positive Δz indicates that the measured glove contour is outside of the design contour. The reference lines drawn through the deviation curves represent a first order change to the contour. The pressure differences caused by such changes can be shown to be very small and of no significance relative to the boundary layer stability. The deviation increment measured relative to the new reference line in each case can be interpreted in terms of higher order waves that can be evaluated individually in relation to the smoothness criteria shown in Figure 7-12. With the exception of the lower surface at the inboard station (WBL 296.3) the wave amplitudes for the relatively large wavelengths involved all fall below the criteria. The deviation increment in question corresponds to a wavelength of about 16 in and has an amplitude of about .04 in. This would be acceptable for a single wave but not for a multiple wave. However, even though the criteria are stated for large wavelengths, there is some ambiguity about their validity in the upper range of wavelengths. In this context, it should be apparent that the larger waves are not likely to be critical when the desired laminar run is only several wavelengths or less. Based on due consideration of the above qualifications, the contour was accepted in this form since laminar flow was required only to a distance of about 36 in from the leading edge. Deviation increments in the template data corresponding to shorter wavelengths were not analyzed since they are more readily evaluated on the basis of measurements taken with the waviness gage.

Waviness was checked with a three-point dial indicator gage having a 2-in wheelbase. The measured waviness for the finished surface (prior to painting) is shown in Figures 7-13 and 7-14. The tabulation for the maximum double amplitude h_{max} is given for each station, which shows the overall wavelike excursions to be within the objective of .003 in (or less) for most of the areas surveyed. The .003-in objective is appropriate for multiple wave criteria. This general indicator of the overall deviation was chosen as a working basis for determining areas where further effort was needed in the surface finishing process. It will be noted that there are several areas where the .003-in objective was not met. However, in almost all cases it is a single wave which exceeds the objective rather than multiple waves. For single waves the allowable amplitude is approximately three times that of multiple waves (ref. 16). It should be noted that stations WBL 300 and WBL 296.3 are inboard of the region instrumented for laminar flow, so the waviness at these stations was not a concern. On the upper surface, the .003-in indicated wave height objective was met everywhere with the exception of a single wave of .004-in indicated height at WBL 310. Deviations at WBL 296.3 were of no concern since it was covered by strip-a-tube. For wavelengths smaller than 1 in, the chosen finishing technique ensured the virtual absence of such waves, which was readily verified by visual and manual (i.e., feel) techniques.

The results of the analysis of the final surface measurements can be summarized as follows:

- The contour deviations were relatively small and would not be expected to produce an observable variation in static pressure from that corresponding to the design contour.
- Longer wavelength deviations ($\lambda > 6$ in) are well within acceptable limits with the possible exception of the inboard lower surface (WBL 296.3) where the presence of instrumentation would preclude the attainment of laminar flow anyway.
- The waviness gage measurements indicated that the critical shorter wavelengths ($\lambda < 4$ in) were well within the criteria.
- Very short wavelengths ($\lambda < 1.0$ in) were not detected by any of the methods used in final evaluation of the surface tolerances.

The above points lead to the conclusion that the glove surface was finished to a condition compatible with the development of natural laminar flow in the test areas.

The final finish comprised (1) a gray polyurethane primer coat, (2) a pin-hole filler and surfacer, (3) a conductive coating consisting of Dexter 28-C-1 static conditioner and Dexter 8-10-5 surfacer applied per BAC 5837, and (4) several coats of gray automotive lacquer. The resulting surface was hand-rubbed to a mirror-like finish. Slight imperfections or depressions uncovered during the rubbing phase were filled using spot applications of lacquer followed by local sanding and polishing to be indistinguishable from the surrounding surface.

Application of the surface-mounted instrumentation was the final phase of preparation for flight test. Although extreme care was taken during this process, minor damage to the surface occurred in a few places. These were easily repaired using the same techniques as described above. The final glove surfaces with instrumentation installed and ready for flight are shown in Figures 7-15 and 7-16.

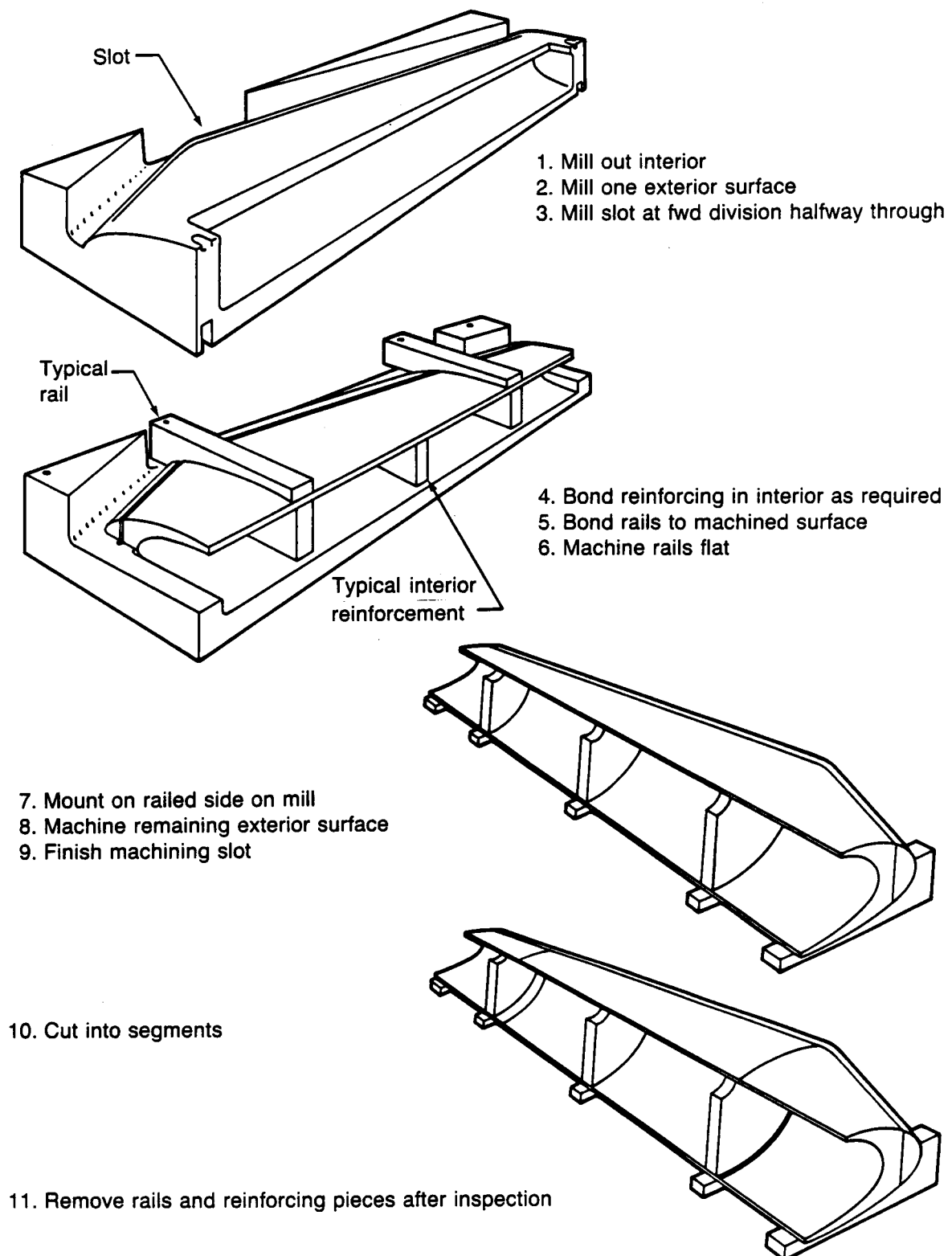


Figure 7-1. Machining Sequence for Glove Leading Edge Segments

ORIGINAL PAGE IS
OF POOR QUALITY



Figure 7-2. Machined Leading Edge Foam Piece

Handwritten signature or mark.

ORIGINAL PAGE IS
OF POOR QUALITY

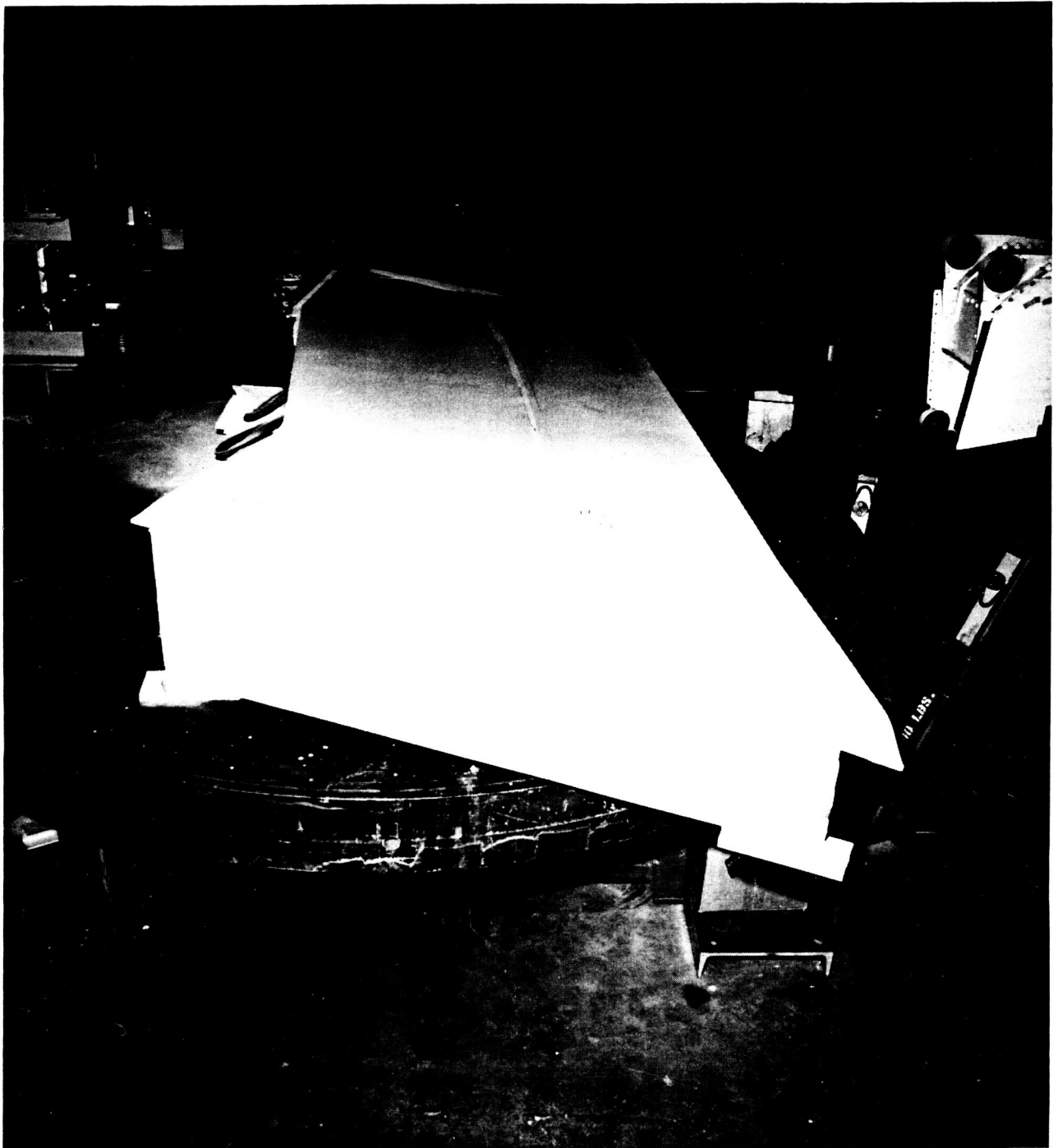


Figure 7-3. Machined Upper Surface Foam Panel

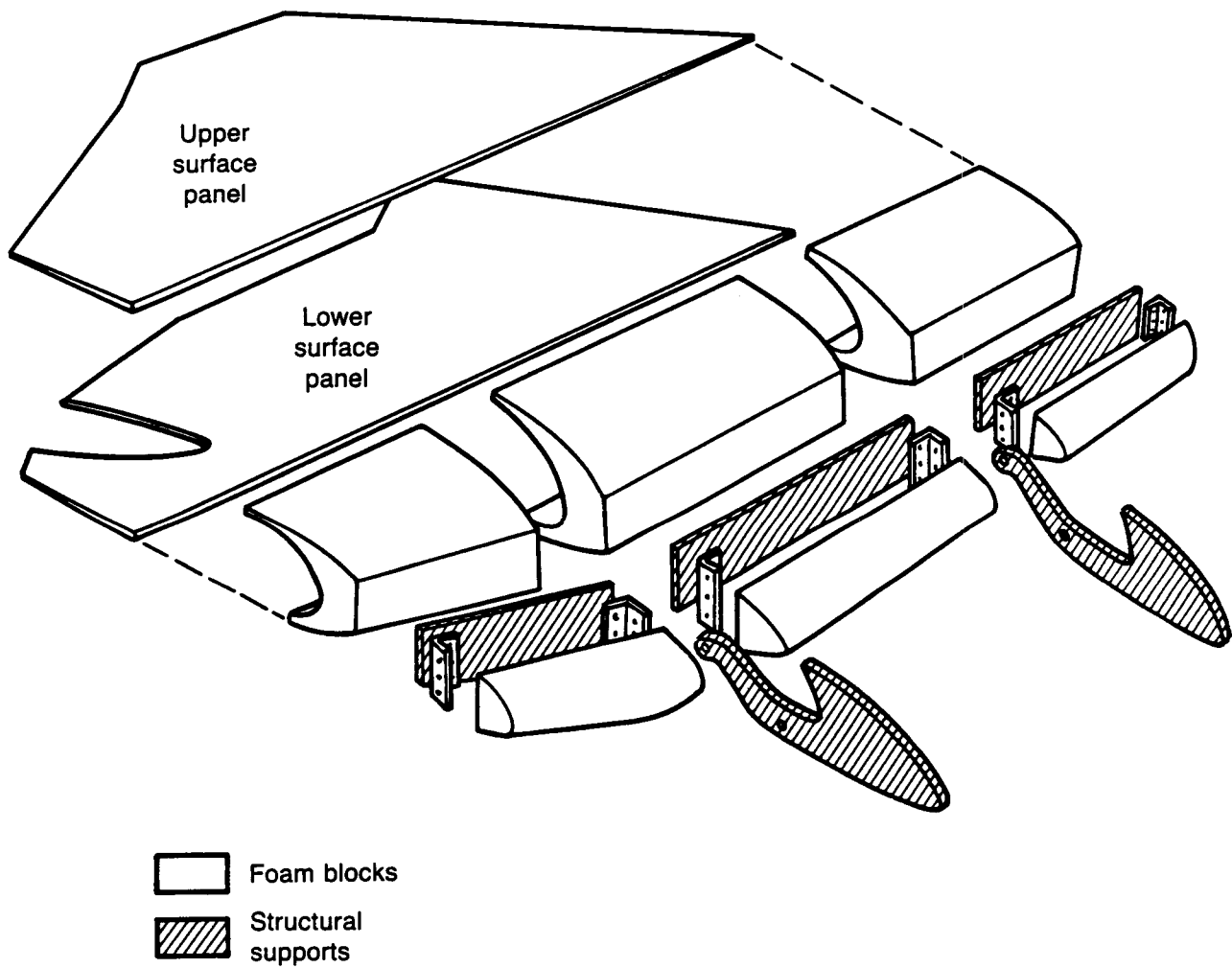


Figure 7-4. Glove Parts Arrangement

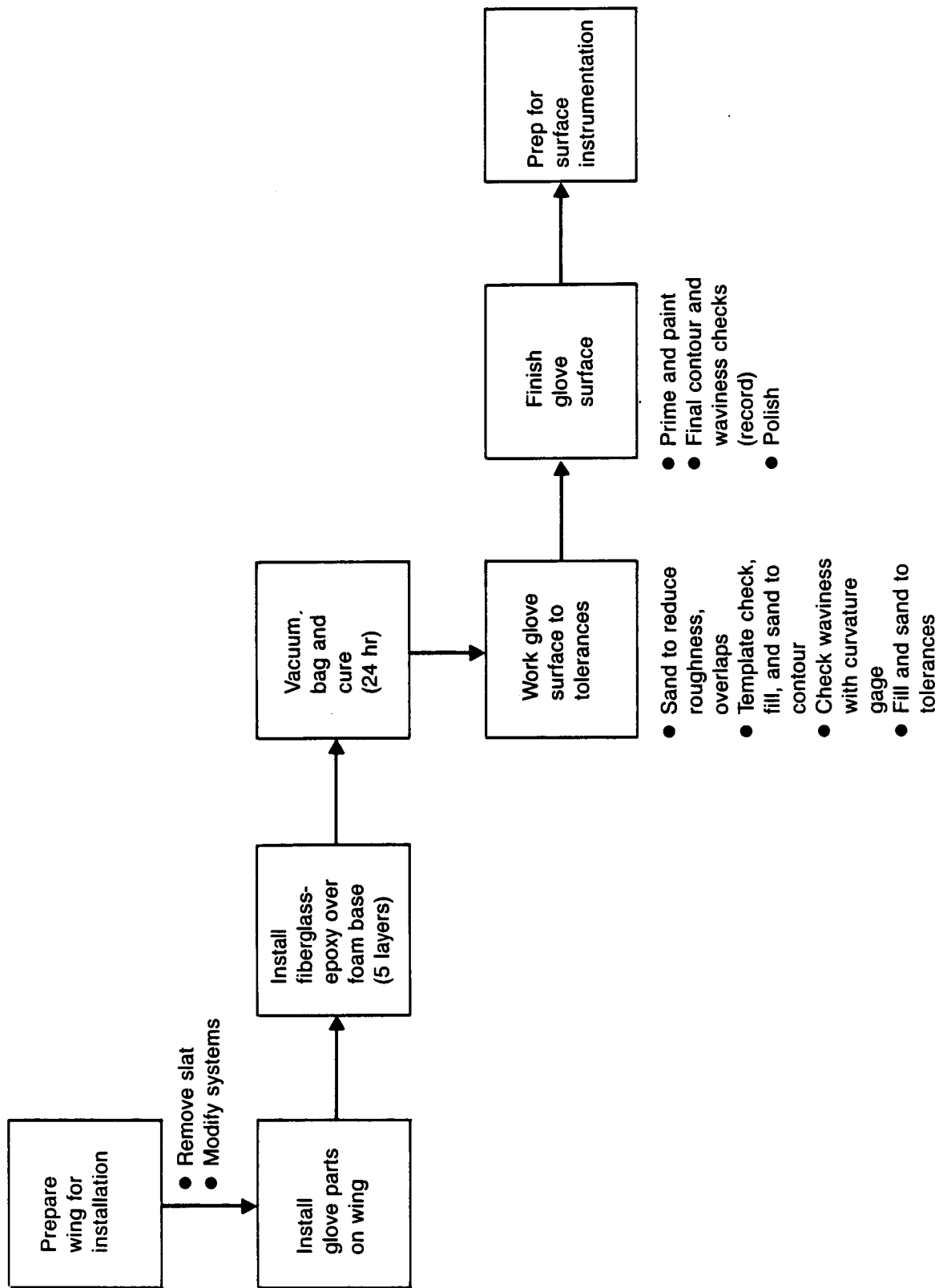


Figure 7-5. Glove Installation Technique

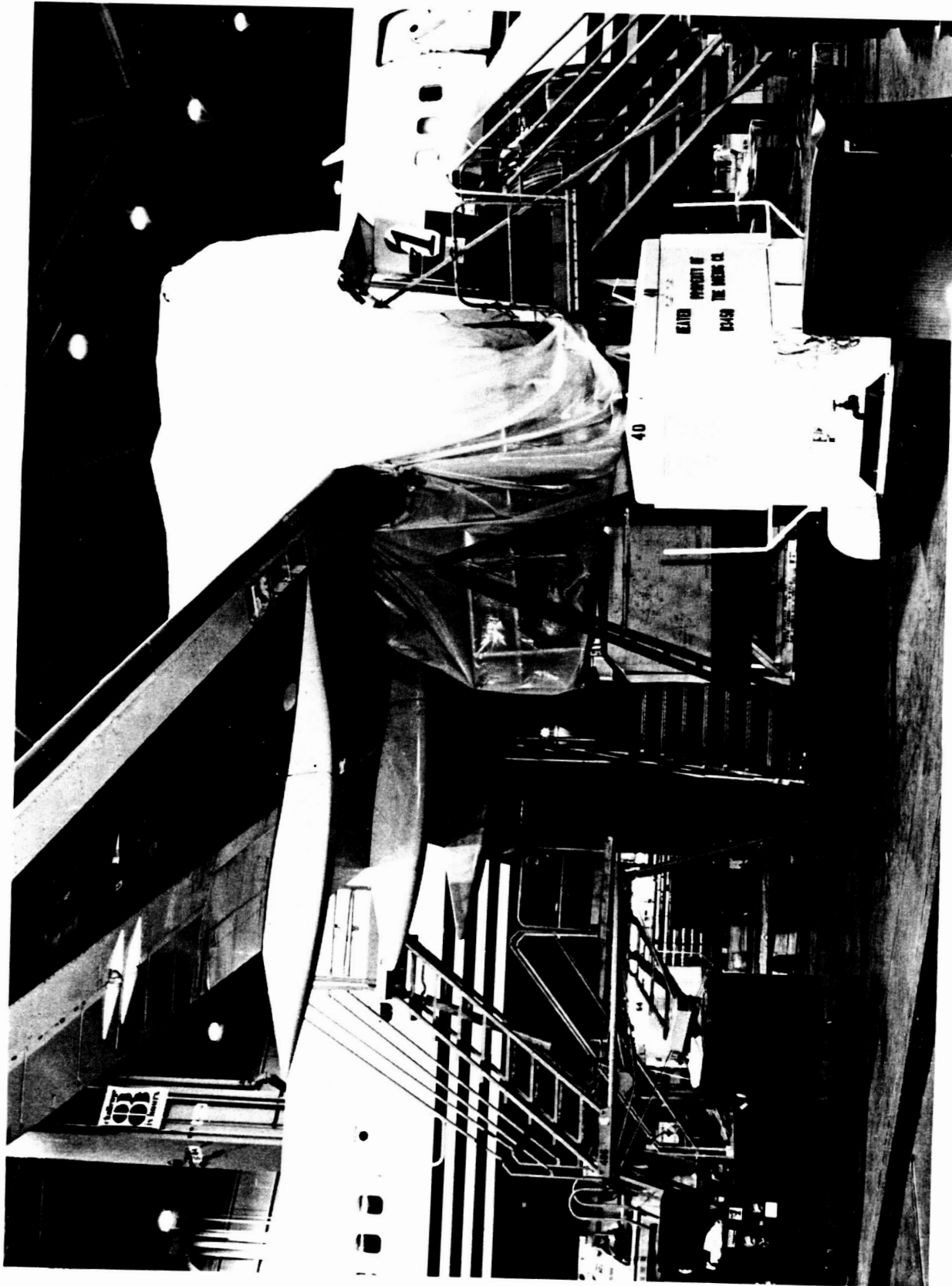


Figure 7-6. Wing Cocoon for Glove Installation

ORIGINAL PAGE IS
OF POOR QUALITY

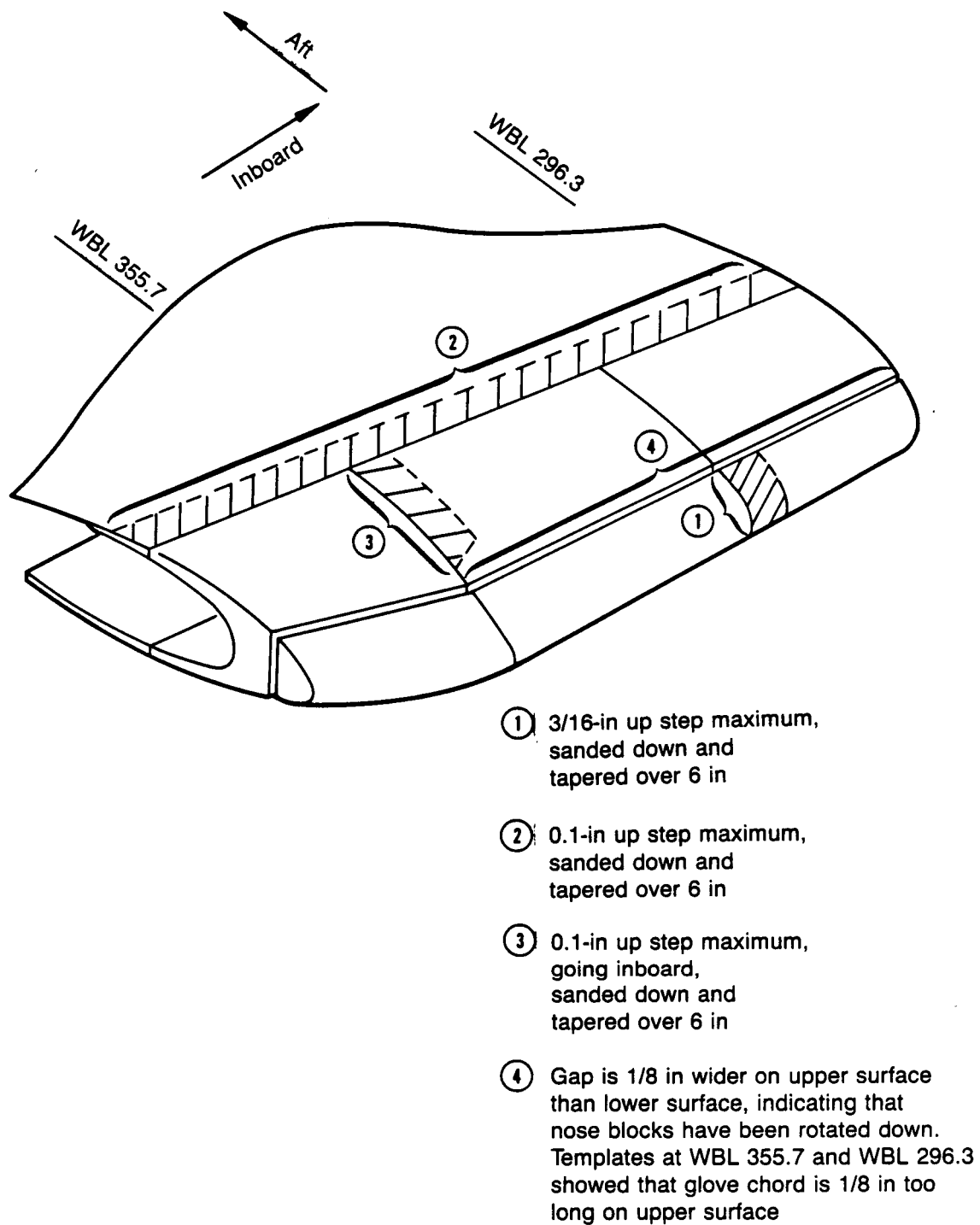


Figure 7-7. Assembly Mismatches for Glove Upper Surface

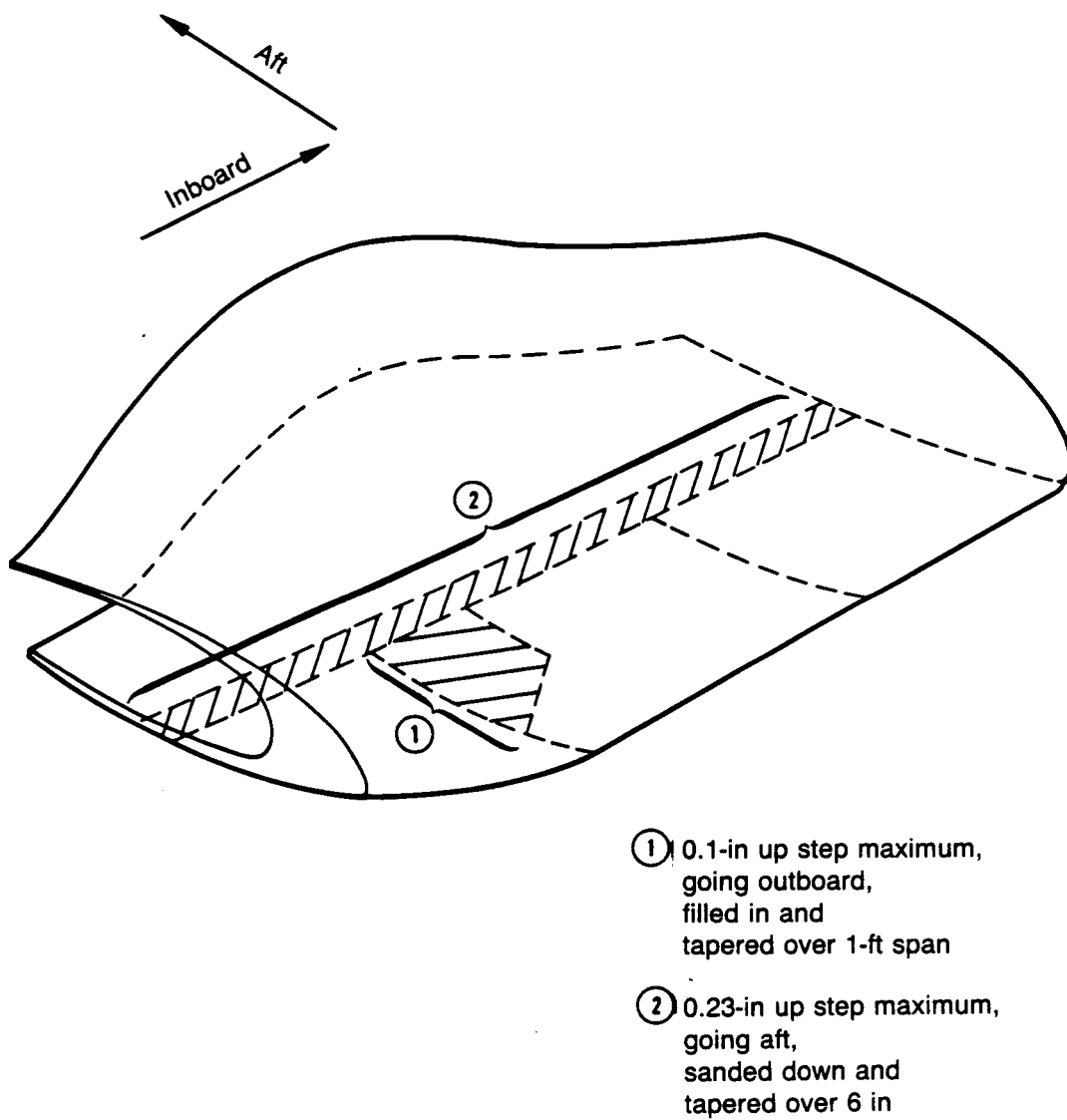


Figure 7-8. Assembly Mismatches for Glove Lower Surface

ORIGINAL PAGE IS
OF POOR QUALITY

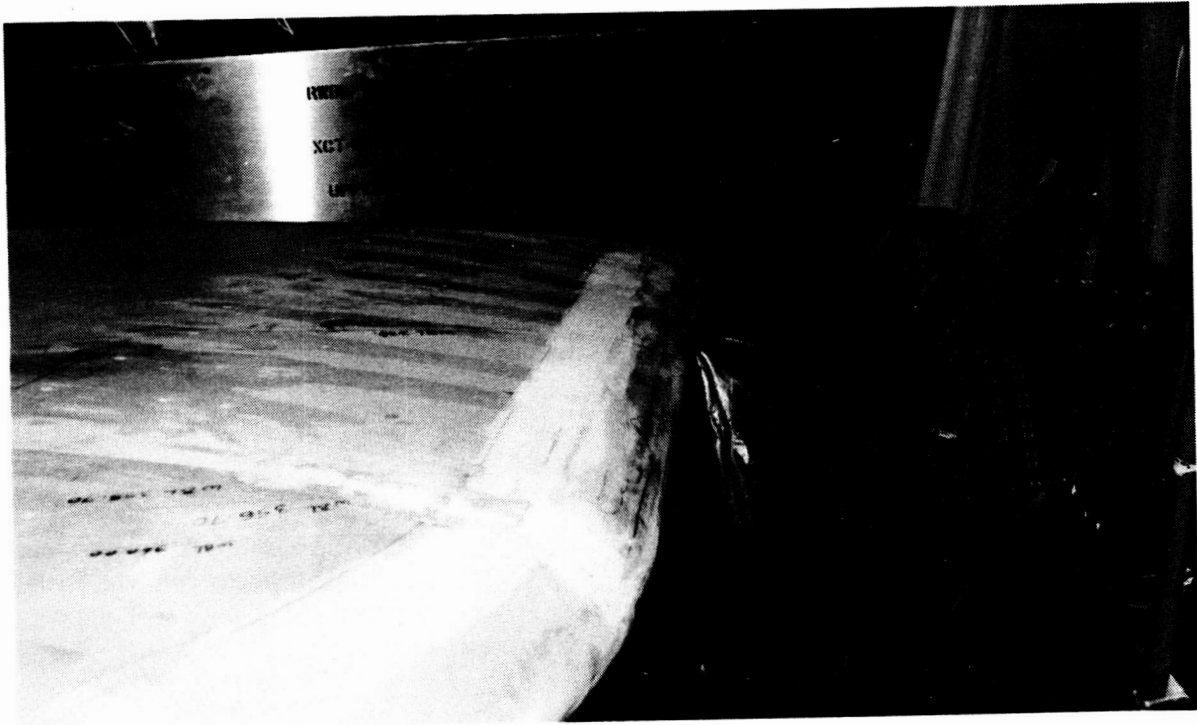
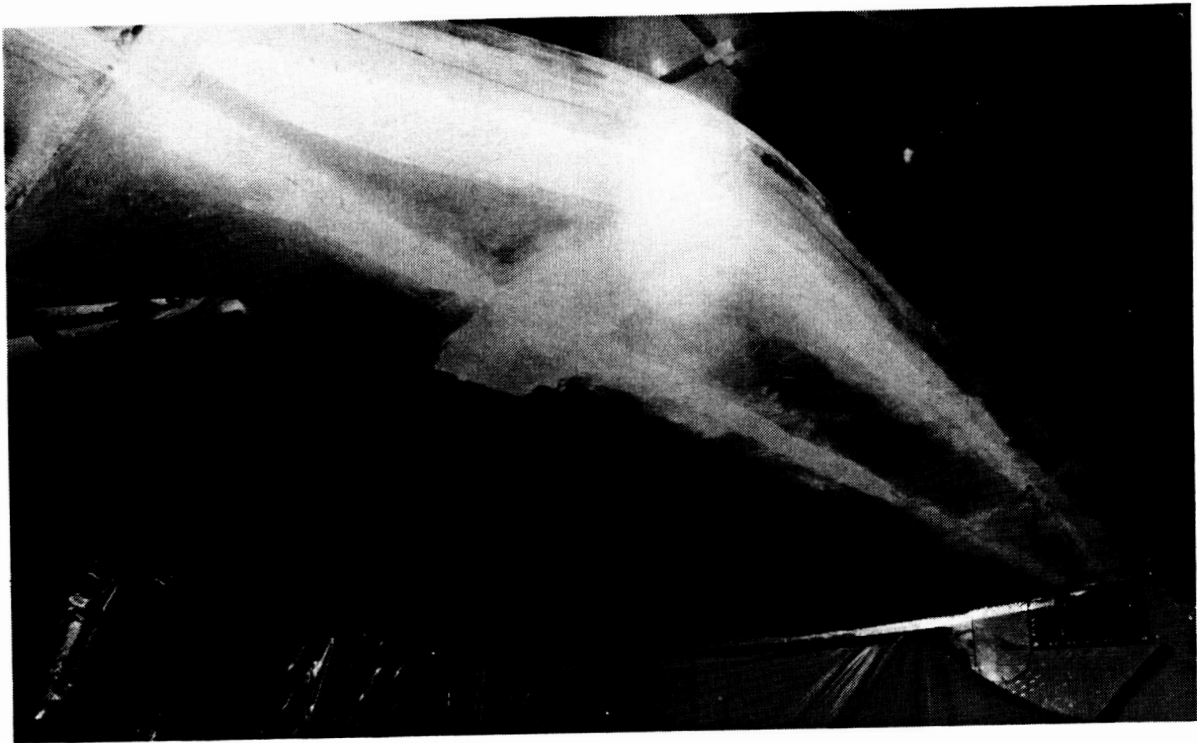
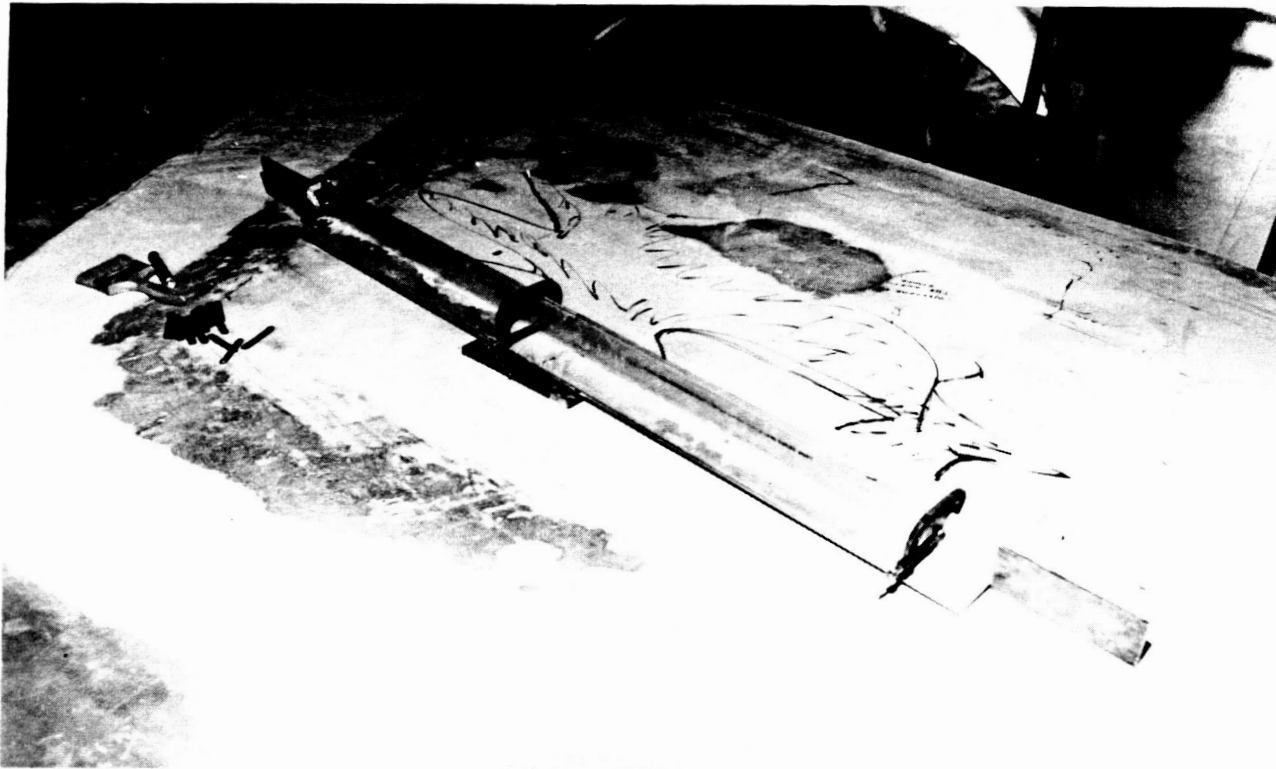


Figure 7-9. Glove Surfaces Prior to Fiberglass Installation

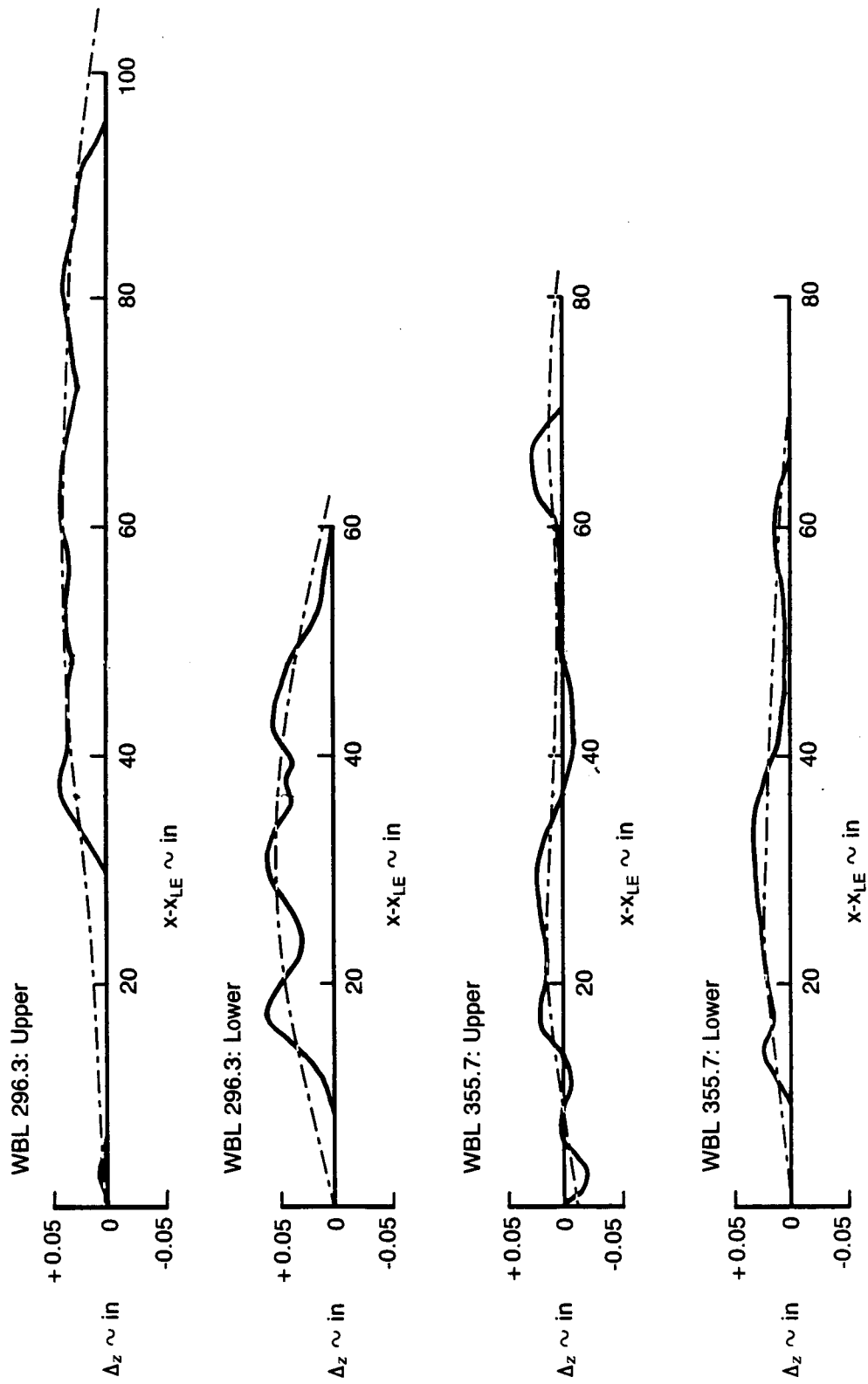


(a)



(b)

Figure 7-10. Steps In Glove Contouring and Finishing Process



Note: A positive Δ_z value indicates that the measured glove contour is outside of the design contour.

Figure 7-11. Deviation of Glove Contour From Design Loft

Special conditions:

- For chordwise waves double amplitude limits
- For a single wave (spanwise or chordwise) triple amplitude limits

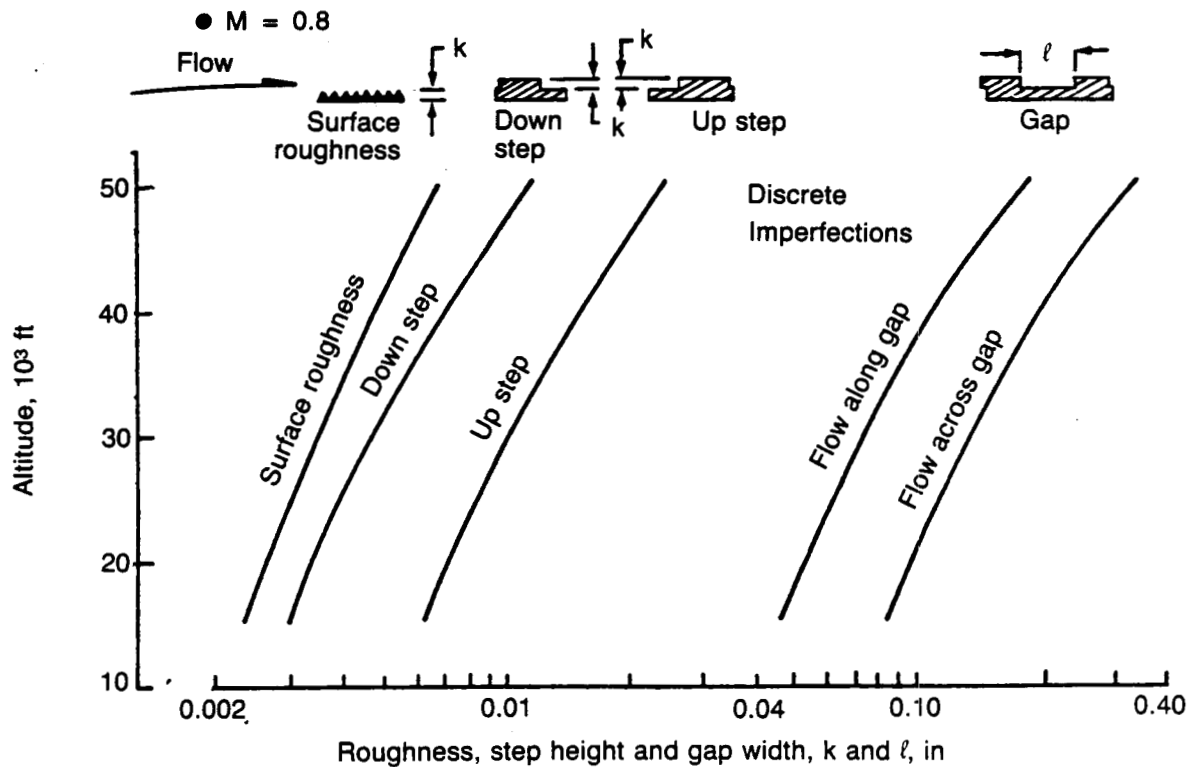
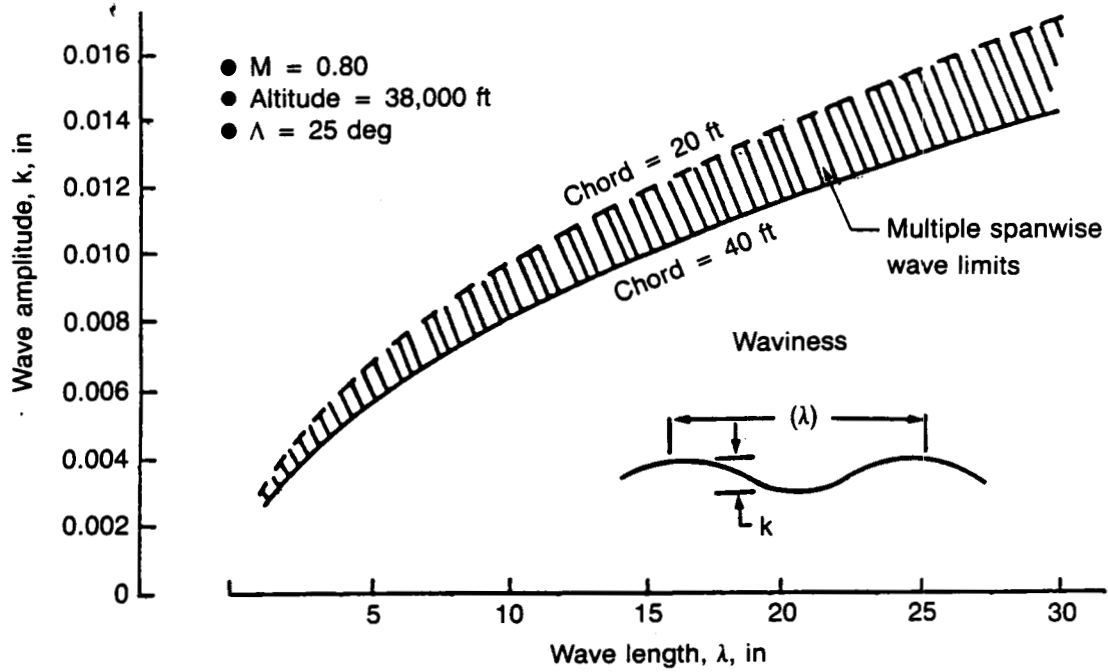


Figure 7-12. Smoothness Criteria for Laminar Flow Surfaces

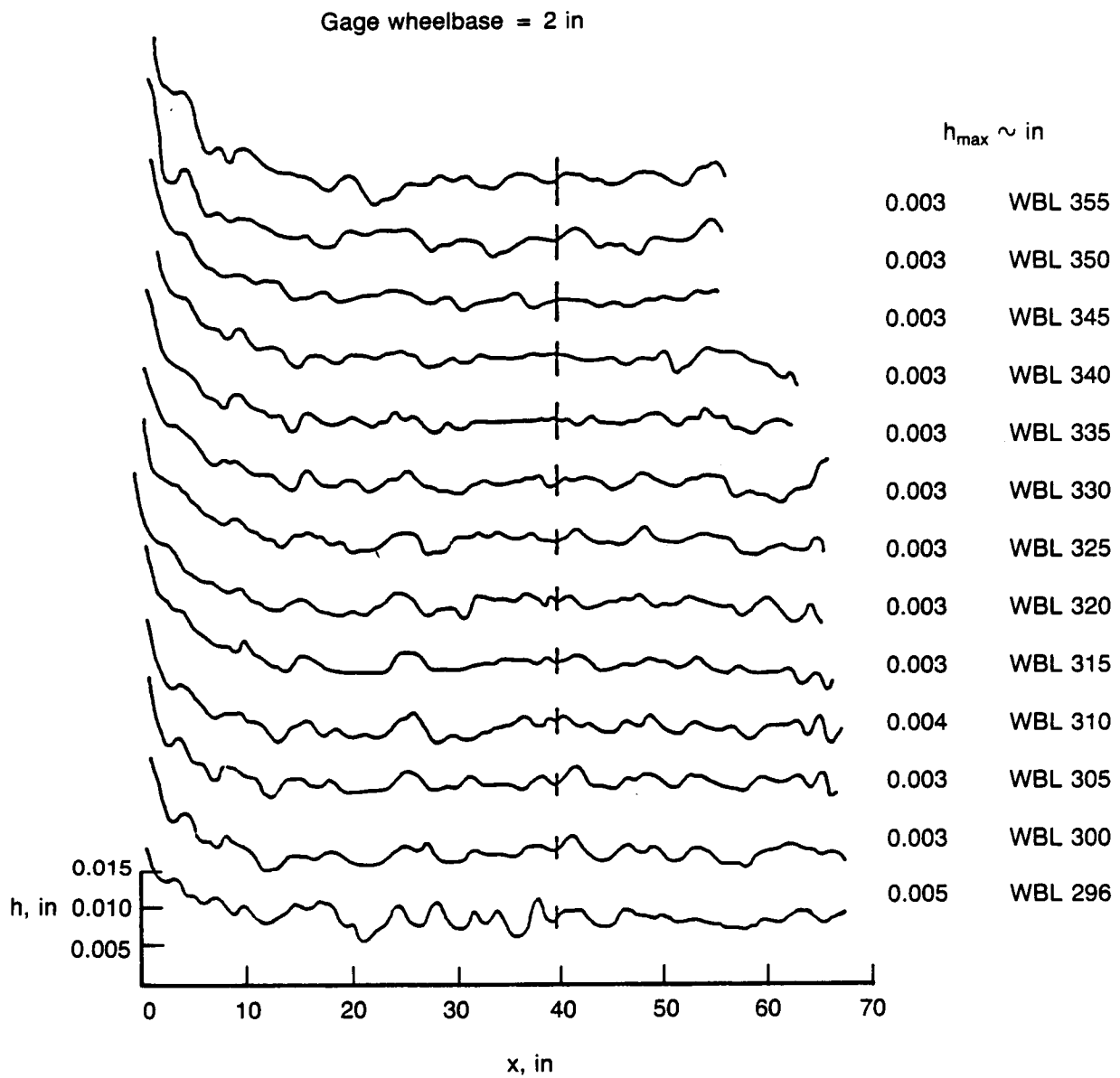


Figure 7-13. Waviness Survey for Glove Upper Surface

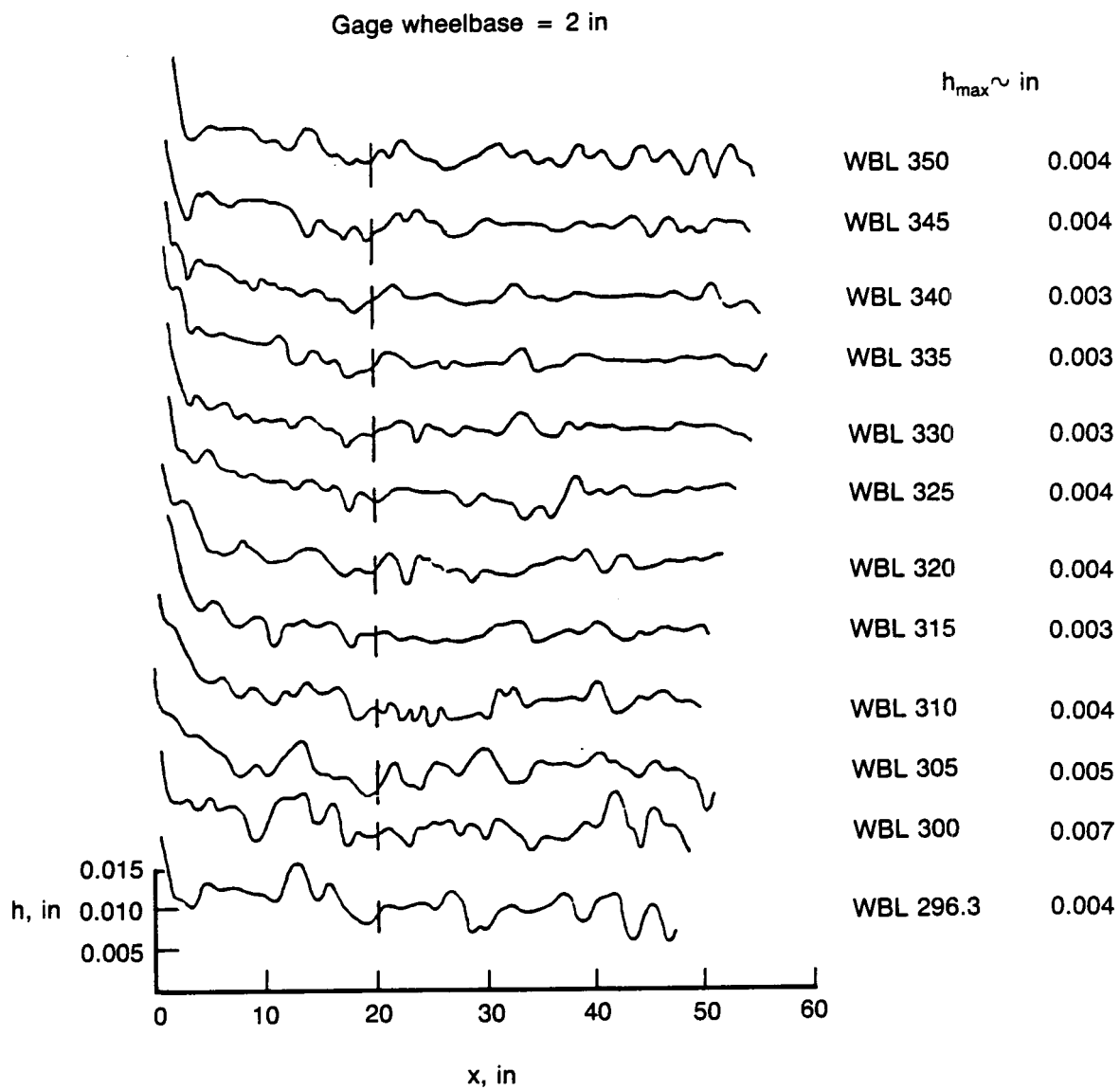


Figure 7-14. Waviness Survey for Glove Lower Surface

ORIGINAL PAGE IS
OF POOR QUALITY

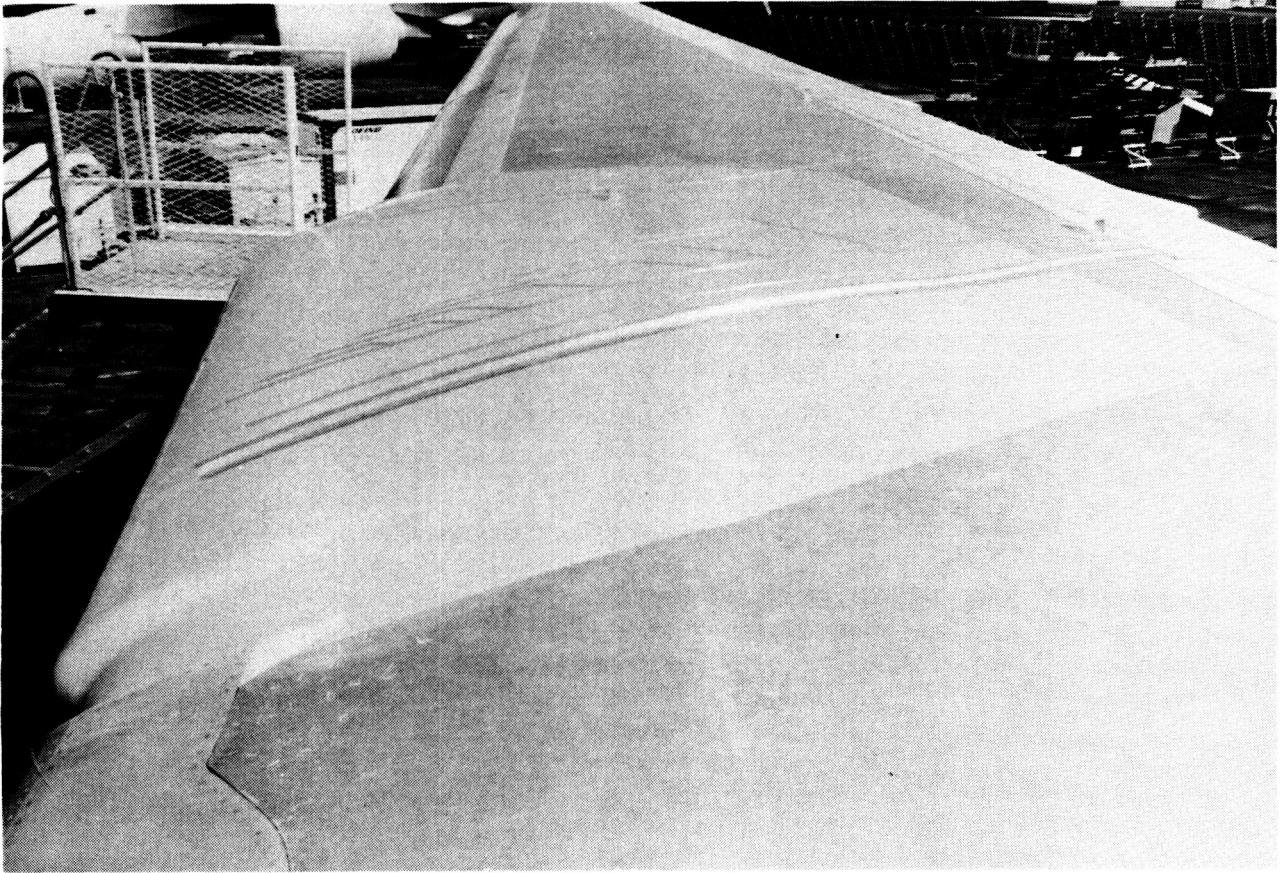


Figure 7-15. Finished Glove Upper Surface Instrumentation Installed

ORIGINAL PAGE IS
OF POOR QUALITY

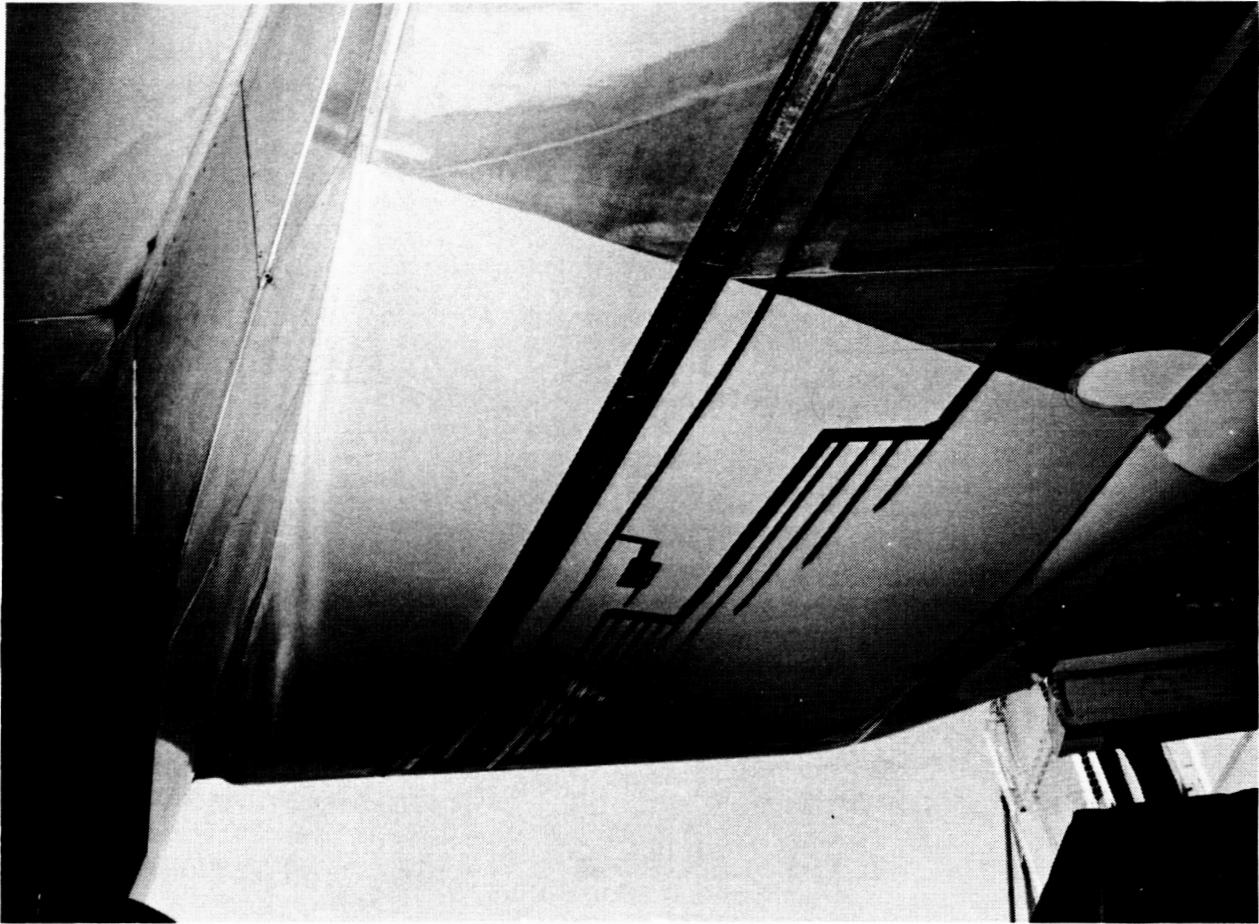


Figure 7-16. Finished Glove Lower Surface Instrumentation Installed

8.0 TEST DATA ANALYSIS

The flight tests were conducted on four separate flights on June 3, 10, 24, and 26, 1985. The first two flights were used to complete the initially planned series, for which a complete set of noise, static pressure, and transition data were acquired. The last two flights provided data for a more detailed evaluation of the aerodynamic characteristics of the NLF glove. Static pressures in the outboard portion of the glove were obtained as well as expanded coverage of the transition phenomena by relocation of the hot-film gages. No noise data was taken during these latter flights. Details of the instrumentation arrangement in all cases are provided in Section 6.0.

The test vehicle was the Boeing Model 757-200, Airplane NA001, powered by two P&W 2037 engines. The NLF glove was installed on the right-hand wing near the wing leading edge just outboard of the no. 2 engine. Pressure belts with a total of 12 ports, 20 hot-film probes, 5 surface-mounted microphones, and 2 probe-mounted microphones were installed on the NLF glove. Ten additional microphones, 4 surface-mounted and 6 probe-mounted, were on the wing outside the NLF glove region. For these tests slat no. 4 was deactivated and slat no. 7 removed. All remaining slat segments were fully operable.

8.1 FLIGHT TEST CONDITIONS

The airplane instrumentation systems were activated as follows:

High speed pulse code modulation (HSPCM)	- On
Airborne data analysis and monitoring system (ADAMS)	- Operable BA, GW, FC and PC programs (see below)
Manual notes	- Condition time
	- Gross weight and center of gravity
	- Altitude
	- Mach number
	- Stabilizer setting
	- Total air temperature
	- Engine r/min and exhaust gas temperature

The specific codes of the ADAMS system are defined as follows:

BA	- Basic airplane data
GW	- Gross weight data
FC	- Flight controls data
PC	- Pressure coefficient data

The range of airplane test parameters chosen is listed below for the first two flights for which noise data were obtained:

Gross weight, lb	- As specified (160,000 to 200,000)
Flaps and gear	- Up
Altitude, ft	- As required (30,000 to 42,000)
Mach number	- As noted, $\pm .01$ (.60 to .84)
Fin cone	- Extended 125 ft

The test procedure followed a generally accepted approach for this type of testing. The airplane was stabilized at the specified Mach number and altitude which was held constant for most conditions. In several cases where engine power conditions were insufficient to maintain altitude, low descent rates were permitted and the average altitude for the data recording period listed. Engine thrust setting and airplane trim were set and held constant while on condition. The condition period was defined to provide 1 min of data acquisition while airplane flight and atmospheric conditions were stabilized.

The actual conditions flown were selected to be compatible with the preliminary plan outlined in Chapter 4.0, which covers the main requirements for the acquisition of data to achieve the program objectives. Additional conditions were provided as appropriate to permit evaluation of instrumentation characteristics, atmospheric conditions, and other issues not originally anticipated.

8.2 ACOUSTIC ENVIRONMENT

Noise data were recorded only for Flights 1 and 2. Table 8-1 is a listing, in the order taken in flight, of selected airplane and engine data measured during the relevant noise recording period for Flight 1. Table 8-2 lists the comparable data taken during Flight 2. The fan exhaust Mach number was calculated using the measured fan exhaust pressure ratio in each case. Engine 1 refers to the left wing engine and engine 2 to the right wing (glove side) engine. Numbers missing from the sequence indicate that the test was truncated (i.e., conditions not achieved) due to unsatisfactory atmospheric conditions.

Tables 8-3 and 8-4 are listings of selected data grouped into categories which were useful for presentation and comparisons of the analyzed data. Some of the categories are arbitrary and were chosen for plotting convenience. One-third-octave spectra for all of the conditions shown are contained in Volume 2 and grouped according to these categories. The data analysis reported in Volume 1 concentrates primarily on categories 5, 6, 7, and 8 of Flight 2. Categories 1 and 4 of Flight 2 are also discussed. Very little analysis was conducted of data from Flight 1 or from categories 2, 3, 9, 10, 11, and 12 of Flight 2.

8.2.1 Sound Level Distributions

Figures 8-1, 8-2, 8-3, and 8-4 show OASPL distributions on the wing measured for the maximum power condition (right wing engine) for categories 5, 6, 7, and 8, respectively. The overall sound pressure level (OASPL) data for all conditions tested are tabulated in Volume 2. As further elaborated below, the noise levels measured on the lower wing surface are dominated by engine noise whereas those measured on the upper wing surface are dominated by nonengine sources. In general, the nonengine sources dominating the upper wing noise distributions have not been defined. Boundary layer turbulence, shock-boundary layer interactions, or other aerodynamic sources are believed to be major contributors. Other possible sources are boundary layer acoustic radiation (generally small compared to boundary layer turbulence levels), trailing edge acoustic radiation, and atmospheric turbulence (generally low at high altitudes). The above data are presented to give an overview of the magnitude of the maximum noise levels experienced. Engine noise levels (OASPL) in the range of approximately 120 dB to 140 dB are in evidence on the lower wing. The upper wing surface is subjected to a range of approximately 110 dB to 130 dB. Some of the upper wing surface microphones indicate higher levels than corresponding microphones on the lower surface. Generally, however, the upper surface noise levels are less than the lower surface levels. Possible reasons for this will be explored in the discussions which follow.

Figures 8-5, 8-6, 8-7, and 8-8 show the effect of flight Mach number on normalized OASPL vs. fan exhaust Mach number (right engine). The OASPLs are normalized to an altitude of 40,000 ft using a 20 log (ambient pressure) dependence. As shown in Figures 8-5 and 8-6, all of the lower wing microphones indicate noise levels increasing with increasing engine power except for microphone 2. Since, at a given airplane Mach number, the airplane flight parameters were held nearly constant as engine power was increased, the increasing measured noise levels are attributed to engine-generated noise. Microphone 2, which does not show an engine power dependence, is felt to be dominated by turbulent airflow noise. The engine fan and core exhaust jets are believed to be the dominant engine noise sources. Therefore

the forward location of microphone 2 together with rearward convection of sound waves by the free-stream flow (relative to the airplane) probably accounts for the low engine noise at that location. Microphone 4 is on the same side of the engine as the compressor bleed valve exhaust port. Depending on altitude, this bleed port is exhausting high-pressure air at the lower engine power conditions. A comparison between bleed-on bleed-off conditions was conducted to identify the bleed flow noise influence. The results are discussed in Section 8.2.3. In Figure 8-5, the microphone 4 points dominated by bleed flow noise can clearly be distinguished from those dominated by engine noise. The trends with fan Mach number appear to be consistent with those shown for other microphone locations.

The upper wing surface microphone data presented in Figures 8-7 and 8-8 do not indicate the clear engine power dependence seen for the lower wing surface microphones. With increasing engine power the general tendency is for a nearly constant noise level at a given flight Mach number. However, some irregular noise variations with engine power are evident and have not been explained. The lowest fan exhaust Mach number data point for the airplane Mach number .7 series was obtained by shutting the right-hand engine down and allowing it to "windmill." In this case, the airplane was allowed a shallow descent to maintain airplane Mach number since the engine thrust was insufficient for level flight. Turbulent airflow shed by the engine nacelle appeared to strongly affect microphone 5 as well as other microphones to a lesser degree. A number of data points were measured in the presence of cirrus clouds. Cirrus clouds have been known to trip laminar boundary layer flow and may generate impulse noise when the ice crystals strike the microphone surface. The aerodynamic source influences on the upper wing microphones are also considered to be important. At flight Mach numbers of .7 and greater, supersonic flow exists on the upper surface of the wing, which generates a shock wave. The wing shock will cause a sudden boundary layer thickness increase and will interact with the turbulence to generate sound. In addition, a shock wave can form in front of the probe microphone in supersonic flow.

The leading edge microphone (microphone 12) may give an indication of an "upper limit" to the engine noise influence on the upper wing surface. This microphone appears to be dominated by engine noise at the higher engine power conditions. At an airplane Mach number of .8, the microphones at 5% chord on the lower surface of the NLF glove indicated noise levels (normalized OASPL) in the range of 130 dB. For these same conditions, the leading edge microphone indicates levels in the range of 117 dB. It could be expected that this level difference is primarily due to wing shielding since a line drawn from the region at which the engine noise is generated to the leading edge microphone intercepts the wing surface. This tends to indicate that the upper wing surface microphones are exposed to engine noise levels less than 117 dB.

8.2.2 One-Third-Octave Spectra Data

Lower wing microphone spectra are shown in Figures 8-9 through 8-16 and upper wing spectra are shown in Figures 8-17 through 8-24. The spectra for microphones 5, 14, and 15 show a high level tone at 400 Hz (band 26) which is due to airplane electrical system interference. The contribution of this tone to the OASPL has been removed for the OASPL plots previously presented. Bleed flow noise, nacelle spillage noise, and turbomachinery tones are also indicated on the spectrum plots. For the lower wing microphones, the definite trend of increasing noise with increasing engine power (right engine) as discussed above for the OASPL plot is clearly seen. Also, for a given microphone, the spectrum shapes for the entire range of airplane Mach numbers .63, .7, .8, and .82 are somewhat similar.

On the inboard upper wing, the data from the 5% chord microphone (microphone 1) is particularly interesting because of the nearly constant shape observed for the entire airplane Mach number range from .63 to .82. Predictions of boundary layer turbulence spectra were calculated using Reference 17 for the airplane Mach number .63 and .80 conditions and are shown in Figures 8-21 and 8-23. This procedure applies to flat plate turbulent boundary layers. Although the predicted spectrum shapes are similar to the measured data, the predicted peak spectrum levels were approximately 5db lower than measured and peak noise frequencies were high. These differences may not be significant since an exact

correspondence should not be expected because the measurement is not for a flat plate boundary layer. However, the predictions are sufficiently different to indicate that the microphone protrusion into the flow may have caused a local separation and resulted in stronger turbulence pressure fluctuations than predicted. Depending upon the airplane Mach number, the other upper wing microphones located at 5% chord indicate spectral shapes and levels very similar to that of microphone 1 data. However the data from these microphones is not nearly as consistent as microphone 1. The presence of cirrus clouds has been suggested as one possible cause of noise changes for these microphones. However, it is not clear why microphone 1 would not be affected by cirrus clouds as well.

Microphone 5 is located in a region where the boundary layer was expected to be laminar for the airplane Mach numbers greater than approximately .76. It is observed that the spectrum shape measured at microphone 5 for airplane Mach number .63 is significantly different from those for the higher flight Mach numbers. Also, the values of normalized OASPL for Mach no. = .63 are correspondingly higher than for the higher flight Mach numbers. It is possible that the laminar boundary layer is in transition near microphone 5 for this flight condition. At the higher flight Mach numbers, microphone 5 provides data similar to that from microphone 1. This is unexpected since microphone 1 is believed to be dominated by turbulent boundary layer pressure fluctuations whereas the flow near microphone 5 was expected to be laminar for these conditions. A likely explanation of these discrepancies is turbulence caused by the adjacent instrumentation or possibly turbulence from the microphone installation itself. The apparent engine power dependence of the noise data at microphone 5 for the airplane Mach numbers higher than .63 may also be attributable to intermittent turbulence since transition was measured between 5% and 10% chord for this condition. Microphone 11 is located in a region of the glove which was probably turbulent for all conditions tested because of the peaky pressure distribution. However, the noise level dependence on engine power is not readily explainable unless there is some diffraction of the noise from this source around the wing leading edge.

8.2.3 Compressor Bleed Flow Noise

In general, at lower engine power conditions the compressor bleed valve opens and high pressure air exhausts through a port located just downstream of the fan exhaust nozzle and on the inboard side of the right wing engine. It was expected that the noise generated by the bleed exhaust jet would affect the noise inboard of the engine but would not have a large influence on the microphones outboard of the engine. To measure the bleed flow noise influence, a condition which normally has the bleed valve open was also flown with the bleed valve closed. The spectra from these conditions are shown in Figures 8-25 through 8-28. Microphone 4, which is on the same side of the engine as the bleed exhaust port, indicates more than 10-dB increase in noise level when the bleed is open. Microphone 2, which is also on the same side of the engine as the bleed but forward of the engine, shows approximately a 5-dB increase for the same condition. Microphones 8 and 10 on the outboard side of the engine also showed approximately 5-dB increase when the bleed valve was open. Although microphone 13 indicated an apparent change in level when the bleed valve was open there is some doubt that the change was due to bleed flow noise. Condition 233, for which data is plotted in Figure 8-14, has nearly the same airplane and engine conditions as condition 218 with the bleed port open. However, the peak spectrum level at microphone 13 is much closer to that of condition 217 with bleed closed. An examination of the same conditions for the wing upper surface shows that the bleed noise did not significantly affect the microphones on the upper wing surface although microphones 12, 7, and 3 did show a small apparent increase when the bleed valve was open.

8.2.4 Altitude Normalization

A systematic study of noise trends is facilitated greatly when the data can be normalized and plotted in relation to fundamental parameters. Since the data from microphone 1 is independent of engine power it was used to study the effect of altitude changes. The category 1 conditions from Flight 2 (Table 8-3) correspond to a range of altitudes of 30,000 ft to 41,000 ft. Flight Mach number for the category 1 data is nearly constant between .80 and .81. For the preliminary analysis reported in this document, only an ambient pressure altitude normalization was investigated. The ambient pressure normalization is appropriate dimensionally and can be validated when Mach number, Reynolds number, and geometry are held constant. In analytical form, the sound pressure can be expressed as:

$$\begin{aligned} P_{rms} &= \rho/2 V^2 f(M, \dots, \text{other nondimensional parameters}) \\ &= \rho/2 c^2 M^2 f(M, \dots) \end{aligned}$$

$$\text{But since } \frac{\rho}{2} c^2 = \frac{\gamma}{2} P_{amb},$$

$$P_{rms} = P_{amb} \frac{\gamma}{2} M^2 f(M, \dots)$$

Now we have also,

$$\begin{aligned} \text{SPL} &= 20 \log \frac{P_{rms}}{P_{ref}}, \text{ where } P_{ref} \text{ is the reference pressure, } (20 \mu\text{Pa}) \\ &= 20 \log P_{amb} + 20 \log \left[\frac{\gamma}{2} \frac{M^2 f(M, \dots)}{P_{ref}} \right] \end{aligned}$$

Figure 8-29 is a plot of OASPL versus $\log P_{amb}$ for the category 1, microphone 1 data from Flight 1. The data set appears to correlate best with two line segments (separated by about 1 dB), both of which have a slope of about 20 as predicted from dimensional analysis. The separation of lines seems to occur above altitudes of about 35,000 feet for which the airplane lift coefficients are significantly higher than those below (see tabulated data). This may indicate a change in flow over the wing which corresponds to a transition shift near the leading edge. The latter could be due to the airplane attitude change associated with C_L or perhaps a move into higher altitude where the atmosphere is smoother and with lower ice crystal concentration. In any case, the normalization of SPL with $20 \log P_{amb}$ would appear to be appropriate.

The effect of the ambient pressure normalization on the 1/3 octave spectra data from category 1, microphone 1 is shown in Figure 8-30. The compression of the spectra into a narrow band illustrates the applicability of this normalization procedure which can be seen to be independent of frequency. For the OASPL data in category 1, Figures 8-31 and 8-32 demonstrate the effect of using the $20 \log P_{amb}$ normalization. Microphone 1 is thought to be dominated by turbulent boundary layer pressure fluctuations whereas the microphone 10 OASPL data (Figure 8-32), is dominated by engine noise. In both cases the normalization provides an improved collapse of the data which approaches a single curve relationship. Based on these comparisons, ambient pressure normalization was used for all the OASPL data examined in the present analysis.

8.2.5 Noise Correlation With Engine Parameters

Two parameters were examined as correlating parameters for the engine noise: corrected fan r/min, N_{1C} , and fan exhaust jet Mach number, M_{FAN} . It would be expected that noise from turbomachinery-related sources would correlate best with N_{1C} whereas noise from jet exhaust flow shocks would correlate best with M_{FAN} . Figure 8-33 compares microphone 10 data for constant altitude plotted versus N_{1C} with the same data plotted against M_{FAN} . It is seen that, when plotted versus N_{1C} , the data tends to fall on separate curves for each flight Mach number. This stratification tends to disappear when the data is plotted versus M_{FAN} .

Examining the normalized OASPL versus M_{FAN} plots for other under wing microphones in Figures 8-5 and 8-6 will show that there appears to be a tendency for all of the aft (60% chord) probe microphones to be independent of airplane Mach number at the higher engine power conditions. The probe at 30% chord as well as the surface microphones at 5% chord indicate an airplane Mach number dependence. This may be consistent with the conclusion that jet flow-related noise is the dominant component on the lower surface since an aft shift in directivity (e.g., 8 to 10 deg) could change the forward microphone levels without a significant change in the aft microphone levels depending on the initial directivity pattern. Based on the evaluation discussed above, M_{FAN} has been selected as the appropriate parameter to correlate engine power effects and all noise data is therefore presented using M_{FAN} as the independent variable.

8.2.6 Narrowband Analysis

Most noise spectra data in this report are shown on a 1/3-octave band basis, which is satisfactory for noise comparisons between different wing locations and flight conditions. However, narrowband analyses are more appropriate for the study of sound source types and possible extraneous influences on the noise spectra.

Narrowband spectra were only analyzed for category 5, "Engine Power Variation, $M = .63$," and category 6, "Engine Power Variation, $M_{AP} = .8$," of Flight 2. Plots for all 17 microphones for the above conditions and categories are contained in Volume 2 of this report. Figures 8-34 to 8-43 of Volume 1 show the category 6 narrowband results. Table 8-4 lists the frequencies of the turbomachinery blade passing harmonics for the fan rotor, first stage low pressure compressor and low pressure turbine stages for the conditions making up category 6. Many of these tones are identifiable in the narrowband plots for the lower wing microphones. In addition, tones and narrowband random noise contributions are found which do not relate to the frequencies of readily identifiable sources. For example, Figure 8-37 shows a blowup of the microphone 6 spectra in the 5000-Hz to 8000-Hz range for conditions 223, 224, and 225. A narrowband random noise peak is seen around 6000 Hz. Although the peak shows a slight frequency increase with increasing N_1 it is not proportional to N_1 as is the case for turbomachinery tones such as the fan third harmonic seen in the figure. The source of this peak is not known.

In general, the effects of the discrete tones are significant contributors to the noise spectra although they would not be expected to play a dominant part in the boundary layer transition phenomena. The extraneous sources such as the airplane electrical system are quite obvious and can be removed from the microphone outputs to yield the representative noise environment.

Table 8-1. Noise-Related Airplane and Engine Data — Flight 1

Cond. no.	Airplane Mach no.	Pressure altitude, ft	C _L	Sideslip, deg	N _{1C} , r/min (left eng)	N _{1C} , r/min (right eng)	N ₁ , r/min (right eng)	Mach no. (fan exhaust)
005	0.81	38 952	.52	-0.2	4366	4010	3644	1.23
006.1	0.79	39 008	.54	5.8	4388	4382	3971	1.28
001	0.82	38 950	.49	-0.3	4348	4175	3800	1.27
002	0.81	39 012	.50	5.4	4359	4353	3974	1.29
109	0.79	38 957	.53	-0.7	4391	3810	3461	1.17
006.2	0.80	38 926	.51	-6.4	4369	4348	3962	1.28
035	0.81	39 952	.53	-0.3	4359	4017	3633	1.23
036	0.78	39 957	.56	-0.4	4394	3908	3519	1.18
013	0.80	40 948	.55	0.2	4129	4366	3934	1.28
014	0.81	40 946	.54	0	4222	4220	3823	1.27
015	0.81	40 946	.54	-0.2	4367	4115	3733	1.25
016	0.80	41 002	.56	6.3	4383	4245	3848	1.26
017	0.80	40 878	.55	-7.1	4374	4366	3986	1.28

Compressor bleed closed for all conditions

Table 8-2. Noise-Related Airplane and Engine Data — Flight 2

Cond. no.	Airplane Mach no.	Pressure altitude, ft	C _L	Sideslip, deg	N _{1C} , r/min (left eng)	N _{1C} , r/min (right eng)	N ₁ , r/min (right eng)	Mach no. (fan exhaust)
201	0.80	30 011	.35	-0.6	4161	3227	3109	1.06o
202	0.79	30 080	.36	3.2	4174	3240	3114	1.05o
203	0.79	30 075	.36	-4.0	4179	3294	3167	1.07o
204	0.81	34 001	.42	-0.2	4300	3424	3224	1.10o
205	0.79	34 008	.43	3.9	4317	3437	3230	1.09o
206	0.80	34 000	.42	-3.9	4304	3481	3274	1.11o
207	0.81	36 000	.45	0	4359	3585	3333	1.17o
210	0.80	36 998	.48	-0.3	4376	3660	3380	1.14c
211	0.80	37 994	.50	-0.2	4361	3850	3538	1.19c
212	0.79	37 988	.51	3.9	4382	3867	3545	1.18c
213	0.80	37 927	.50	-3.7	4361	3796	3485	1.17c
214	0.81	38 987	.52	-0.1	4365	3954	3614	1.21c
215	0.82	38 988	.50	-0.1	4346	4042	3701	1.24c
216	0.83	38 986	.48	0	4331	4327	3971	1.30c
218	0.70	37 007	.62	-0.6	4437	3582	3265	1.05o
217	0.71	37 007	.60	-0.5	4350	3557	3248	1.06c
219.1	0.64	35 020	.67	0.7	2491	4493	4121	1.19c
220.1	0.62	35 009	.71	-0.8	4502	2928	2683	0.86o
221	0.63	35 007	.68	-0.6	4500	2315	2123	0.76o
222	0.81	38 991	.50	0.1	4365	3903	3571	1.20c
248	0.82	38 990	.48	0.2	4344	4023	3692	1.24c
249	0.78	38 993	.53	0	4393	3717	3391	1.14o
250	0.75	38 999	.57	0	4438	3723	3382	1.12o
251	0.76	38 997	.56	0.2	3623	4426	4023	1.26c
252	0.75	38 994	.57	-0.4	3977	4007	3638	1.19c
223	0.80	40 483	.53	-0.2	4004	4340	3934	1.28c
224	0.80	40 482	.54	-0.4	4081	4102	3714	1.24c
225	0.80	40 483	.54	-0.7	4373	3793	3437	1.18o
226	0.79	40 426	.55	4.8	4383	3965	3587	1.20c
227	0.80	40 449	.54	-4.0	4373	3993	3617	1.21c
228	0.79	41 296	.57	-0.5	4395	2645	2384	0.94o
229	0.75	40 793	.61	-0.4	4442	3330	2994	1.04o
231	0.70	39 015	.64	0.7	3575	4508	4059	1.23c
232	0.70	39 008	.65	0	3993	4019	3618	1.15c
233	0.70	39 005	.65	-0.3	4518	3631	3270	1.06o
234	0.70	39 042	.64	6.8	4512	3786	3412	1.09c
235	0.71	38 954	.62	-6.7	4505	3816	3443	1.11c
236	0.71	38 920	.63	-0.8	4510	2602	2349	0.85o
237	0.71	39 005	.62	-0.5	4506	3280	2962	0.99o
239	0.80	38 000	.46	-0.5	4376	3557	3271	1.12o
240	0.80	38 003	.46	3.9	4382	3673	3377	1.14o
241	0.80	40 971	.53	0	4373	4034	3653	1.23c
242	0.83	40 968	.49	0.3	4338	4321	3930	1.30c
243	0.82	38 976	.46	0.2	3700	4345	3985	1.29c
244	0.82	38 972	.45	-0.3	4085	4116	3776	1.26c
245	0.82	38 974	.45	-0.3	4351	3865	3542	1.20c
246	0.82	38 989	.46	4.0	3895	4355	3987	1.29c
247	0.81	38 548	.45	-0.7	4364	2501	2293	0.93o
238	0.69	36 497	.53	-0.7	4501	1097	1001	0.70o

o — Bleed vave open c — Bleed valve closed

Table 8-3. One-Third-Octave Band Plot Categories — Flight 1

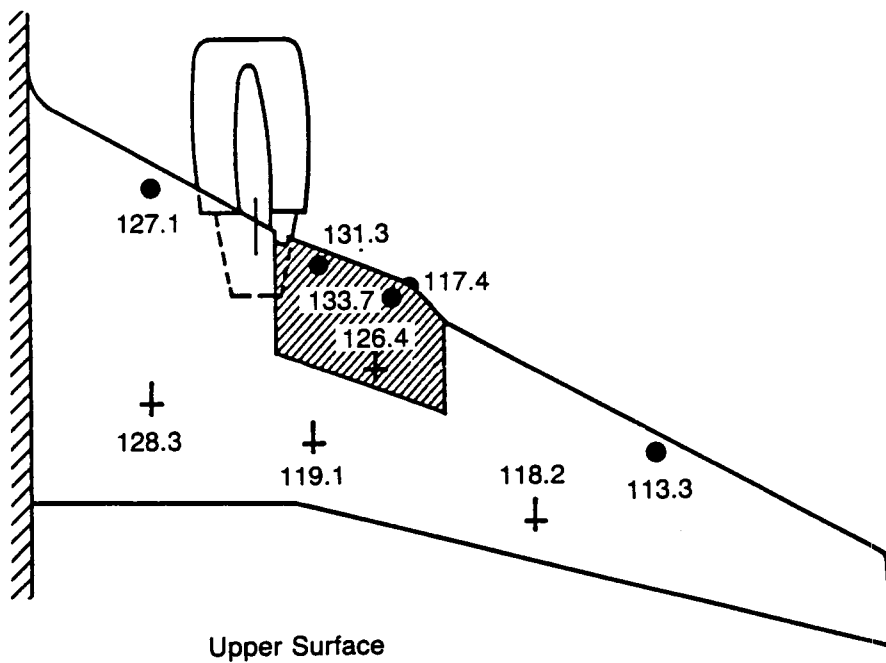
	Cond. no.	Airplane Mach no.	Altitude (10 ³ ft)	Right engine N _{1C} (r/rim)	Sideslip, (deg)
Category 1, Zero sideslip	001	0.82	39	4175	0
	005	0.81	39	4010	0
	035	0.81	40	4019	0
	036	0.78	40	3908	0
	109	0.79	39	3810	0
Category 2, Positive sideslip	002	0.81	39	4353	5.4
	006.1	0.79	39	4382	5.8
	016	0.80	41	4245	6.3
Category 3, Negative sideslip	006.2	0.80	39	4348	-6.4
	017	0.80	41	4366	-7.1
Category 6, Engine power variation	013	0.80	41	4366	0
	014	0.81	41	4221	0
	015	0.81	41	4115	0

Table 8-4. One-Third-Octave Band Plot Categories — Flight 2

	Cond. no.	Mach no.	Altitude (10 ³ ft)	Right engine N _{1C}	Sideslip, deg	
Category 1— Altitude variation— no sideslip	201	0.80	30	3227	0	
	204	0.81	34	3424	0	
	207	0.81	36	3585	0	
	210	0.80	37	3660	0	
	211	0.80	38	3850	0	
	239	0.80	38	3557	0	
	214	0.81	39	3954	0	
	241	0.80	41	4034	0	
Category 2— Positive sideslip	202	0.79	30	3240	3.2	
	205	0.79	34	3437	3.9	
	212	0.79	38	3867	3.9	
Category 3— Negative sideslip	203	0.79	30	3294	-4.0	
	206	0.80	34	3481	-3.9	
	213	0.80	38	3796	-3.7	
Category 4— Bleed valve check	217	0.71	37	3557	0	
	218	0.70	37	3582	0	
Category 5— Engine power variation M _{AP} = 0.63	219	0.64	35	4493	0	Narrowband analyzed
	220	0.62	35	2928	0	
	221	0.63	35	2315	0	
Category 6— Engine power variation M _{AP} = 0.8	223	0.80	40.5	4340	0	Narrowband analyzed
	224	0.80	40.5	4102	0	
	225	0.80	40.5	3793	0	
	228	0.79	41.3	2645	0	
Category 7— Engine power variation M _{AP} = 0.7	231	0.70	39	4508	0	
	232	0.70	39	4019	0	
	233	0.70	39	3631	0	
	237	0.71	39	3280	0	
	236	0.71	39	2602	0	
	238	0.69	36.5	1097	0	

Table 8-4. One-Third-Octave Band Plot Categories — Flight 2 (Continued)

	Cond. no.	Mach no.	Altitude (10 ³ ft)	Right engine N _{1C}	Sideslip, deg	
Category 8— Engine power variation $M_{AP} = 0.82$	243	0.82	39	4345	0	
	244	0.82	39	4116	0	
	245	0.82	39	3865	0	
	247	0.81	38.5	2501	0	
Category 9— Sideslip variation $M_{AP} = 0.8$	224	0.80	40.5	4102	0	
	225	0.80	40.5	3793	0	
	226	0.79	40.5	3965	4.8	
	227	0.80	40.5	3993	-4.0	
Category 10— Sideslip variation $M_{AP} = 0.7$	232	0.70	39	4019	0	
	233	0.70	39	3631	0	
	234	0.70	38	3786	6.8	
	235	0.71	39	3816	-6.7	
Category 11— Other sideslip data	240	0.80	38	3673	3.9	
	246	0.82	39	4355	4.0	
Category 12— Other zero sideslip	242	0.83	43	4321	0	
	249	0.78	39	3717	0	
	250	0.75	39	3723	0	
	251	0.76	39	4426	0	
	252	0.75	39	4007	0	
	229	0.75	40.5	3330	0	
	215	0.82	39	4042	0	
	216	0.83	39	4331	0	
	248	0.82	39	4023	0	
	222	0.81	39	3903	0	



Altitude: 35,000 ft
Mach no. = 0.64
 N_{1c} = 4493 r/min
Fan exhaust Mach no. = 1.19

● Surface microphone
+ Probe microphone

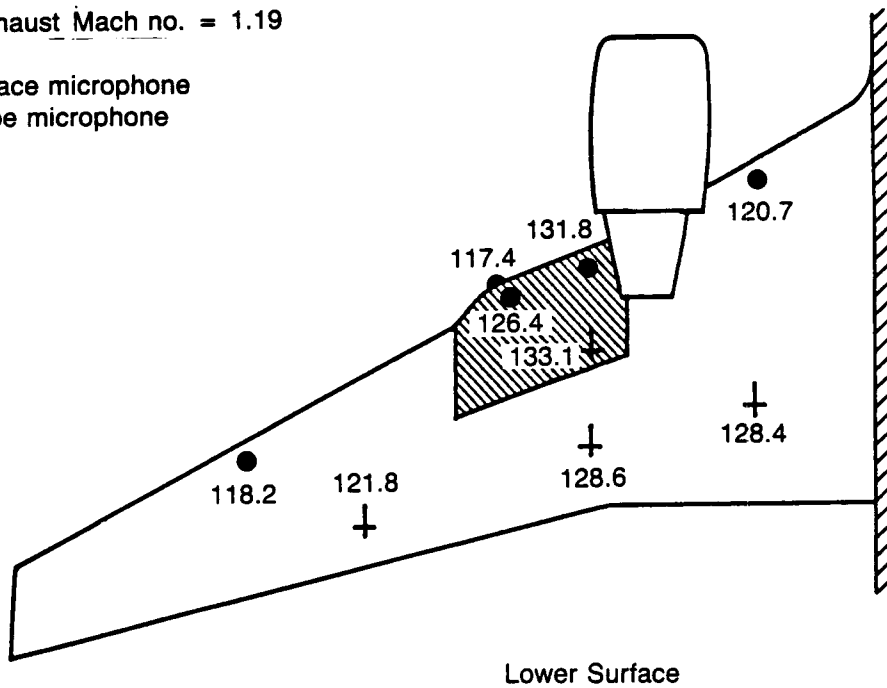
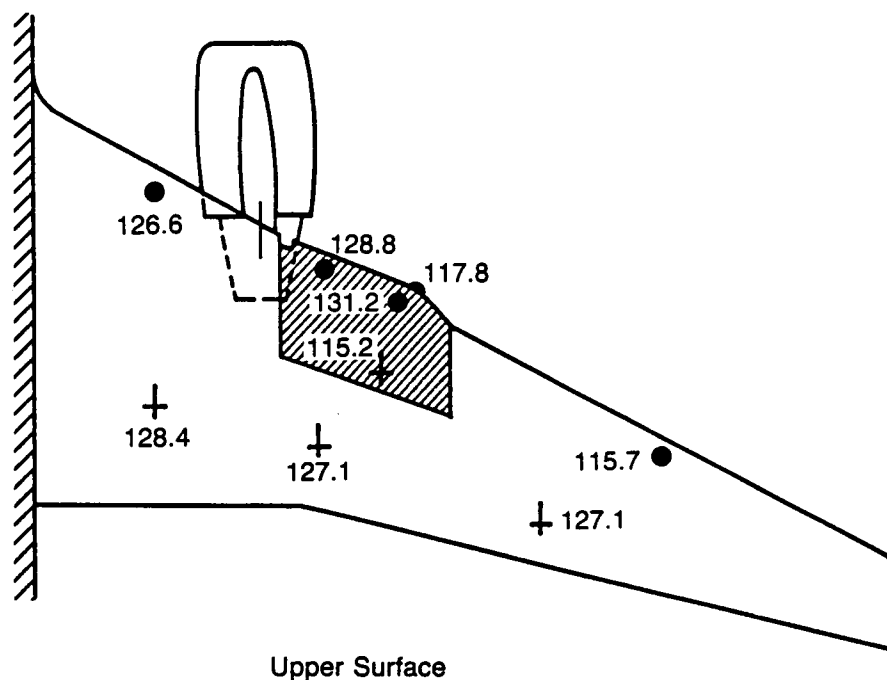


Figure 8-1. OASPL Distribution on 757 Wing, Category 5, Condition 219



Altitude = 40,500 ft
 Mach no. = 0.80
 $N_{1c} = 4,340$ r/min
 $C_L = 0.534$
 Fan exhaust Mach no. = 1.28

● Surface microphone
 † Probe microphone

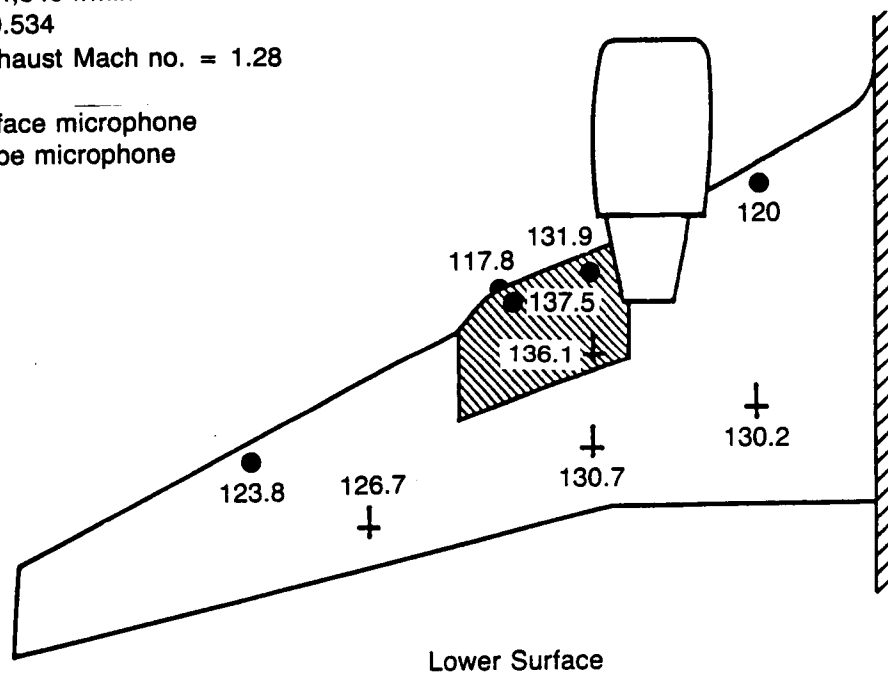
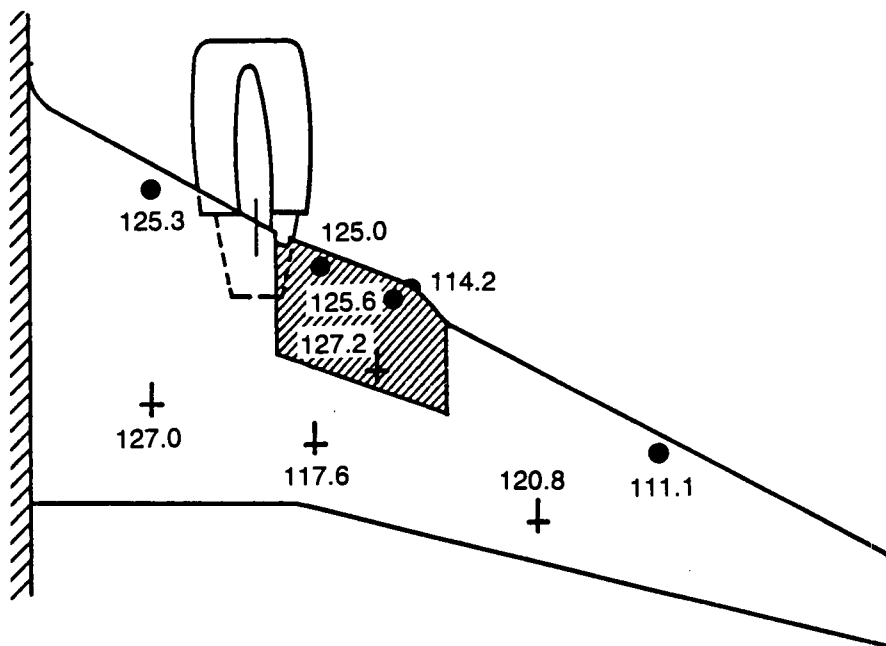


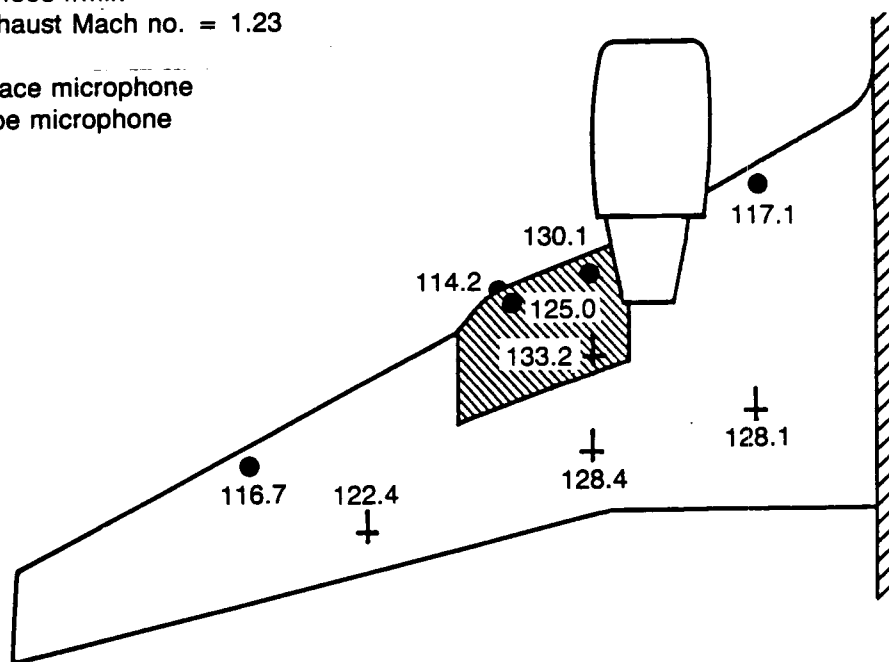
Figure 8-2. OASPL Distribution on 757 Wing, Category 6, Condition 223



Upper Surface

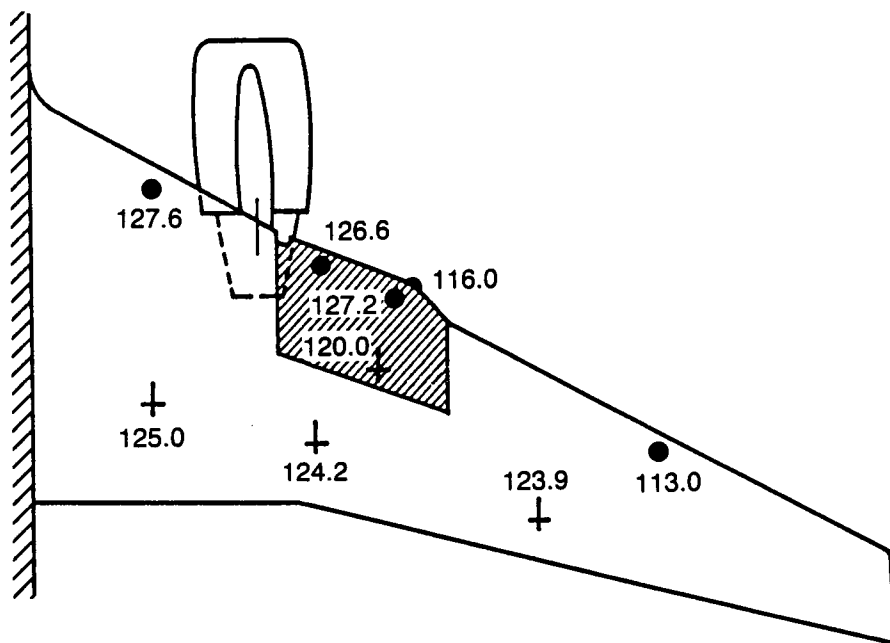
Altitude = 39,000 ft
 $Mach_{AP} = 0.70$
 $N_{1c} = 4508 \text{ r/min}$
 Fan exhaust Mach no. = 1.23

● Surface microphone
 + Probe microphone



Lower Surface

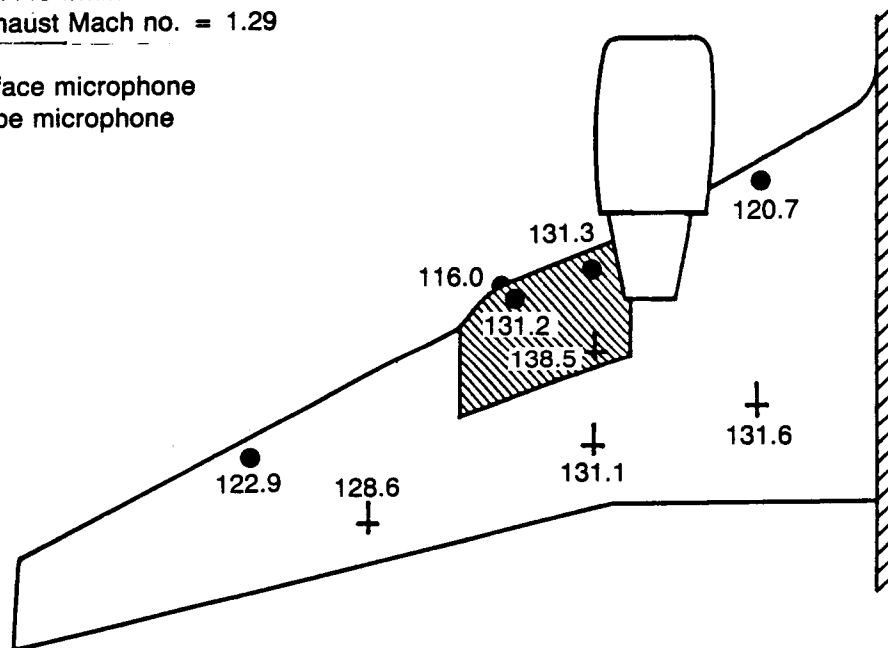
Figure 8-3. OASPL Distribution on 757 Wing, Category 7, Condition 231



Upper Surface

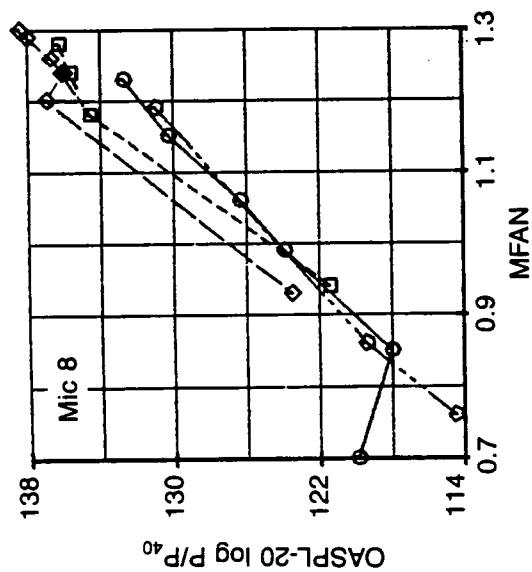
Altitude: 39,000 ft
Mach no. = 0.82
 $N_{1c} = 4445$ r/min
Fan exhaust Mach no. = 1.29

● Surface microphone
+ Probe microphone



Lower Surface

Figure 8-4. OASPL Distribution on 757 Wing, Category 8, Condition 243



\diamond M_{AP} 0.63
 \circ M_{AP} 0.70
 \square M_{AP} 0.80
 \diamond M_{AP} 0.82

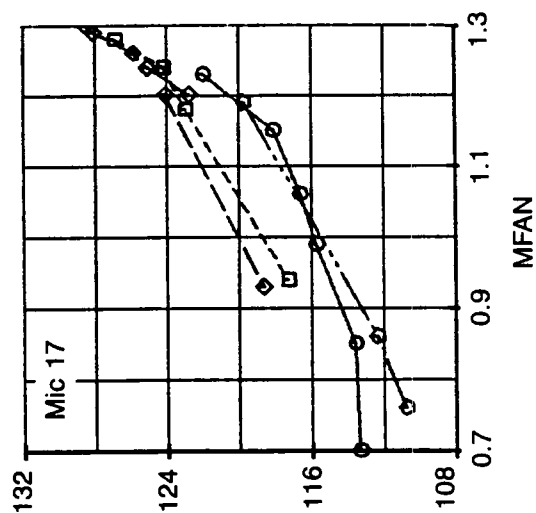
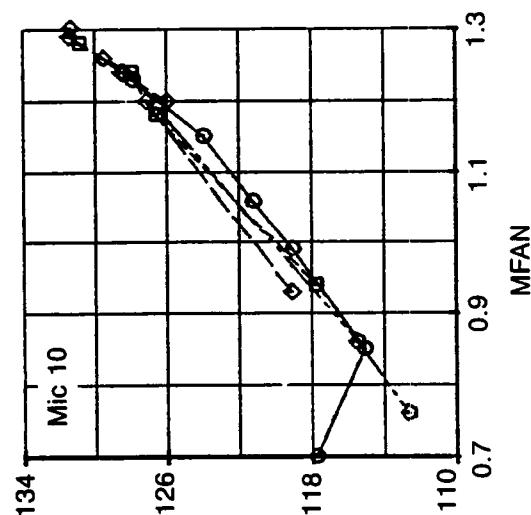
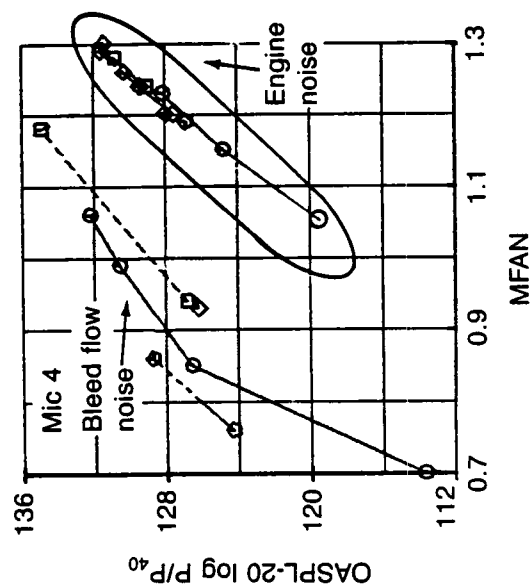
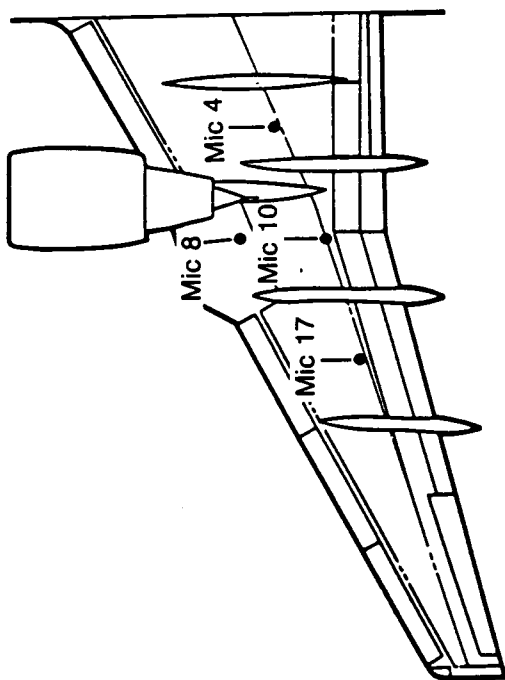


Figure 8-5. Normalized OASPL on Wing Lower Surface, Probe Microphones

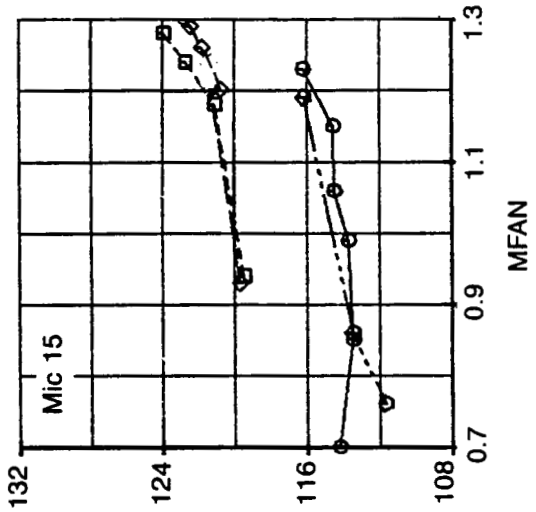
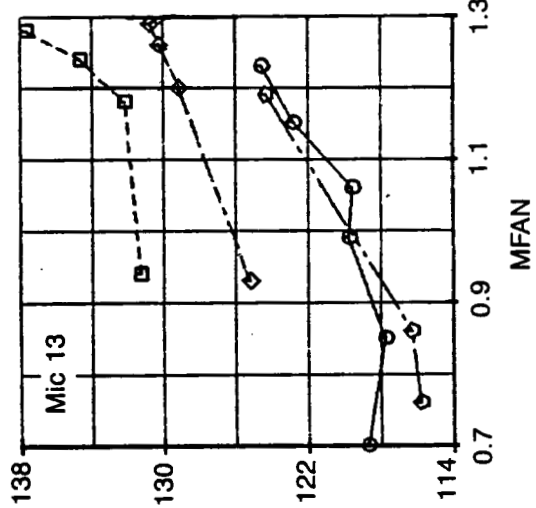
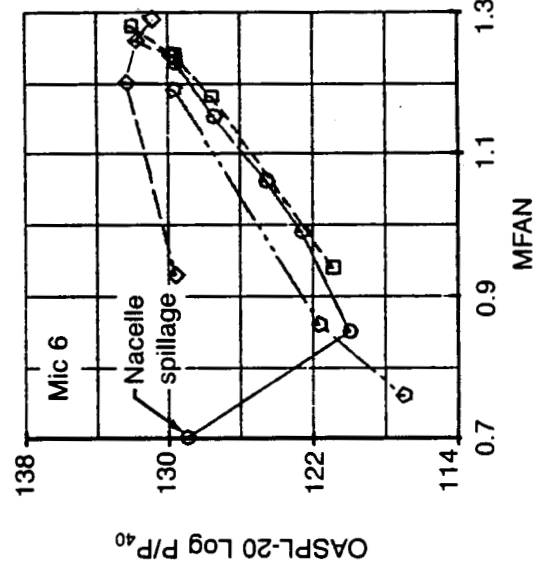
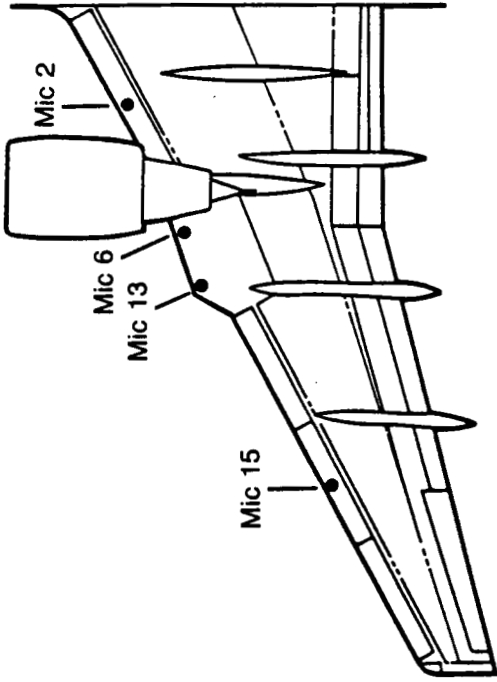
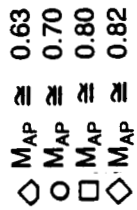
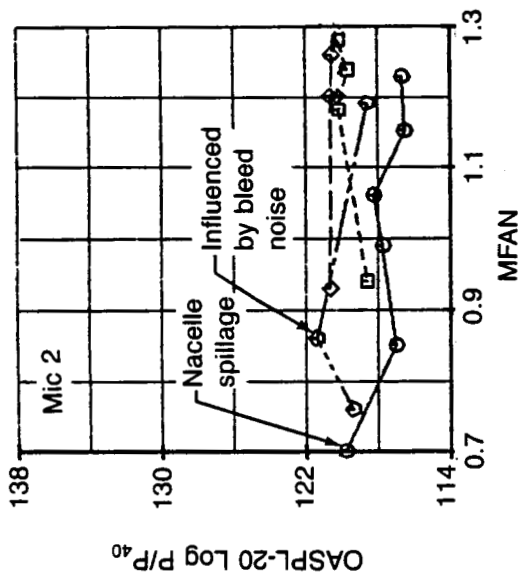


Figure 8-6. Normalized OASPL on Wing Lower Surface, Leading Edge Surface Microphones

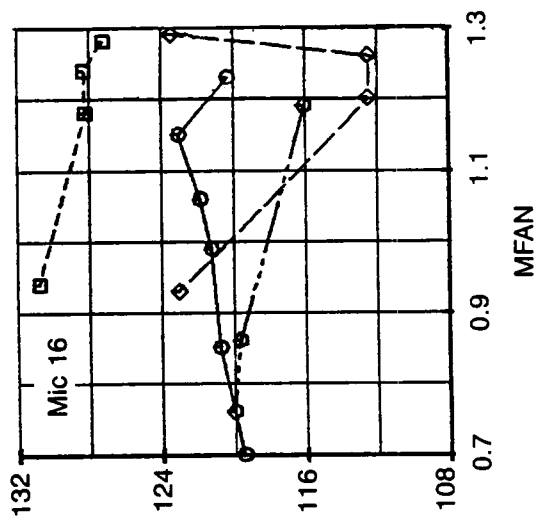
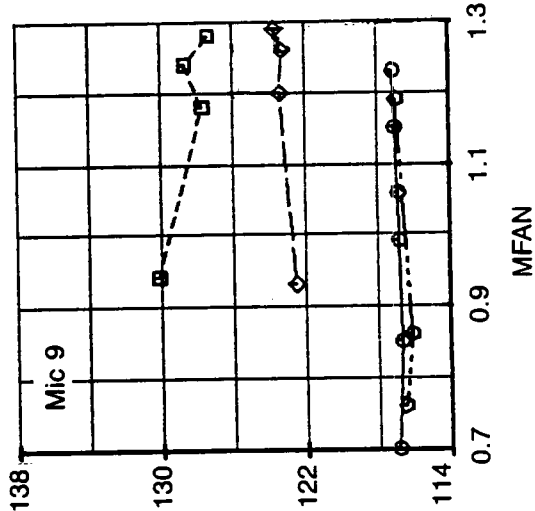
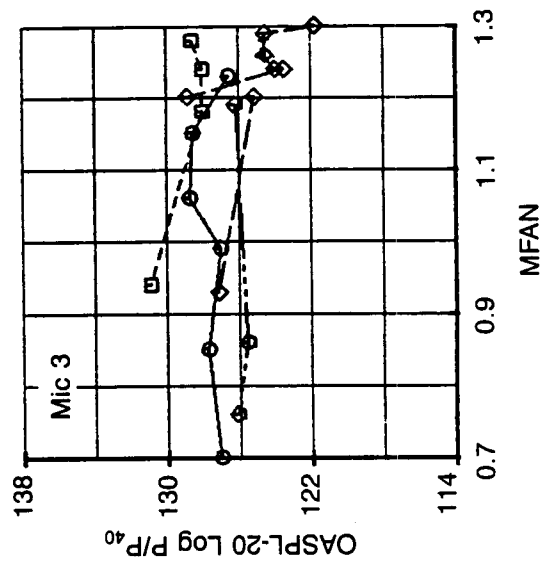
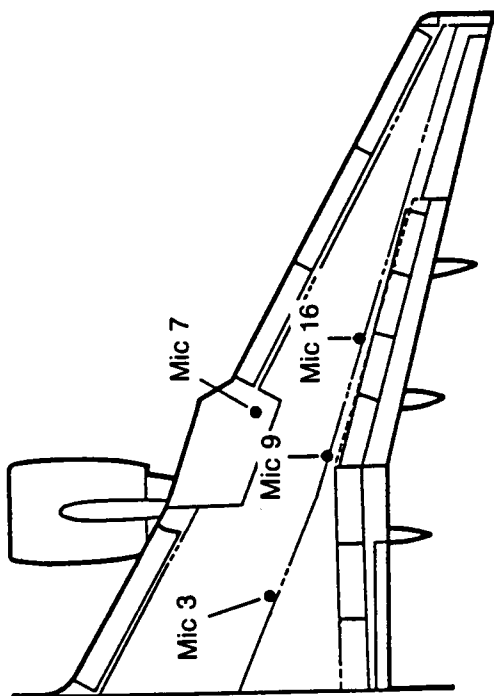
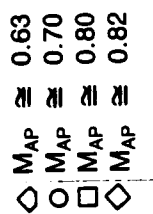
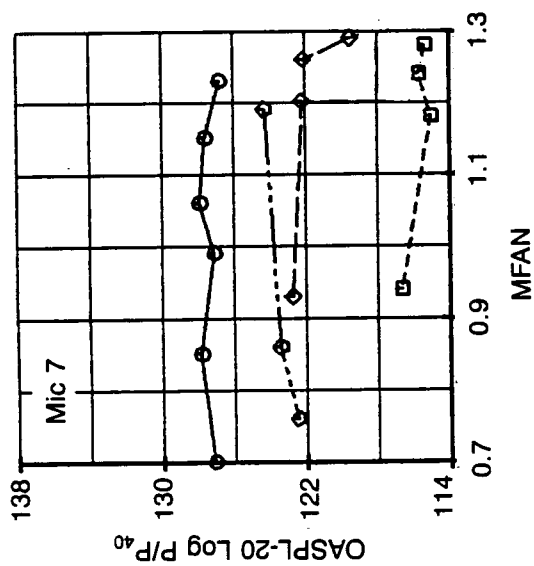


Figure 8-7. Normalized OASPL on Wing Upper Surface, Probe Microphones

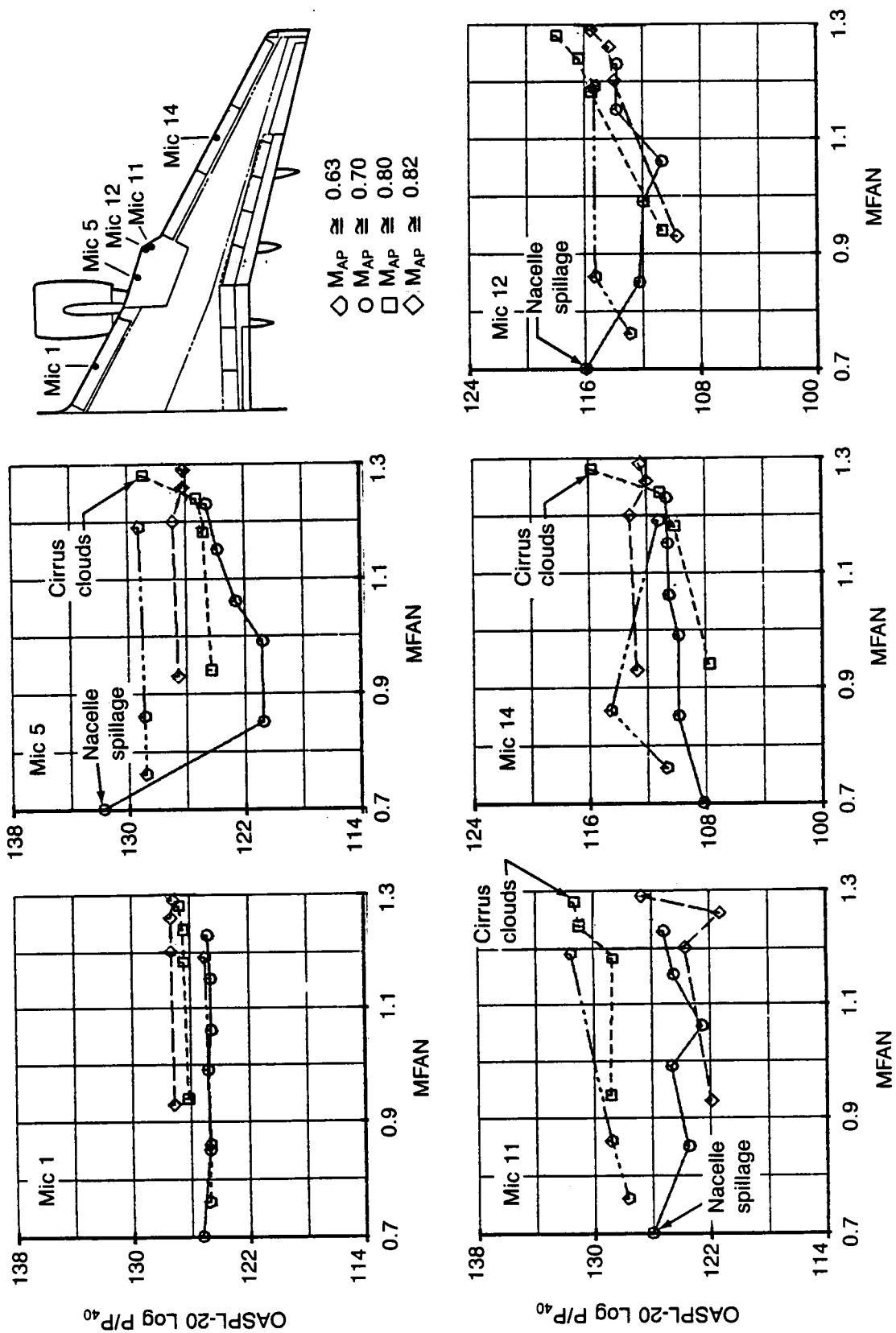


Figure 8-8. Normalized OASPL on Wing Upper Surface, Leading Edge Surface Microphones

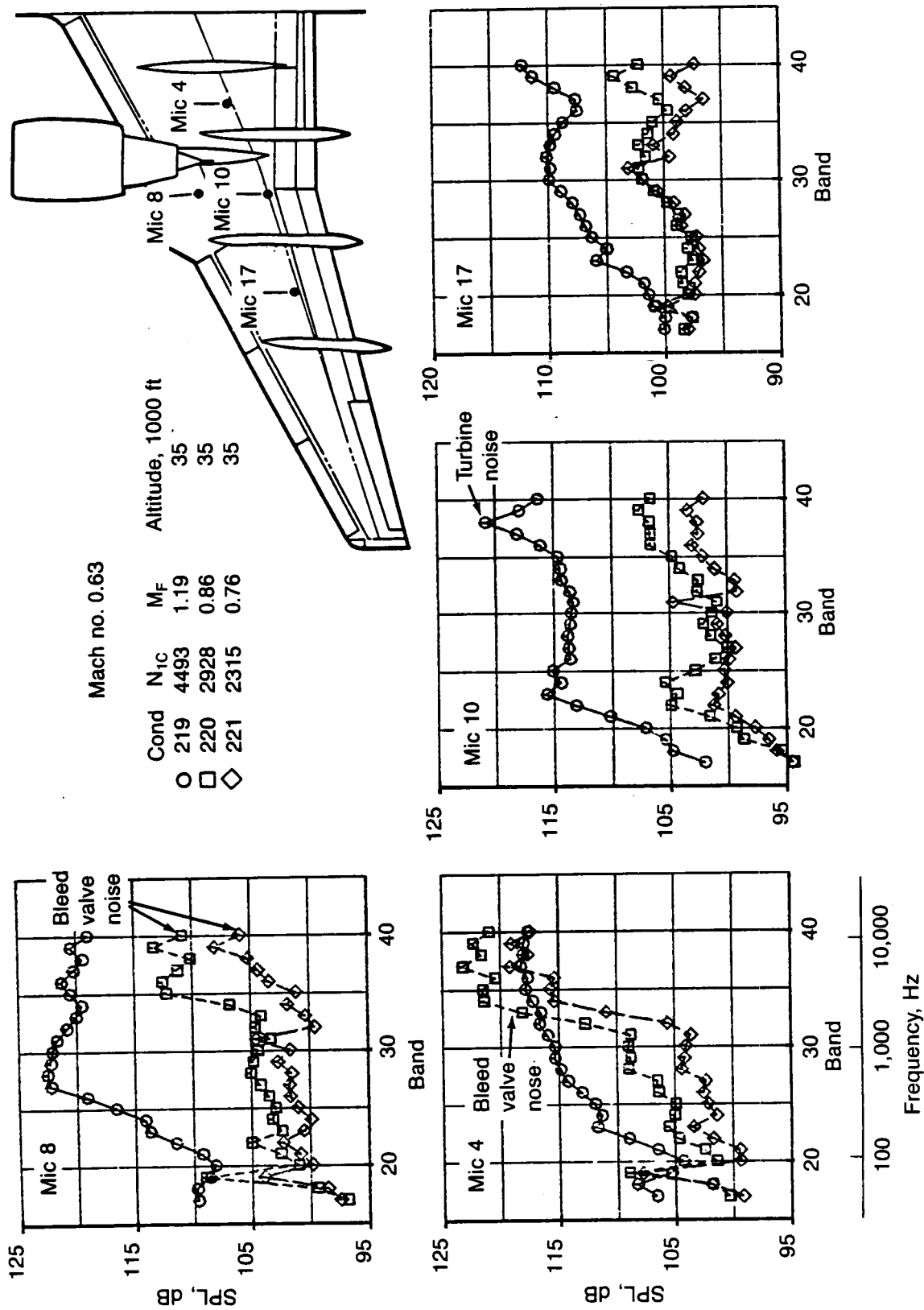


Figure 8-9. Engine Power Effects on Wing Lower Surface Spectra, Probe Microphones

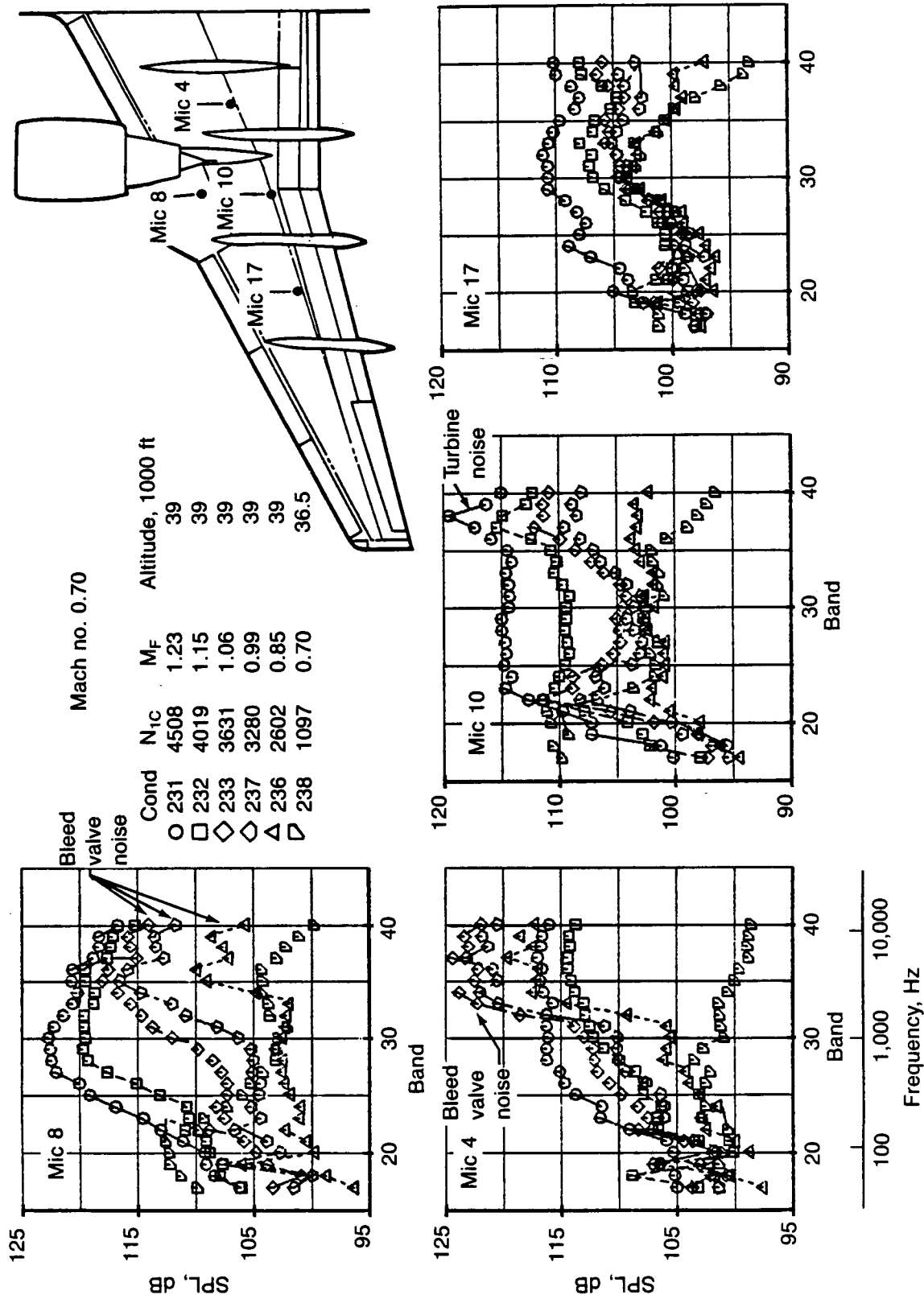
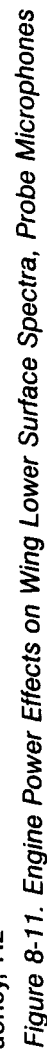
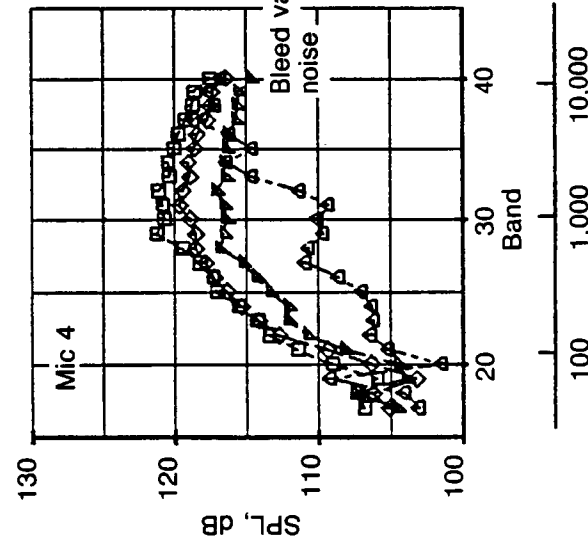
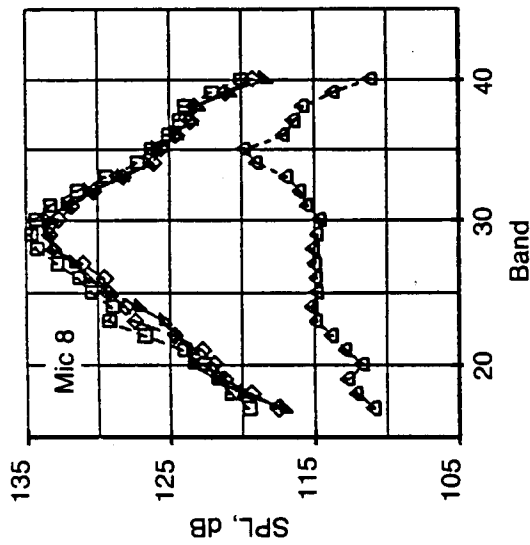


Figure 8-10. Engine Power Effects on Wing Lower Surface Spectra, Probe Microphones





Frequency, Hz

Mach no. 0.82

Cond	N _{1c}	M _F	Altitude, 1000 ft
□	243	4345	39
◇	244	4116	39
▧	245	3865	39
△	247	2501	38.5

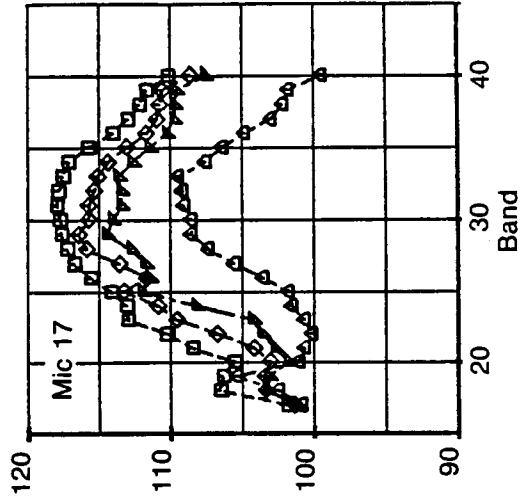
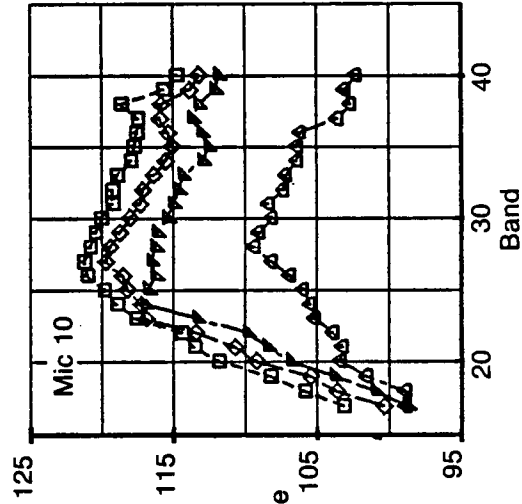
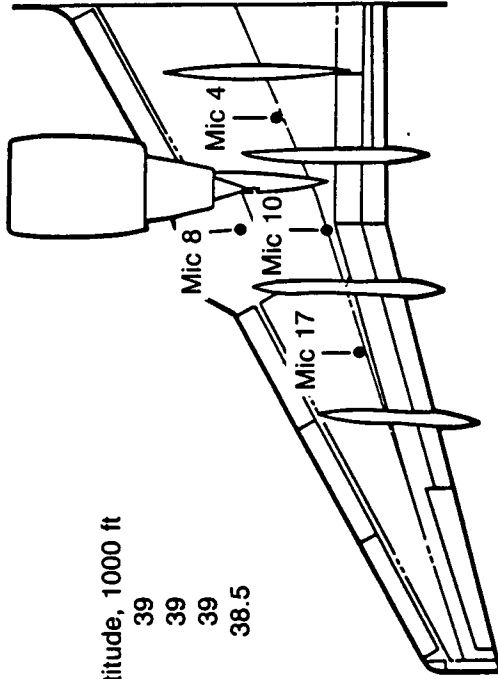
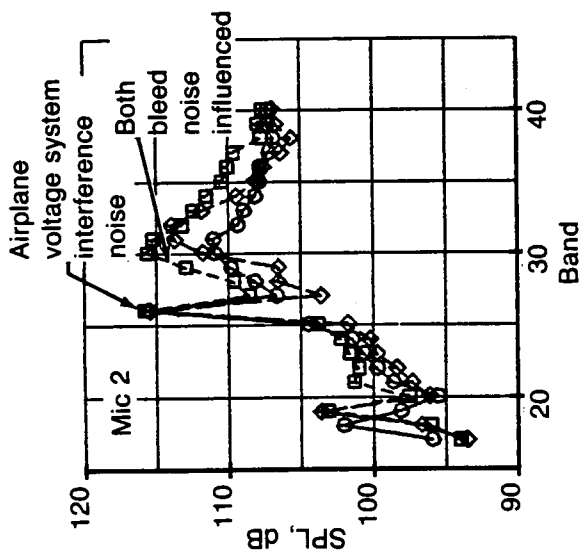


Figure 8-12. Engine Power Effects on Wing Lower Surface Spectra, Probe Microphones



Mach no. 0.63

Cond N_{IC} M_F Altitude, 1000 ft
 O 219 4493 1.19 35
 □ 220 2928 0.86 35
 ◇ 221 2315 0.76 35

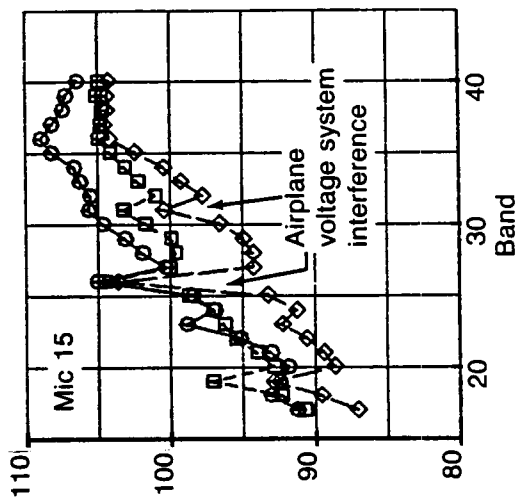
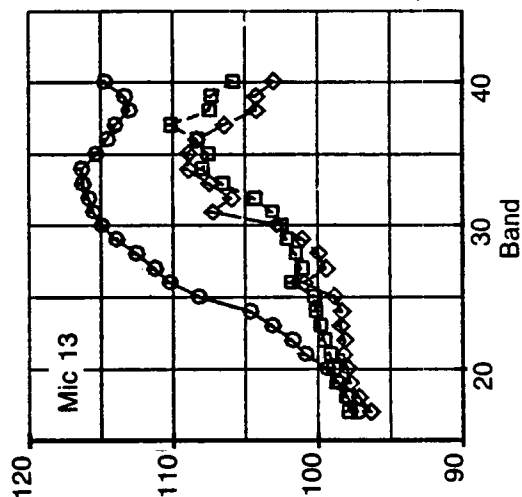
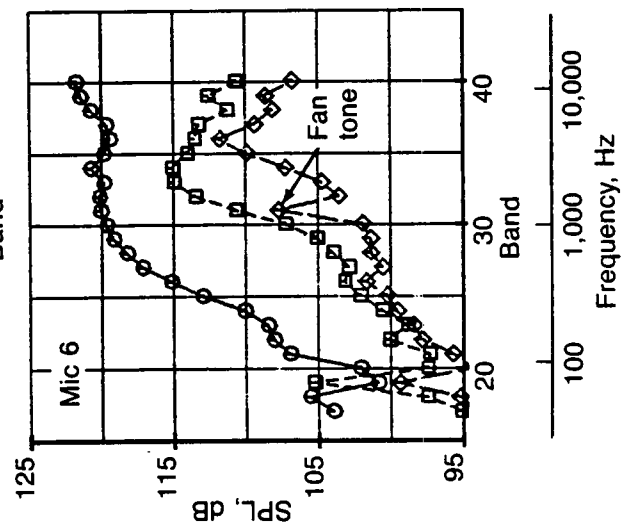
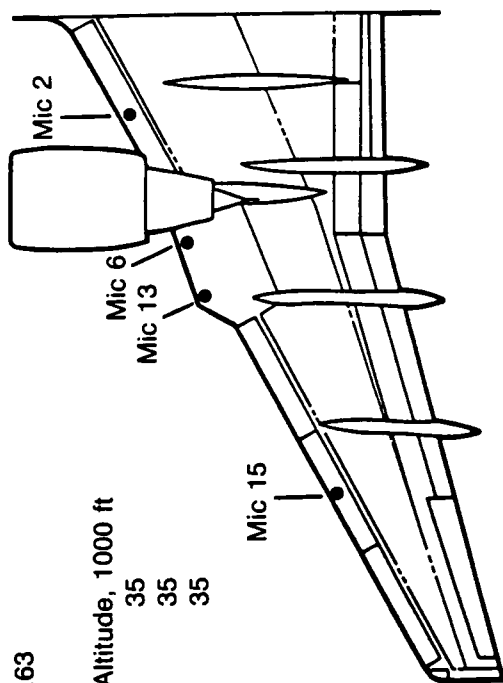


Figure 8-13. Engine Power Effects on Wing Lower Surface Spectra, Leading Edge Surface Microphones

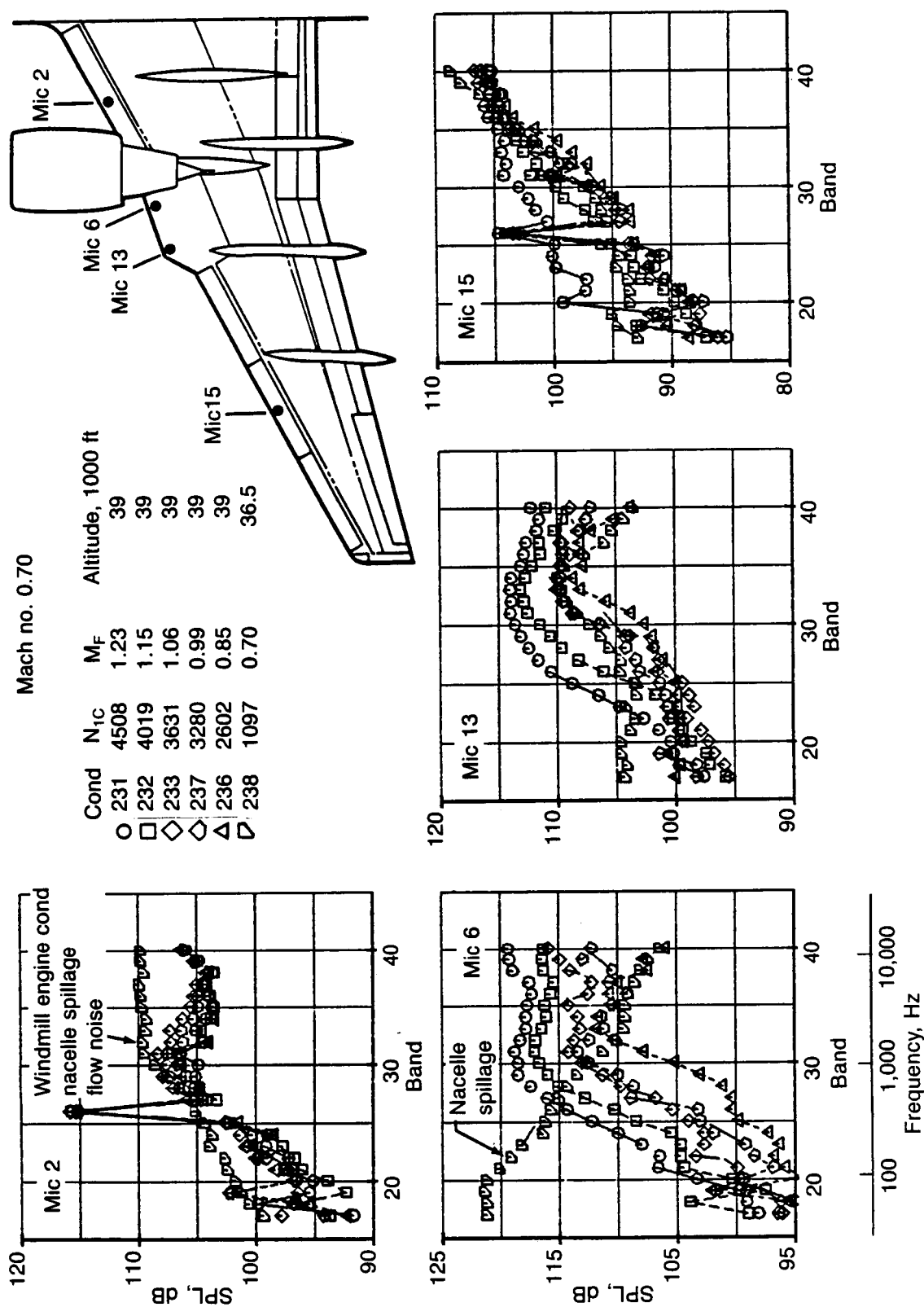


Figure 8-14. Engine Power Effects on Wing Lower Surface Spectra, Leading Edge Surface Microphones

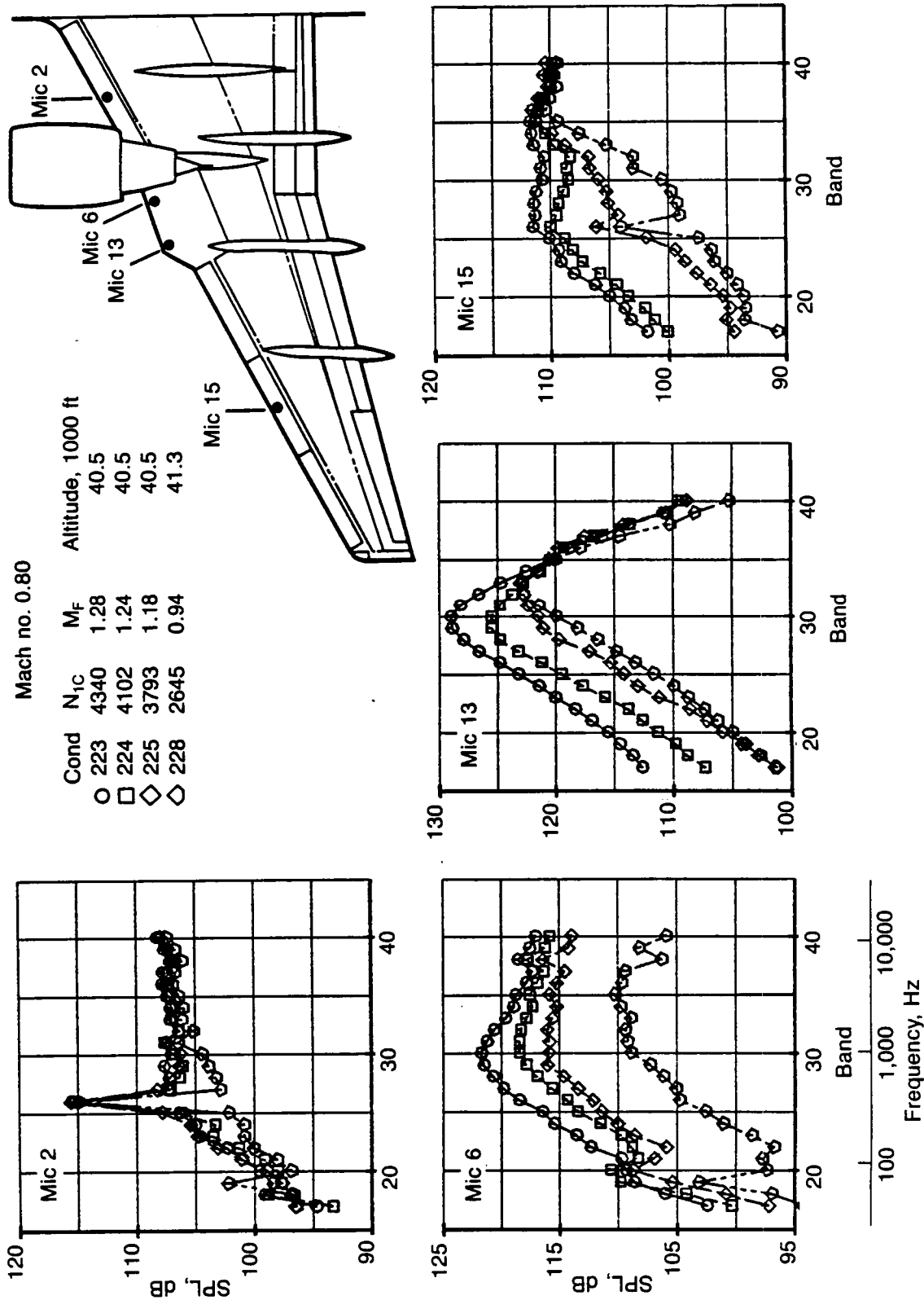
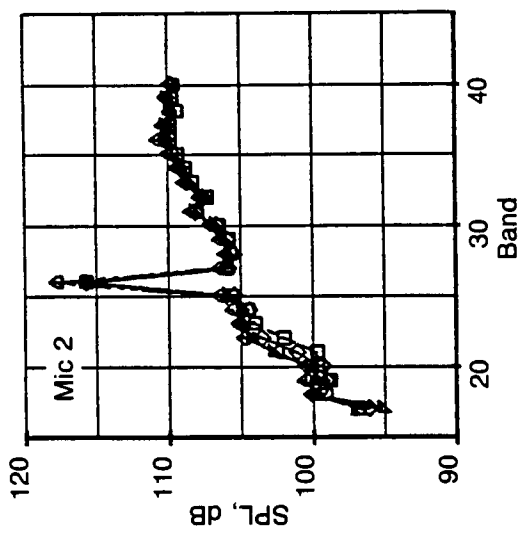


Figure 8-15. Engine Power Effects on Wing Lower Surface Spectra, Leading Edge Surface Microphones



Mach no. 0.82

Cond	N _{1C}	M _F	Altitude, 1000 ft
□	243	4345	39
◇	244	4116	39
▽	245	3865	39
△	247	2501	38.5

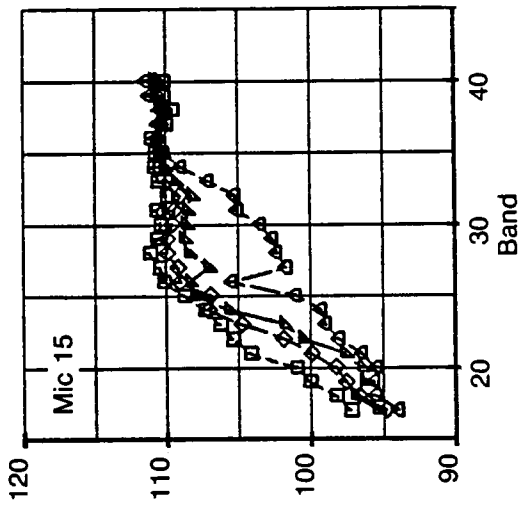
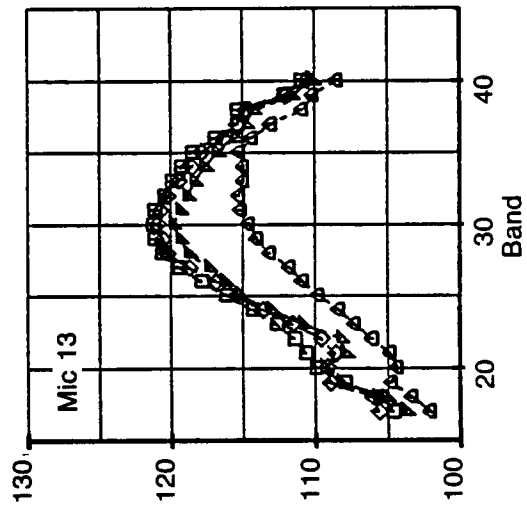
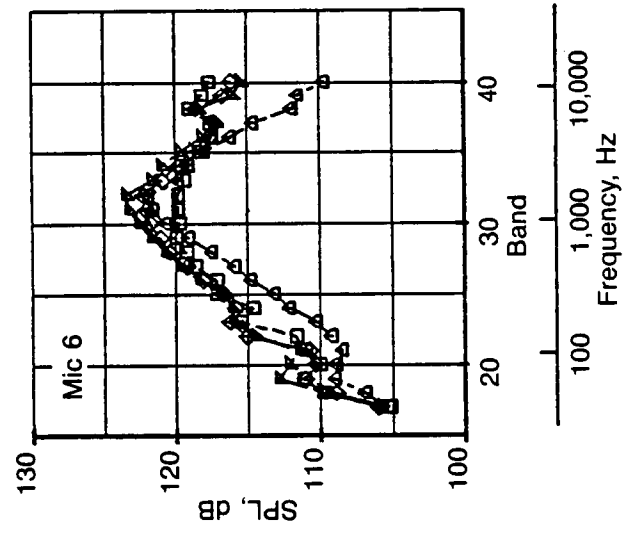
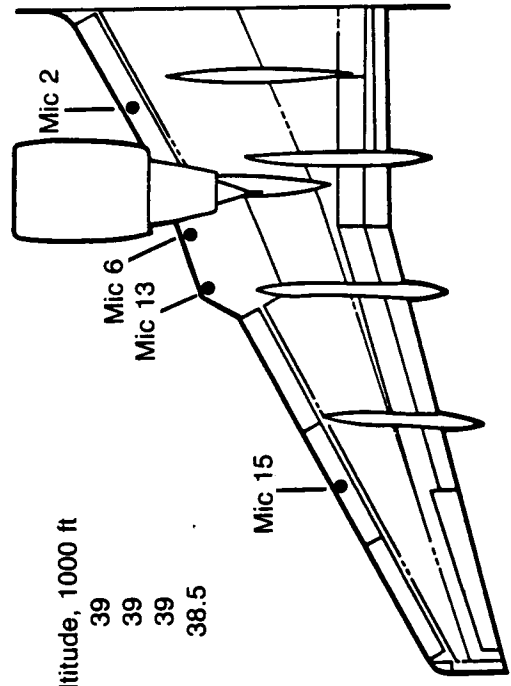
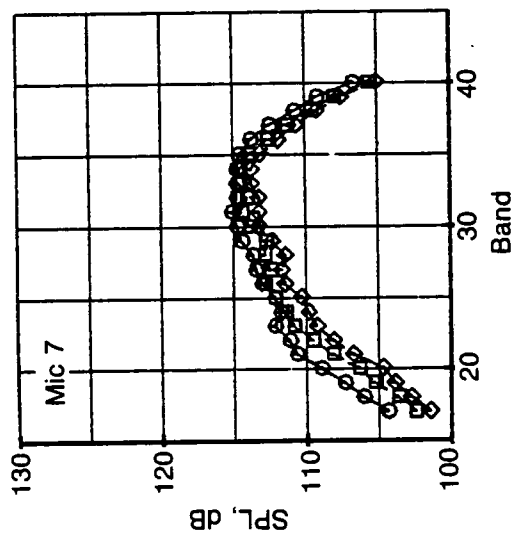


Figure 8-16. Engine Power Effects on Wing Lower Surface Spectra, Leading Edge Surface Microphones



Mach no. 0.63

Cond	N _{1C}	M _F	Altitude, 1000 ft
○	219	1.19	35
□	220	0.86	35
◇	221	0.76	35

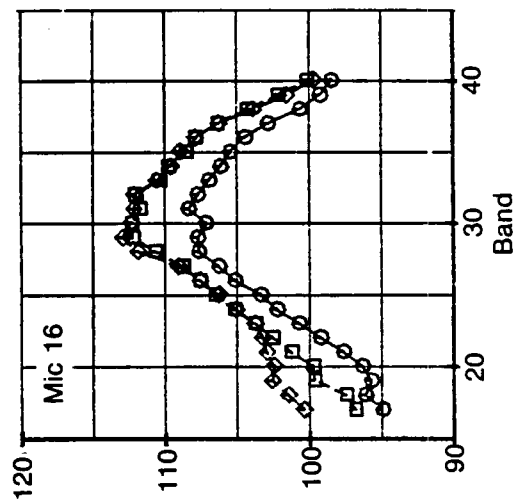
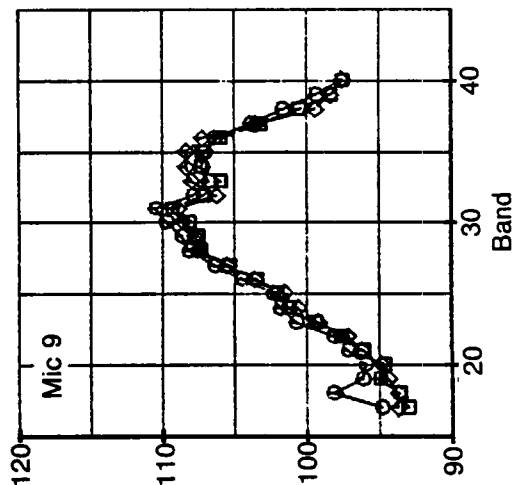
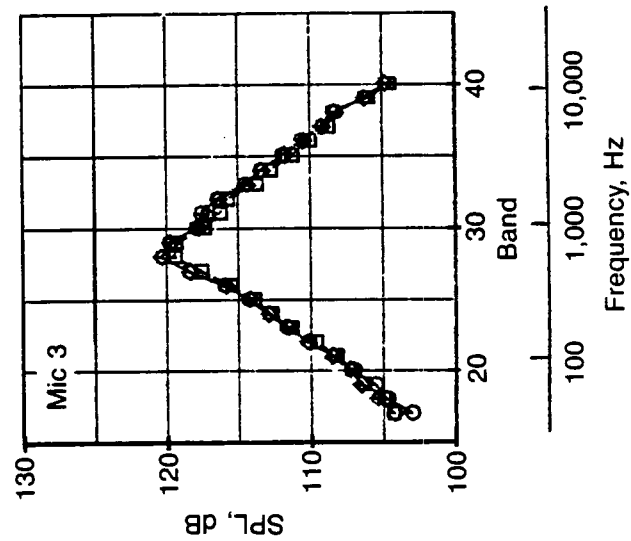
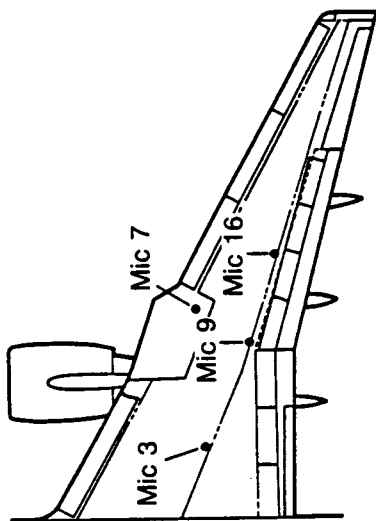
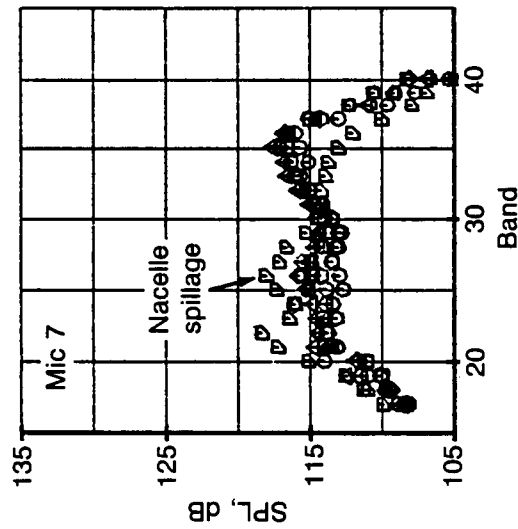


Figure 8-17. Engine Power Effects on Wing Upper Surface Spectra, Probe Microphones



Mach no. 0.70

Cond	N _{IC}	M _F	Altitude, 1000 ft
○ 231	4508	1.23	39
□ 232	4019	1.15	39
◇ 233	3631	1.06	39
◇ 237	3280	0.99	39
△ 236	2602	0.85	39
▽ 238	1097	0.70	36.5

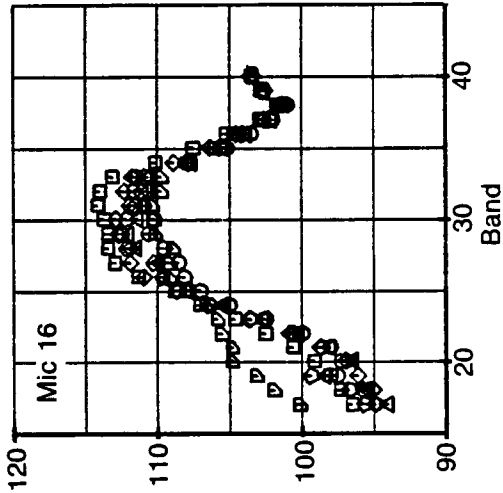
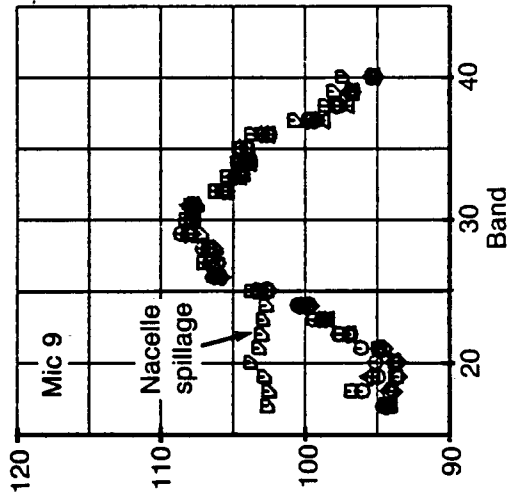
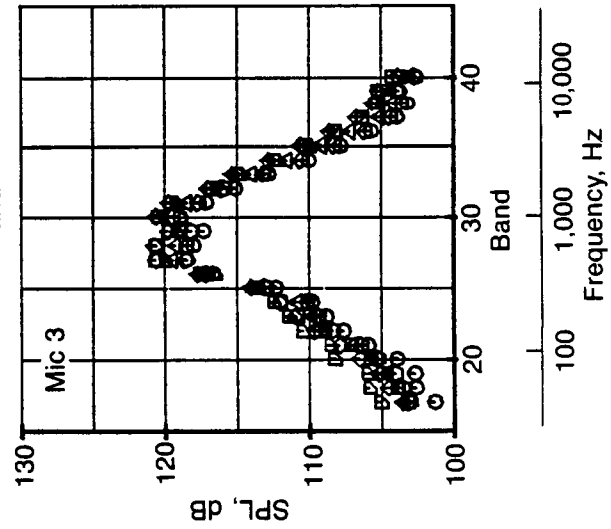
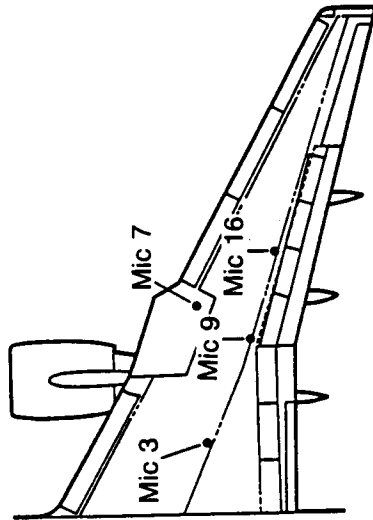
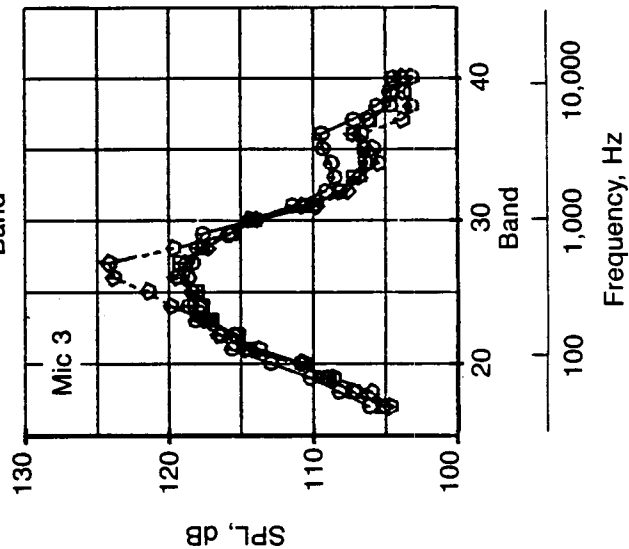
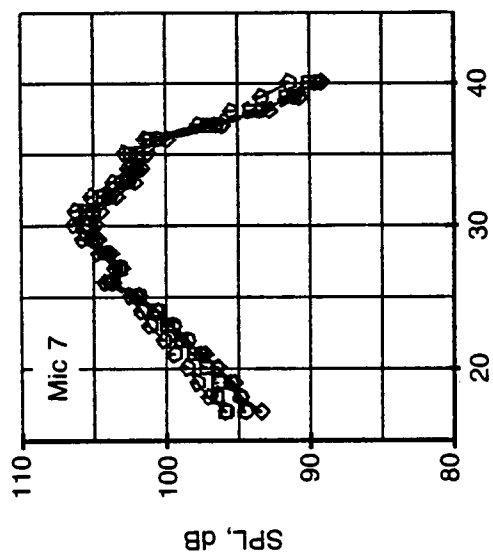


Figure 8-18. Engine Power Effects on Wing Upper Surface Spectra, Probe Microphones



Mach no. 0.80

Cond	N_{TC}	M_F	Altitude, 1000 ft
○	223	4340	1.28
□	224	4102	1.24
◇	225	3793	1.18
◊	228	2645	0.94
			40.5
			40.5
			40.5
			41.3

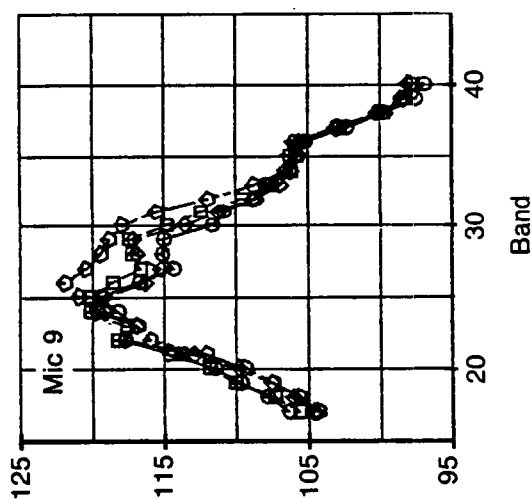
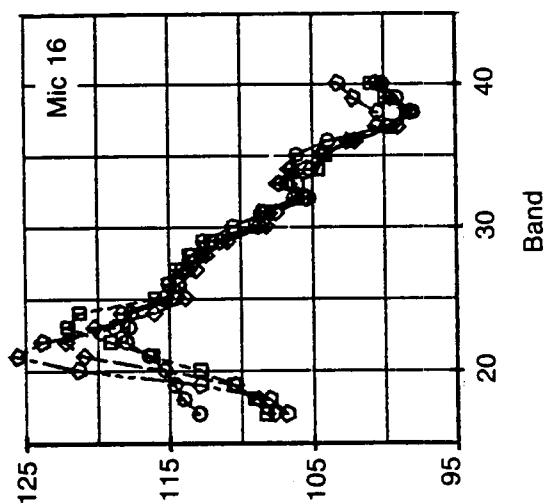
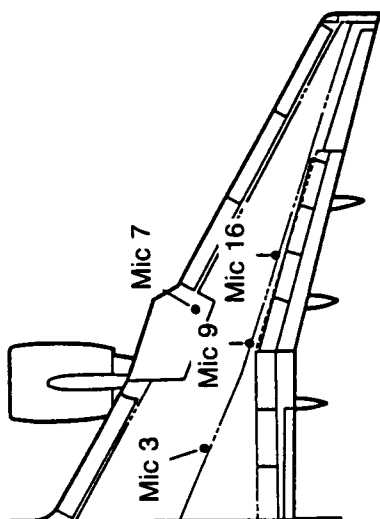
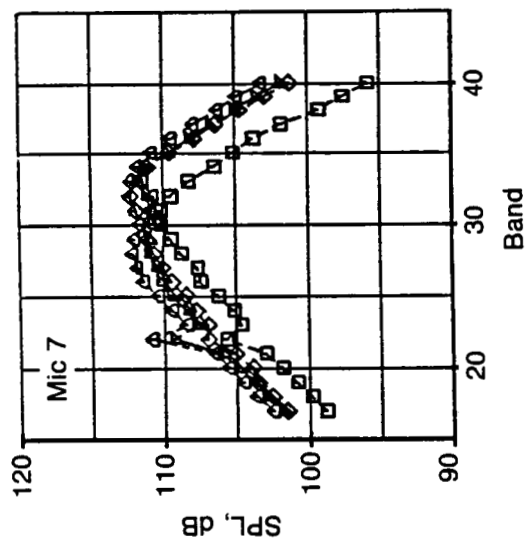


Figure 8-19. Engine Power Effects on Wing Upper Surface Spectra, Probe Microphones



Mach no. 0.82

Cond	N _{1C}	M _F	Altitude, 1000 ft
□	243	1.29	39
◇	244	1.26	39
▽	245	1.20	39
△	247	0.92	38.5

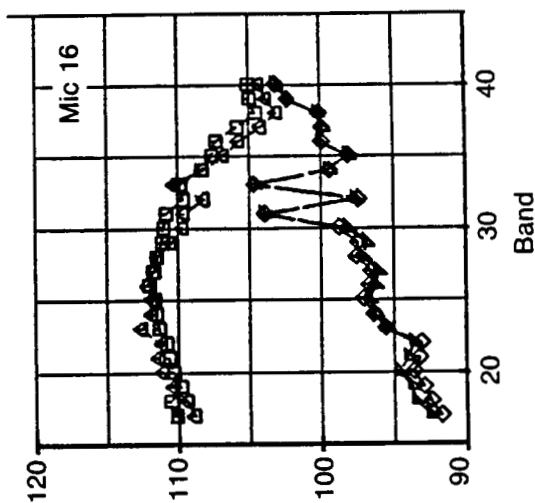
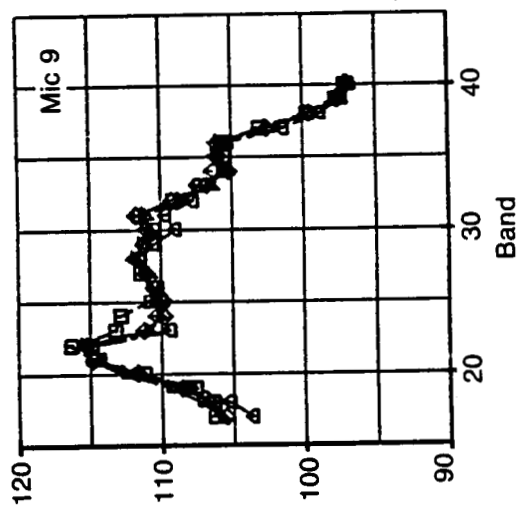
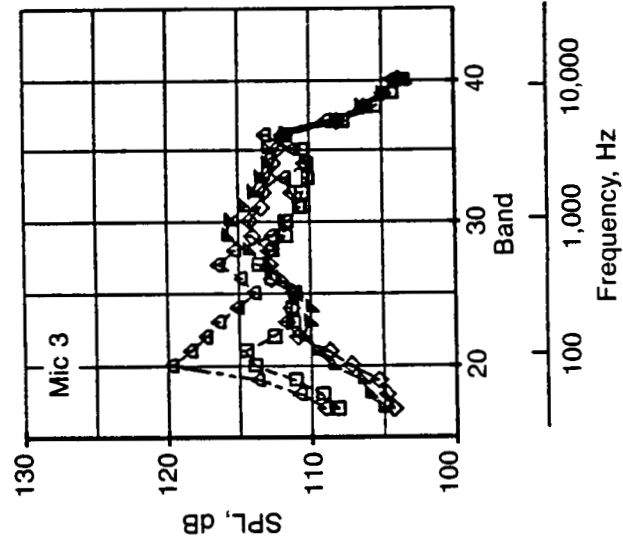
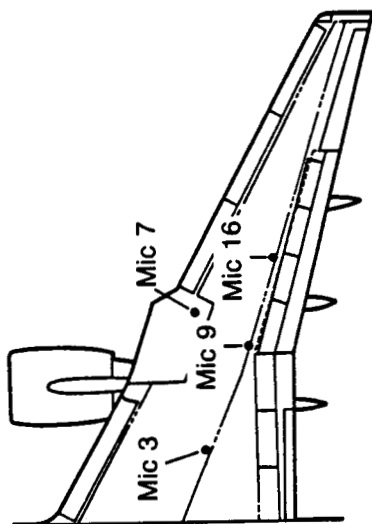


Figure 8-20. Engine Power Effects on Wing Upper Surface Spectra, Probe Microphones

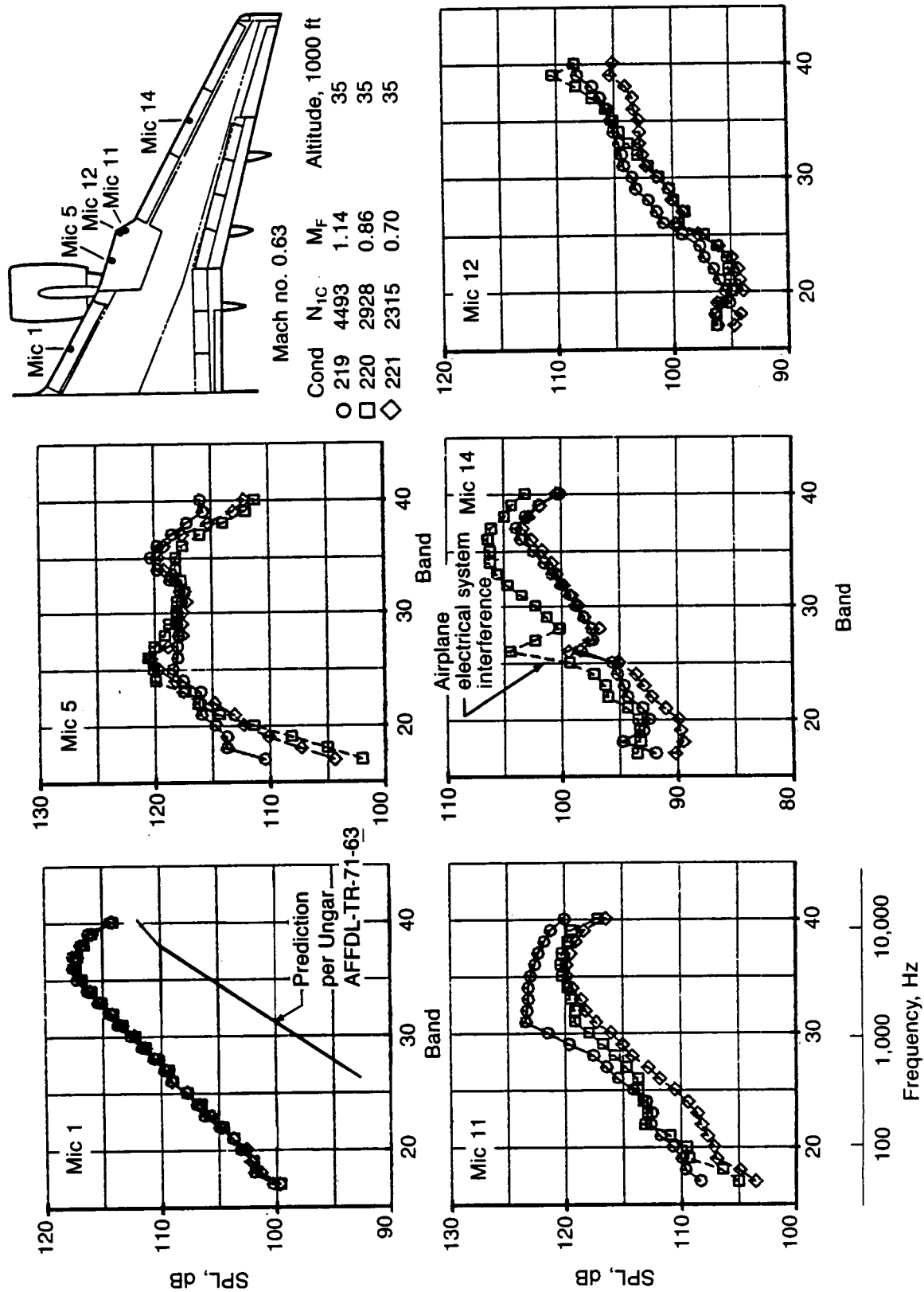


Figure 8-21. Engine Power Effects on Wing Upper Surface Spectra, Leading Edge Surface Microphones

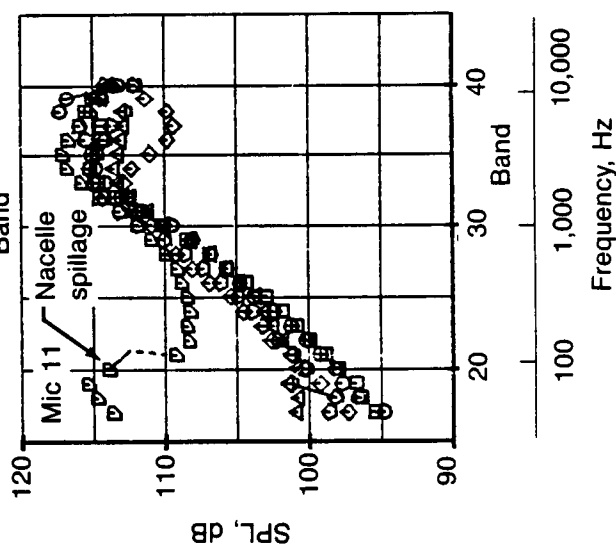
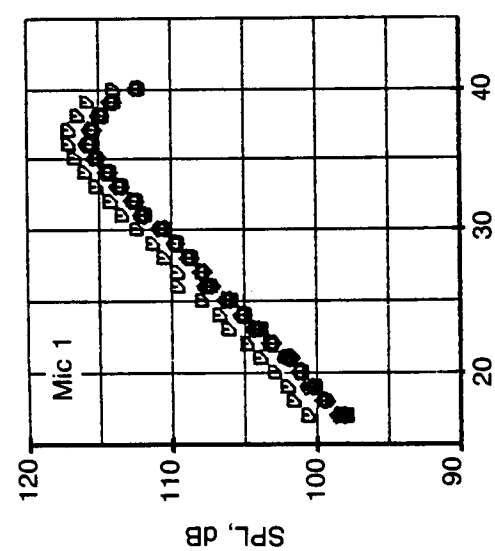
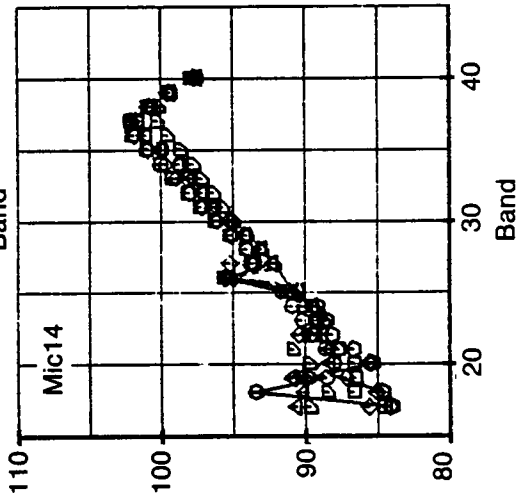
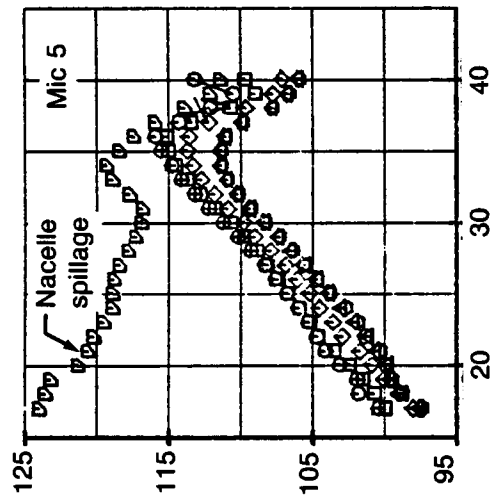
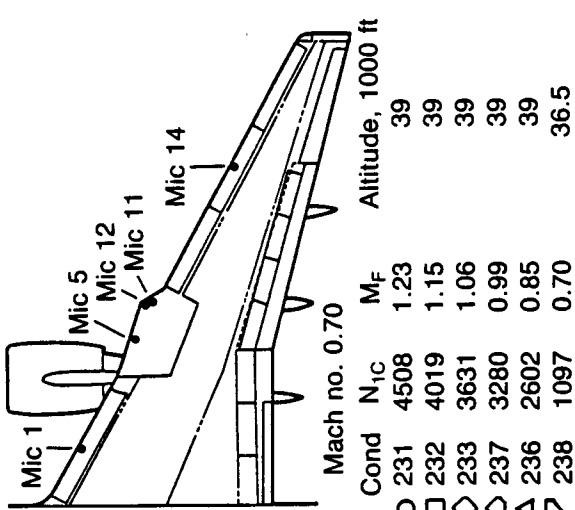


Figure 8-22. Engine Power Effects on Wing Upper Surface Spectra, Leading Edge Surface Microphones

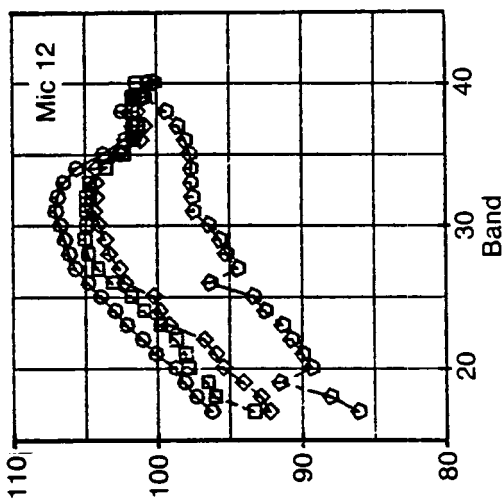
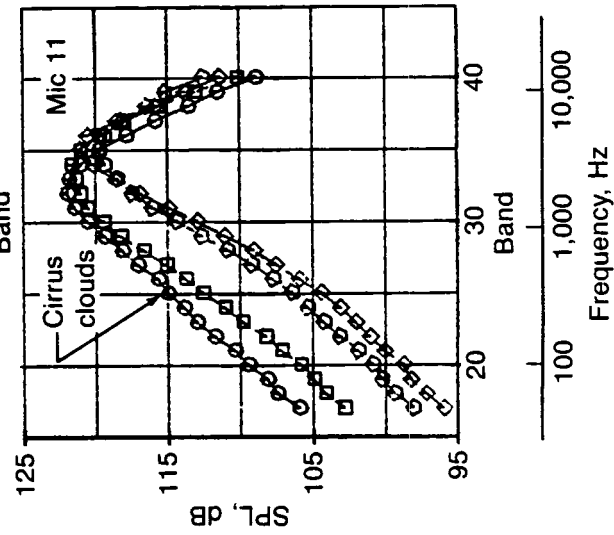
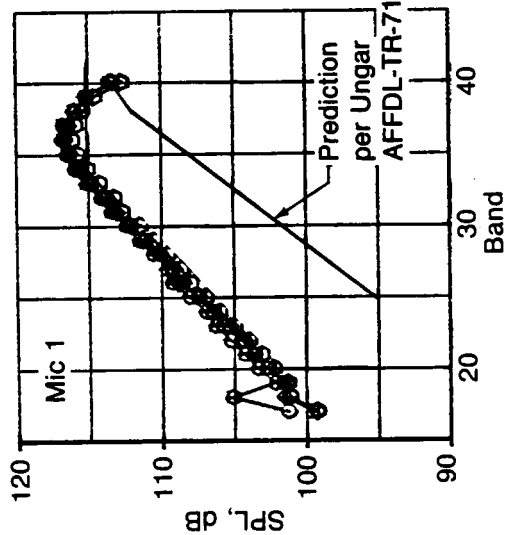
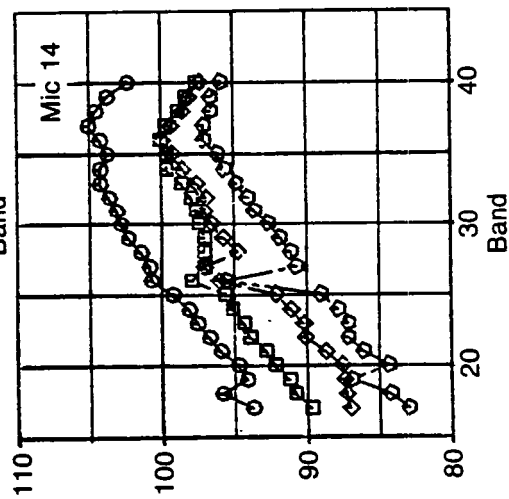
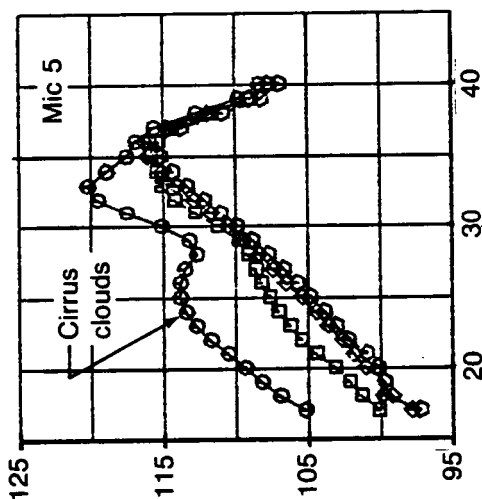
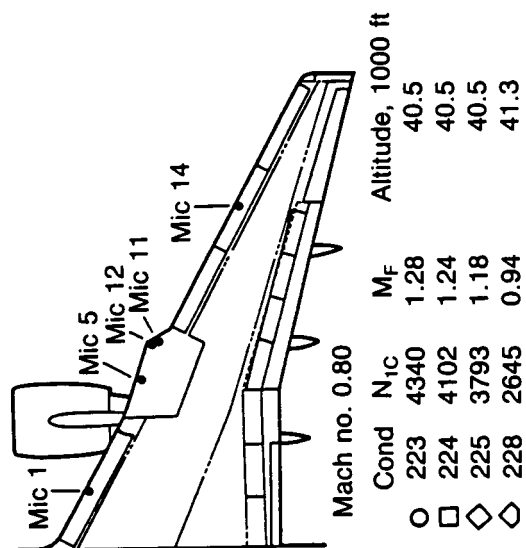


Figure 8-23. Engine Power Effects on Wing Upper Surface Spectra, Leading Edge Surface Microphones

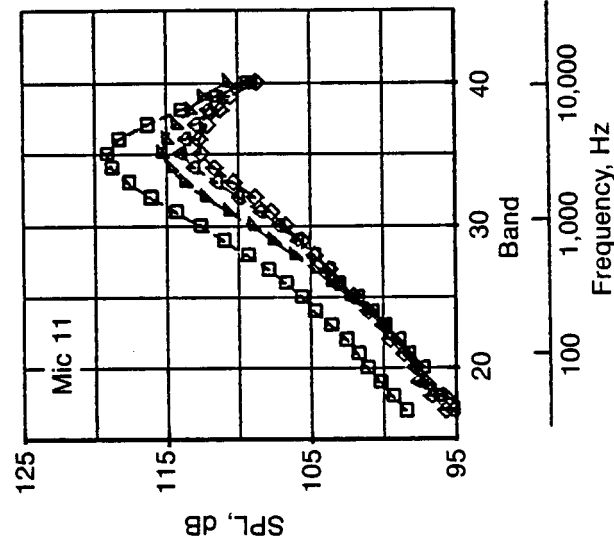
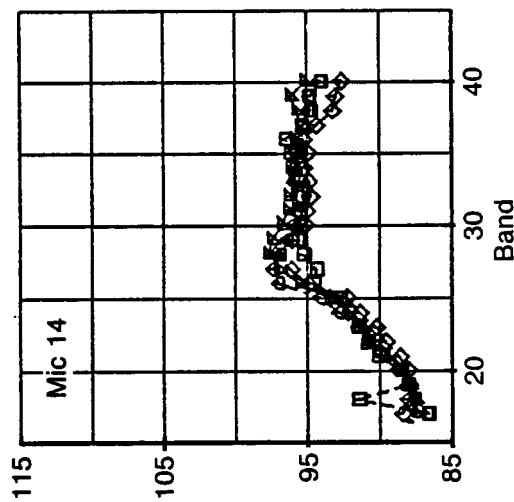
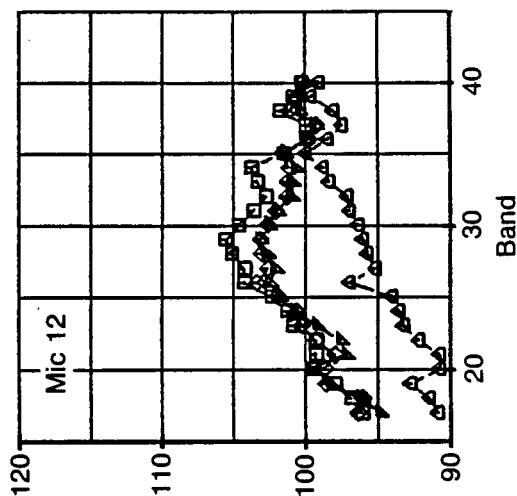
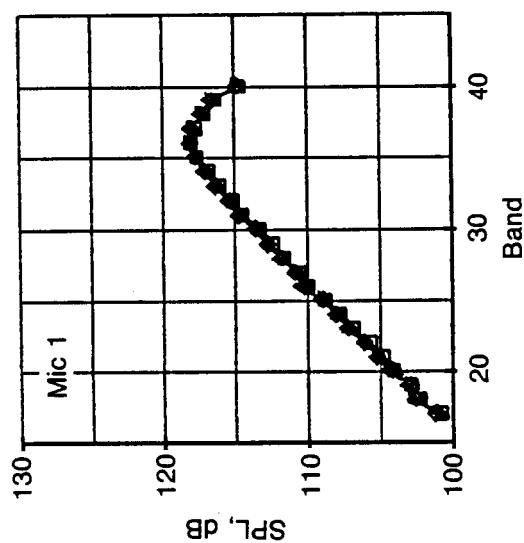
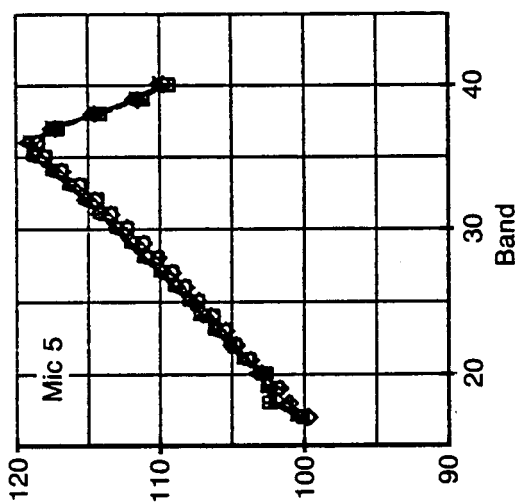
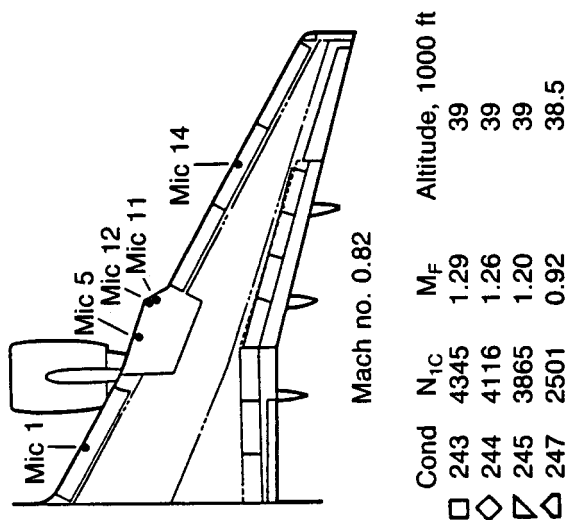
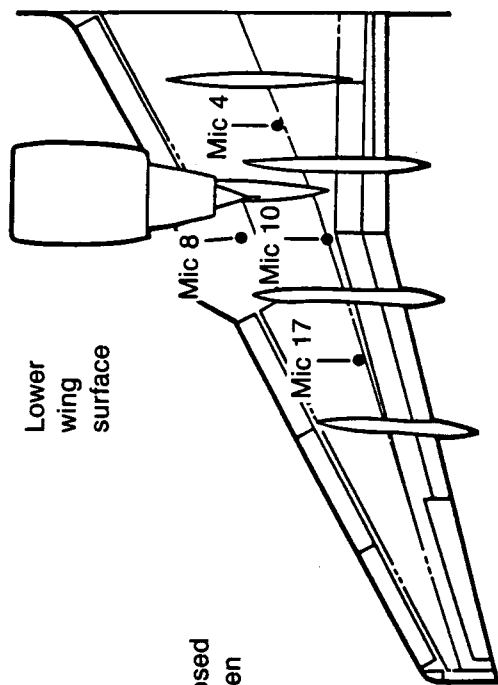
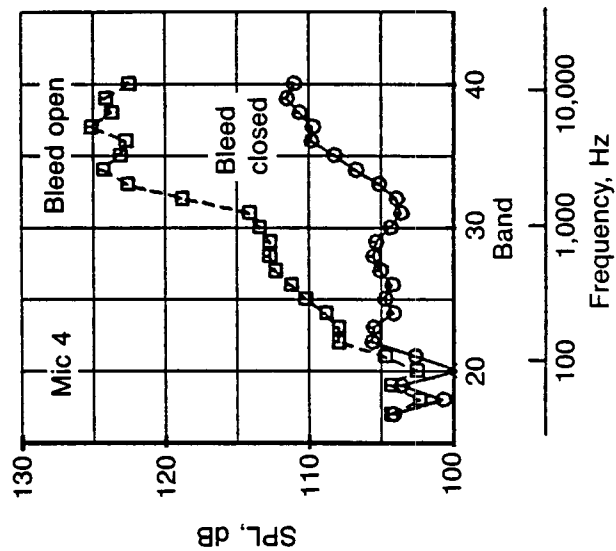
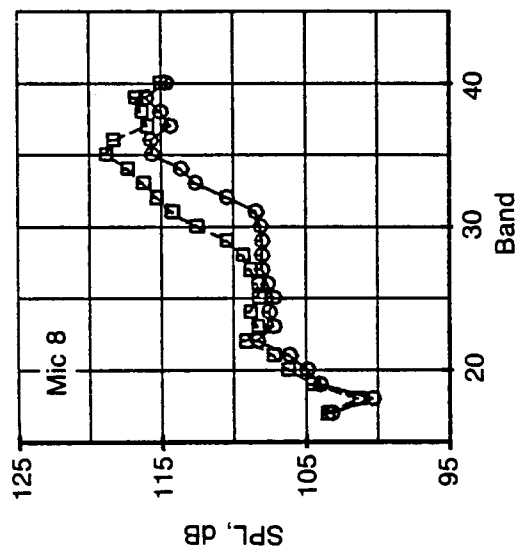


Figure 8-24. Engine Power Effects on Wing Upper Surface Spectra, Leading Edge Surface Microphones



Mach no. 0.70

Cond N_{1C}
 O 217 3557 bleed closed
 □ 218 3582 bleed open

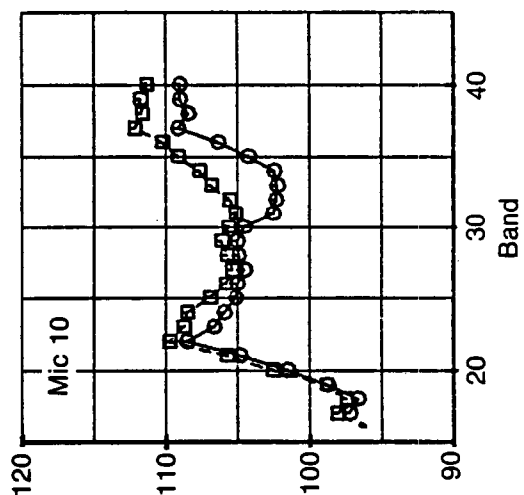
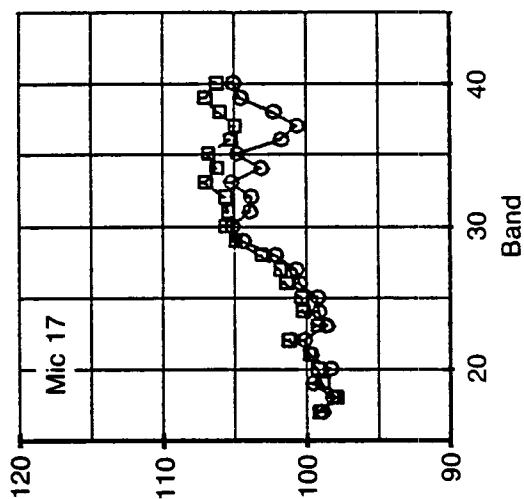
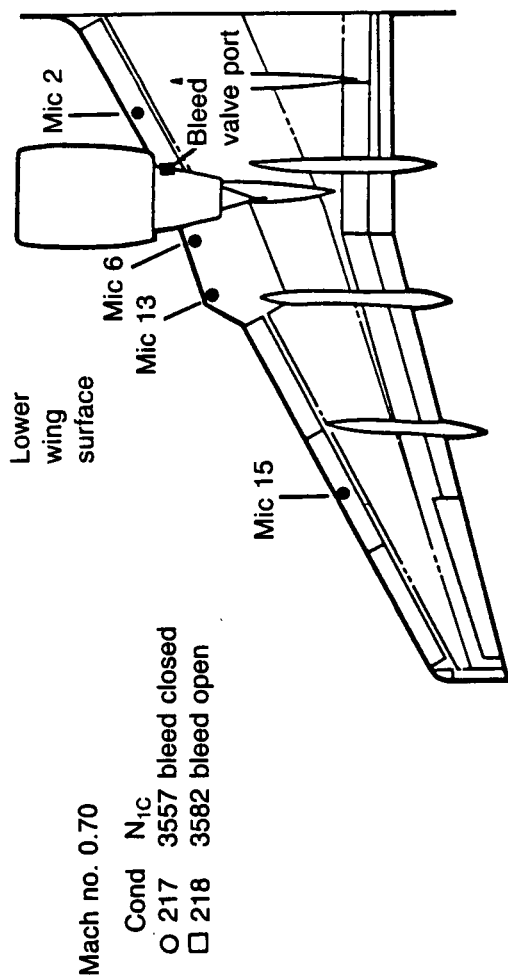
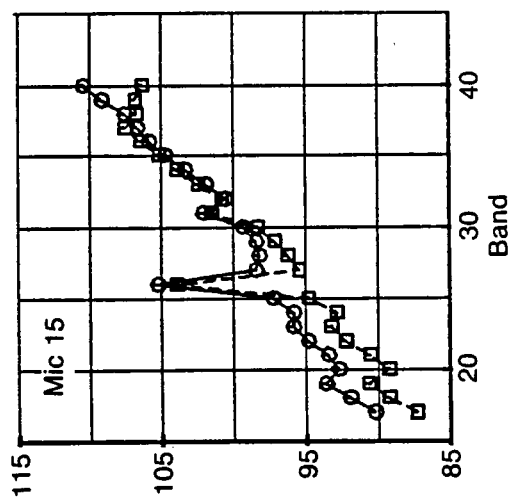
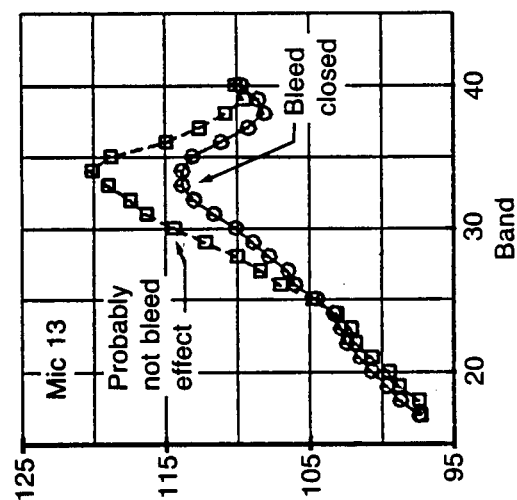
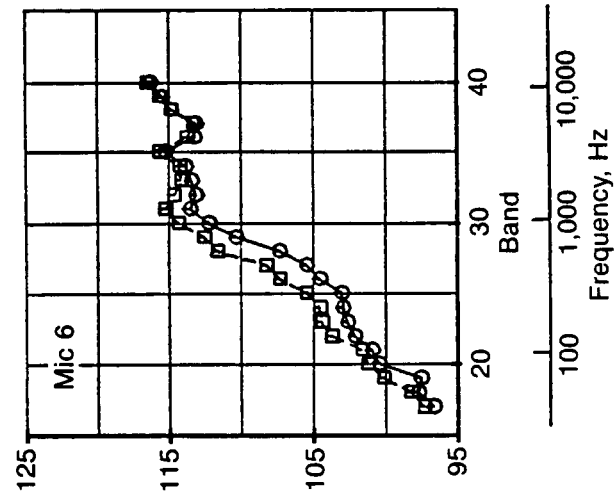
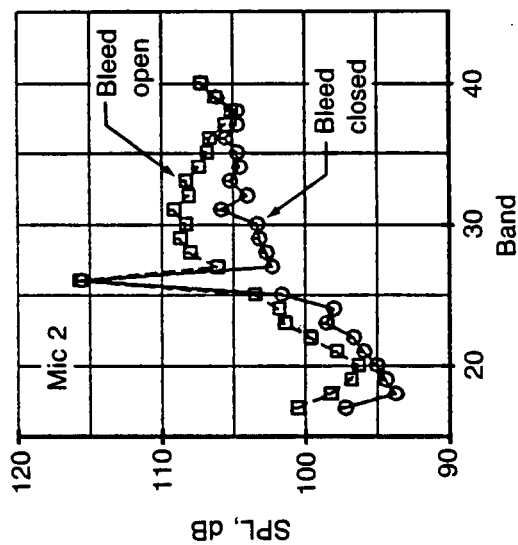
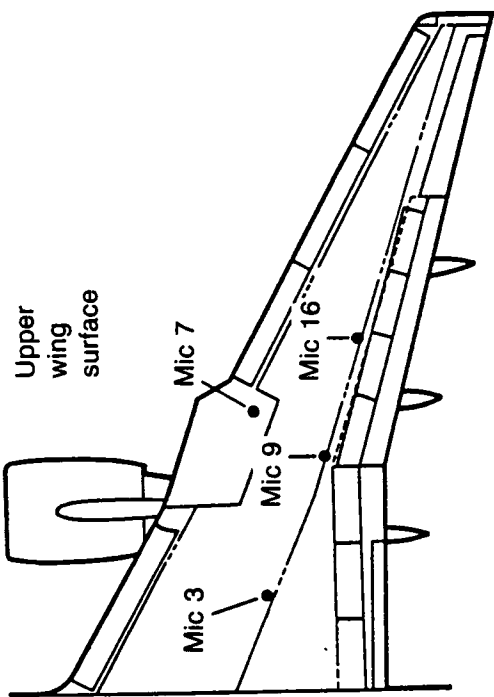
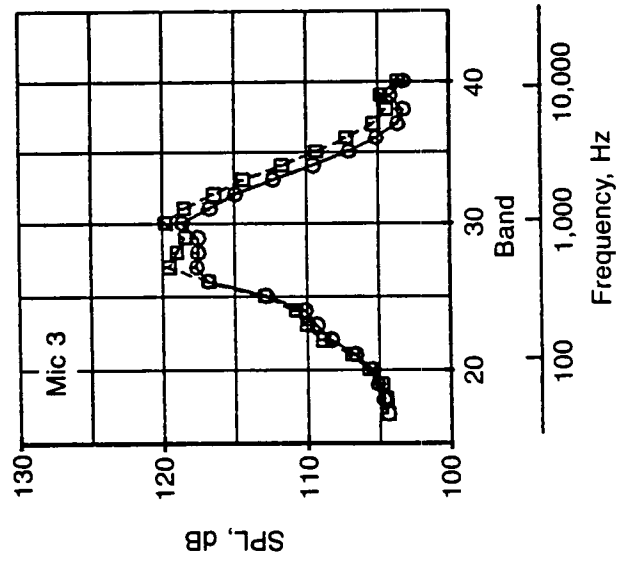
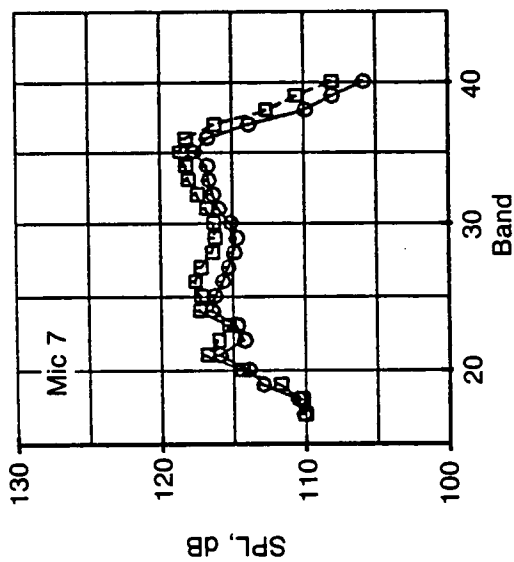


Figure 8-25. Engine Bleed Effects on Wing Lower Surface Spectra, Probe Microphones



Mach no. 0.70
Cond N_{1C}
O 217 3557 bleed closed
□ 218 3582 bleed open

Figure 8-26. Engine Bleed Effects on Wing Lower Surface Spectra, Leading Edge Surface Microphones



Mach no. 0.70

Cond N1c
 O 217 3557 bleed closed
 □ 218 3582 bleed open

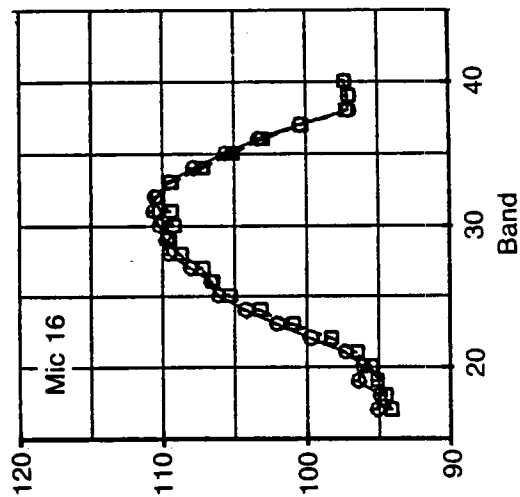
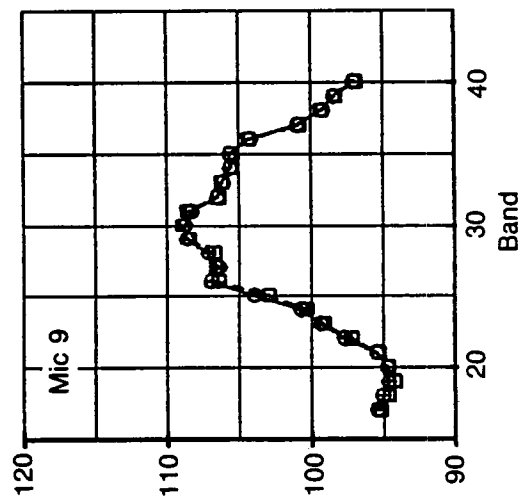


Figure 8-27. Engine Bleed Effects on Wing Upper Surface Spectra, Probe Microphones

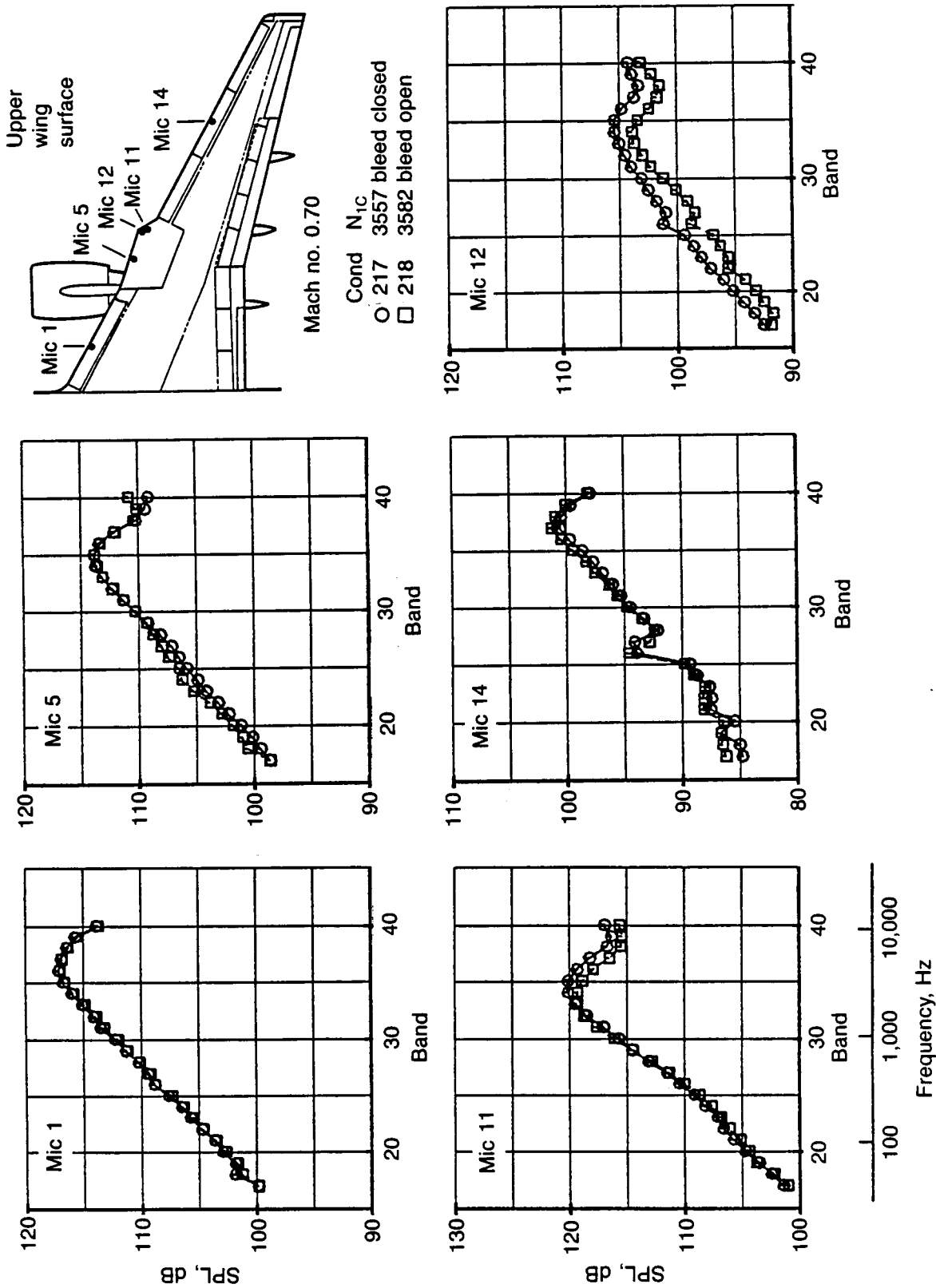


Figure 8-28. Engine Bleed Effects on Wing Upper Surface Spectra, Leading Edge Surface Microphones

Applicable Flight Conditions and Variables

Condition	Altitude, 1000 ft	Mach no.	M _{FAN}	C _L	Sideslip angle, deg	Left aileron angle, deg	Rudder angle, deg
201	30	0.80	1.06	0.35	-0.6	-2.6	0.3
204	34	0.81	1.10	0.42	-0.2	-1.3	0.7
207	36	0.81	1.17	0.45	0	-0.5	0.8
210	37	0.80	1.14	0.48	-0.3	-1.2	0.6
239	38	0.80	1.12	0.46	-0.5	-2.1	0.7
211	38	0.80	1.14	0.50	-0.2	-0.9	0.6
222	39	0.81	1.20	0.50	0.1	-0.1	0.9
214	39	0.81	1.21	0.52	-0.1	-0.5	0.7
224	40.5	0.80	1.24	0.54	-0.4	-0.8	0.1
223	40.5	0.80	1.28	0.53	-0.2	-0.2	0.1
241	41.0	0.80	1.23	0.53	0	-0.3	0.9
228	41.3	0.79	0.94	0.57	-0.5	-2.0	0.8

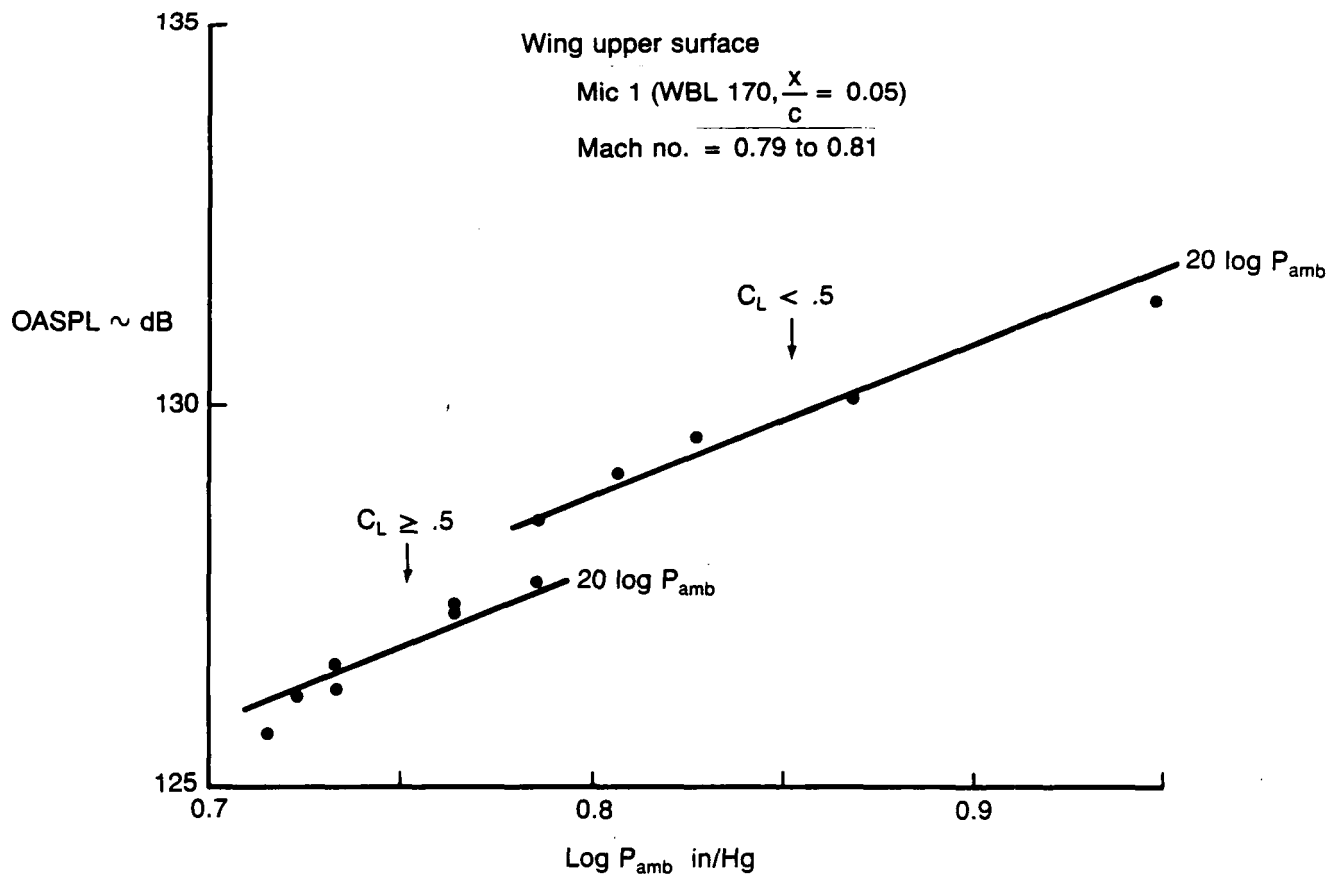


Figure 8-29. OASPL Correlation With Ambient Pressure

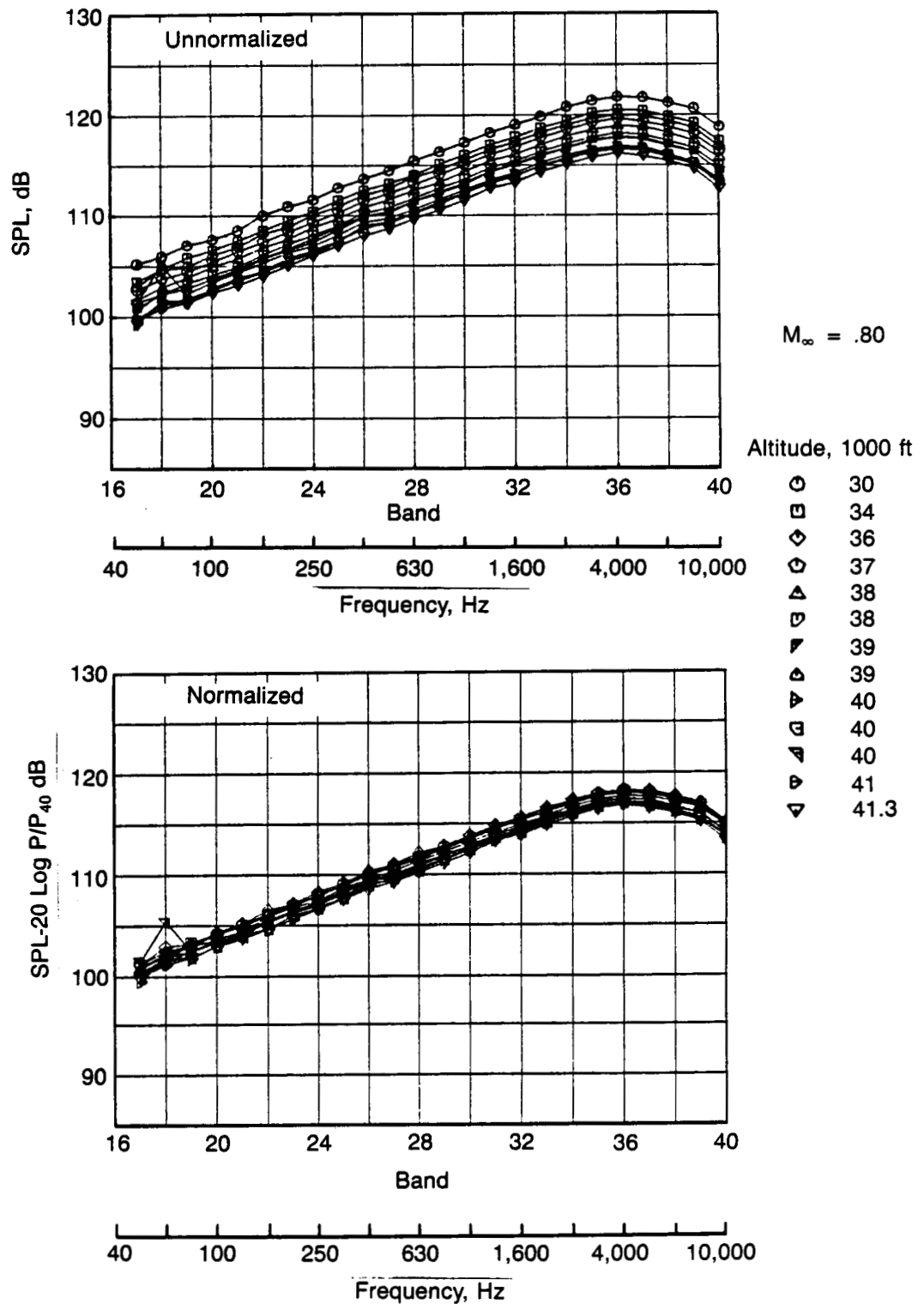


Figure 8-30. Altitude Normalization of Noise Spectra, Upper Surface Microphone 1

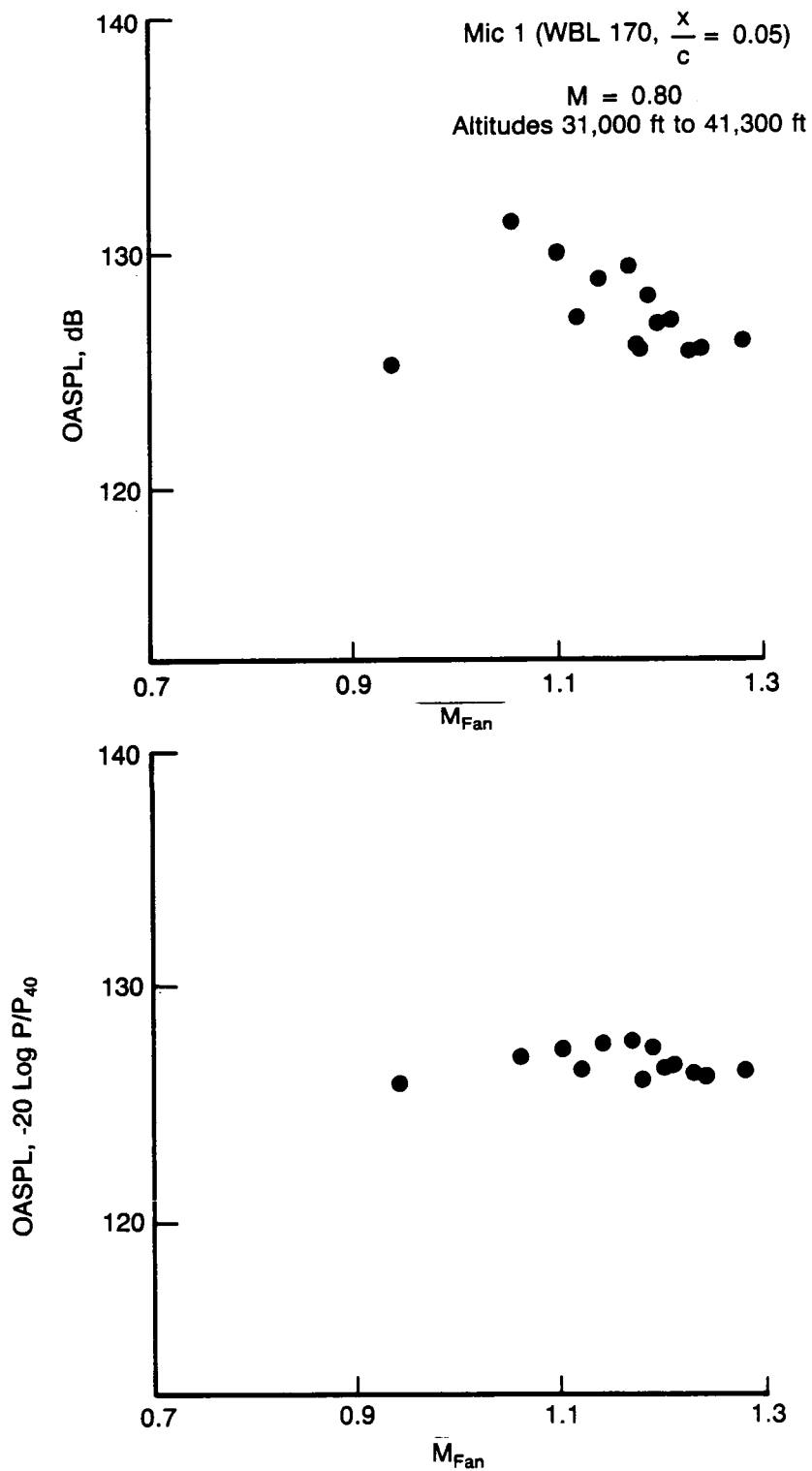


Figure 8-31. Effect of Altitude Normalization, Upper Surface Microphone 1

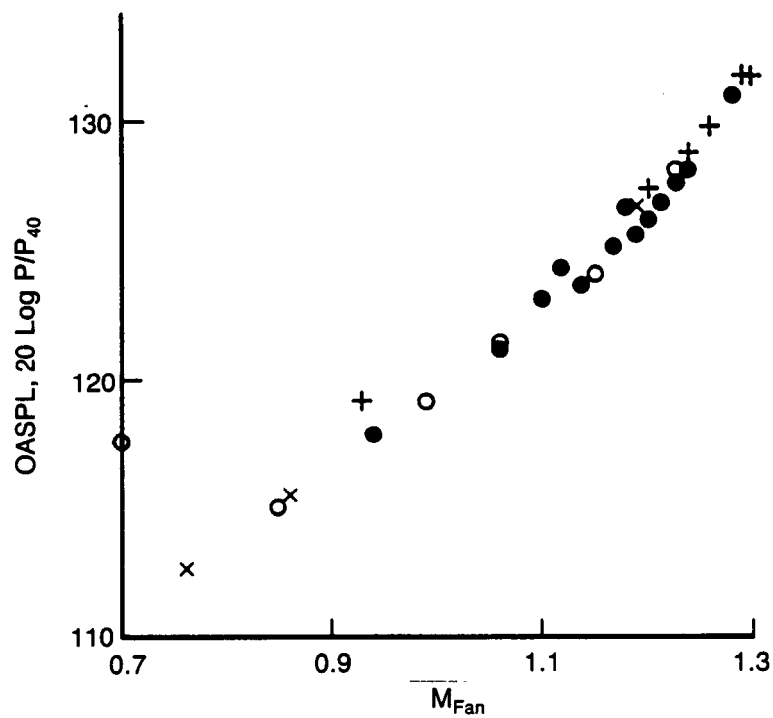
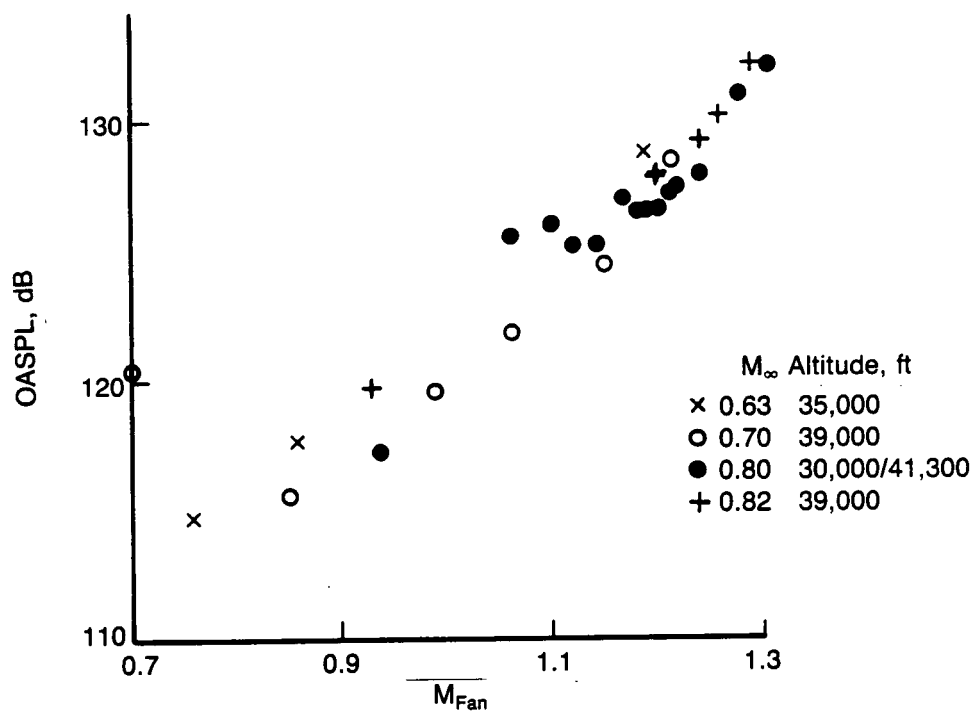


Figure 8-32. Effect of Altitude Normalization, Lower Surface Microphone 10

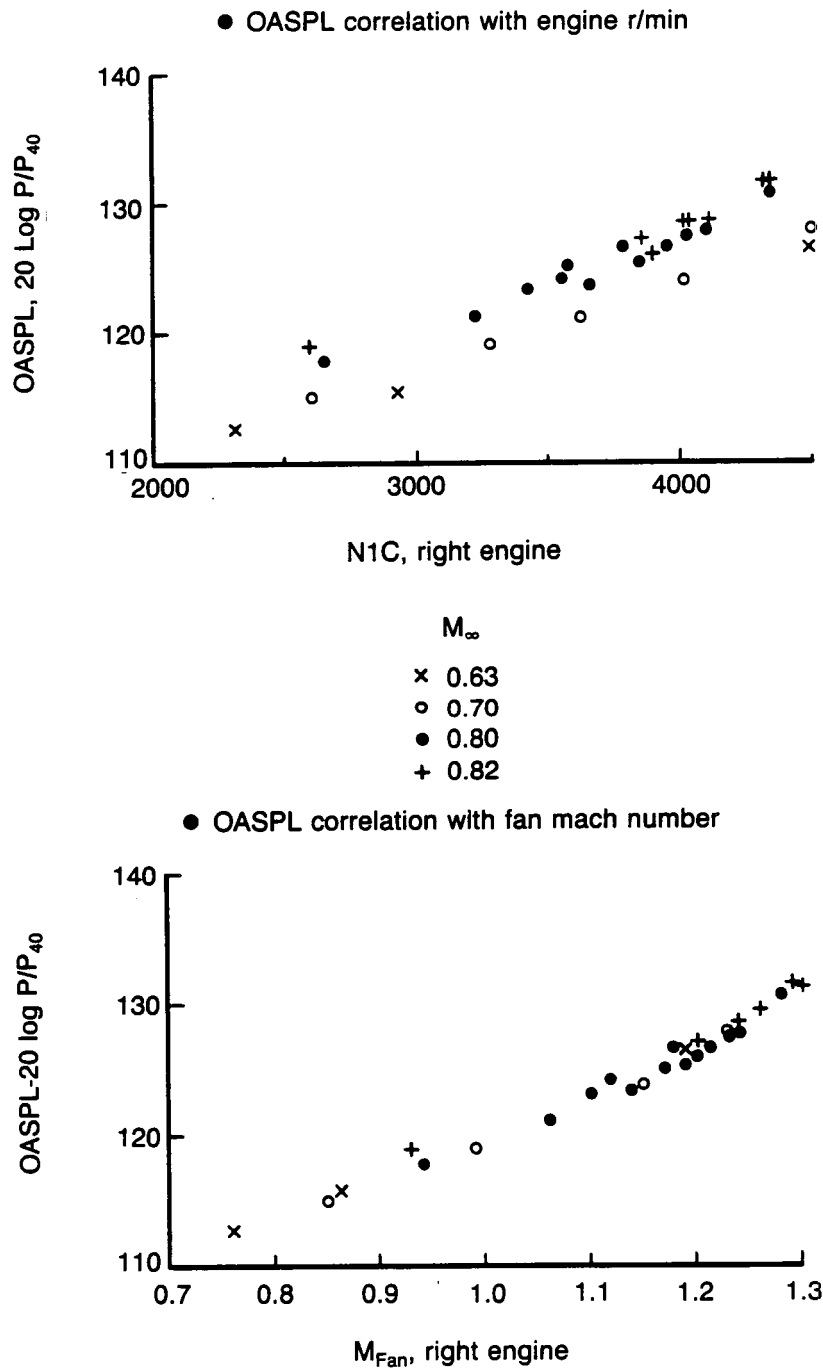


Figure 8-33. Engine Parameters Correlation, Lower Surface Microphone 10

Table 8-5. Prominent Turbomachinery Tones For P&W 2037 Engine

Component	Number of blades	Harmonic order, n	Tone frequency			
			Cond 223 $N_1 = 3934$	Cond 224 $N_1 = 3714$	Cond 225 $N_1 = 3437$	Cond 228 $N_1 = 2384$
Fan	36	= 1	2360	2228	2062	1430
		= 2	4721	4457	4124	2861
		= 3	7081	6685	6187	4291
		= 4	9442	8914	8249	5722
Low pressure compressure 1st stage	66	= 1	4327	4085	3781	2622
Turbine						
5th stage	94	= 1	6163	5819	5385	3735
4th stage	90	= 1	5901	5571	5156	3576
3rd stage	102	= 1	6688	6314	5843	4053
2nd stage	138	= 1	9048	8542	7905	5483
1st stage	158	= 1	10360	9780	9051	6278

Tone frequency = n BPF

BPF = Blade pasage frequency, $BN_1/60$

n = Harmonic order

B = Number of blades

N_1 = Fan rotor r/min

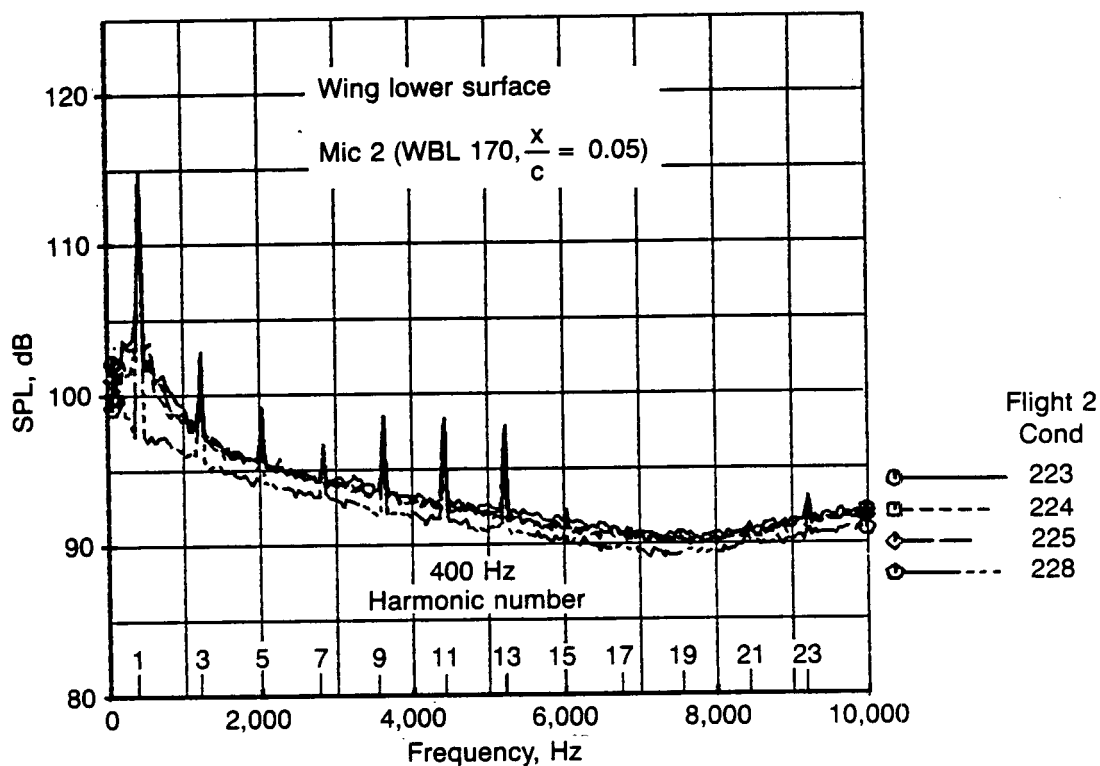
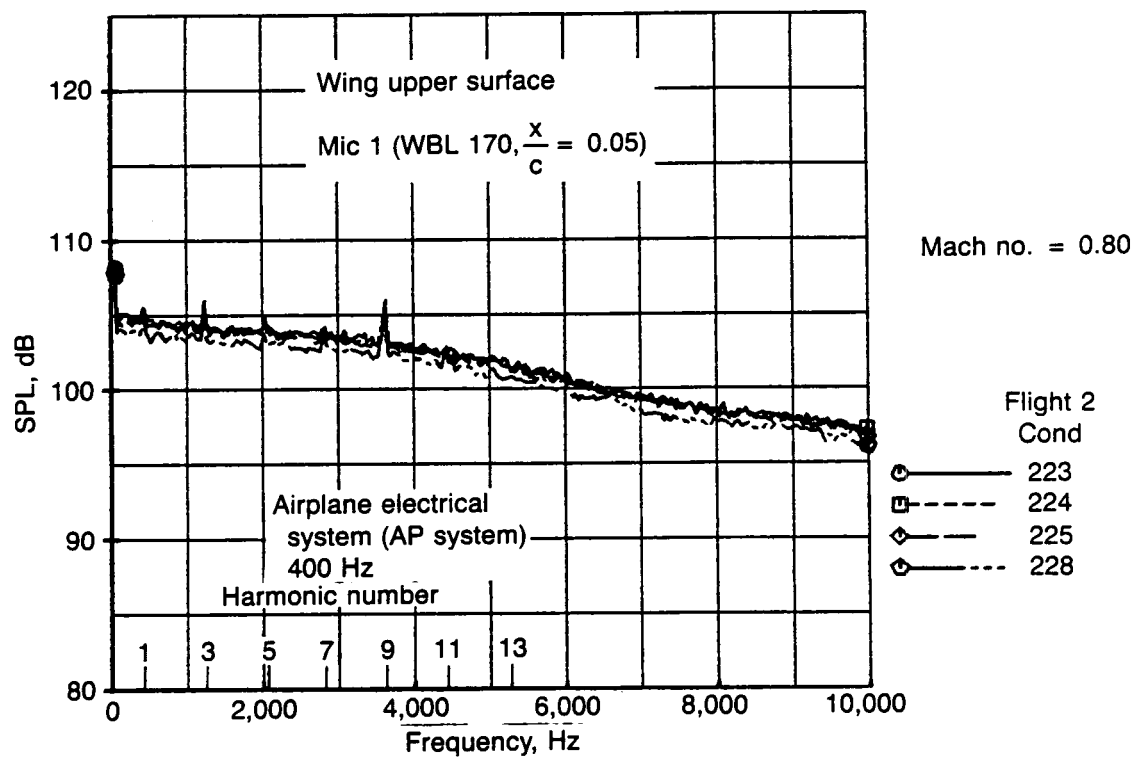


Figure 8-34. Effect of Airplane Electrical Power System Interference on Narrowband (37.5 Hz) Spectra

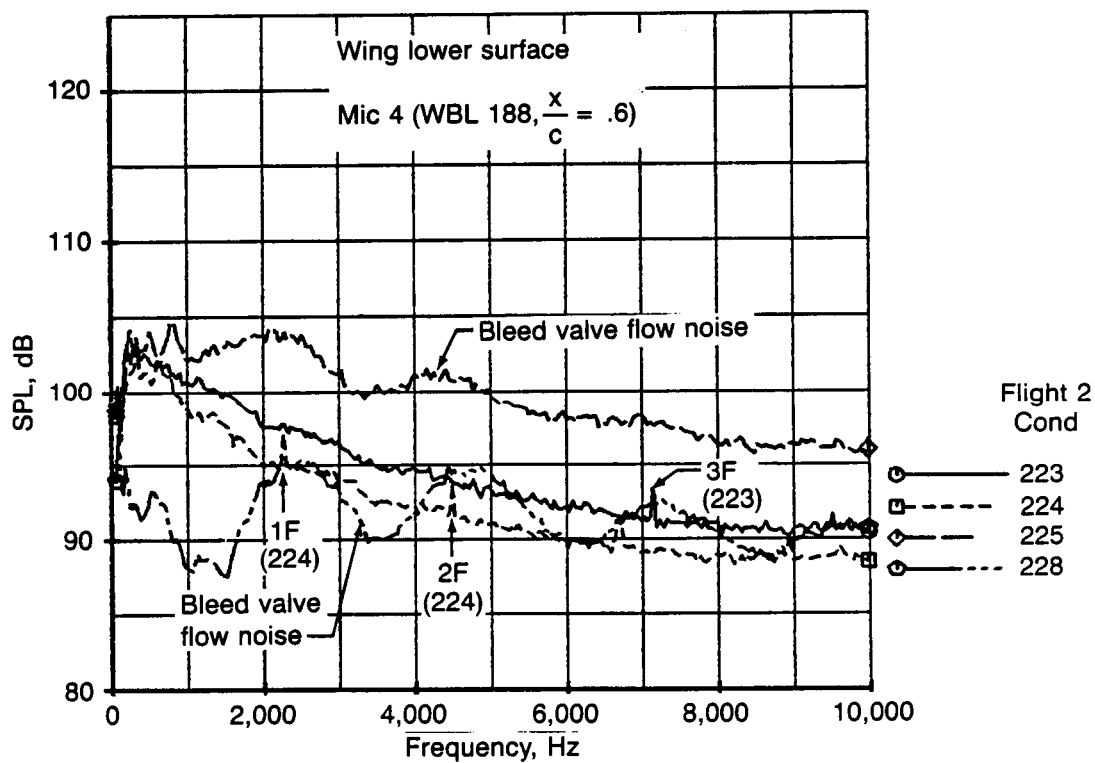
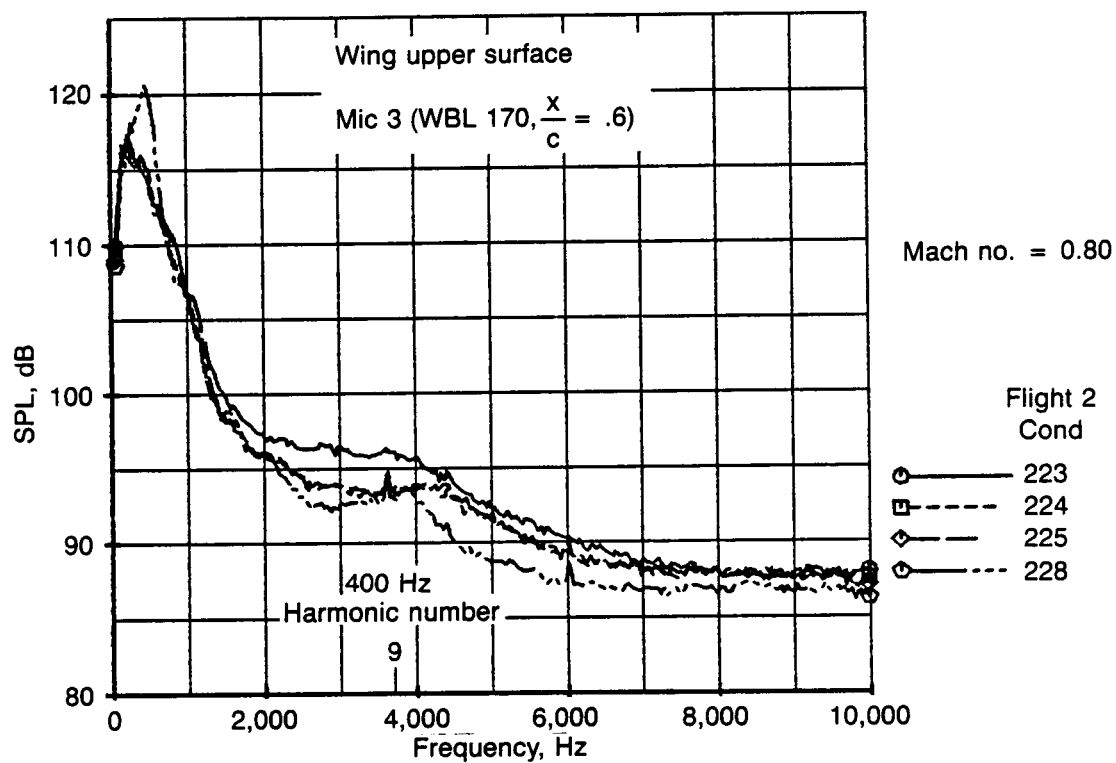


Figure 8-35. Effect of Various Noise Sources on Narrowband (37.5 Hz) Spectra

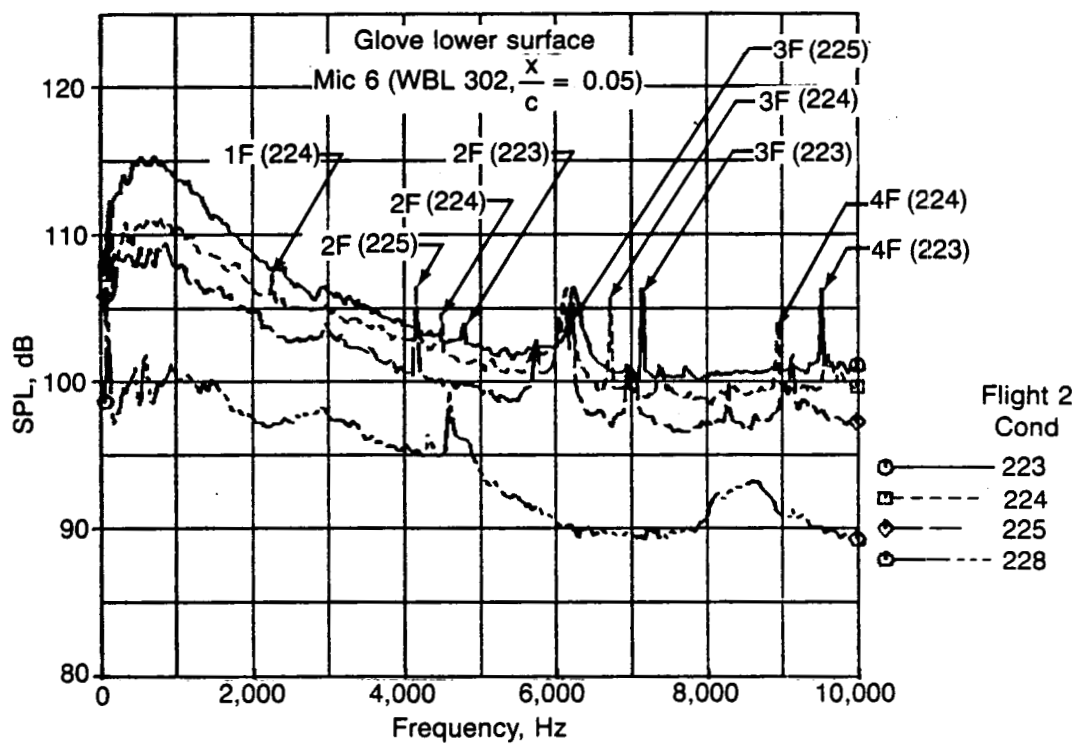
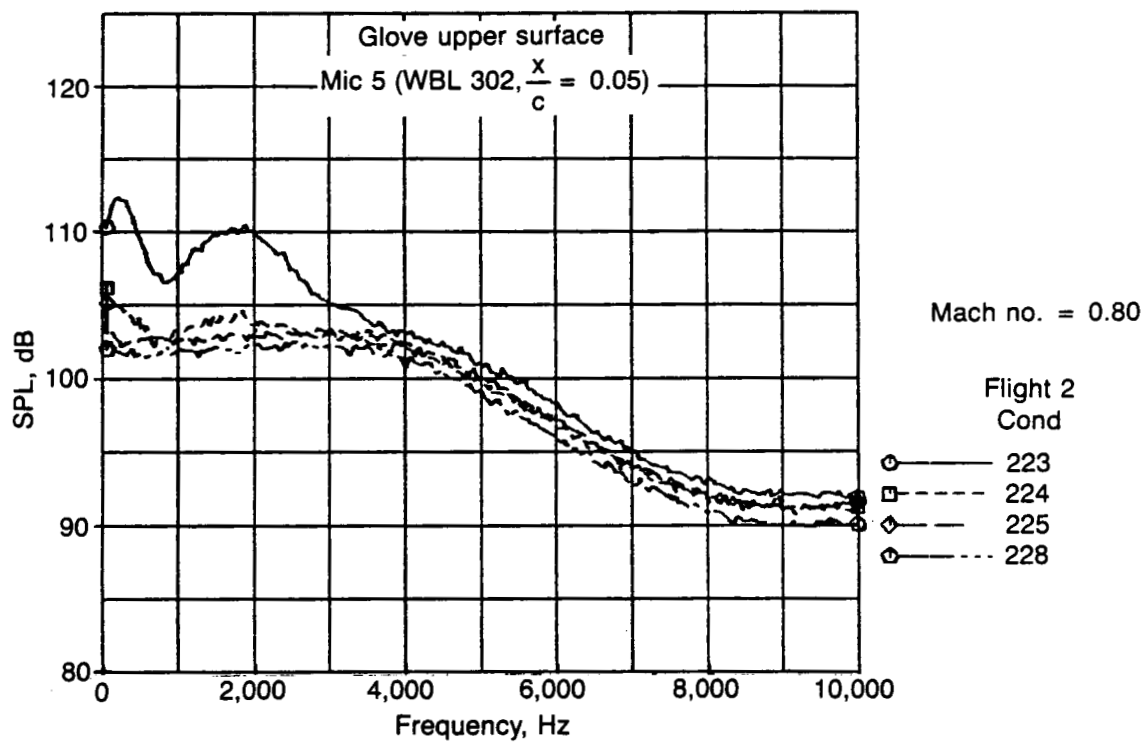
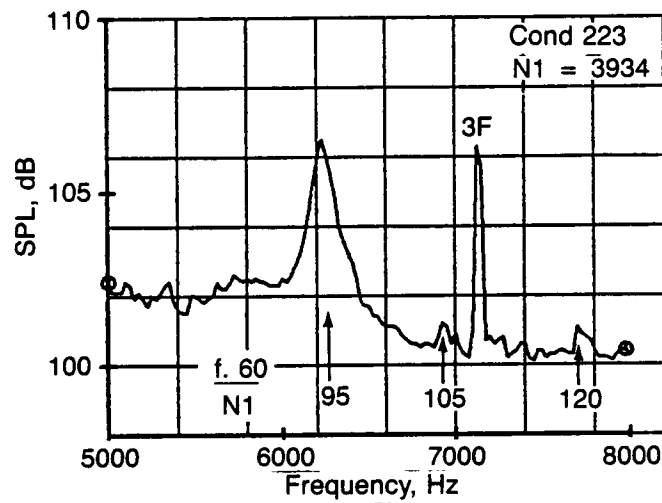


Figure 8-36. Effect of Various Noise Sources on Narrowband (37.5 Hz) Spectra



Glove lower surface

Mic 6 (WBL $302 \frac{x}{c} = 0.05$)

Mach no. = 0.80

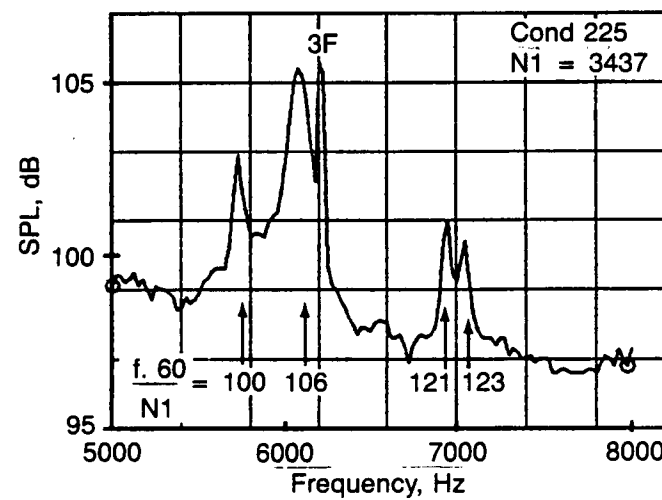
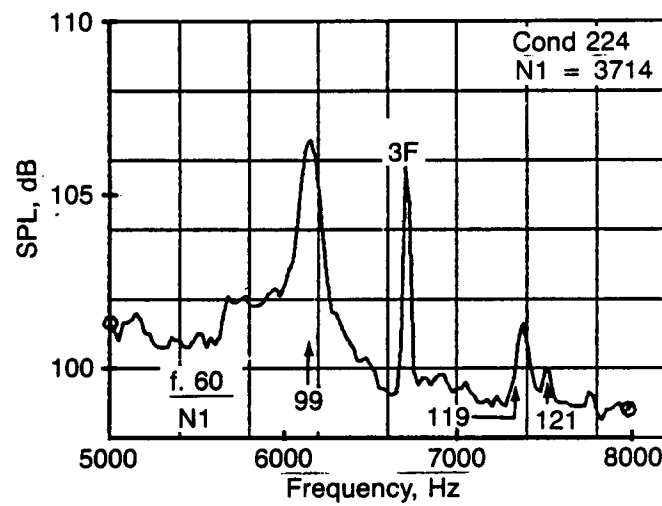


Figure 8-37. Effect of Various Noise Sources on Narrowband (37.5 Hz) Spectra

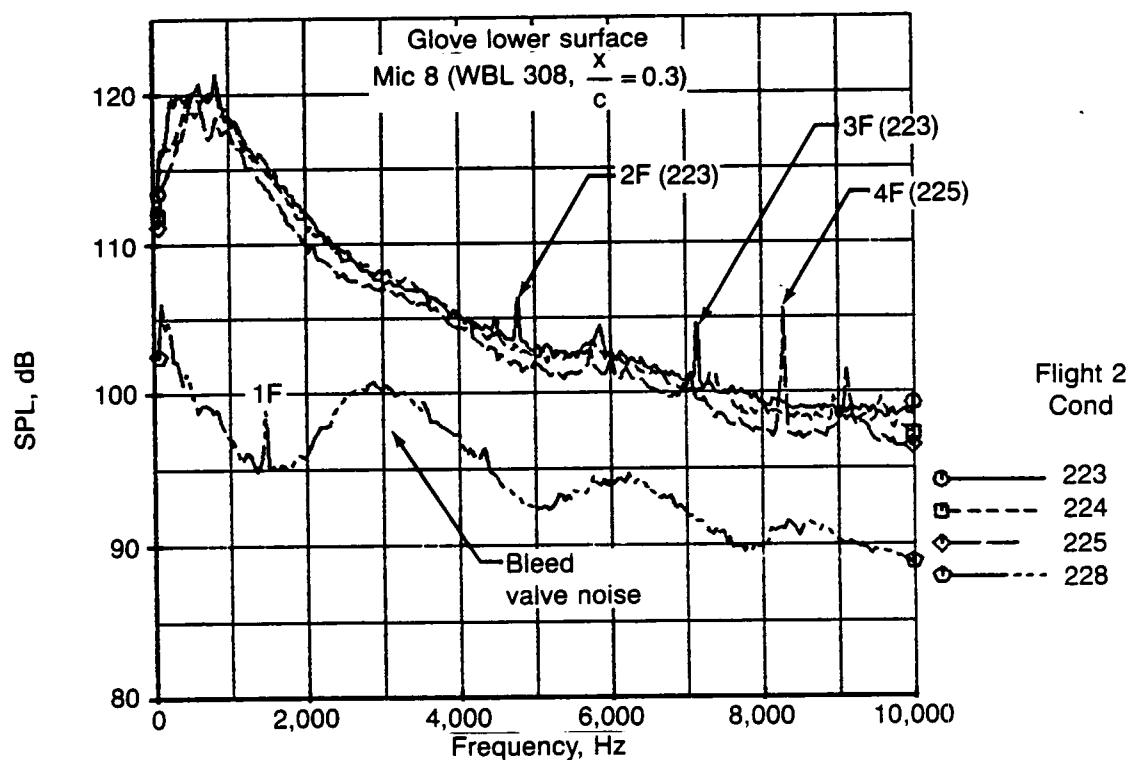
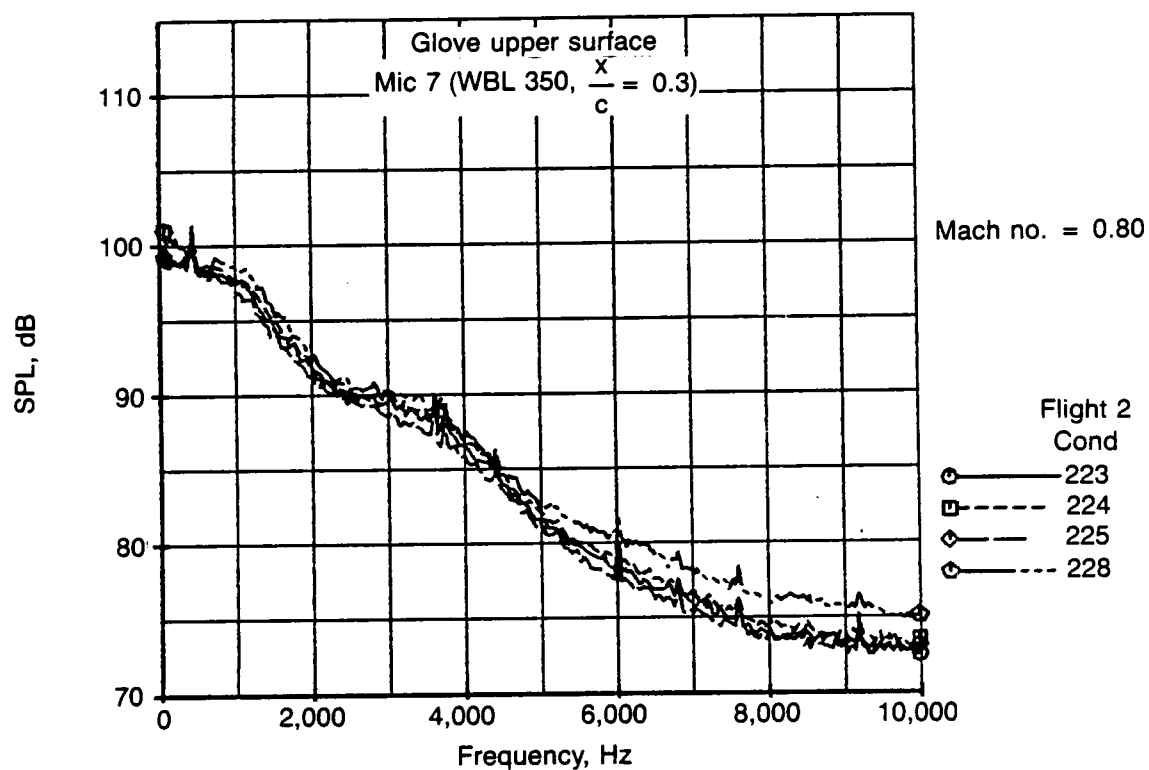


Figure 8-38. Effect of Various Noise Sources on Narrowband (37.5 Hz) Spectra

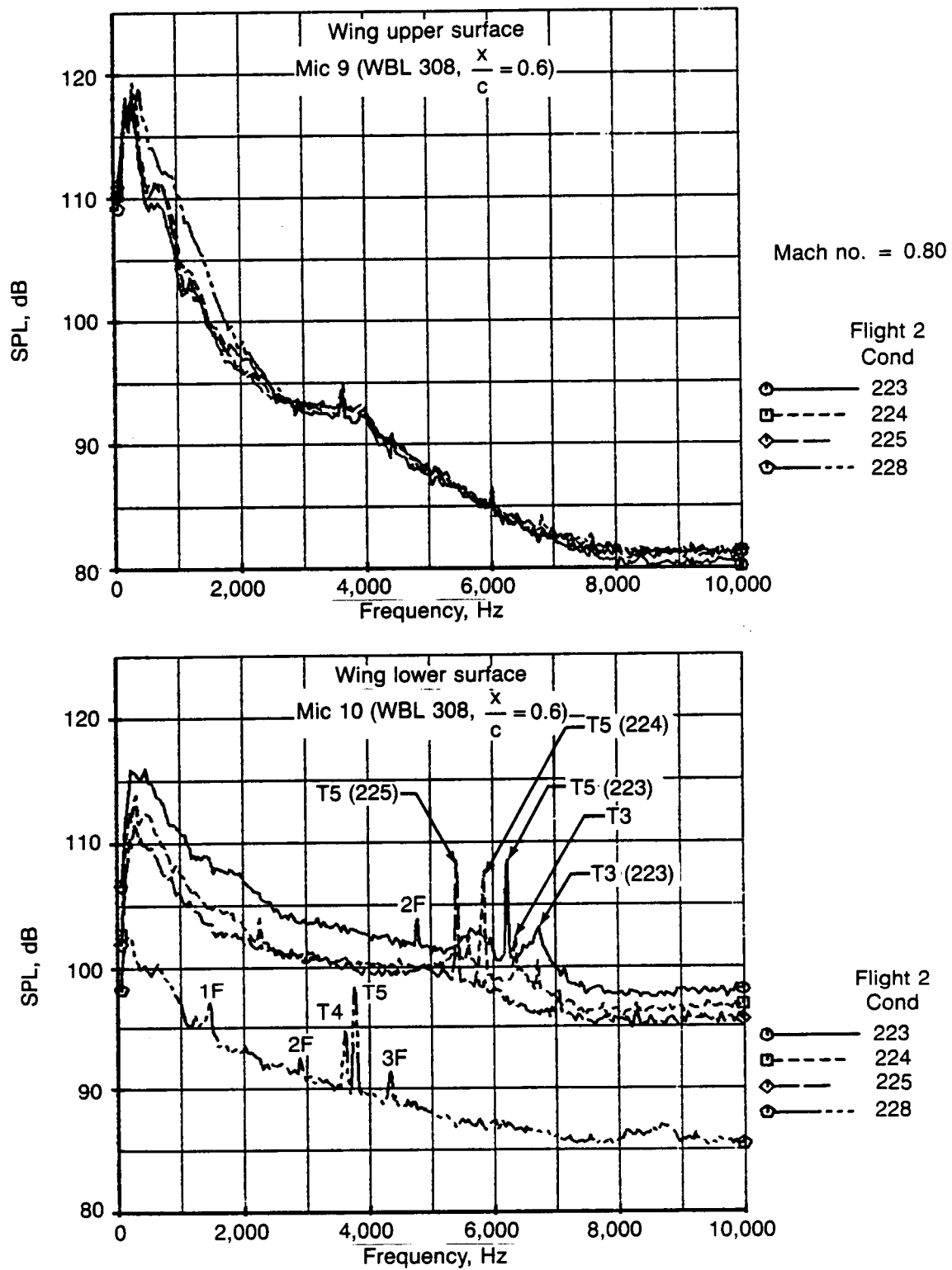


Figure 8-39. Effect of Various Noise Sources on Narrowband (37.5 Hz) Spectra

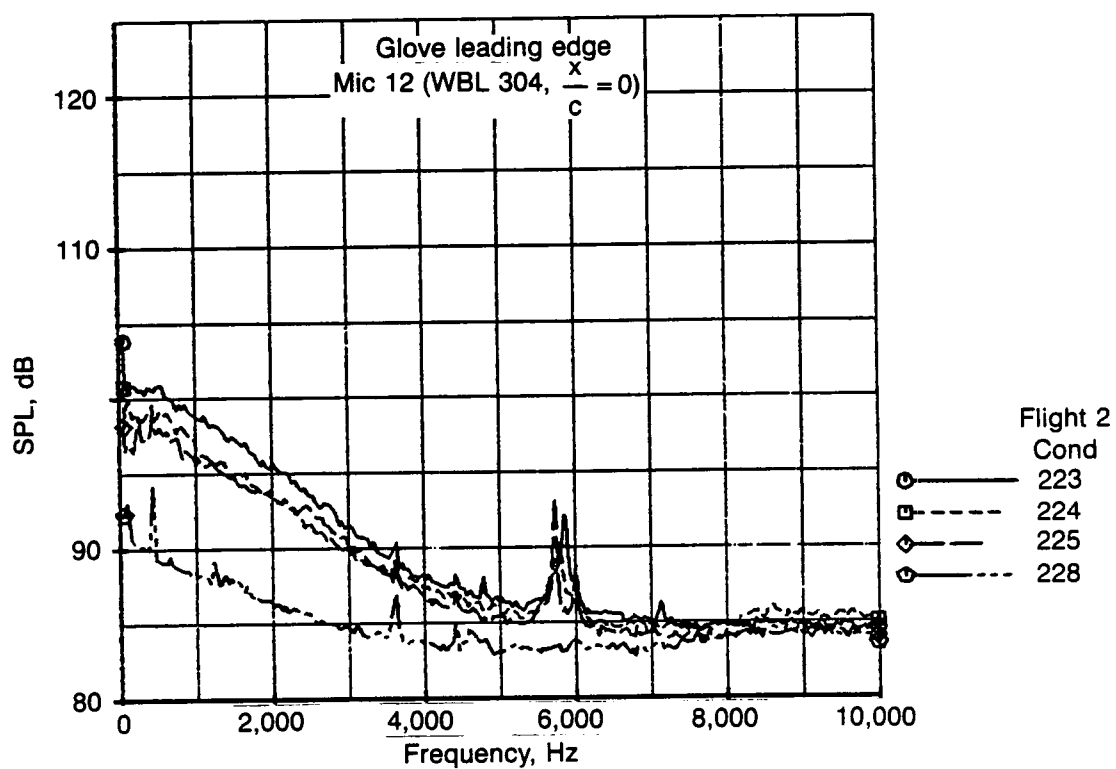
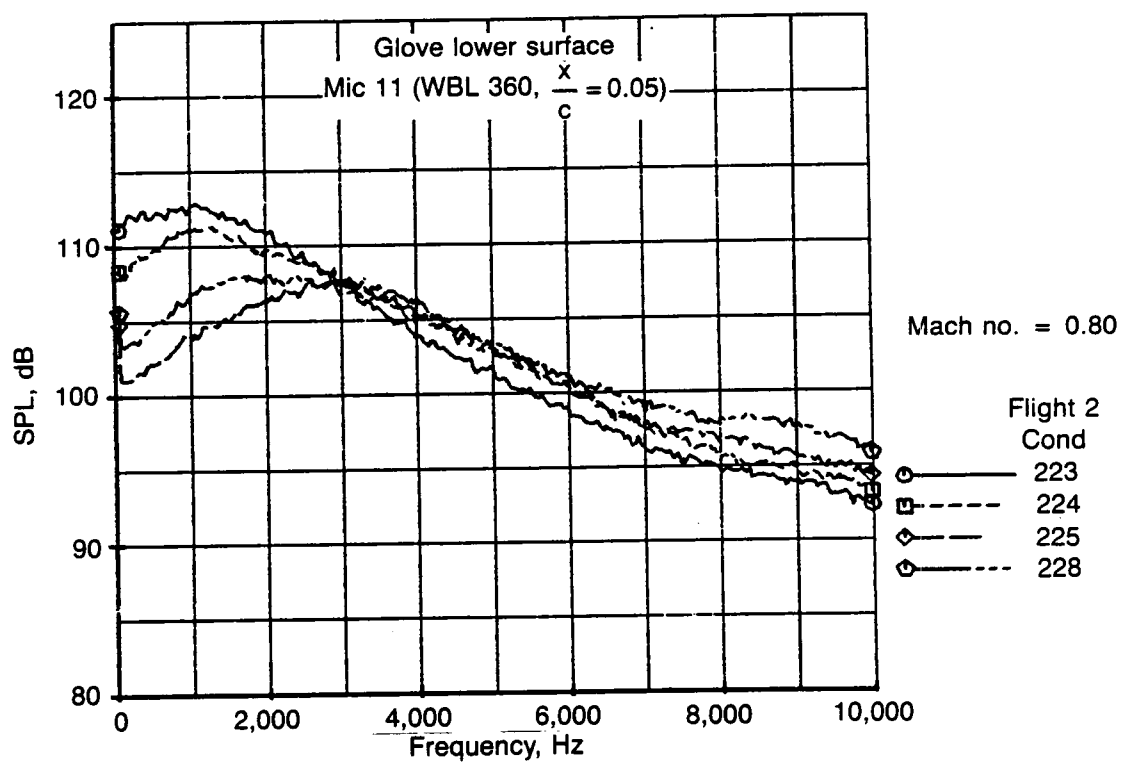


Figure 8-40. Effect of Various Noise Sources on Narrowband (37.5 Hz) Spectra

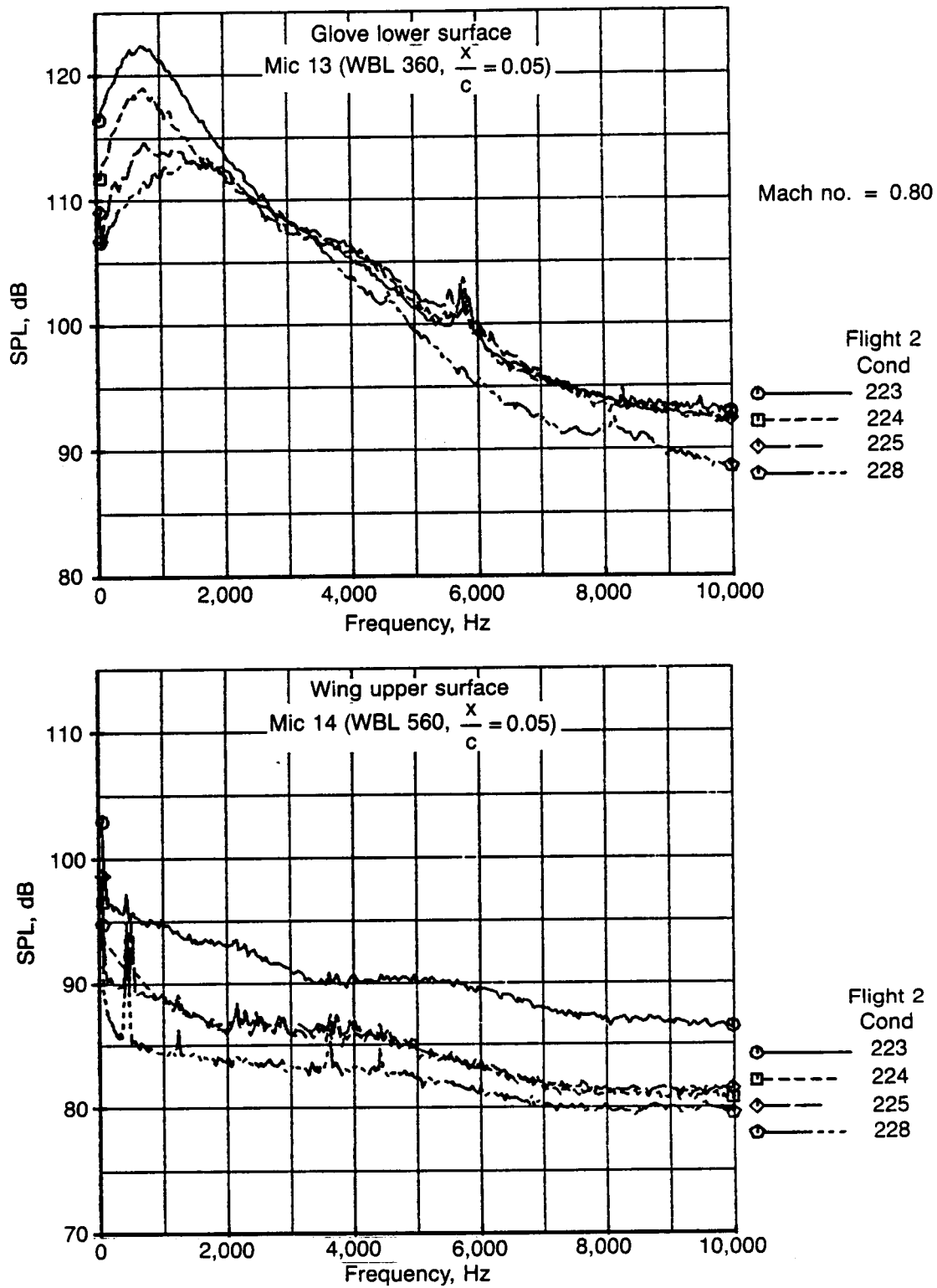


Figure 8-41. Effect of Various Noise Sources on Narrowband (37.5 Hz) Spectra

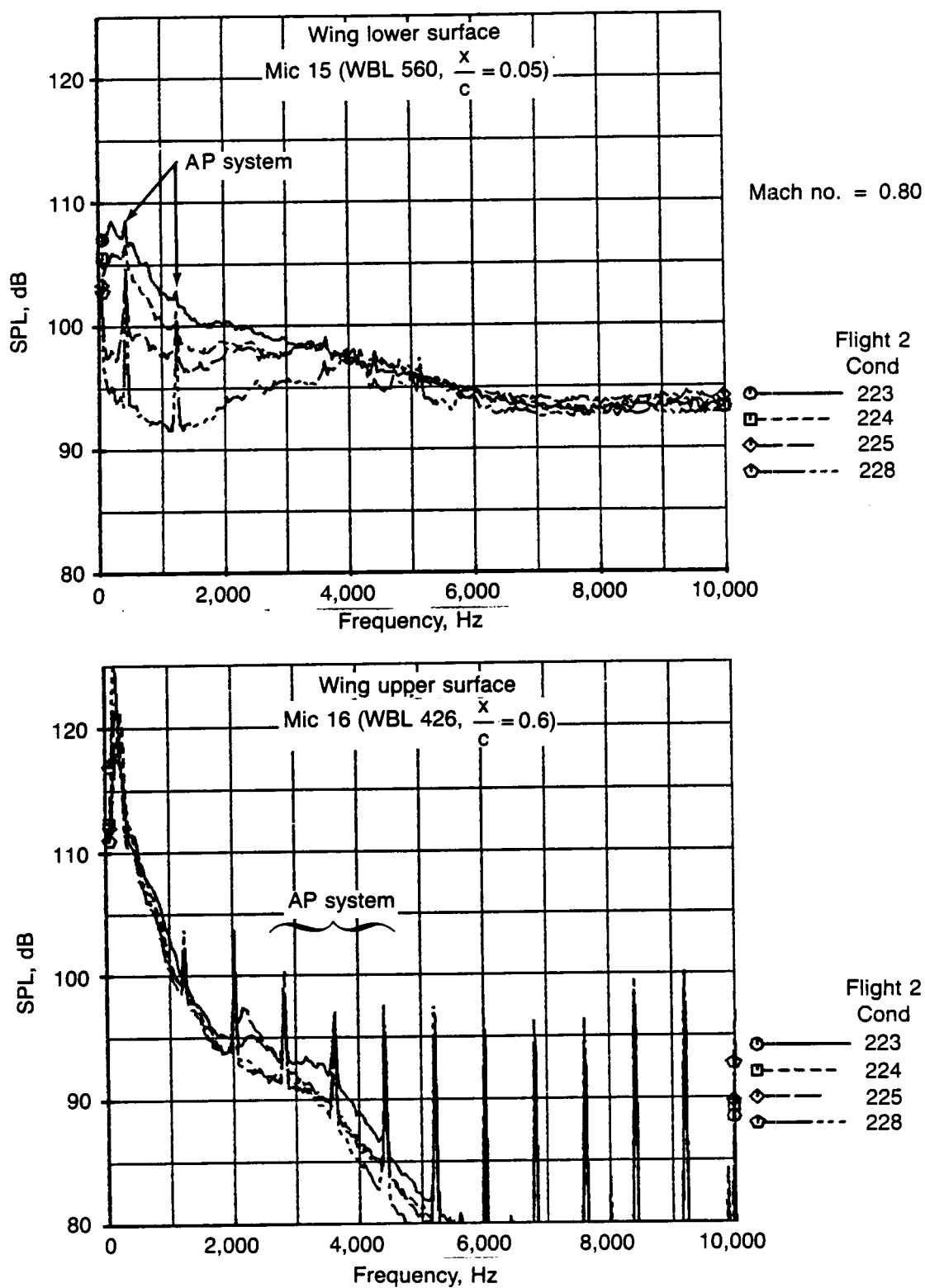


Figure 8-42. Effect of Various Noise Sources on Narrowband (37.5 Hz) Spectra

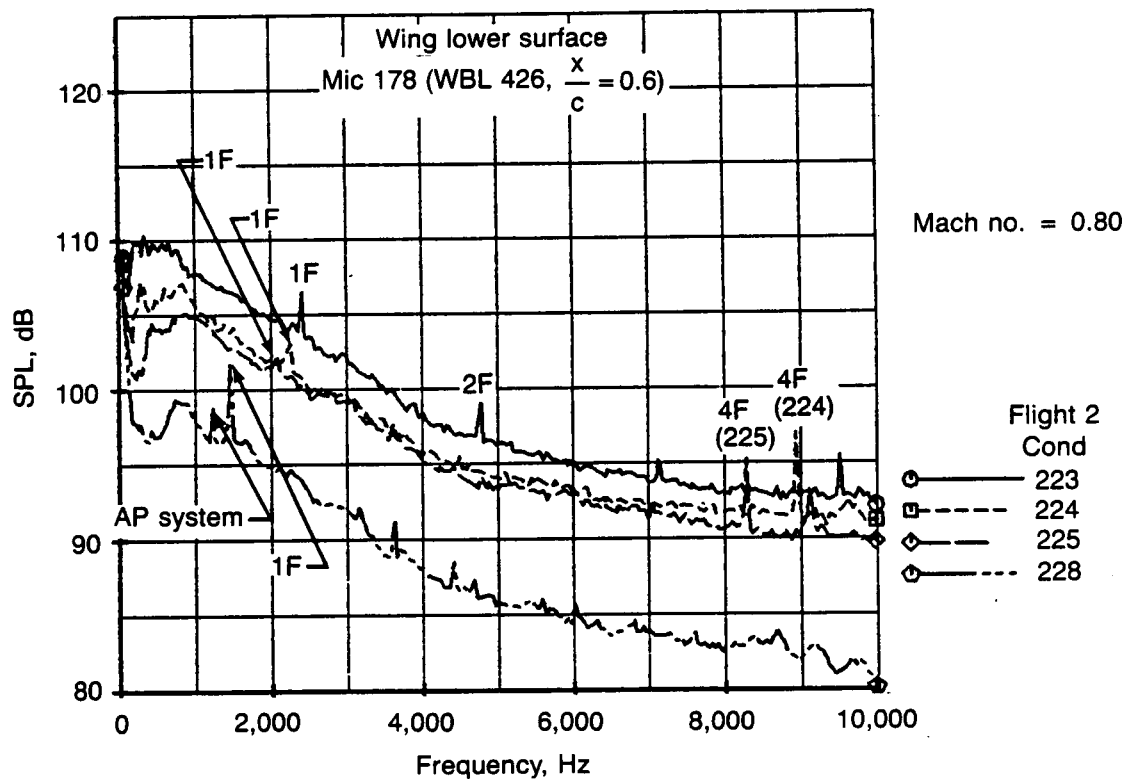


Figure 8-43. Effect of Various Noise Sources on Narrowband (37.5 Hz) Spectra

8.3 AERODYNAMIC CHARACTERISTICS

This section presents the aerodynamic characteristics of the glove and the relationship between the extent of laminar flow (i.e., transition location) and engine noise as well as the other parameters affecting laminar flow. A summary of the flight conditions and the corresponding values of the significant variables and results is presented in Tables 8-6, 8-7, 8-8, and 8-9 for the four flights conducted during the subject program.

The objective of the glove design was to achieve 3 to 4 ft of laminar flow on both glove surfaces so that the effect of engine noise on the extent of laminar flow could be seen directly. Figure 8-44 shows that this objective was met at the design condition. On the upper surface, a maximum of about 28% chord laminar flow was obtained (4.7 ft), and on the lower surface about 18% chord laminar flow was obtained (3.0 ft). This was achieved at maximum continuous engine power for the engine on the glove side. On the upper surface there is more laminar flow inboard than outboard where the peakiness of the pressure distribution can be expected to cause earlier transition. This is illustrated in the lower part of Figure 8-44, which shows the peaky shape at station WBL 355 and the generally favorable shape for WBL 296.

8.3.1 Static Pressure Data

A comparison between measured pressures and calculated values is shown in Figure 8-45, which illustrates the effect of spanwise location on the glove.

Pressure peaks were not predicted by the transonic code on any portion of the glove at $M = .80$ and $C_L = .45$. However, the measured pressure distribution at the inboard location shows a flattening or possible slight peakiness in the 5% to 10% chord region which was not predicted by theory. As previously noted, the significant peakiness at the outboard station (WBL 355) can be expected to cause early transition. Although this trend may extend inboard somewhat, it probably does not have a significant influence at the measuring station (WBL 325). The measured pressure gradients on the upper surface aft of 10% chord are higher than those predicted by theory and should have a stabilizing effect on the boundary layer.

On the lower surface no data point is shown at $x/c = .10$ because it is suspected that the pressure data at this location was in error for Flight 2, on which most of the inboard pressure data was acquired. This situation is discussed in more depth in Volume 2 of this report. The measured lower surface pressure distribution at the inboard station shows a steeper pressure gradient and a slightly further forward recovery point than theory. Outboard, the lower surface recovery point is much further forward than the theory predicted.

The effect of airplane lift coefficient on the glove pressure distribution at the inboard station (WBL 296) is shown in Figure 8-46. On the upper surface, the flattening of the measured pressure distribution between 5% and 10% chord disappears at $C_L = .54$ (i.e., the design condition). On the lower surface, the measured pressure gradient is higher than the theory at all lift coefficients, and pressure recovery is slightly further forward.

The effect of airplane lift coefficient on the glove pressure distribution at the outboard station (WBL 355) is shown in Figure 8-47. The measured pressure distribution on the upper surface is peaky at all lift coefficients, with the strength of the peak increasing with increasing C_L . Also, the local Mach number is increasing rapidly to supersonic values ($C_p^* \approx .42$) in the peaky areas. In contrast, theory has indicated no actual peaks, although an increasing tendency towards peakiness with increasing C_L is evident. The measured pressure gradients on the upper surface aft of 10% chord are higher than those predicted by theory at all lift coefficients. On the lower surface, the measured pressure recovery location is at about 15% chord, which is much further forward than the theory predicted. Also, there is a leading edge peak on the lower surface at the highest lift coefficient which was not predicted by theory and is not explainable by known data trends.

The effect of Mach number on the glove pressure distribution at the inboard station (WBL 296) at a lift coefficient of .45 is shown in Figure 8-48. The theory shows decreasing peakiness on the upper sur-

face with increasing Mach number. At this lift coefficient, flight data at the inboard station was obtained only at $M = .80$ and $M = .82$. In both cases the pressure distribution flattens on the upper surface between 5% and 10% chord. For the lower surface, theory predicts a decreasing pressure gradient and increasing peakiness with increasing Mach number. Also, the measured lower surface data shows a higher pressure gradient and further forward recovery point than theory with no tendency toward peakiness.

Figure 8-49 shows the effect of Mach number on the outboard glove station (WBL 355) at a lift coefficient of .45. The forward peak predicted by the theory at $M = .70$ on the upper surface is also indicated by the measured data. However, at all of the higher Mach numbers the measured data shows a peak at 5% chord that theory did not predict. The measured pressure gradient is higher than that predicted by theory at $M = .78$, $M = .80$, and $M = .82$. On the lower surface, the recovery point of the measured pressure data is much further forward than predicted by theory at all Mach numbers.

The pressure measurement results can be summarized as follows:

1. There is a tendency toward peakiness of the pressure distributions on the upper surface for almost all flight conditions which was higher than predicted by theoretical analysis. The pressure gradients were also more negative than predicted by theory, particularly behind the leading edge pressure peaks that correspond to supersonic Mach numbers. This is most pronounced on the outboard glove stations.
2. On the lower surface, there is a markedly less tendency toward peakiness than predicted by theory at all flight conditions. The pressure gradients tend to be quite mild to flat and the recovery points are further forward than predicted. Again these tendencies are more noticeable at the outboard station (WBL 355).
3. The variance between theory and experiment can be ascribed to: (1) differences in geometry, and (2) shortcomings of the theory or the modeling techniques. While there were some geometric differences between the actual glove and the design shape, these do not appear to be the major reasons for the observed discrepancies. Also, known anomalies in the measured data do not account for the observed differences.

8.3.2 Transition Location Data

The variation of the measured transition locations on the glove with lift coefficient are shown in Figure 8-50. For this set of data, Mach number is constant at about .80, but altitude (and, therefore, Reynolds number) varies from case to case. Results are shown for both the upper and lower surfaces at the inboard, midspan, and outboard glove regions.

On the upper surface at the inboard location, the extent of laminar flow was greatest (about 28% chord) for lift coefficients of .48 and higher. The extent of laminar flow decreased with decreasing lift coefficient until, for lift coefficients of about .35, transition occurred forward of the most forward hot-film, which was at 15% chord. It should be noted that the lower lift coefficients correspond to lower altitudes and, therefore, increasing Reynolds number. Thus the decreasing extent of laminar flow with decreasing lift coefficient is probably due to a combination of Reynolds number effects and pressure distribution effects. At the midspan location on the upper surface, the transition location varies from 20% to 25% chord. Also, there is less sensitivity to lift coefficient at this station than at the inboard station. In the outboard region on the upper surface, transition occurred somewhere forward of the most forward hot film at 15% chord. As previously stated, the probable cause of this result is the peakiness of the pressure distribution in this region.

On the lower surface, the inboard region had about 17% chord laminar flow at the high lift coefficients. For lift coefficients below .45, transition occurred somewhere forward of the most forward hot film at 15% chord. At the midspan location on the lower surface, the decreasing extent of laminar flow with decreasing lift coefficient is very apparent. However, in the outboard region of the glove lower surface there was no noticeable variation of the transition location with lift coefficient.

The effect of flight Mach number on the transition location is shown in Figure 8-51. For this set of data, both C_L and altitude vary from case to case, resulting in a range of transition locations at a given Mach number.

On the upper surface, the transition location exhibits a strong Mach number dependency at both the inboard and midspan locations. At the outboard location, transition occurred forward of the most forward hot film at 15% chord at all Mach numbers. Again, this was probably due to the peakiness of the pressure distributions in this region. There was more laminar flow at the inboard location than at the midspan location, and at both stations the most laminar flow was obtained at Mach numbers of .8 and higher.

On the lower surface, the greatest extent of laminar flow was obtained at the midspan location (about 20% chord) at Mach numbers between .75 and .78, with the extent of laminar flow decreasing at both higher and lower Mach numbers. However, the Mach number dependency was not as strong as on the upper surface. In the inboard region of the lower surface, the most laminar flow (17% chord) was obtained at a Mach number of 0.8, with the amount decreasing at lower Mach numbers. For Mach numbers near 0.7, transition occurred somewhere forward of the most forward hot film at 15% chord and thus is not shown in the figure. In the outboard region of the lower surface, the greatest extent of laminar flow was obtained at $M = .75$.

8.3.3 Sideslip Effects

The effects of sideslip on the measured transition location on the glove are shown in Figure 8-52. A change in sideslip angle produces two primary effects: (1) a change in the effective sweep angle of the glove, and (2) a change in the glove pressure distribution. A positive sideslip angle results in a lower effective sweep angle on the glove, whereas a negative sideslip angle results in a higher effective sweep angle. The glove pressure distribution changes because of the change in the component of Mach number normal to the leading edge and because of the change in local angle of attack caused by the wing dihedral and the requirement to maintain airplane roll attitude.

On the upper surface, the general trend changes from favorable to unfavorable as lift coefficient and sideslip angle increase. It appears that as lift coefficient increases, the sideslip angle for maximum laminar flow decreases. Apparently, the effects of the sideslip increase on the pressure distributions, as shown in Figure 8-53, are offsetting the beneficial effects resulting from the reduction in effective sweep angle.

On the lower surface, the general effect of increasing sideslip is to increase the extent of laminar flow (fig. 8-52). As shown in Figure 8-53 (for the $M = .8$ cases, only) the lower surface pressure gradient becomes more favorable and the pressure recovery point moves aft as the sideslip angle increases. This, combined with the reduction in effective sweep angle, results in increased laminar flow. The 27% chord location was the greatest extent of laminar flow observed on the lower surface during the entire flight test. The reason for the failure of the point at $\beta = 5^\circ$, $C_L = .54$ to follow the trend is not known at this time.

8.4 EFFECT OF ENGINE POWER ON TRANSITION

The trends exhibited in this section are of primary interest since the main purpose of the flight program was to determine the influence of engine noise on transition. Figure 8-54 shows the variation in transition location on the glove with variations in N_1 (Fan r/min) of engine number 2, which is the engine nearest the glove. On the upper surface, for a nominal condition of $M = .80$, $C_L = .54$, there was an increase in extent of laminar flow from the lowest to the higher r/min settings. This is the only variance from what would normally be expected on the basis of previous experience. It should be noted, however, that because of the difficulty of maintaining this Mach number at such a high altitude (41,500 ft) with one engine at idle r/min, the actual average Mach number for the idle condition was 0.79 and C_L was .567. This may have been the cause of the reduced laminar flow at this power setting. At $M = .70$,

$C_L = .64$ there was a slight reduction in laminar flow at the higher power settings. However, since there is very little laminar flow on the upper surface at this condition because of the large leading edge pressure peak, little significance is attached to such a change. At all other conditions on the upper surface, no effect of engine power setting on extent of laminar flow was observed. This result is not surprising in view of the minimal dependence of upper surface noise on engine power.

On the lower surface, most of the test series show a reduction in extent of laminar flow as N_1 increases. However, the changes are relatively small and at other conditions there is either no change or there is an increase in the extent of laminar flow as r/min increases. A closer examination of the actual flight conditions for the two cases having the unexpected trends shows that these cases corresponded to somewhat different conditions than the nominal. For example, the point labeled 1 was taken at a lower Mach number (.62 vs. .63) and higher C_L (.70 vs. .68), thus possibly causing a forward shift in transition. The point labeled 2 was taken at a negative sideslip relative to the others (i.e., -.5 vs. +1.2), which could also result in a forward transition shift. On the basis of the above results it is concluded that even though engine power does increase the noise level significantly on the lower surface, only very slight trends toward forward transition movement appear evident.

Table 8-6. Flight Test Data Summary — Flight 1

Cond. no.	Mach no.	Altitude, ft	C _L	β , deg	Engine 2 N ₁ r/min	Transition location, $\frac{x_{tr}}{c}$ (upper/lower)
0.001	0.822	38 950	0.492	- 0.3	3800	.25/.13
0.002	0.812	39 012	0.501	+ 5.4	3974	.20/.20
0.005	0.807	38 952	0.516	- 0.2	3644	.23/.18
*0.006.1	0.790	39 009	0.537	+ 5.8	3971	.13/.26
0.006.2	0.800	38 926	0.514	- 6.4	3962	.25/.13
0.013	0.801	40 948	0.553	+ 0.2	3934	.23/.18
0.014	0.807	40 946	0.544	0.0	3823	.23/.18
0.015	0.806	40 949	0.543	- 0.2	3733	.23/.18
0.016	0.797	41 002	0.556	+ 6.3	3848	.15/.25
0.017	0.797	40 878	0.552	- 7.1	3986	.25/.13
*0.035	0.807	39 952	0.525	- 0.3	3633	.24/.19
*0.036	0.780	39 956	0.560	- 0.4	3519	.23/.19
0.109	0.787	38 956	0.534	- 0.7	3461	.20/.18

*Data affected by cirrus clouds

Table 8-7. Flight Test Data Summary — Flight 2

Cond. no.	Mach no.	Altitude, ft	C _L	β , deg	Engine 2 N ₁ r/min	Transition location, $\frac{x}{c}$ (upper/lower)
0.201	0.800	30 011	0.353	- 0.6	3109	.22/.12
0.202	0.793	30 080	0.359	+ 3.3	3114	.23/.18
0.203	0.794	30 075	0.358	- 3.9	3167	.10/.05
0.204	0.805	34 001	0.416	- 0.2	3224	.25/.15
0.205	0.793	34 008	0.427	+ 3.9	3230	.20/.23
0.206	0.801	34 000	0.417	- 3.8	3274	.25/.15
0.207	0.809	36 000	0.450	0.0	3333	.25/.15
0.210	0.801	36 998	0.480	- 0.3	3380	.23/.18
0.211	0.804	37 994	0.498	- 0.2	3538	.23/.18
0.212	0.791	37 988	0.513	+ 3.9	3545	.20/.20
0.213	0.800	37 927	0.500	- 3.7	3485	.23/.15
*0.214	0.805	38 988	0.516	- 0.1	3614	.25/.20
*0.215	0.821	38 988	0.496	- 0.1	3701	.25/.20
0.216	0.832	38 986	0.478	0.0	3972	.25/.13
0.217	0.709	37 007	0.601	- 0.5	3248	.06/.15
0.218	0.701	37 007	0.617	- 0.6	3265	.06/.13
0.219.1	0.636	35 020	0.674	+ 0.7	4123	.03/.12
0.220.1	0.621	35 009	0.705	- 0.8	2683	.03/.10
0.221	0.632	35 007	0.679	- 0.6	2123	.03/.12
0.222	0.805	38 992	0.502	+ 0.1	3571	.23/.18
*0.223	0.804	40 483	0.534	- 0.2	3934	.23/.20
*0.224	0.796	40 482	0.544	- 0.4	3714	.23/.20
*0.225	0.800	40 483	0.537	- 0.7	3437	.23/.18
0.226	0.792	40 426	0.545	+ 4.8	3587	.18/.20
0.227	0.797	40 449	0.537	- 4.0	3615	.25/.18
0.228	0.790	41 295	0.567	- 0.5	2384	.20/.20
0.229	0.754	40 793	0.606	- 0.4	2994	.13/.20
0.231	0.701	39 015	0.641	+ 0.7	4059	.06/.14
0.232	0.697	39 009	0.647	0.0	3618	.06/.15
0.233	0.697	39 005	0.645	- 0.3	3259	.06/.15
0.234	0.699	39 042	0.644	+ 6.8	3412	.08/.27
0.235	0.708	38 954	0.623	- 6.7	3441	.08/.10
0.236	0.705	38 920	0.627	- 0.8	2349	.08/.15
0.237	0.707	39 005	0.623	- 0.5	2962	.08/.15
0.238	0.694	36 497	0.555	- 0.7	1001	.05/.18
0.239	0.802	37 999	0.460	- 0.5	3271	.25/.17
0.240	0.798	38 003	0.464	+ 3.9	3377	.20/.20
0.241	0.802	40 971	0.527	0.0	3653	.23/.18
0.242	0.830	40 968	0.488	+ 0.3	3930	.25/.18
0.243	0.816	38 976	0.457	+ 0.2	3985	.25/.17
0.244	0.821	38 972	0.452	- 0.3	3757	.25/.15
0.245	0.821	38 974	0.450	- 0.3	3542	.25/.15
*0.246	0.816	38 989	0.455	+ 4.0	3988	.25/.23
*0.247	0.813	38 548	0.447	- 0.7	2260	.25/.17
0.248	0.822	38 990	0.480	+ 0.2	3692	.25/.18
0.249	0.784	38 993	0.527	0.0	3392	.20/.20
0.250	0.752	38 999	0.573	+ 0.1	3382	.10/.20
0.251	0.757	38 997	0.563	+ 0.2	4023	.10/.20
0.252	0.753	38 994	0.569	- 0.4	3638	.10/.20

*Data affected by cirrus clouds

Table 8-8. Flight Test Data Summary — Flight 3

Cond. no.	Mach no.	Altitude, ft	C_L	β , deg	Engine 2 N_1 r/min	Transition location, $\frac{x_{tr}}{c}$ (upper/lower)		
						Inboard	Midspan	Outboard
0.001	0.703	30 009	0.442	+0.5	3468	-/-**	-.15	-.15
0.002	0.701	30 005	0.445	+5.3	3535	-.20	-.20	-.20
0.003	0.801	30 728	0.350	0.0	3602	-/-	.20/-	-.15
0.004	0.798	30 721	0.352	+3.5	3606	.25/.18	.23/.18	-.15
0.005	0.799	30 682	0.350	-3.4	3677	-/-	.20/-	-/-
0.006	0.807	34 669	0.410	0.0	3677	.25/-	.25/.15	-.15
0.006.1	0.800	35 062	0.422	+0.2	3619	.25/-	.23/.15	-.15
0.007	0.820	34 668	0.398	0.0	3746	-/-	.25/.15	-/-
0.007.1	0.817	35 065	0.405	+0.1	3691	—	.25/.15	-/-
0.008	0.780	35 067	0.444	+0.2	3585	.25/-	.20/.17	-.15
0.009	0.753	35 075	0.476	+0.3	3558	.20/-	-.17	-.15
0.010	0.704	35 080	0.543	+0.3	3477	-/-	-.15	-.15
0.011	0.698	35 080	0.553	+6.7	3628	-.25	-.25	-.23
0.012	0.799	36 588	0.451	+0.1	3631	.23/-	.23/.15	-.15
0.013	0.801	38 035	0.479	+0.1	3649	.28/-	.23/.18	-.15
0.014	0.823	39 863	0.492	+0.1	3919	.28/-	.23/-	-.15
0.015	0.834	39 862	0.480	+0.1	3945	.28/-	.25/.15	-.15
0.016	0.802	40 480	0.530	+0.4	3964	.28/.17	.23/.18	-.15
0.017	0.802	40 419	0.529	+0.1	3795	.28/.17	.23/.18	-.15
0.018	0.805	40 477	0.525	0.0	3653	.28/.17	.23/.18	-.15
0.019	0.797	40 544	0.537	+4.0	3661	.25/.23	.20/.25	-.20
0.020	0.792	40 443	0.540	-4.1	3661	.27/-	.23/.15	-.15
0.021	0.703	39 137	0.640	+0.9	4056	-/-	-.15	-.15
0.022	0.700	39 128	0.647	+0.4	3667	-/-	-.15	-.15
0.023	0.695	39 190	0.655	-0.4	3068	-/-	-.15	-.15
0.024	0.692	39 180	0.660	+7.0	3502	-.25	-.25	-.23
0.025	0.719	39 075	0.608	-7.8	4037	.15/-	-/-	-/-
0.026	0.801	39 092	0.494	+0.2	3708	.28/.17	.23/.18	-.15
0.027	0.821	38 440	0.451	+0.1	3754	.27/-	.25/.18	-.15
0.028	0.778	39 646	0.531	+0.2	3681	.25/.15	-.20	-.17
0.029	0.752	39 661	0.567	+0.2	3638	.18/.15	-.20	-.18
0.030	0.825	40 761	0.495	0.0	3953	.29/-	.25/.18	-.15
0.031	0.706	35 180	0.513	+1.2	4084	-/-	-.17	-.15
0.032	0.704	35 213	0.515	-0.5	2537	-/-	-.15	-.15
0.033	0.706	35 154	0.513	+0.1	3528	-/-	-.18	-.15
0.034	0.800	35 325	0.400	-0.1	3568	.23/-	.25/.15	-/-
0.035	0.800	25 005	0.248	-0.6	3570	-/-	-/-	-/-
0.036	0.794	24 979	0.251	+2.6	3569	-/-	-/-	-/-
0.037	0.798	38 015	0.462	+0.1	3649	.28/.17	.23/.18	-.15
0.038	0.698	35 215	0.525	-0.7	2099	-/-	-.17	-.15

**Indicates transition ahead of $\frac{x}{c} = .15$

Table 8-9. Flight Test Data Summary — Flight 4

Cond. no.	Mach no.	Altitude, ft	C_L	β , deg	Engine 2 N_1 r/min	Transition location, $\frac{x_{tr}}{c}$ (upper/lower)		
						Inboard	Midspan	Outboard
0.001	0.700	30 001	0.448	0.0	3412	-/-**	-.15	-/-
0.002	0.708	29 897	0.436	+5.2	3539	-.20	-.20	-.20
0.003	0.800	30 517	0.350	-0.3	3586	-/-	.25/-	-/-
0.004	0.797	30 585	0.354	+3.6	3736	-.19	.22/.18	-.15
0.005	0.805	30 590	0.346	-3.5	3688	-/-	-/-	-/-
0.006	0.799	34 447	0.419	-0.2	3640	.15/-	.23/.15	-/-
0.007	0.820	34 448	0.398	-0.2	3680	-/-	.23/.15	-/-
0.008	0.780	34 449	0.439	-0.1	3595	.15/-	.23/.15	-.15
0.009	0.752	34 453	0.472	-0.1	3555	-/-	-.15	-.15
0.010	0.701	34 471	0.542	-0.1	3510	-/-	-/-	-.15
0.011	0.701	34 451	0.541	+6.4	3699	-.20	-.25	-.20
0.012	0.800	36 176	0.450	-0.1	3654	.15/-	.23/.15	-.15
0.013	0.801	37 563	0.478	-0.1	3679	.15/-	.23/-	-.15
0.014	0.819	39 460	0.498	-0.1	3861	.15/-	.23/-	-.15
0.015	0.829	39 459	0.484	-0.2	3953	.15/-	.23/.15	-.15
0.016	0.800	39 960	0.531	-0.2	3962	.15/.15	.23/.18	-.15
0.017	0.800	39 961	0.531	+0.1	3768	.15/.15	.23/.18	-.15
0.018	0.800	40 065	0.532	+0.4	3690	.15/.15	.23/.18	-.15
0.019	0.802	40 091	0.531	+3.6	3840	-.20	.23/.20	-.17
0.020	0.800	40 086	0.532	-3.7	3898	.17/-	.23/.15	-.15
0.021	0.700	38 592	0.644	-0.3	4048	-/-	-/-	-.15
0.022	0.701	38 668	0.644	+0.2	3679	-/-	-/-	-.15
0.023	0.699	38 670	0.647	+0.3	3332	-/-	-/-	-.15
0.024	0.700	38 615	0.643	+6.4	3339	-.20	-.25	-.20
0.025	0.700	38 790	0.647	-6.0	3961	-/-	-/-	-/-
0.026	0.798	38 806	0.497	+0.2	3737	.15/.15	.23/.18	-.15
0.027	0.824	37 973	0.447	0.0	3782	.15/-	.23/.15	-.15
0.028	0.777	39 167	0.531	+0.1	3715	.15/.15	.20/.20	-.17
0.029	0.752	39 176	0.567	+0.1	3707	-/-	-.18	-.16
0.030	0.827	40 353	0.493	-0.1	3995	.15/-	.23/.18	-.15
0.031	0.700	34 694	0.522	-0.3	4078	-/-	-.15	-.15
0.032	0.703	34 697	0.517	+0.5	2669	-/-	-.18	-.17
0.033	0.703	34 692	0.518	-0.1	3501	-/-	-.15	-.15
0.034	0.802	34 776	0.397	-0.3	3581	-/-	.23/.15	-.15
0.037	0.802	37 569	0.457	-0.2	3648	.15/-	.23/.17	-.15
0.039	0.702	33 024	0.478	+5.0	4061	-.20	-.22	-.22
0.040	0.711	32 961	0.463	+4.8	2406	-.23	-.25	-.22

**Indicates transition ahead of $\frac{x}{c} = .15$

- $M = 0.80$
- $C_L = 0.53$
- Altitude = 40,500 ft

- $\beta = 0$
- $N_{1E2} = 3964$ (MCT)

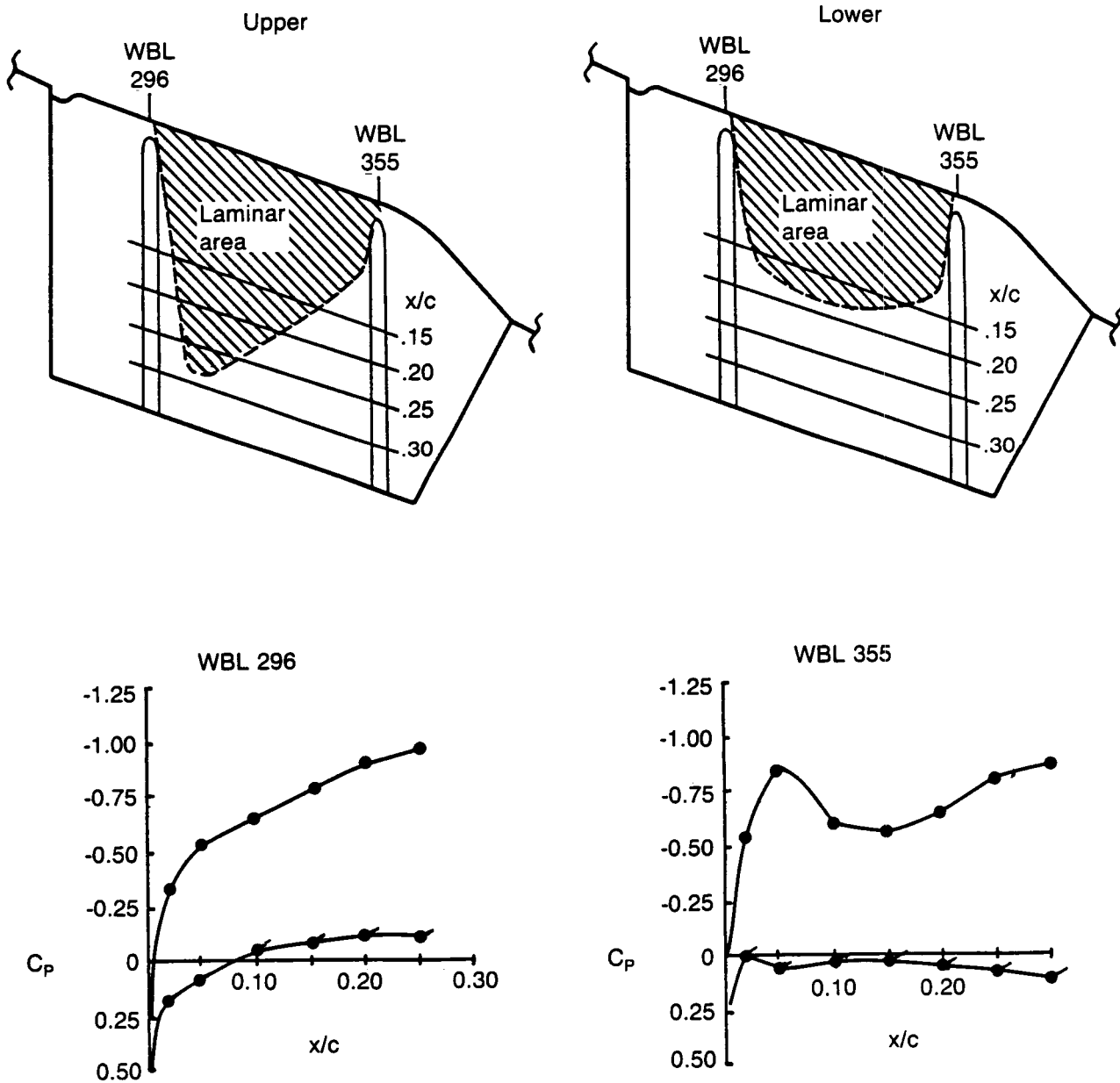


Figure 8-44. Laminar Areas on Glove in Flight—Design Condition

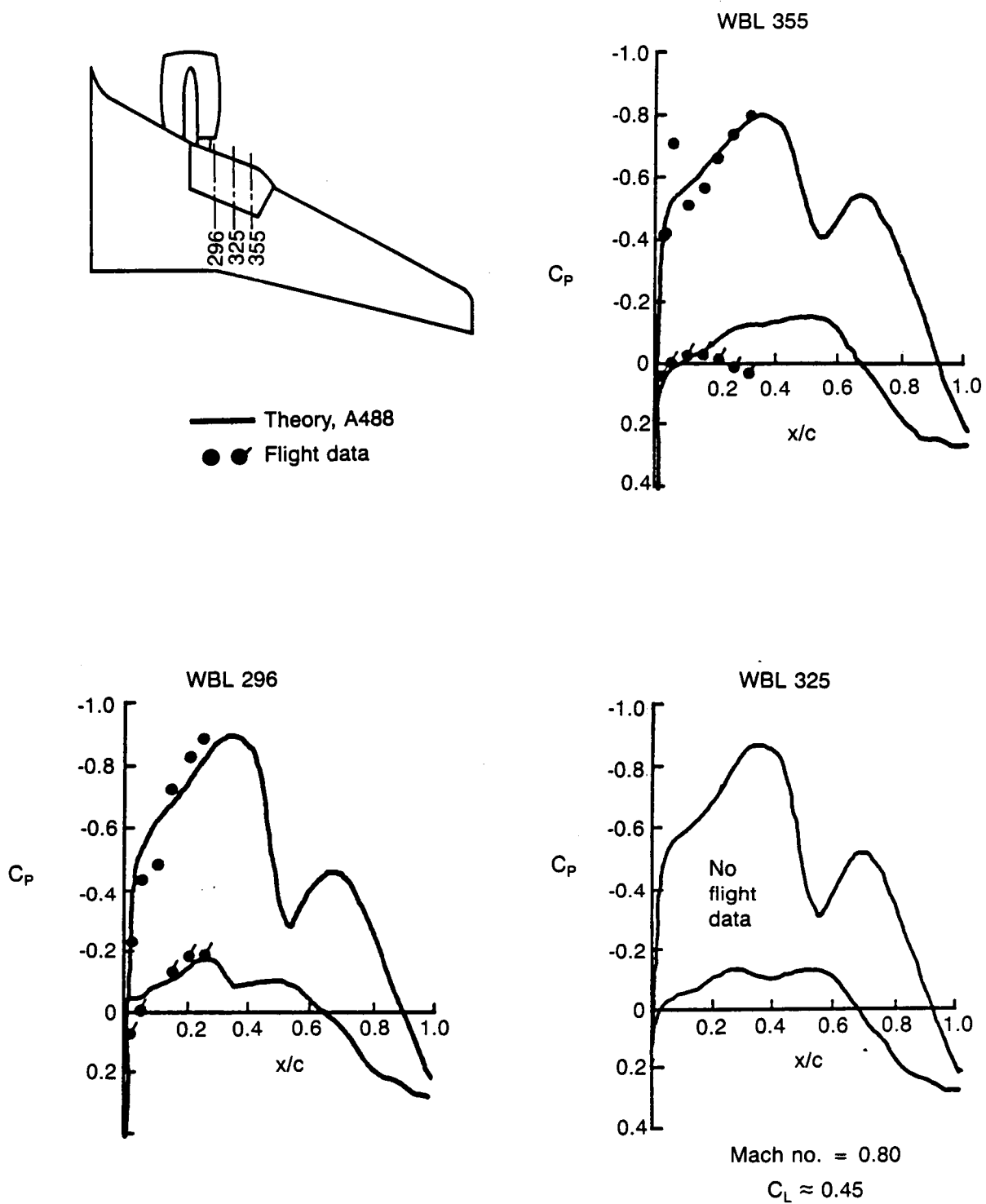


Figure 8-45. Spanwise Effects on Glove Pressure Distributions

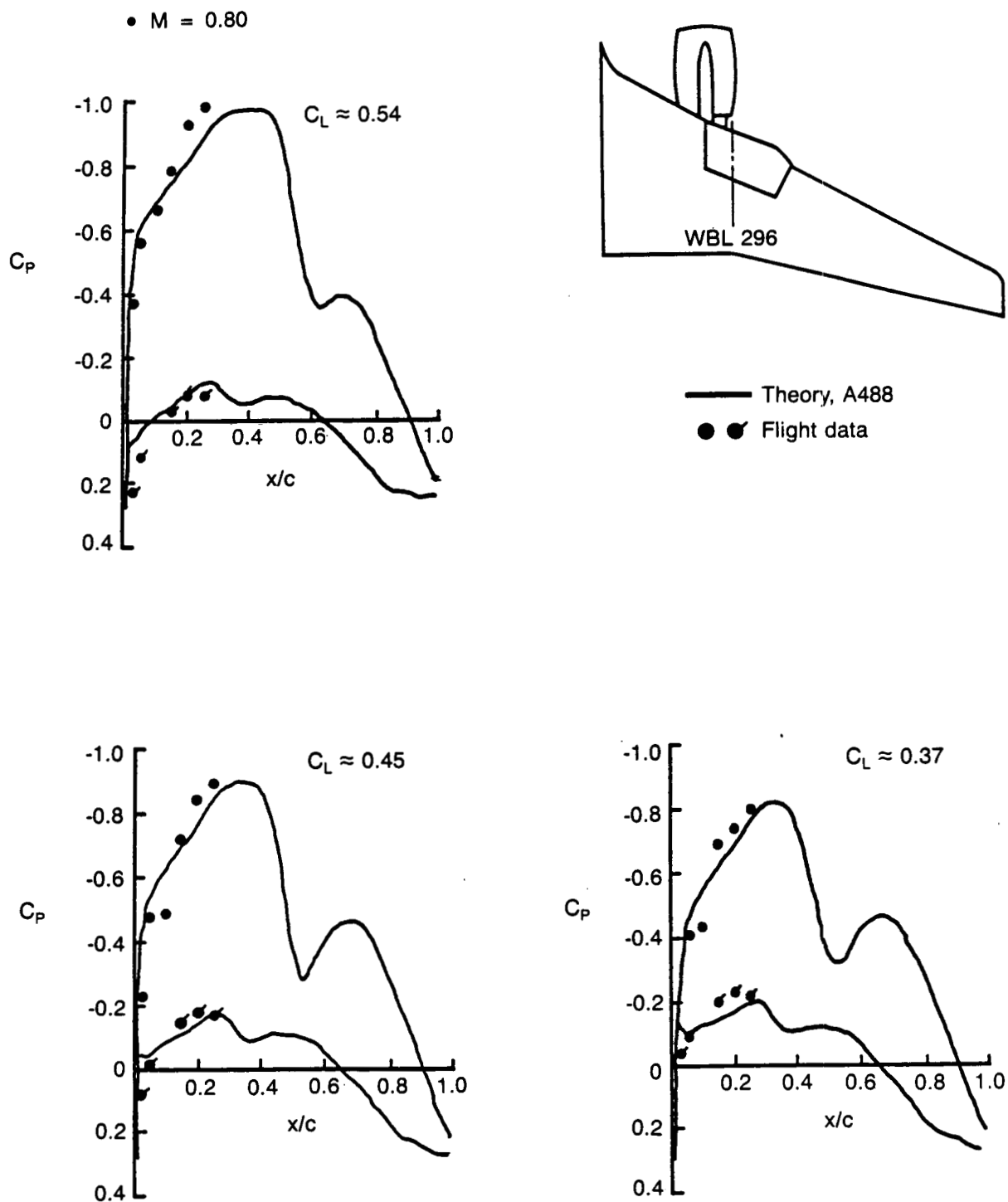
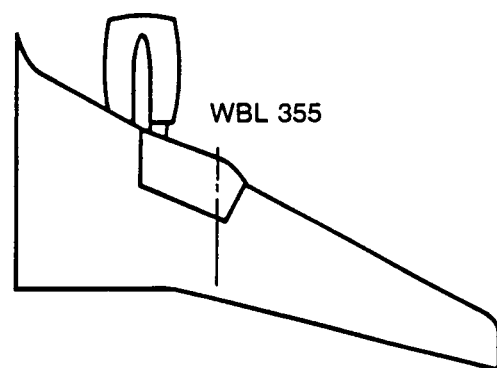
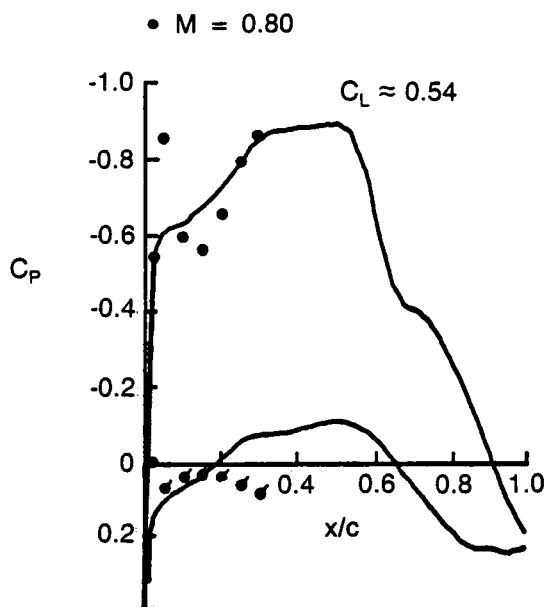


Figure 8-46. Comparison of Inboard Glove Pressure Distributions—Effect of C_L



— Theory, A488
● ● Flight data

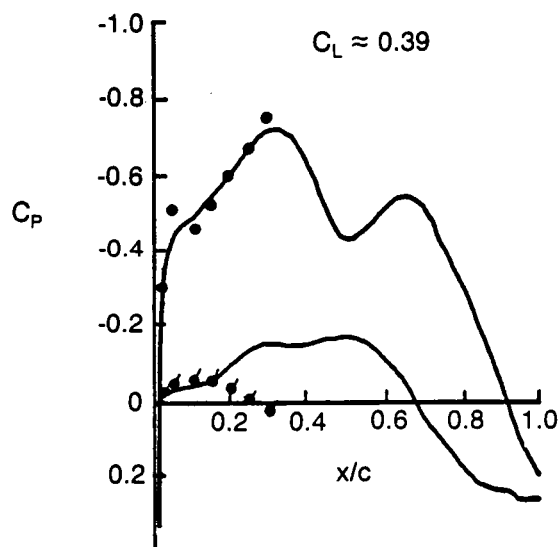
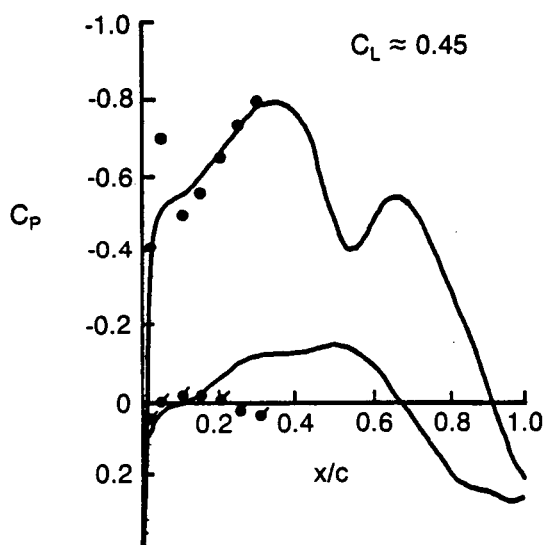


Figure 8-47. Comparison of Outboard Glove Pressure Distributions—Effect of C_L

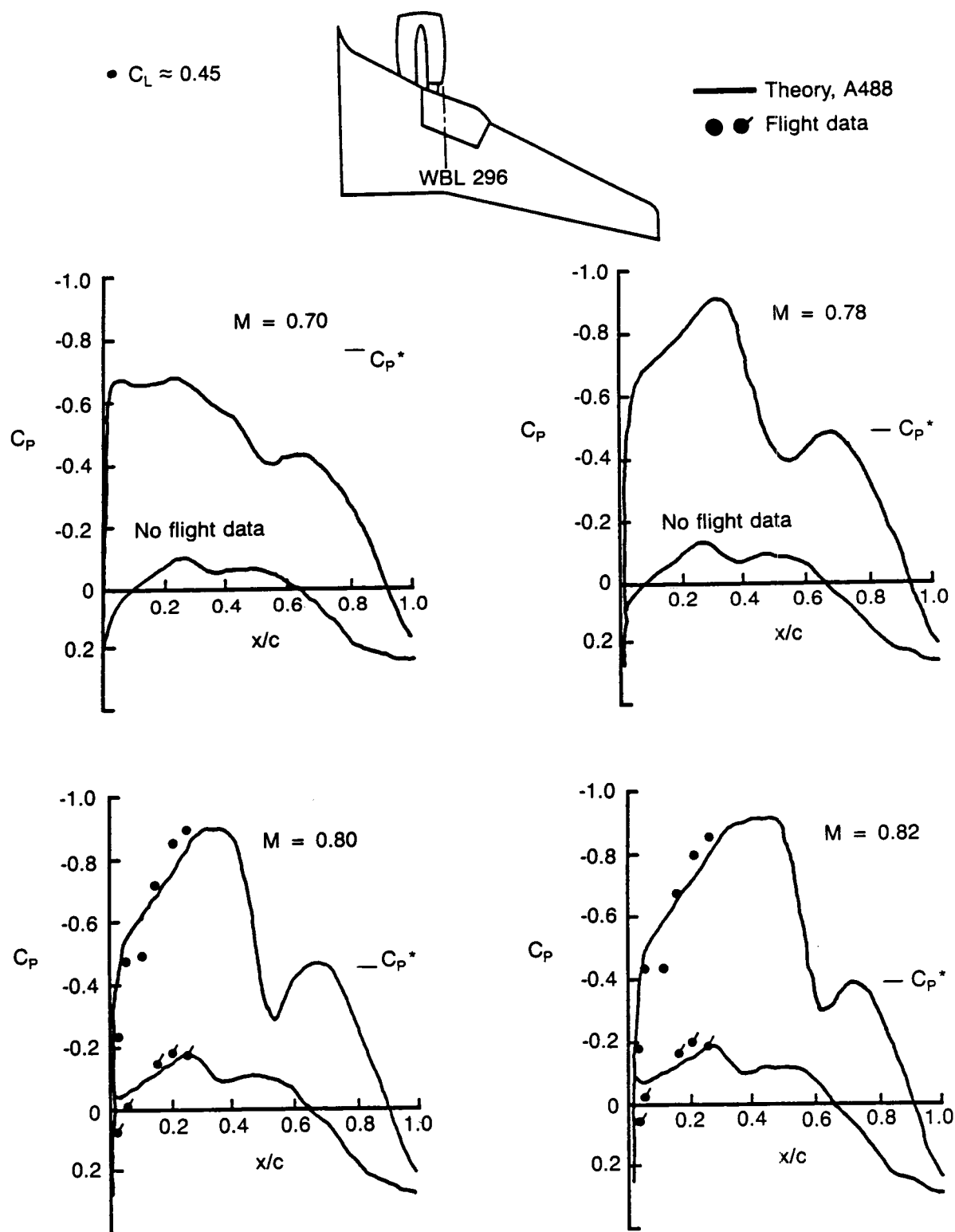


Figure 8-48. Comparison of Inboard Glove Pressure Distributions—Effect of Mach Number

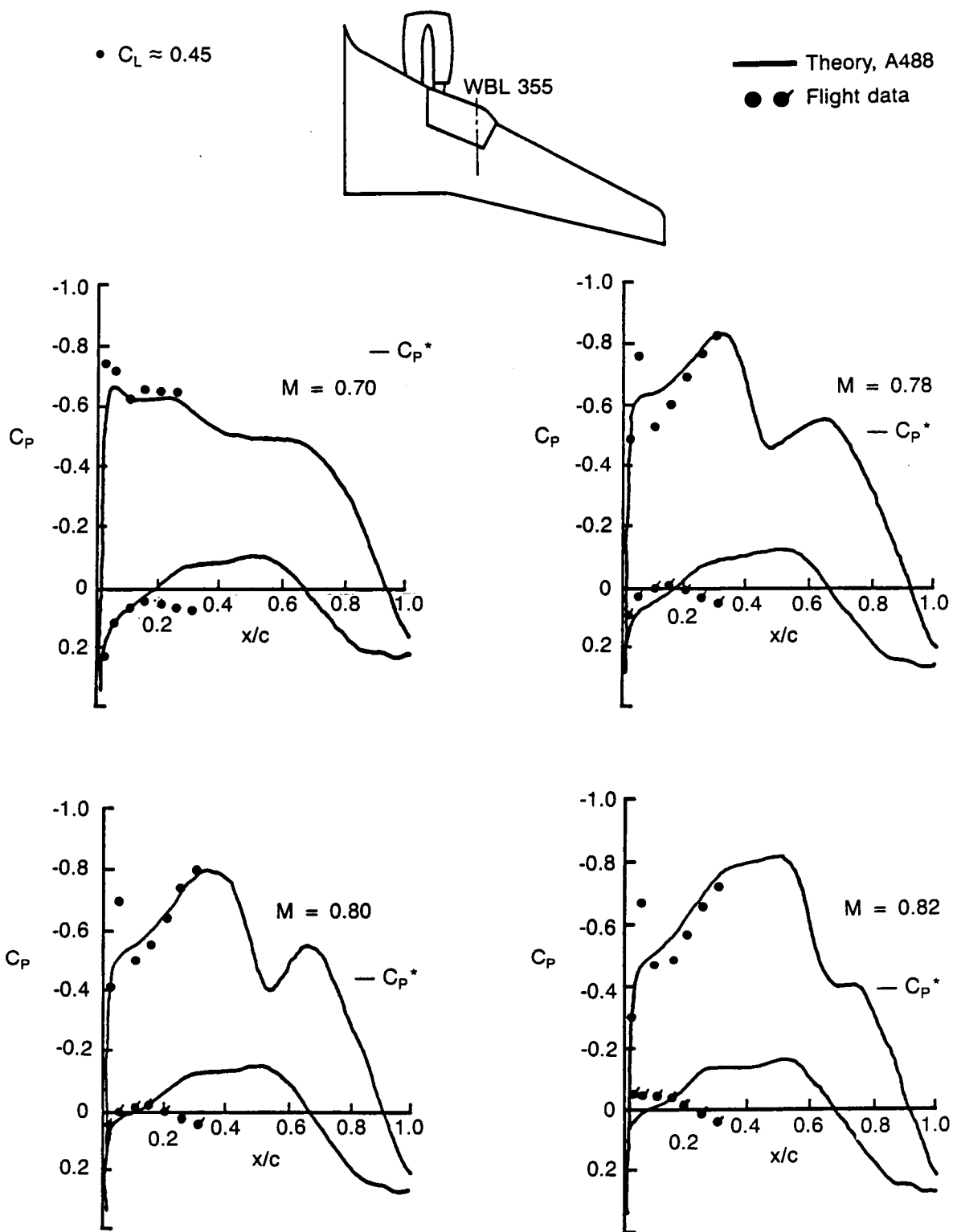


Figure 8-49. Comparison of Outboard Glove Pressure Distributions—Effect of Mach Number

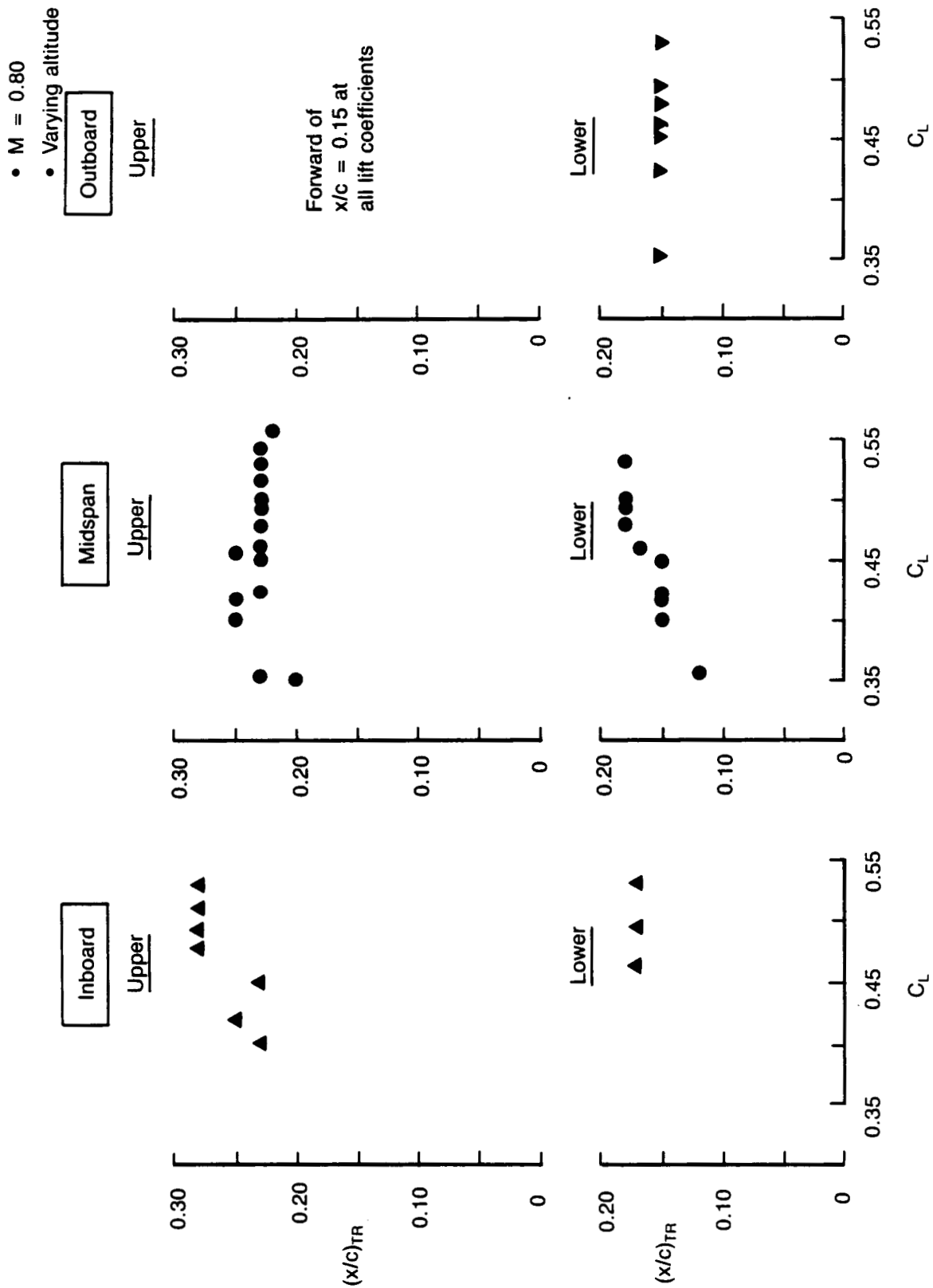


Figure 8-50. Transition Distribution on 757 Glove—Effect of C_L

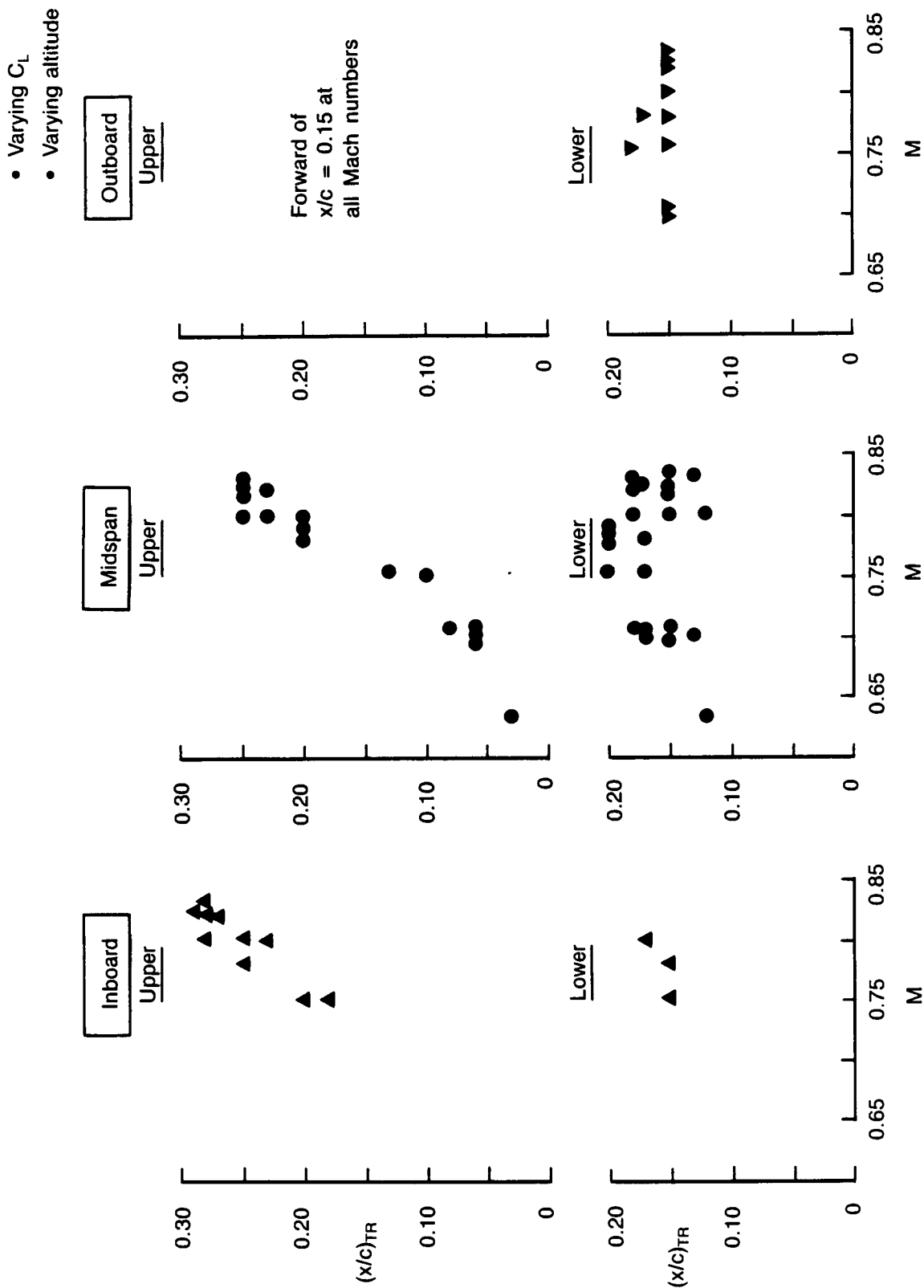


Figure 8-51. Transition Distribution on 757 Glove—Effect of Mach Number

• $M = 0.80$ (except as noted)

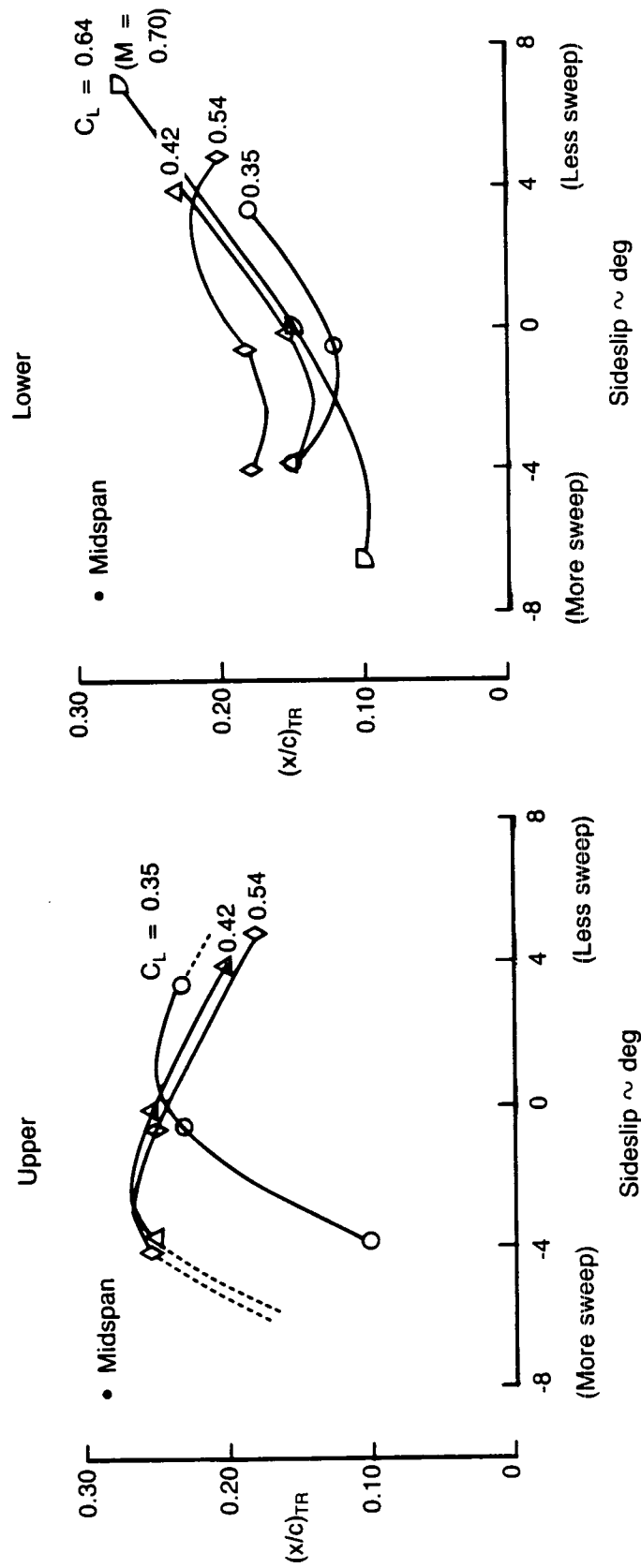
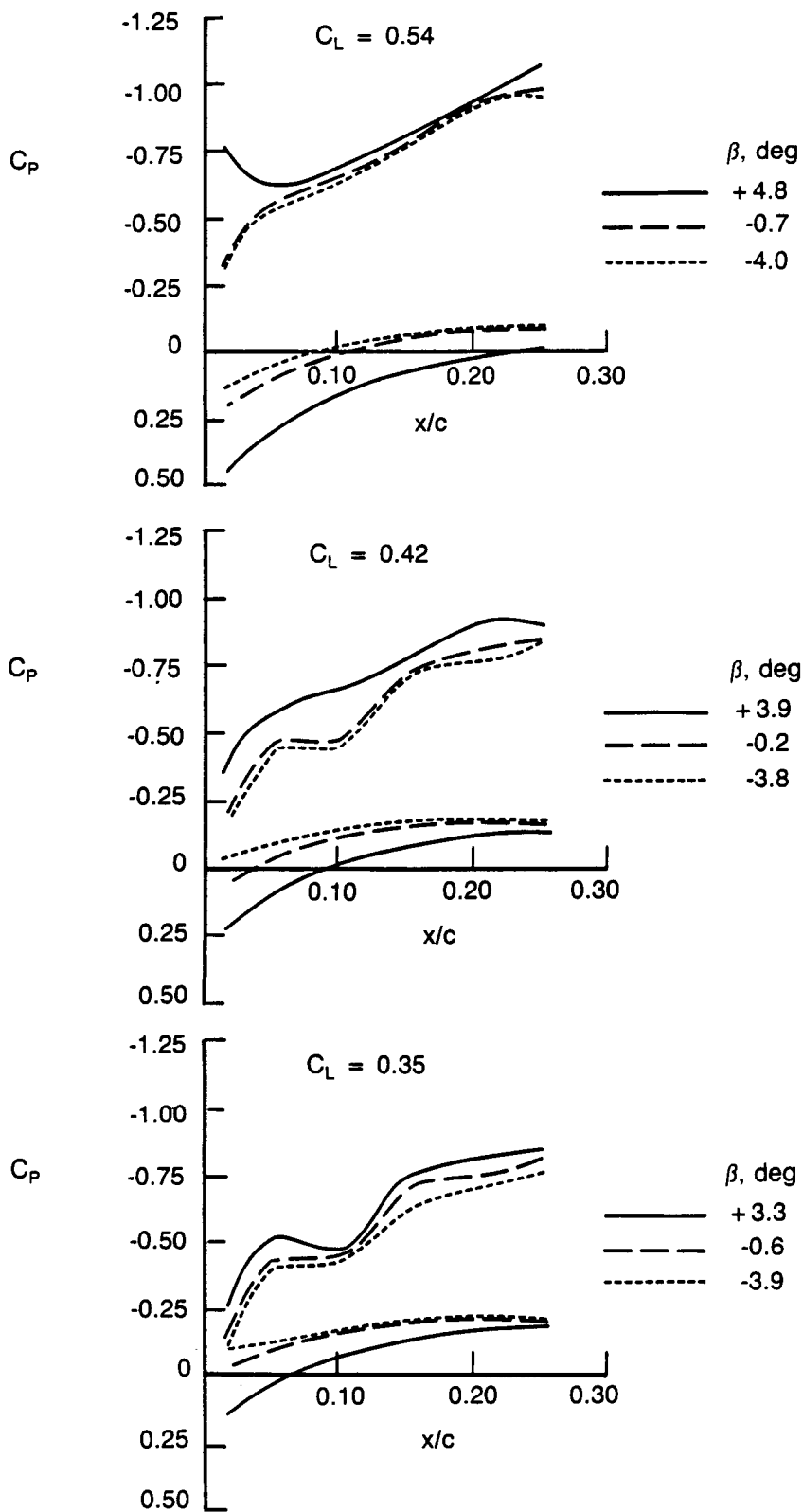


Figure 8-52. Transition Variation With Sideslip (Sweep)—Effect of C_L



- $M = 0.80$
- WBL 296

Figure 8-53. Effect of Sideslip on Glove Pressure Distributions

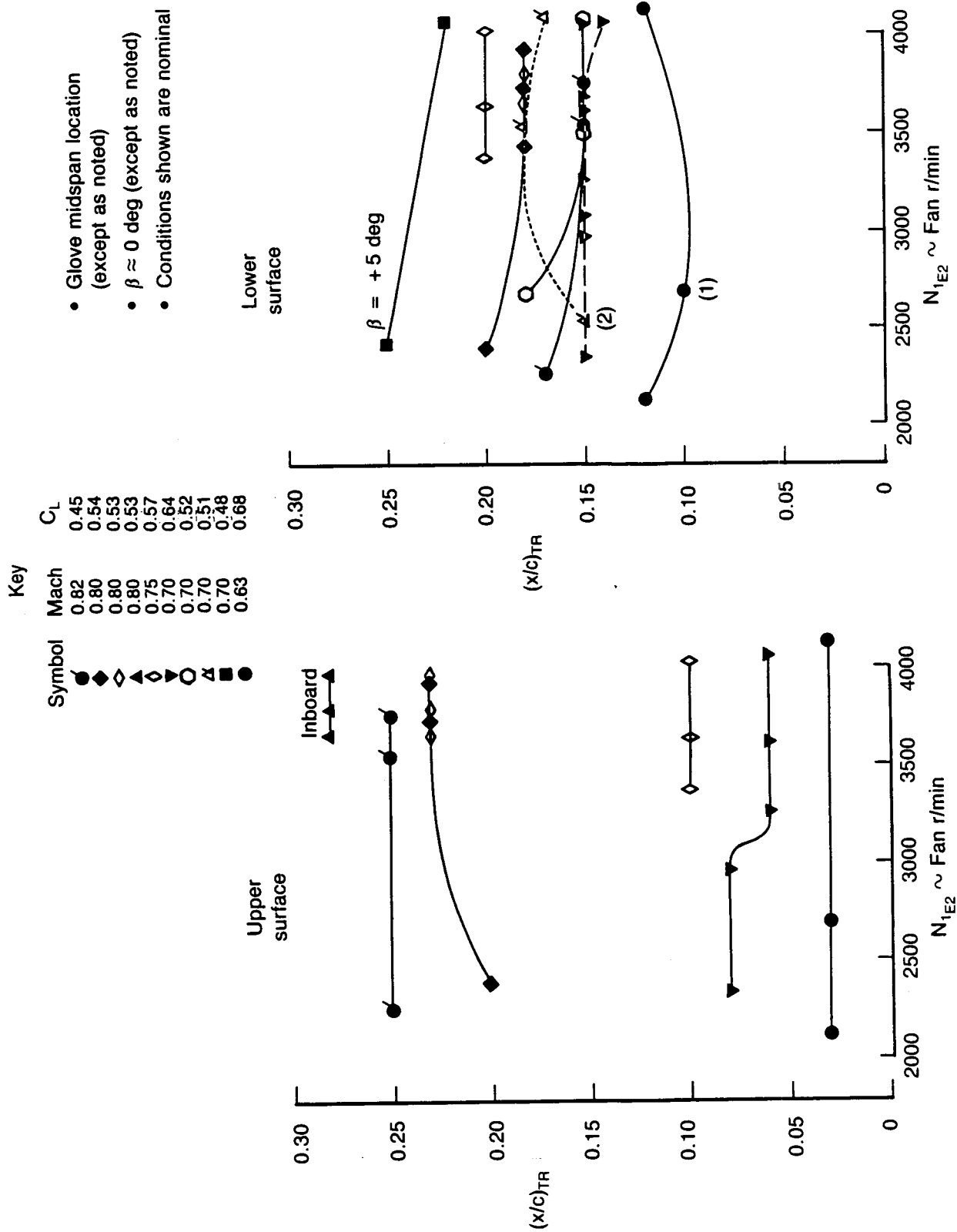


Figure 8-54. Effect of Engine Power Setting on Extent of Laminar Flow

9.0 CONCLUSIONS AND RECOMMENDATIONS

The major conclusion of this study is that extensive natural laminar flow can be obtained consistently on the wing of a transport configuration with wing-mounted fan engines. Transition location was influenced by pressure distribution, Reynolds number, C_L , Mach number, sideslip (sweep), and roughness in ways that are generally in accord with other experience and tests. Specific detail conclusions of the study are as follows:

1. Noise generated by the wing airflow, such as the wing shock, the wing turbulent boundary layer, and the vortex from the outboard planform break appears to dominate on the wing upper surface, although there is some sensitivity to engine power in the leading edge region. Engine noise clearly dominated on the lower surface where the levels are proportional to fan jet Mach number.
2. Engine noise produced by the PW 2037 turbofan engine had only a very weak effect on lower surface transition and no measurable effect on upper surface transition.
3. The wing notch incorporated to protect the glove leading edge was effective in preventing turbulent flow transfer from adjacent areas such as the strut-wing or fuselage-wing intersections.
4. Although significant atmospheric turbulence was encountered during some periods in flight, no effect on the extent of laminar flow was observed.
5. The NLF transition locations moved forward in visible cirrus clouds, consistent with previous observations of the effect of ice crystals. However, in faint or invisible clouds there was little effect on transition even when their presence was apparent in the disturbed hot-film output traces. Change in altitude or location was an effective avoidance procedure.
6. Insect residues accumulated during Flight 4 (for which no protective measures were used) were sufficient to cause turbulent flow. This effect was not alleviated by operation at higher altitudes (i.e., lower unit Reynolds numbers). Although various protective measures are potentially available, only the removable paper cover technique was used (in Flights 1, 2, and 3). It can only be considered applicable for experimental purposes.
7. Compliance with surface smoothness and waviness tolerances for laminar flow surfaces was adequate for the glove tests and was achieved without excessive effort. Minor local damage sustained at various stages during the instrumentation installation and preparation for flight was easily repaired.

Recommendations:

1. Even though no large effects of engine noise were observed in the tests reported here, additional analyses should be done to maximize the value of the data obtained, namely:
 - (a) Determine the contribution of the various noise sources to the spectra measured on the 757 wing. In addition to the conventional engine noise sources, these include surface flow phenomena, turbulence, shock waves, vortices, etc.
 - (b) Evaluate and update current methods of predicting noise fields. This should be done in relation to other sources of data besides the 757 flight test program.
 - (c) Quantify and systematize the effects of noise on boundary layer transition by correlating existing data (e.g., 757 tests, NASA and Boeing wind tunnel experiments, Northrop X-21 flights, etc.).
2. The data base for laminar flow technology should be augmented with selected experiments. Since the extent of laminar flow in the 757 glove tests was limited by the choice of NLF, testing an HLFC wing section would be important to obtain data for longer laminar runs. It is possible that noise influences may be much more important for longer laminar runs. This approach would also correspond more closely to the type of application of most interest for transport aircraft.

3. Based on the experience of the 757 glove tests, it is apparent that a number of improvements in testing technique would be useful in the future.
- (a) A refinement of the normal pressure belt installation to avoid pressure errors should be implemented in the future. This is important for cases where the expense and other limitations preclude the use of buried static orifices.
 - (b) Current tests have indicated a relationship between ice crystal concentration and transition movement which should be quantified. To accomplish this, better means of defining ice crystal size and number density are required.
 - (c) The definition of transition location is subject to a number of limitations (e.g., accuracy, coverage, interference, cost, etc.) which could probably be surmounted by developing better detection means. Other sensor types and installation approaches should be examined.
 - (d) Current experience with noise measurements in flight has again demonstrated that the microphone system design and installation can have substantial effects on the recorded results. Variations between microphone types appear to be important but difficult to interpret, particularly in relation to the observed effects of noise on boundary layer transition. Better arrangements need to be developed in conjunction with theoretical analysis and laboratory evaluation of their properties. Boundary layer turbulence and wing shock influence in particular need to be addressed. The complex airflow over a wing surface needs to be considered.

10.0 REFERENCES

1. Mangiarotty, R. A., "Effects of Engine Noise on Aircraft Wing Laminar Boundary Layer Stability," *Journal Acoustical Society America*, Vol. 70, No. 1, pp. 98-109, July 1981.
2. BCAC Preliminary Design Staff, "Evaluation of Laminar Flow Control System Concepts for Subsonic Commercial Transport Aircraft," NASA CR 158976, Langley Research Center, 1978.
3. Mangiarotty, R. A. and Bohn, A. J., "Wind Tunnel Evaluation of Induced Acoustical Effects on Laminar Flow Control," Boeing Report D6-47017, January 1979.
4. Mangiarotty, R. A. and Bohn, A. J., "Wind Tunnel Study on the Effects of Acoustical Disturbances on Controlled Laminar Flow," *Journal AIAA*, Vol. 18, No. 7, pp. 801-807, September 1980.
5. Swift, G. and Munger, D., "A Study of the Prediction of Cruise Noise and Laminar Flow Control Noise Criteria for Subsonic Air Transports," NASA CR-159104, Langley Research Center, 1979.
6. Eldred, K. M., Roberts, W. H., and Yancey, L. J., "In-Flight Noise Measurements on F94-C Aircraft," Report No. NOR 60-284, September 1960, Norair Division, Northrop Corporation.
7. Carmichael, R. F. and Pelke, D. E., "In-Flight Noise Measurements Performed on the X-21A Laminar Flow Aircraft," Contract AF33(600)-42052, Document NOR-64-81, April 1964.
8. Mack, L. M., "Computation of the Stability of the Laminar Compressible Boundary Layer," *Methods in Computational Physics*, edited by B. Adler, Academic Press, N.Y., pp. 247-299, 1965.
9. Pfenninger, W. "Flow Problems of Swept Low-Drag Suction Wings of Practical Construction at High Reynolds Numbers," *Annals of the N.Y. Academy of Sciences*, Vol. 154, Art. 2, pp. 672-703, November 1968.
10. Mack, L. M., "On the Stability of the Boundary Layer on a Transonic Swept Wing," AIAA Paper 79-0164, AIAA 17th Aerospace Sciences Meeting, New Orleans, La., January 15-17, 1979.
11. Srokowski, A. J. and Orzag, S. A., "Mass Flow Requirements for LFC Wing Design," AIAA Paper 77-1222, AIAA Aircraft Systems and Technology Meeting, Seattle, Washington, August 22-24, 1977.
12. Hefner, Jerry N. and Bushnell, Dennis M., "Status of Linear Boundary Layer Stability Theory and the e^n Method, with Emphasis on Swept-Wing Applications," NASA Technical Paper 1645, April 1980.
13. Runyan, L. J., Navran, B. H., and Rozendaal, R. A., "F-111 Natural Laminar Flow Glove Flight Test Data Analysis and Boundary Layer Stability Analysis," NASA CR-166051, October 1983.
14. "Flight Tests on 'King Cobra' FZ.440 to Investigate the Practical Requirements for the Achievement of Low Profile Drag Coefficients on a 'Low Drag' Aerofoil," Smith, F. and Higton, D. J., R.A.E. Report No. AERO 2078, October 13, 1945.
15. Boeing Acoustics Laboratory Staff, "ADP-2 System Operation," Document D6-51129, October 1981.
16. Nennie, Joseph P. and Gluyas, George L., "Aerodynamic Design and Analysis of an LFC Surface," *Astronautics and Aeronautics*, July 1966.
17. Ungar, Eric E., et al., "A Guide For Predicting the Vibrations Of Fighter Aircraft in the Preliminary Design Stages," Technical Report AFFDL-TR-71-63, April 1973.

APPENDIX

PROBE DEVELOPMENT

A.1 STING-MOUNTED PROBES

Two different designs of sting-mounted probes were developed in the design and evaluation phase of the test program. The first design, NTL 4027-1 (described in Section 6.3 of this report) was later chosen for the flight test program. The second design, NTL 4027-2, used an ogive-curve probe with a flush-mounted transducer installed on a flattened surface near the probe tip. Both designs were tested in the Noise Technology Laboratory (NTL) in order to determine their directivity and self-noise characteristics. Both configurations were installed on airplane NA001 and tested in flight prior to the installation of the laminar flow glove. A photograph of both probe configurations installed on NA001 is included as Figure A-1.

Directivity testing on the probes was conducted in the NTL large test chamber using the test setup shown in Figure A-2. Both probes were rotated about their transducers in a horizontal plane, 30 in from a pink noise sound source. The noise spectrum of the sound source was shaped to be flat over the 1/3-octave bands between 250 Hz and 10 kHz (see fig. A-3). Negligible directivity effects were noted on the side-mounted transducer probe configuration which, at the time, was fitted with a nonvented LQ-125-5 Kulite transducer (see fig. A-4). During directivity testing of the B&K bullet nose configuration, a frequency response that contained a resonant peak near 630 Hz was observed (see fig. A-5). Subsequent testing after the resolution of transducer vent tube problems (see sec. A.2) showed the B&K bullet nose configuration to have negligible directivity characteristics.

The self-noise checkout of the probes was run in the NTL quiet air facility using the test setup shown in Figure A-6. The probes were tested at Mach numbers ranging to 0.65. Example plots are included as Figures A-7 and A-8. The self-noise data indicated that the side-mounted transducer configuration was up to 10 dB noisier above 1000 Hz at the higher airspeeds tested. Self-noise data also indicated the side-mounted transducer configuration to be more sensitive to angle of attack than the B&K bullet nose configuration.

In late February, 1985 the two sting-mounted probe configurations and one wing surface-mounted transducer were installed on the right wing of NA001 approximately at wing buttock line 563 and 60% chord on the top surface of the wing (see figs. A-1 and A-9). The side-mounted transducer configuration was at that time fitted with a vented LQ-101-125-5 Kulite transducer. Flight test data, when reduced, tended to show highest noise levels for the wing surface-mounted LQ-101-125-5 transducer (as expected). The data also tended to show higher noise levels for the side-mounted transducer probe configuration than for the B&K bullet nose configuration (see fig. A-10). An additional flight test was conducted in March, 1985 at airplane Mach numbers up to .8. At $M_{AP} = .8$ much higher low frequency levels were observed with the probe microphones compared to $M_{AP} = .7$. Varying the engine and airplane conditions tended to change these levels (figs. A-11 A13). The B&K bullet nose configuration was chosen for the June 1985 laminar flow flight test program because of its generally superior self-noise characteristics.

A.2 TRANSDUCER VENT TUBE MODIFICATIONS

As discussed in the previous section, a resonant peak was noted in the B&K bullet nose probe configuration. Subsequent testing showed frequency response problems to be related to the vent tubes built into the XCW-093-5 and LQ-101-125-5 transducers. The 1/3-octave frequency response of an XCW-093-5 and LQ-101-125-5 transducer in a pink noise sound field is shown in Figures A-14 and A-15, respectively. Transducer frequency response was improved by the addition of a 3-ft length of Tygon tubing to the existing transducer vent tube (see fig. A-16). The probe evaluation flight tests of late February-early March 1985 were flown with Tygon tubing modified transducers. Subsequent testing showed that an

PRECEDING PAGE BLANK NOT FILMED

improved transducer frequency response could be obtained by reducing transducer vent tube cross-sectional area (see figs. A-17 and A-18). This was done by inserting a wire, sized to make a tight but nonplugging fit, in the transducer's vent tube.

A .008-in wire was inserted into XCW-093-5 vent tubes; a .016-in wire was inserted into LQ-101-125-5 vent tubes. This vent tube modification was performed on all Kulite transducers installed on NA001 for the laminar flow flight tests.

ORIGINAL PAGE IS
OF POOR QUALITY

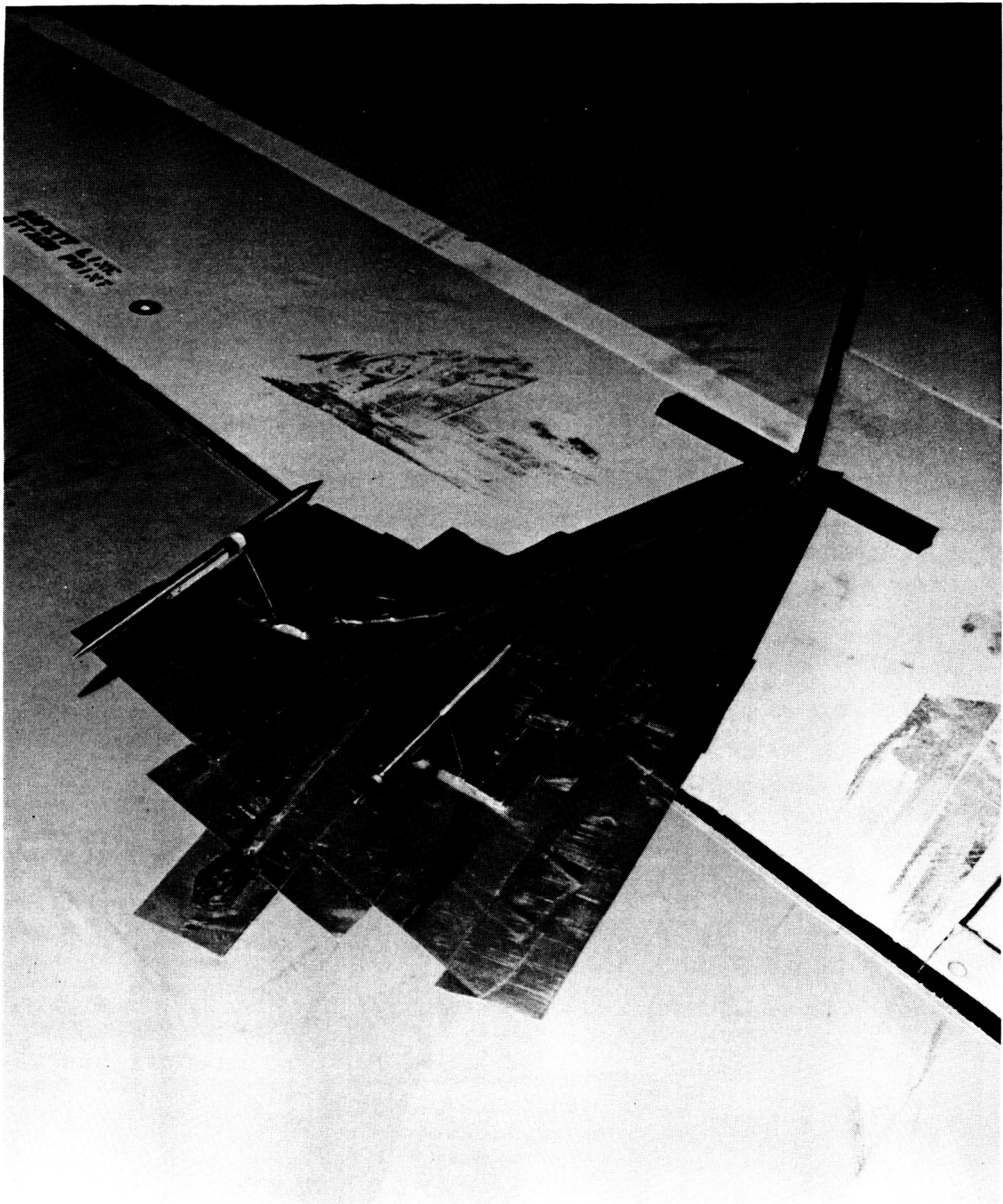


Figure A1. Close-Up View of Transducer Installation on NA001 for Probe Evaluation Flight Tests

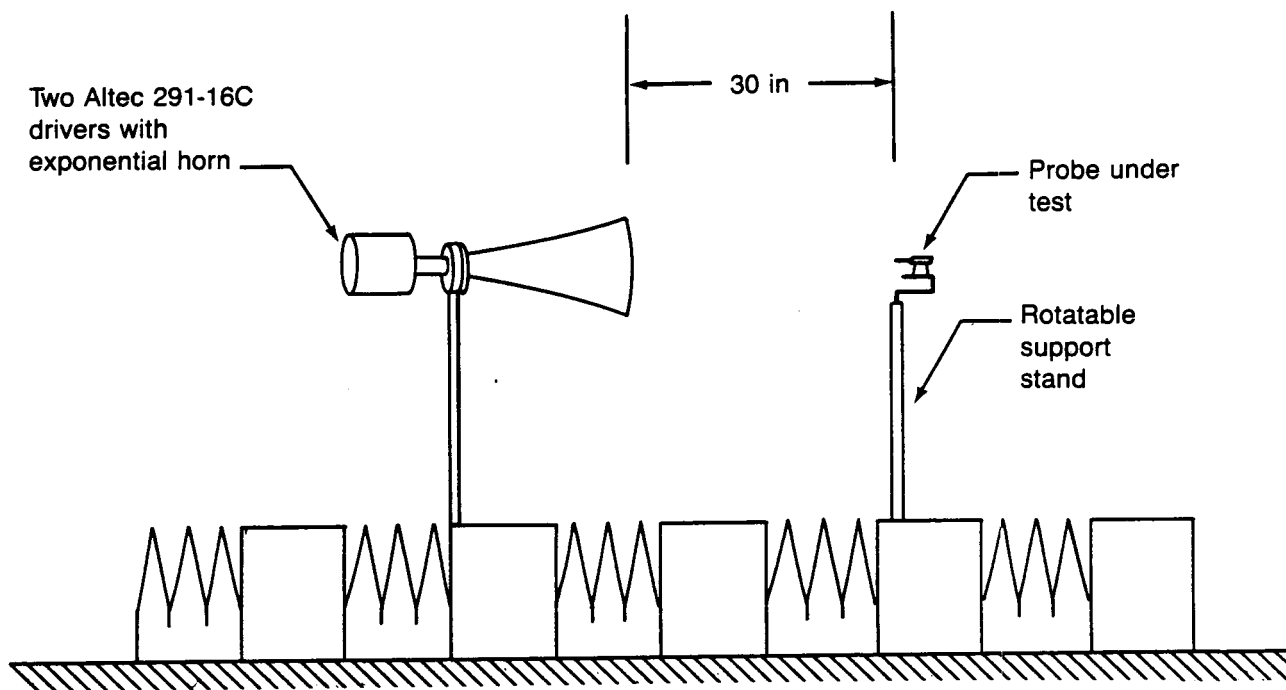


Figure A2. Test Setup for Probe Directivity Comparison

CURVE RUN COND POSITION
1 19 6 M1

AS MEASURED DATA

TIN PRIMARY CHECKOUT

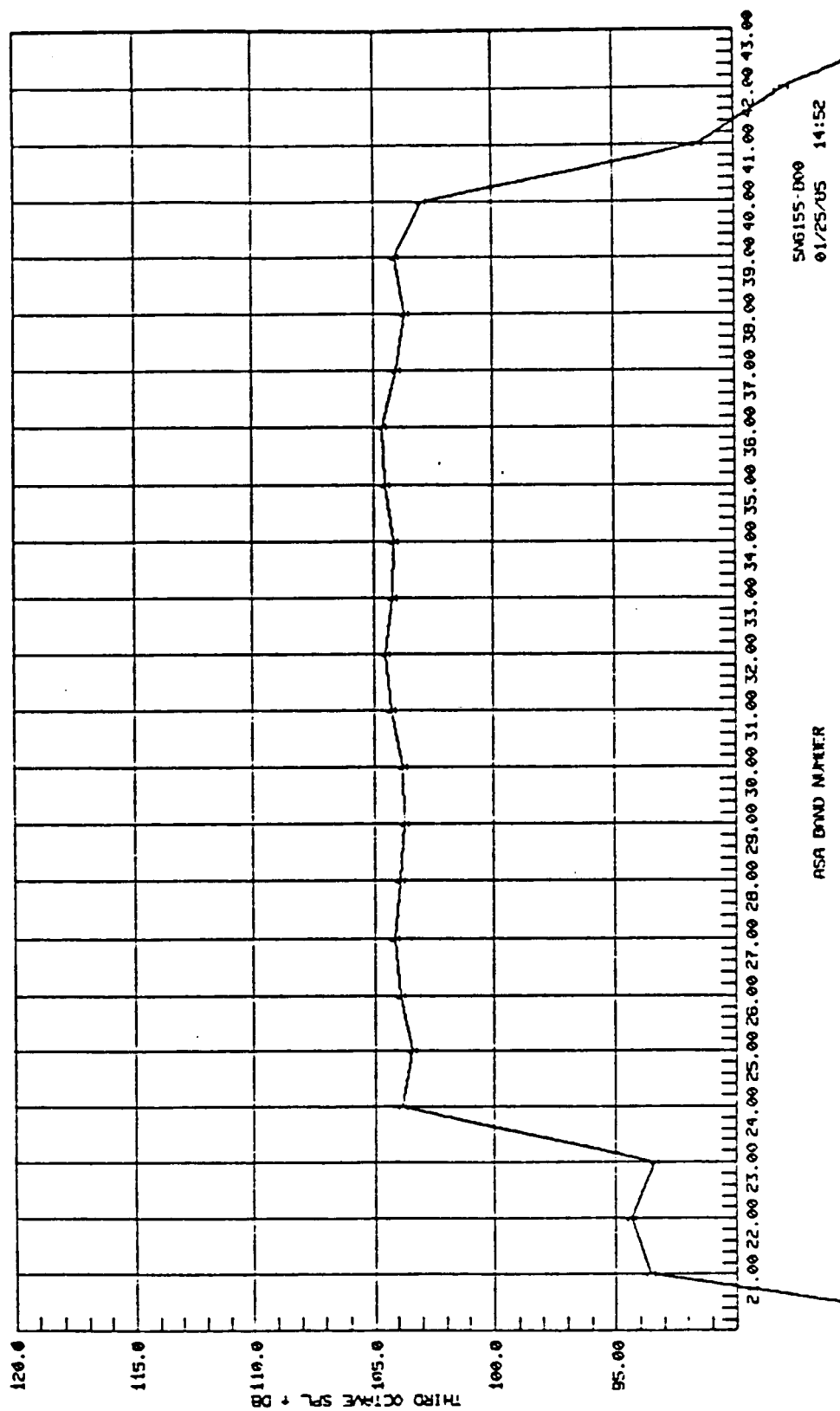
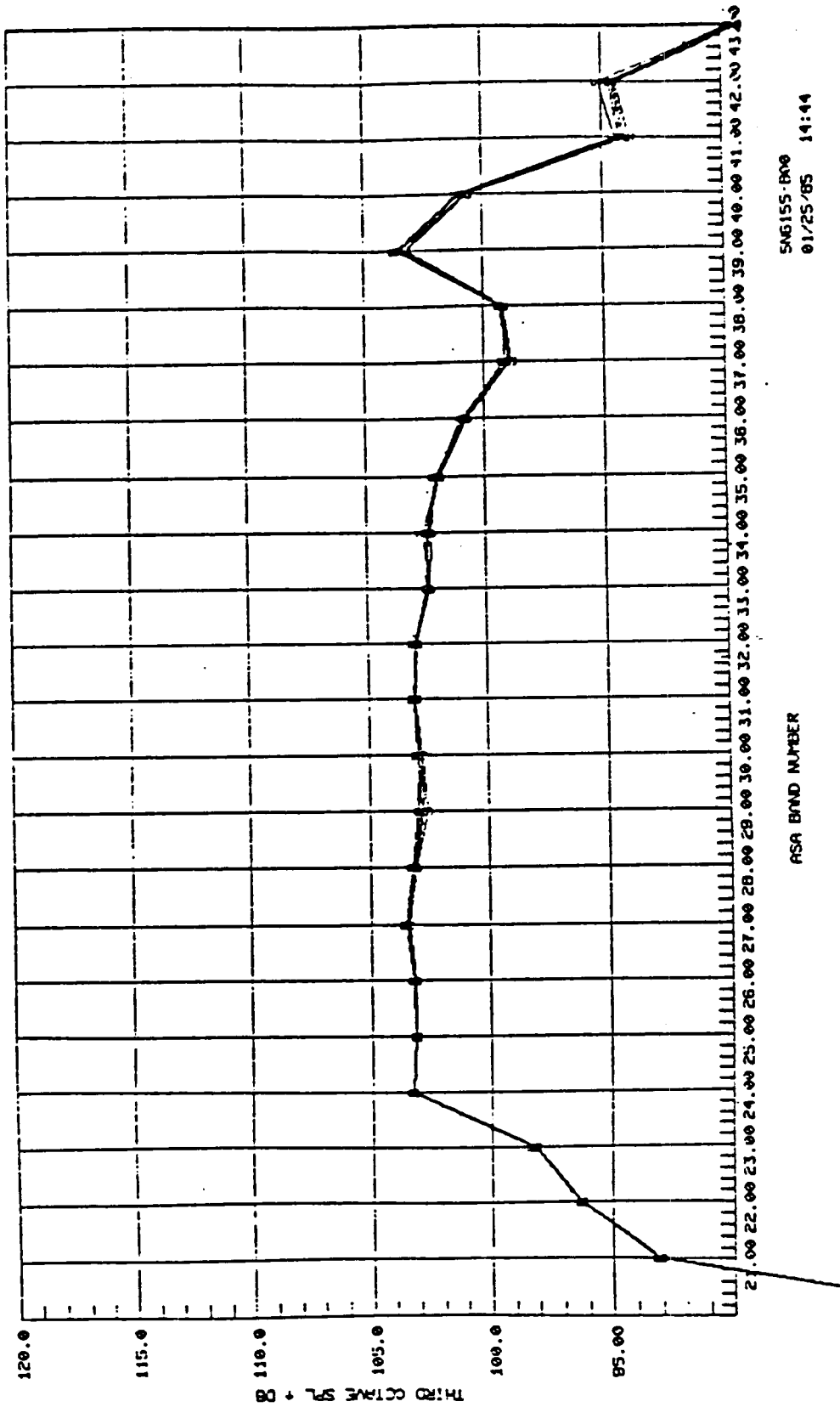


Figure A3. B&K 4134 Reference Spectrum

ORIGINAL PAGE IS
OF POOR QUALITY

AS MEASURED DATA

CURVE RUN	COND	POSITION
1	11	MI 60°
2	11	MI 75°
3	11	MI 90°
4	11	MI 105°
5	11	MI 120°



SN6155-BX0
01/25/85 14:44

ASA BND NUMBER

Figure A4. Side-Mounted Transducer Probe Configuration Tested With Unvented Kullite

AS MEASURED DATA

CURVE	RUN	COND	POSITION
1	15	6	MI 60°
2	15	7	MI 75°
3	15	8	MI 10°
4	15	8	MI 105°

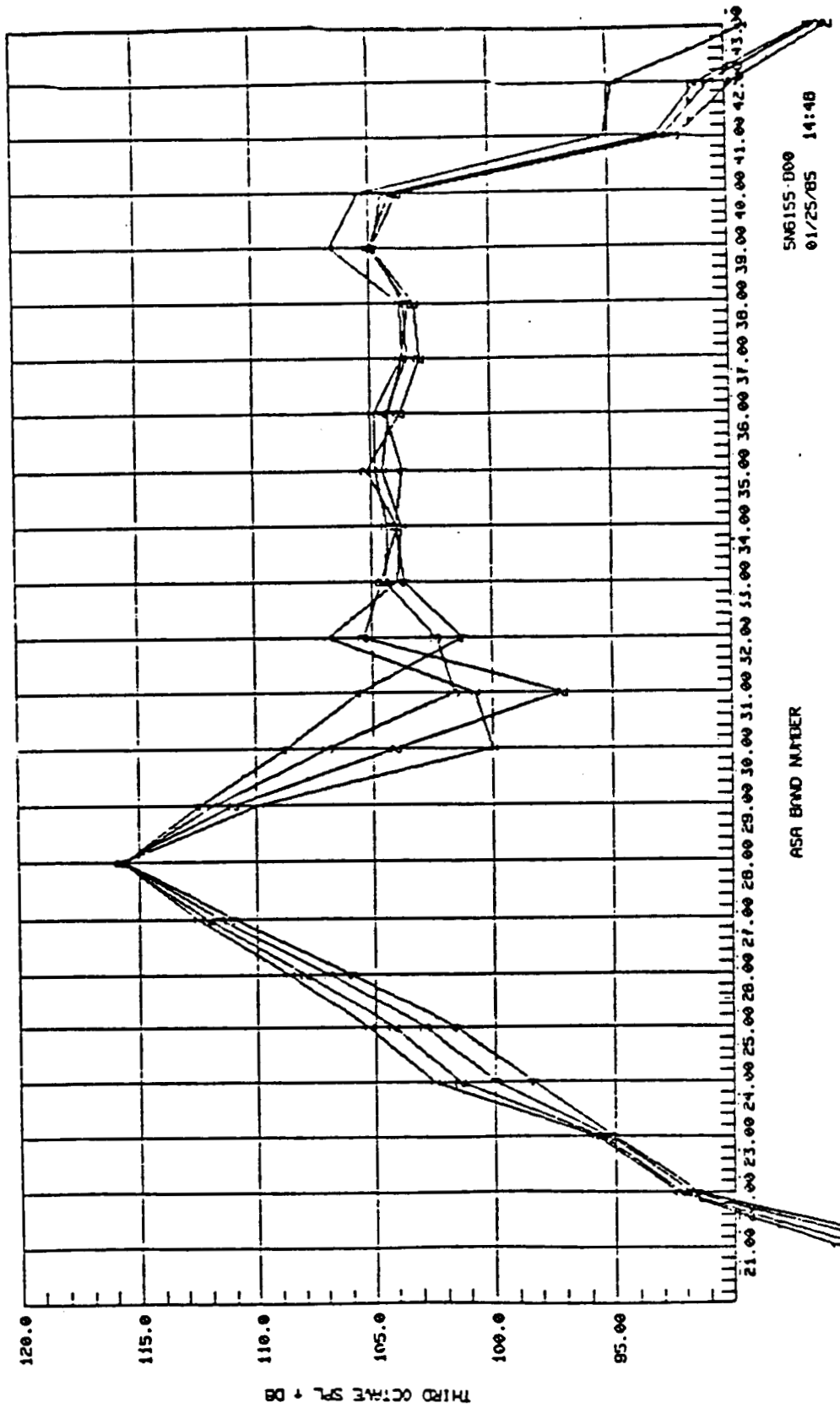
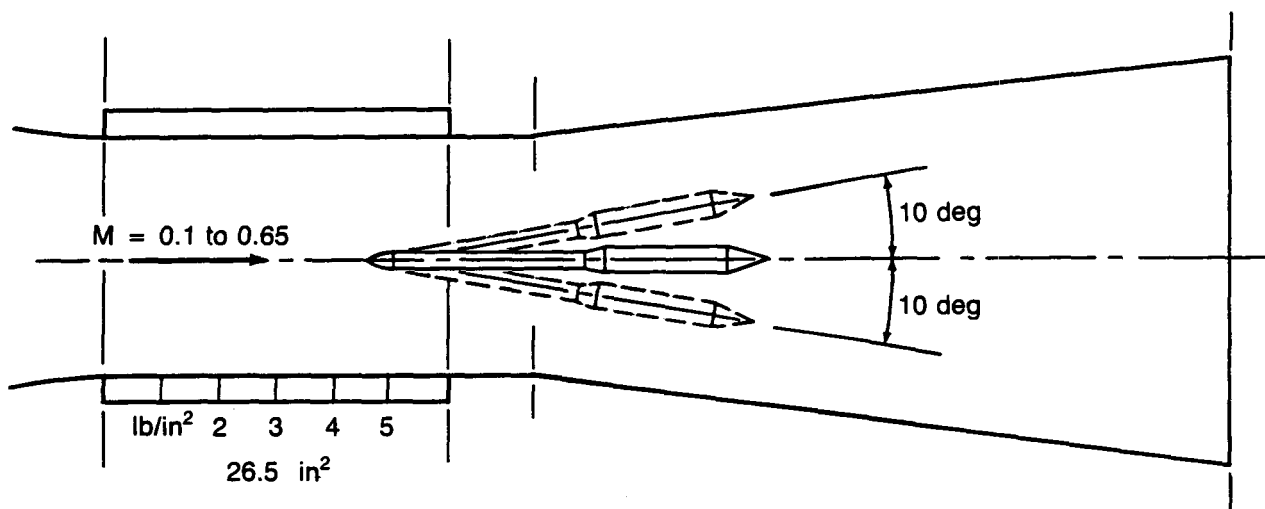


Figure A5. B&K Bullet Nose Probe Configuration—No Modification to Vent Tube

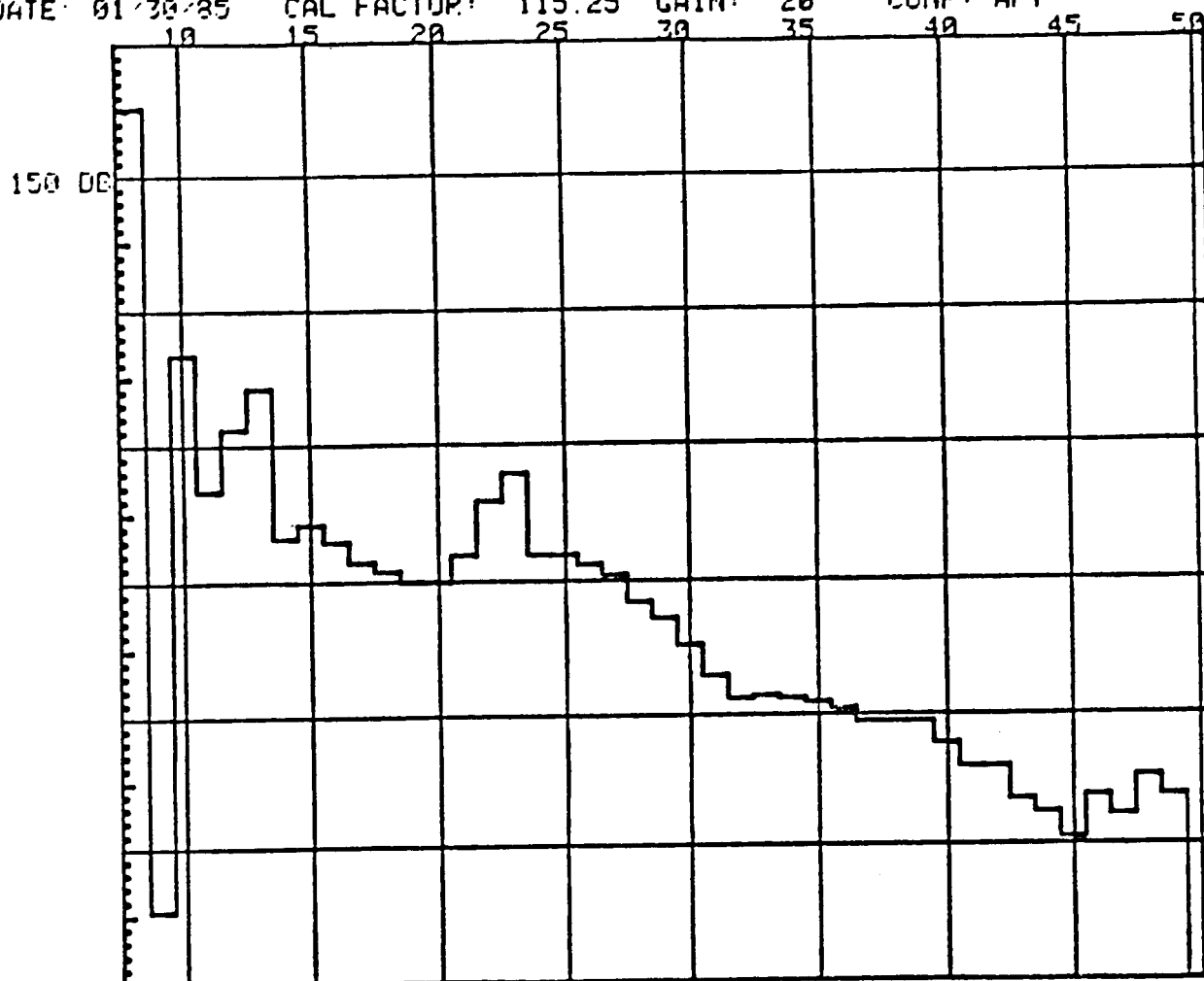
ORIGINAL PAGE IS
OF POOR QUALITY



Note: ± 10 -deg probe orientations are shown by dashed lines

Figure A6. Test Setup in Quiet Air Facility for Probe Self-Noise Test

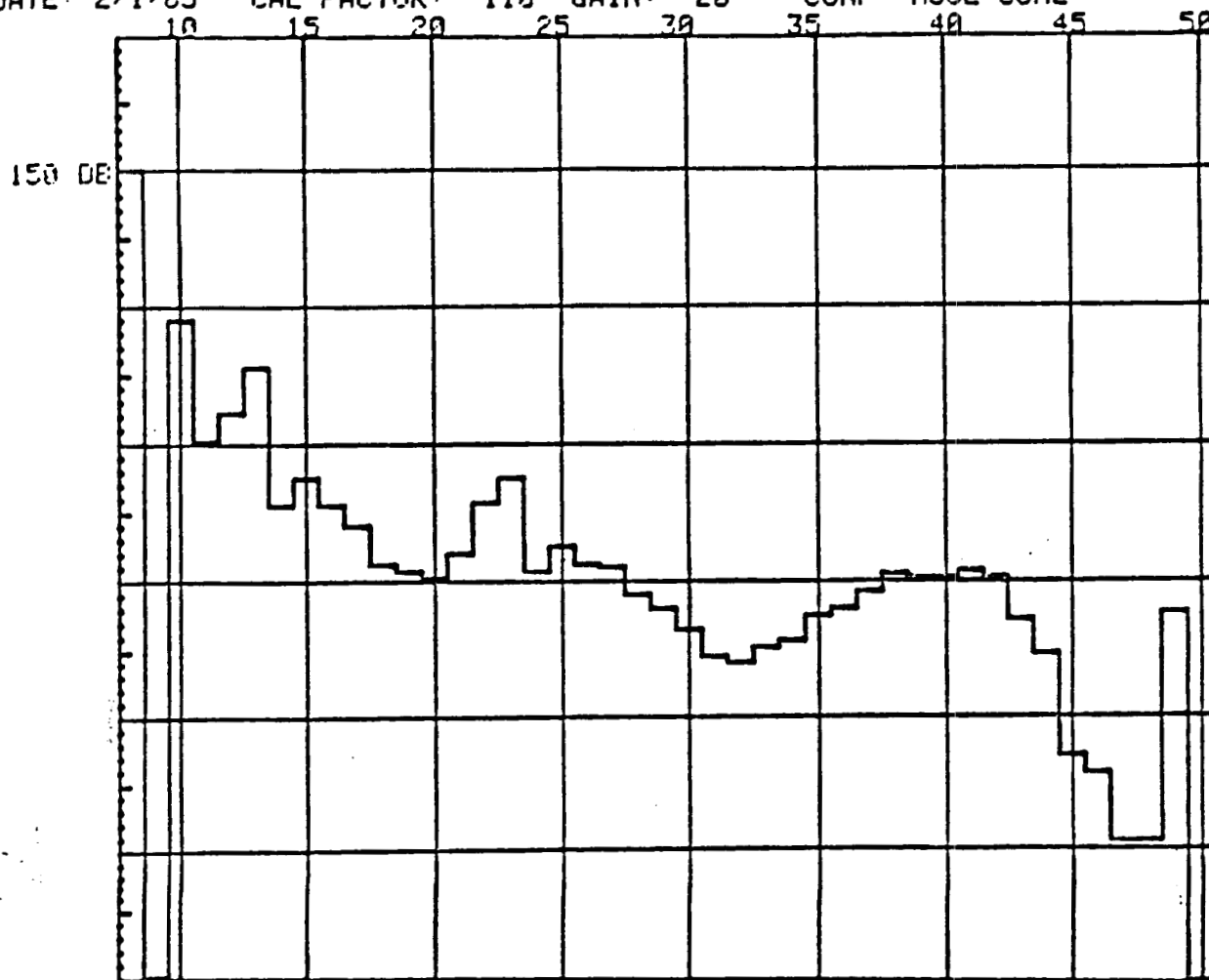
TEST: LAMINAR FLOW PROBE RUN: 1 COND: 4
 DATE: 01/30/85 CAL FACTOR: 115.25 GAIN: 20 CONF: AFT



0-deg angle of attack
 M = 0.55

Figure A7. B&K Bullet Nose Probe Configuration Self-Noise Test

TEST: LAMINAR FLOW PROBE RUN: 4 COND: 4
 DATE: 2/1/85 CAL FACTOR: 110 GAIN: 20 CONF: NOSE CONE



0-deg angle of attack
 $M = 0.55$

Figure A8. Side-Mounted Transducer Probe Configuration Self-Noise Test

ORIGINAL PAGE IS
OF POOR QUALITY

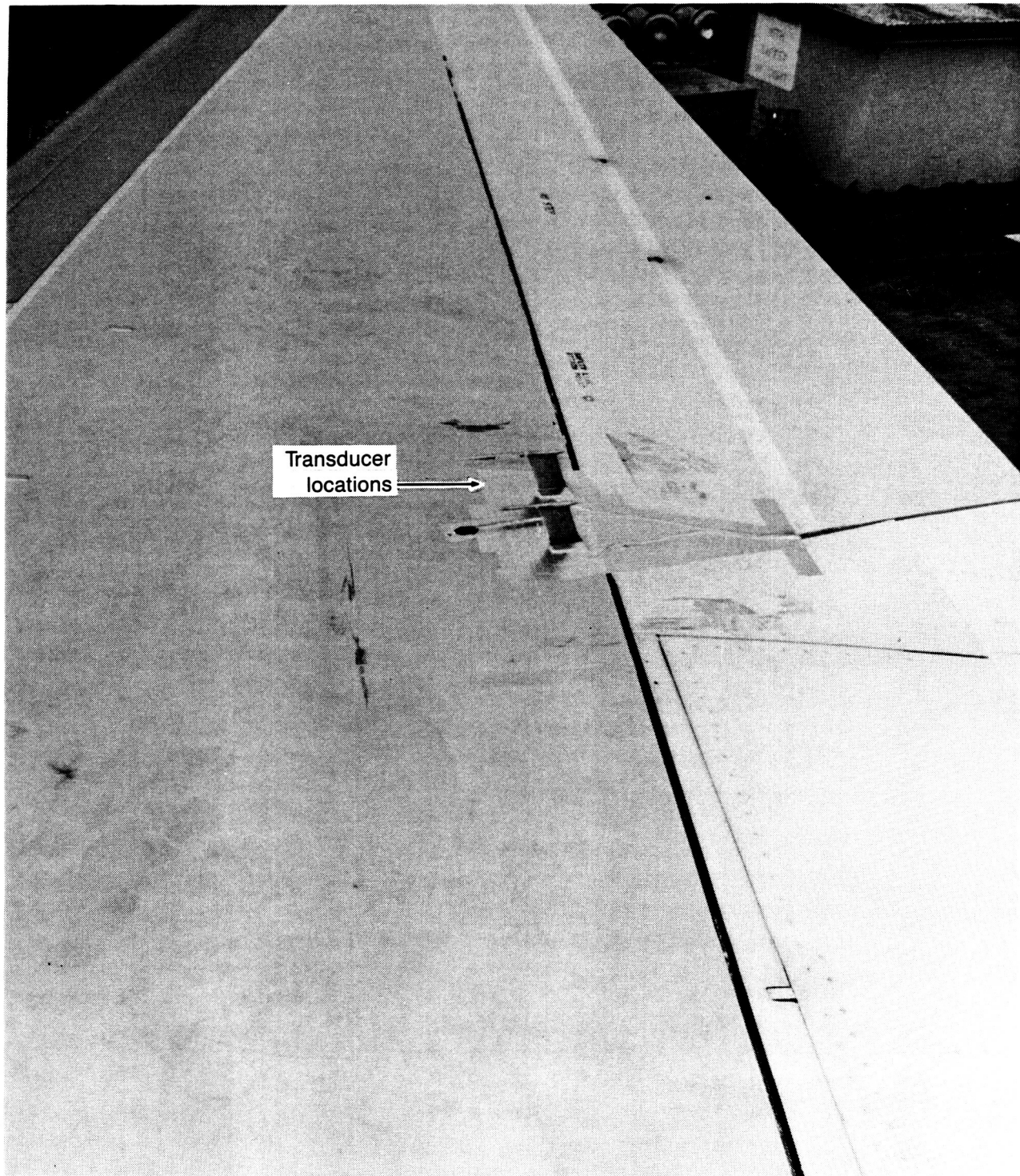
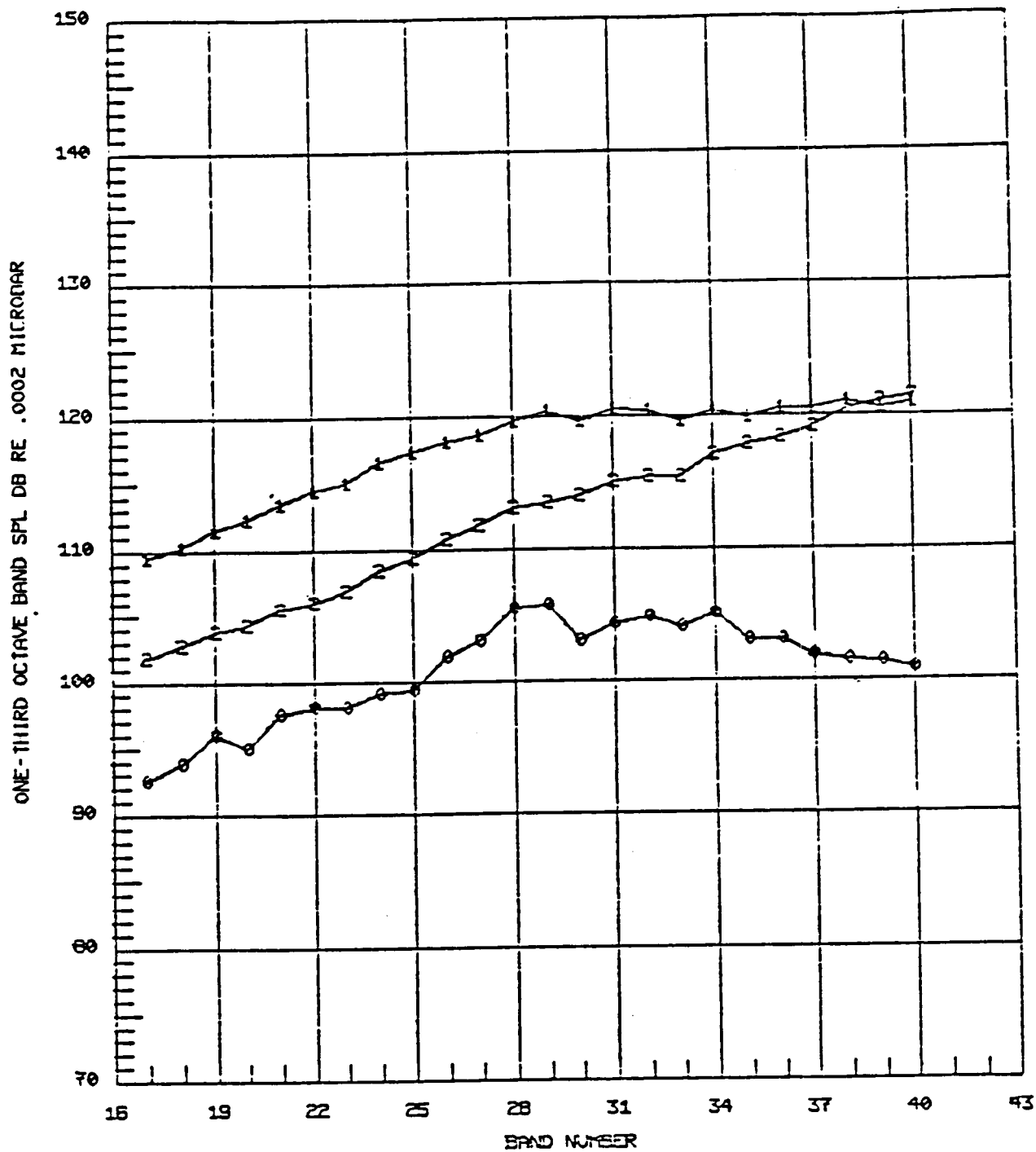


Figure A9. Kulite Transducer Installation on NA001 for Probe Evaluation Flight Tests



PLOT	COND	SEAT	LOC.	STAT.	SYS.	CASPL (DB)
SYN30L						
0	10	B&K bullet nose	K1	0		116.3
1	10	Surface mounted	K2	0		132.6
2	10	Side mfg xducers	K3	0		139.0

20 K ft. M = 0.71

Figure A10. Flight Test Data From February 22, 1985 Probe Evaluation Test

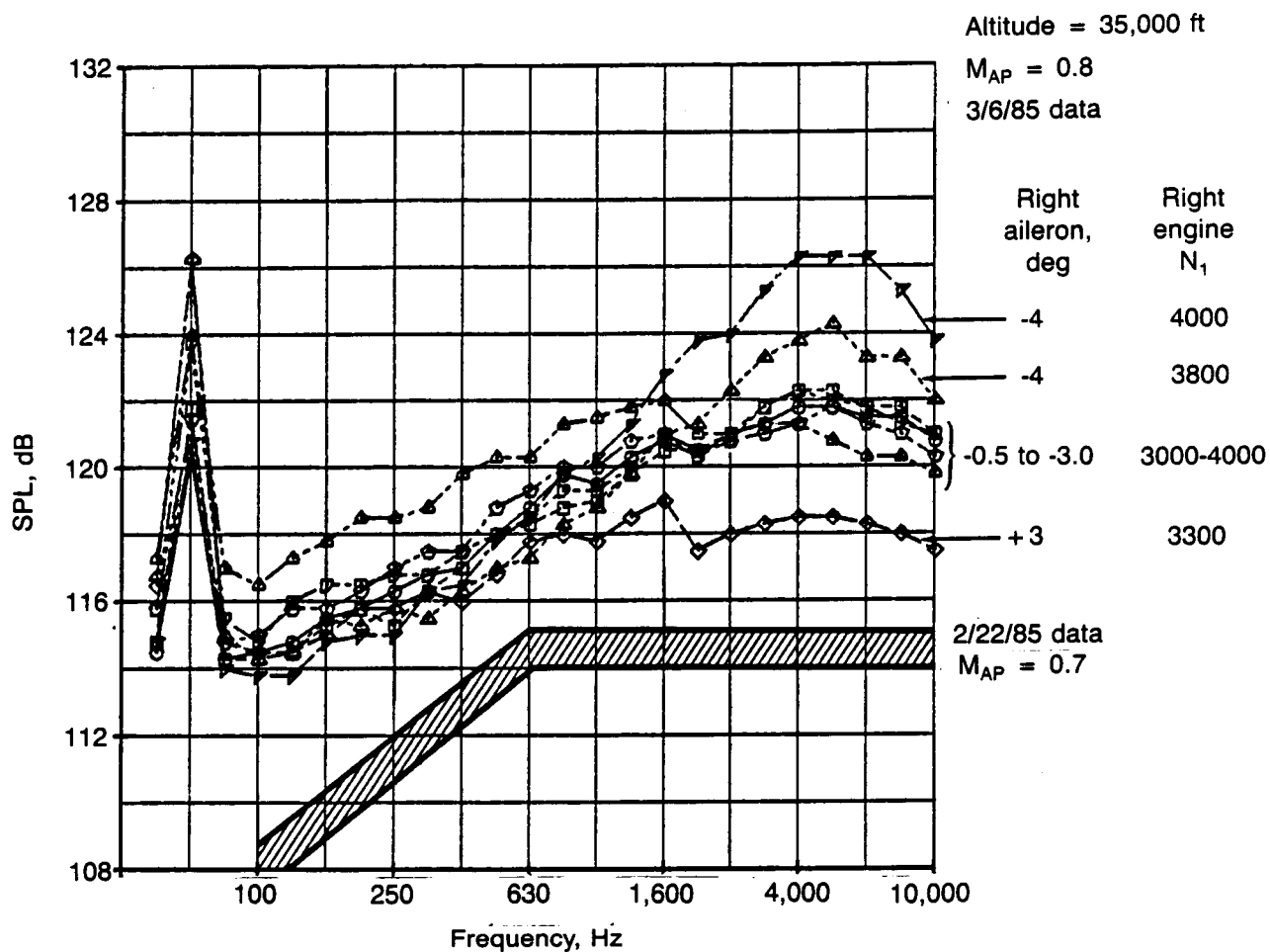


Figure A-11. Flight Evaluation of Surface-Mounted Microphone

ORIGINAL PAGE IS
OF POOR QUALITY

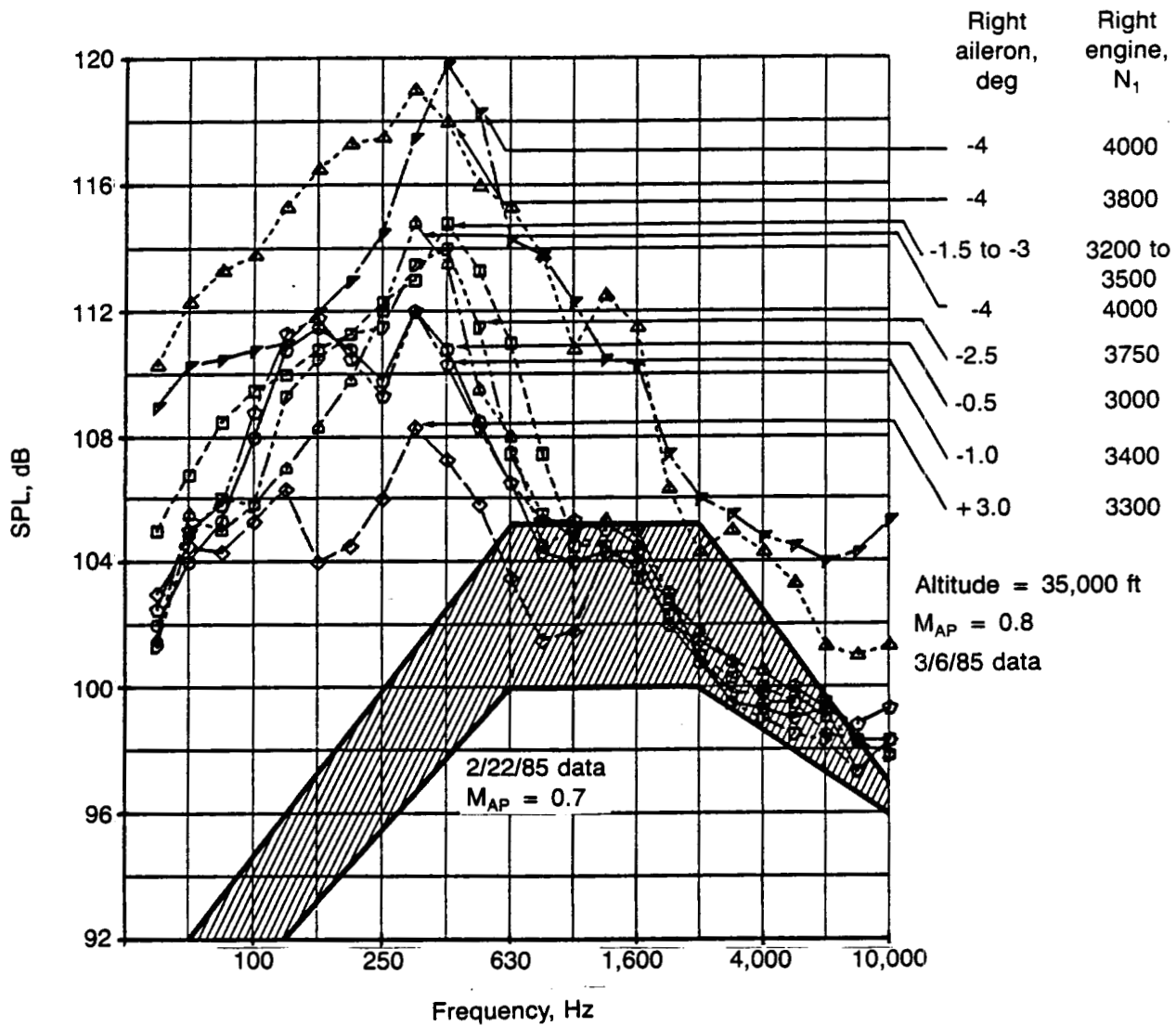


Figure A-12. Flight Evaluation of Probe Microphone (B&K Nose Cone)

ORIGINAL PAGE IS
OF POOR QUALITY

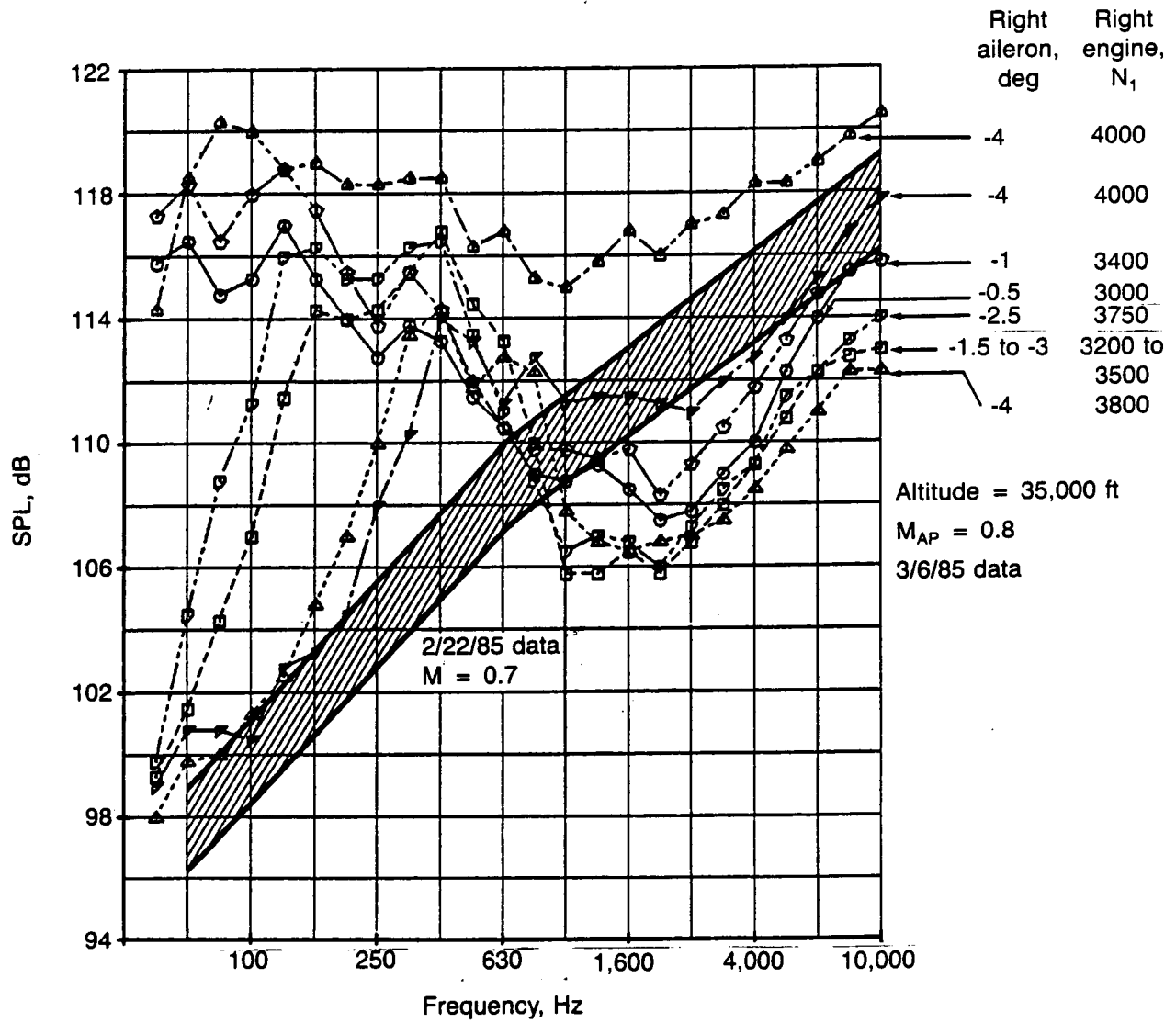
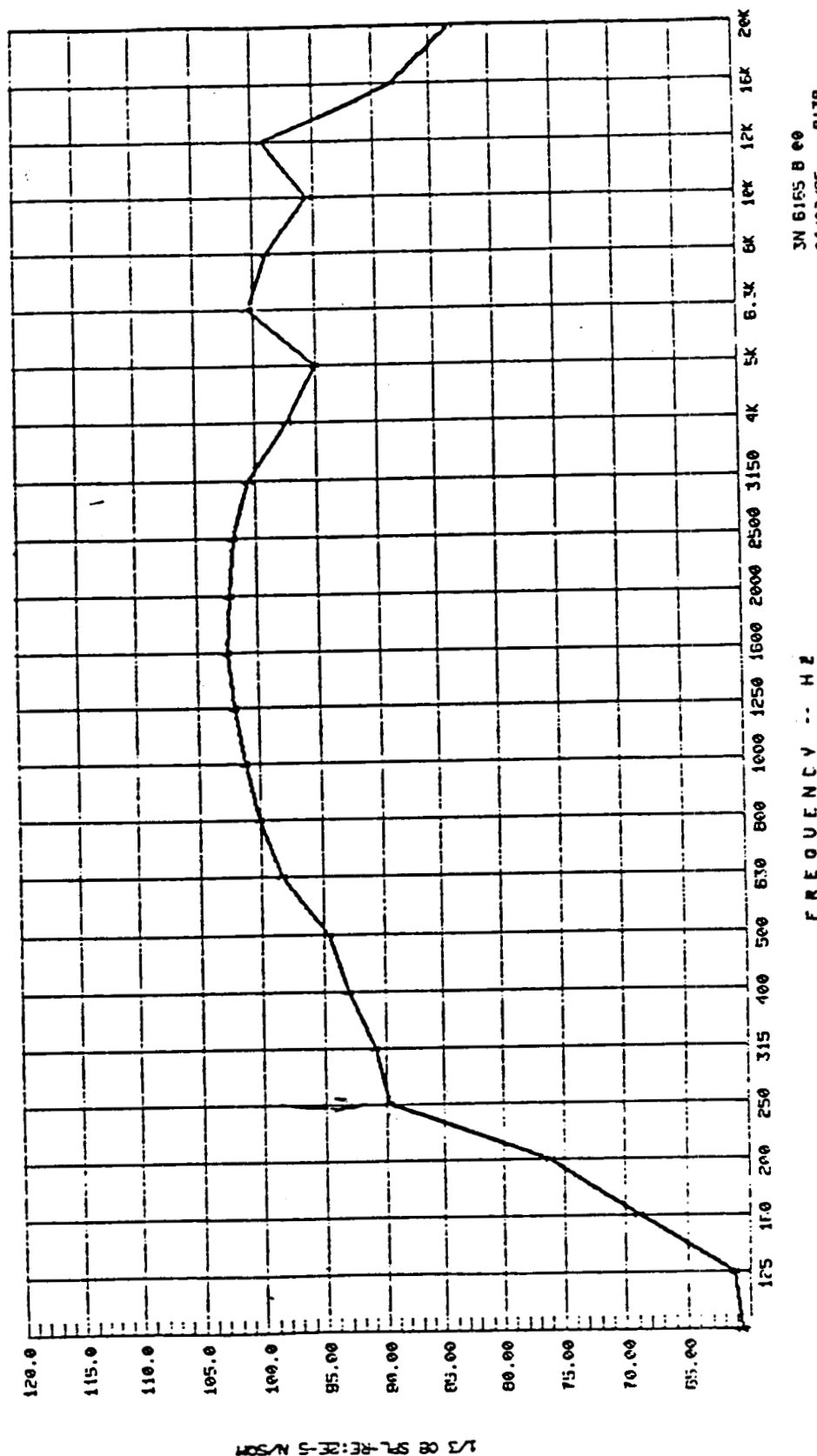


Figure A-13. Flight Evaluation of Probe Microphone (Side Mount)

CURVE SWITCH POSITION
1 1:4

CONFIGURATION : NONE
FUN : 2
CONDITION : 3
TEMPERATURE : 77.0 DEG F
PRESSURE : 23.82 IN/HG
REL HUMIDITY : 70.0 %

LOWINOR FLOW MIC CHECK-OUT



JN 6165 B 00
04/02/85 8138

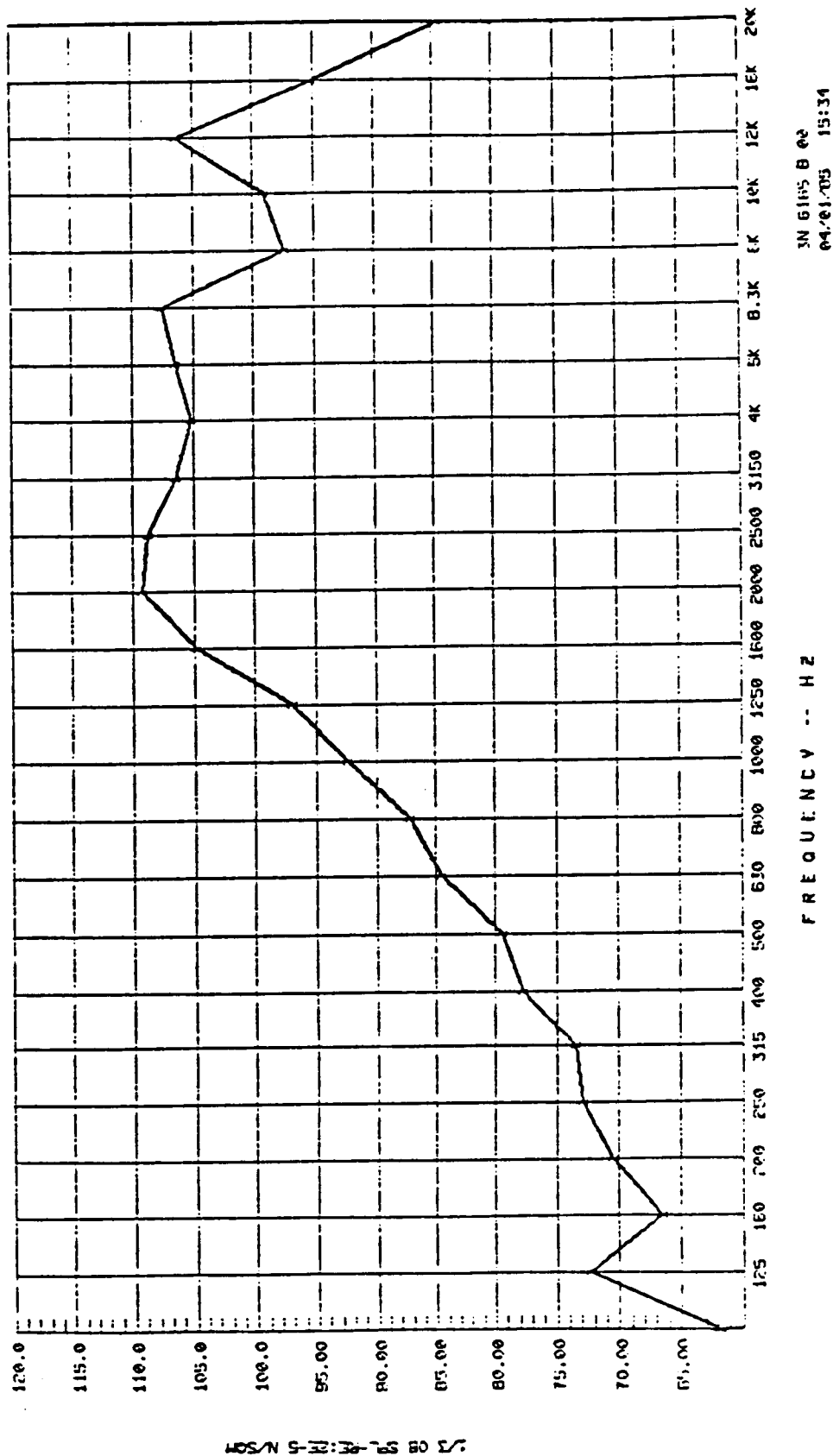
Figure A-14. XCW-093-5 Transducer—No Modifications to Vent Tube

ORIGINAL PAGE IS
OF POOR QUALITY

CURVE SHEET POSITION
1 1:3

CONFIGURATION : NONE
RUN : 1
CONDITION : 3
TEMPERATURE : 17.0 DEG F
PRESSURE : 29.92 IN/HG
REL HUMIDITY : 70.0 %

LOW FLOW MIC CHECK-OUT



IN 6115 B 02
04/01/05 15:34

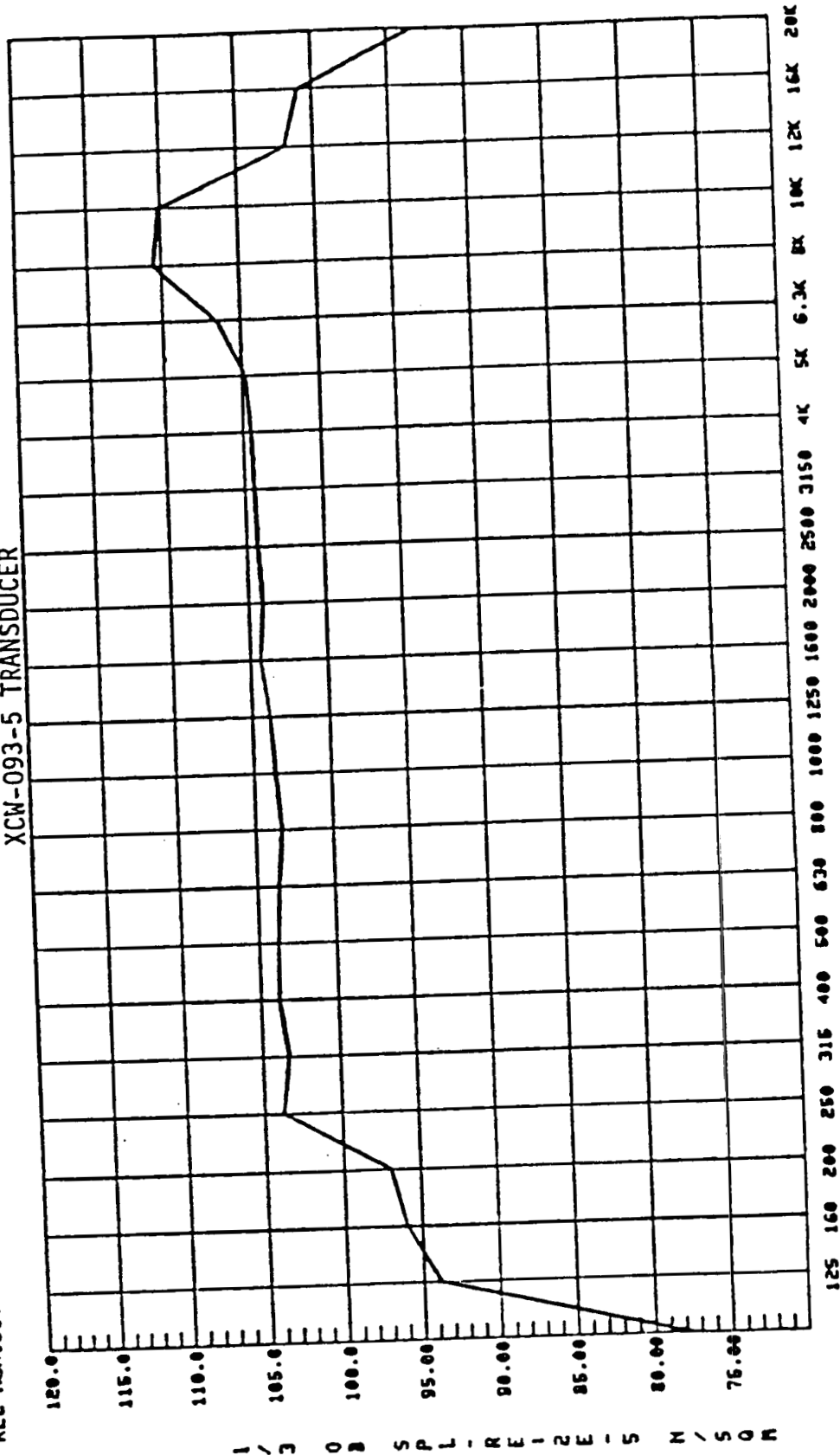
Figure A-15. LQ-101-125-5 Transducer—No Modifications Made to Vent Tube

ORIGINAL PAGE IS
OF POOR QUALITY

-----SWICH-----POSITION-----
11 1 M1

CONFIGURATION : FM90
RUN : 32
CONDITION : 3
TEMPERATURE : 47.0 DEG F
PRESSURE : 20.92 IN/HG
REL HUMIDITY : 70.0 %

XCW-093-5 TRANSDUCER



JN 6165 B 00
01/31/85 14137

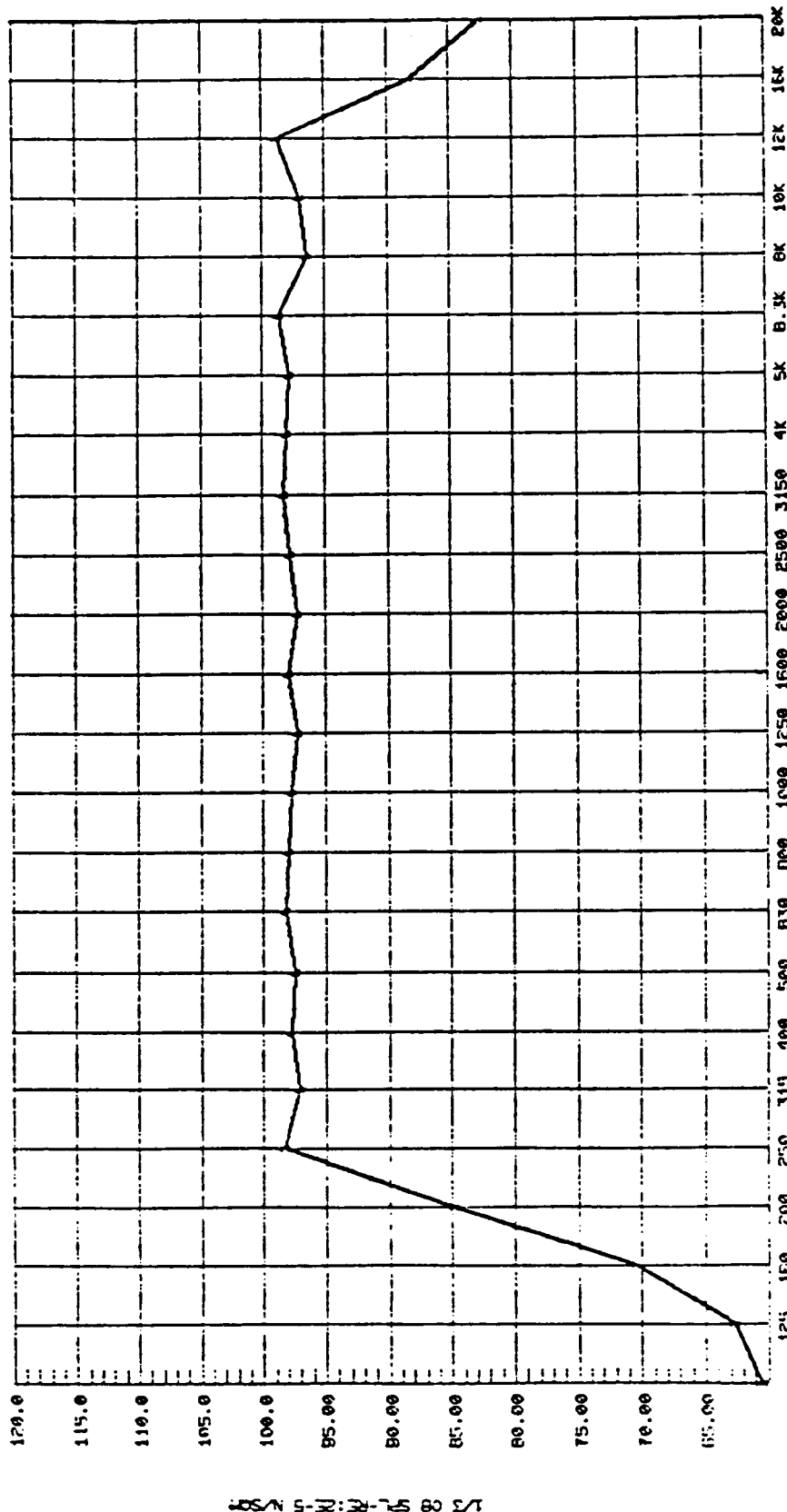
FREQUENCY -- HZ

Figure A-16. B&K Bullet Nose Probe Configuration—3 ft Length of Tygon Tubing Spliced to Transducer Vent Tube

CURVE 1
 SUICH 115
 POSITION

CONCURATION : NONE
 PUN : 132
 CONDITION : B
 TEMPERATURE : 77.0 INCF
 PRESSURE : 29.92 IN/HG
 REL HUMIDITY : 70.0 %

LOHMER FLOW MIC CHECK-OUT



FREQUENCY -- HZ

3N 8165 B 04
 04/02/85 10:37

ORIGINAL PAGE IS
 OF POOR QUALITY

Figure A-17. XCE-093-5 Transducer With 0.008-in Wire Inserted in Vent Tube

CURVE SHEET POSITION
 1 1:3

CONFIDENTIAL 1 PAGE
 RUN 11
 CONDITION 12
 TEMPERATURE 17.0 DEG F
 HUMIDITY 29.92 IN/HG
 AIR PRESSURE 10.0 IN

1000000 HIC CHECK-OUT

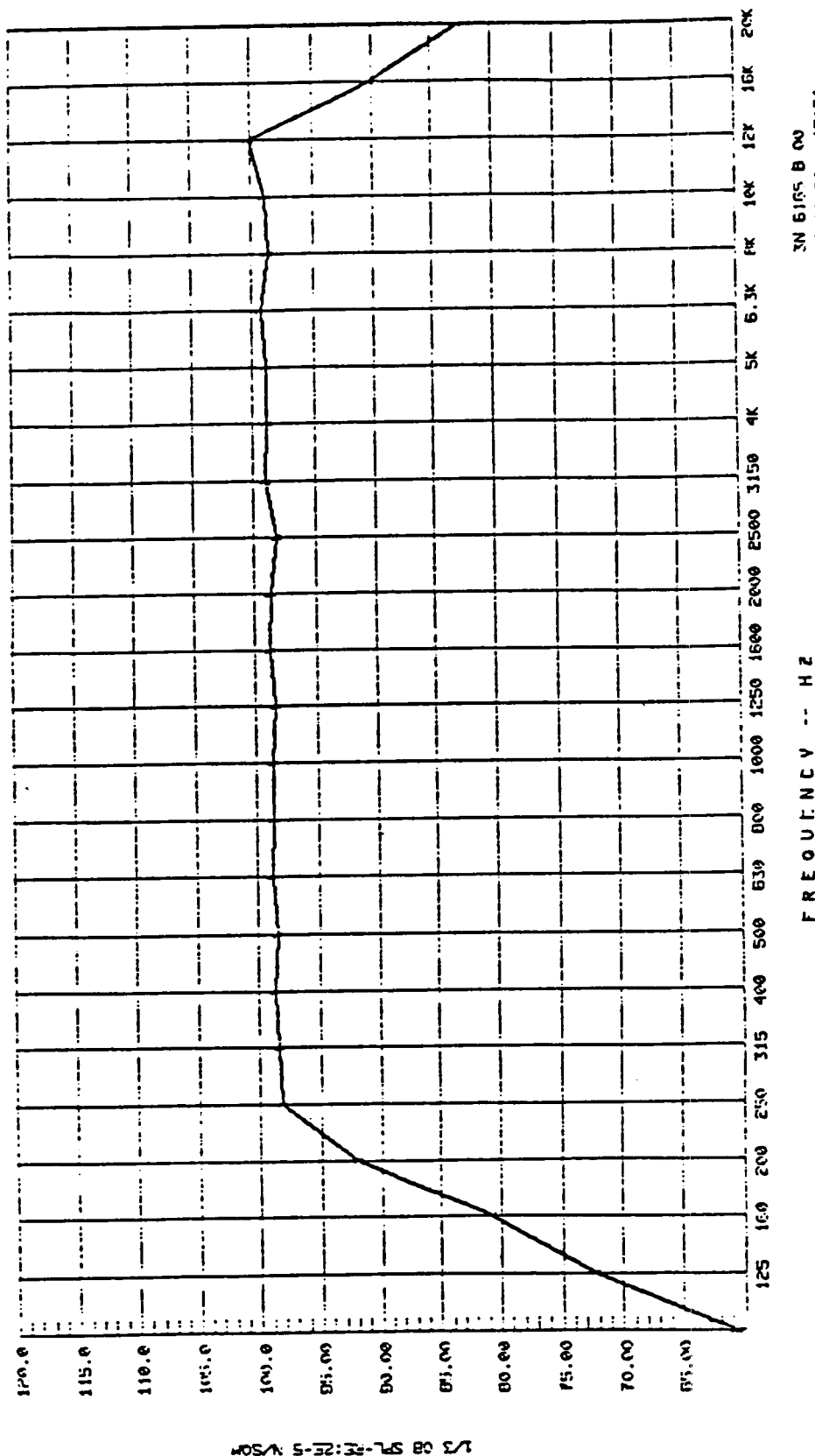



Figure A-18. LQ-101-125-5 Transducer With 0.008-in Wire Inserted in Vent Tube

Standard Bibliographic Page

1. Report No. NASA CR-178216		2. Government Accession No.		3. Recipient's Catalog No.	
4. Title and Subtitle Flight Survey of the 757 Wing Noise Field And Its Effects On Laminar Boundary Layer Transition; Volume I - Program Description and Data Analysis				5. Report Date March 1987	
				6. Performing Organization Code	
7. Author(s) New Product Development Organization Boeing Commercial Airplane Company (BCAC)				8. Performing Organization Report No. D6-53196-1	
9. Performing Organization Name and Address Boeing Commercial Airplane Company P.O. Box 3707 Seattle, WA 98124				10. Work Unit No. NAS1-15325	
				11. Contract or Grant No. Contractor Report	
12. Sponsoring Agency Name and Address National Aeronautics and Space Administration Washington, D.C. 20546				13. Type of Report and Period Covered	
				14. Sponsoring Agency Code	
15. Supplementary Notes Technical Monitors: D. B. Middleton and D. W. Bartlett NASA - Langley Research Center					
16. Abstract A flight test program was performed using the Boeing 757 flight research airplane to investigate the effect of noise from wing mounted engines on laminar boundary layer transition. An NLF glove was installed on the right wing panel just outboard of the engine. The extent of laminar flow on the glove was measured as a function of engine power setting for a range of flight conditions. A combination of surface and probe microphones was distributed over the upper and lower wing surfaces to measure sound spectra. The flight test program was completed in June 1985 and the results of preliminary analysis indicate that a maximum of about 29% of chord laminar flow was obtained on the upper surface and about 28% on the lower surface (at a high sideslip condition). The engine speed was varied from about 2600 (idle) to about 4500 (maximum continuous power) r/min. This produced changes in sound pressure level up to 20 dB on the lower surface. On the upper surface, the noise levels were independent of engine power but sensitive to airplane Mach number. No effect of engine power setting on upper surface transition location was observed, and only a small forward movement of the transition location on the lower surface was observed at the high power settings. Volume I of this report contains the program description and data analysis. Volume II is a compilation of all of the flight test data.					
17. Key Words (Suggested by Authors(s)) Boundary Layer Transition Engine Noise Flight Pressure Data Flight Test Hot Film Sensors Natural Laminar Flow				18. Distribution Statement 	
19. Security Classif.(of this report) Unclassified		20. Security Classif.(of this page) Unclassified		21. No. of Pages 212	
				22. Price	